AGARD-LS-45-71

AGARD-LS-45-71

AGARD

ADVISORY GROUP FOR AEROSPACE RESEARCH & DEVELOPMENT

7 RUE ANCELLE 92 NEUILLY-SUR-SEINE FRANCE

AGARD LECTURE SERIES No. 45

on

Attitude Stabilization of Satellites in Orbit

NORTH ATLANTIC TREATY ORGANIZATION

DISTRIBUTION AND AVAILABILITY
ON BACK COVER

UNLIMITED

AGARD Lecture Series No.45

NORTH ATLANTIC TREATY ORGANIZATION

ADVISORY GROUP FOR AEROSPACE RESEARCH AND DEVELOPMENT

(ORGANISATION DU TRAITE DE L'ATLANTIQUE NORD)

9.71

ATTITUDE STABILIZATION OF SATELLITES IN ORBIT

The material in this book has been collected to support a Lecture Series under the sponsorship of the Guidance and Control Panel, and the Consultant and Exchange Programme, of AGARD
(Brussels, 11-12 October – Stuttgart, 14-15 October 1971)

THE MISSION OF AGARD

The mission of AGARD is to bring together the leading personalities of the NATO nations in the fields of science and technology relating to aerospace for the following purposes:

- Recommending effective ways for the member nations to use their research and development capabilities for the common benefit of the NATO community;
- Providing scientific and technical advice and assistance to the North Atlantic Military Committee in the field of aerospace research and development;
- Continuously stimulating advances in the aerospace sciences relevant to strengthening the common defence posture;
- Improving the co-operation among member nations in aerospace research and development;
- Exchanging of scientific and technical information;
- Providing assistance to member nations for the purpose of increasing their scientific and technical potential;
- Rendering scientific and technical assistance, as requested, to other NATO bodies and to member nations in connection with research and development problems in the aerospace field.

The highest authority within AGARD is the National Delegates Board consisting of officially appointed senior representatives from each Member Nation. The mission of AGARD is carried out through the Panels which are composed of experts appointed by the National Delegates, the Consultant and Exchange Program and the Aerospace Applications Studies Program. The results of AGARD work are reported to the Member Nations and the NATO Authorities through the AGARD series of publications of which this is one.

Participation in AGARD activities is by invitation only and is normally limited to citizens of the NATO nations.

Published September 1971

629.783:629.7.058.47

Printed by Technical Editing and Reproduction Ltd
Harford House, 7-9 Charlotte St, London. W1P 1HD

FOREWORD

It was felt appropriate by the AGARD Guidance and Control Panel to present and discuss the Stabilization of Satellites in Orbit.

The Consultant and Exchange Programme has recruited a team of experts who, under the technical direction of Mr H.Vigneron, will make a survey of the subject. The fundamental equations will be derived.

Cases of non-rigidity, structural vibrations and moving parts are considered. Various types of stabilization are studied: spin, dual-spin, gravity gradient system and associated dampers, flywheels, magnetic torquers, thrusters, and nutation dampers.

Various sensors are described: sun and earth sensors, star trackers, gyros and magnetometers. Their limitations and their accuracy is considered.

The theories and technical problems are illustrated by description of recent missions and projected spacecraft, such as ATS 5, TACSAT 1, SKYLAB B, Apollo, EOLE and PEOLE, SIRIO, OAO, TD.

When typical, acquisition and stationary processes are described.

A Round Table Discussion with the participation of all the speakers will conclude the Lecture Series, which will be presented in Brussels (Belgium) and Stuttgart (Germany) from 11 to 15 October 1971.

SPEAKERS

Mr R.H.BATTIN
Associate Director
Charles Stark Draper Laboratory
Massachusetts Institute of Technology
75 Cambridge Parkway
Cambridge, Massachusetts 02142, USA

Dr.Ing. A.BURATTI
Compagnia Industriale Aerospaziale S.p.A.
Viale di Villa Grazioli, 23
00198 Rome
Italy

Dr M.A.FRIK
Associate Professor
Institut A für Mechanik
Universität Stuttgart
7 Stuttgart 1
Keplerstrasse 17
Germany

Mr T.E.HUBER
Goddard Space Flight Center – NASA
Greenbelt
Maryland 20771
USA

Mr W.G.HUGHES
Ministry of Defence (Aviation Supply)
Space Department
Royal Aircraft Establishment
Farnborough
Hampshire
UK

Mr P.HUGUIER
Ingénieur
Centre National d'Etudes Spatiales
B.P. No.4 – Bretigny S/Orge (91)
France

Dipl.-Ing. W.INDEN
ERNO Raumfahrttechnik GmbH
28 Bremen, Hünefeldstrasse 1-5
W.Germany

Dr P.W.LIKINS
Associate Professor
4731 Boelter Hall
University of California,
Los Angeles
California
USA 90024

Mr H.VIGNERON
Technical Director
SAIT Electronics
Brussels
Belgium

Professor P.Y.WILLEMS
Université de Louvain
Institut de Mécanique
300 Celestijnenlaan
B-3030 Héverlée
Belgium

CONTENTS

ATTITUDE STABILIZATION OF ORBITING SATELLITES

INTRODUCTION

Henri Vigneron
Technical Director - SAIT Electronics
Brussels

The attitude stabilization of an orbiting satellite is certainly one of the most critical problems related to satellite design. This is an extensive problem, as the missions of space vehicles are diversified, and attitude accuracy requirements varied. Besides, the procedures adopted between launch phase and final stabilization are sometimes very complex. Consequently, the disciplines involved are numerous; they call for the most advanced techniques, and it goes without saying that the scope of the problem had to be limited when nine lecture themes had to be selected for a two-day presentation. We first thought of a possible subdivision between active, passive and semi-active stabilization; however, it appeared that some confusion existed between these terms, moreover, hybrid solutions were commonly used.

Finally, the lecture series was limited to the following areas:

- theoretical background, with emphasis on problems of current interest, particularly that related to flexibility,
- design of a servo-control loop in the case of active attitude stabilization,
- description of commonly used sensors and actuators,
- finally, a few typical examples of the stabilization of satellites from those already orbiting or in the planning phase.

The very interesting problem of controls optimization will only be touched on.

To help the audience to get a clear understanding of the papers presented, we have thought it useful to start with a survey of the mathematical problems posed by attitude stabilization. This is the theme of the lecture given by Dr. M. A. FRIK, Professor at the University of Stuttgart. This lecturer reviews various concepts: Euler's angles and equations, Poinsot's ellipsoid, linearization in the case of small deviations. The influence of disturbing torques is described and, finally, the motion equations of a flexible satellite are introduced. This latter part is taken up again in detail by Messrs. Likins and Willems.

Prof. Peter W. LIKINS, from the University of California, discusses the influence of the flexibility of a vehicle. Tracing out the history of a few partial failures, he ascribed some stability anomaly cases to flexibility reflected in the form of dissipated energy or detrimental deformations. Prof. Likins surveys the present state-of-the-art in this field, stressing the fact that the problems raised are not purely academic, but, on the contrary, have to be solved for the large satellites of the future.

Prof. P. WILLEMS, from the University of Louvain, discusses the problem of dual rotation satellites in the case of a free space trajectory, as well as in the case of a circular orbit around the earth; he investigates equilibrium and stability positions. He discusses the case of a flexible junction between the two mobile parts and outlines a strict treatment for this problem.

Mr. W. G. HUGHES, from the Royal Aircraft Establishment (R.A.E.), considers the complete servo-control loop of an active satellite. He briefly describes the various types of engine torques used. He derives equations for a system with three inertia wheels and describes the conditions ensuring a slight intercoupling between the axes. He presents in detail the single axis case, control by inertia wheel including desaturation methods, control moment gyro and control by gas ejection. In the latter case, more appropriate inputs can be generated by means of a dynamic model of the vehicle in the control loop. Finally, the means of obtaining an inertial reference for a vehicle aimed at the earth are examined.

The purpose of the following lectures is of a more technological nature, which does not in the least detract from their interest, as each problem is covered by a specialist having played a very active part in the project described.

Mr. T. I. HUBER, from the Stabilization and Control Branch of NASA, was engaged during many years in the study of the problems related to the attitude control of Orbiting Astronomic Observatory satellites. Besides, he is the responsible engineer for these sub-systems aboard the OAO. With the OAO as an example, he described the various sensors which make it possible to aim a 4,500 lbs. mass at any direction in the sky with an accuracy better than an arc minute. The sensors described are typical of the present status of technology: rough solar sensors, accurate solar sensors, digital sensors, inertial reference providing angle and angle variation data, star tracking systems and finally a high accuracy magnetometer.

Mr. Philippe HUGUIER, an engineer at the National Space Studies Centre (CNES) describes PEOLE and EOLE satellites, for which the two-axis stabilization is achieved by means of a gravity gradient. He gives a detailed description of the acquisition procedure, especially of the half-turn reversal of the PEOLE satellite launched in December 1970 from the French base at Kuru, where the stabilization pole had finally to be pointed at the ascending geocentric.

Mr. W. INDEN, an engineer at ERNO Raumfahrttechnik GmbH, gives a detailed description of the cold gas propulsion system of the European TD satellite, with particular emphasis on manufacturing and qualifying methods.

The attitude control loop of the SIRIO satellite is described by Mr. A. BURATTI, an engineer at the Compagnia Industriale Aerospaziale (C.I.A.); he describes the sensors and actuators of this spacecraft, as well as the manoeuvres to be performed both during the transfer and the final phases. He lays special stress on attitude measurements by means of various terrestrial and solar sensors. He describes ground testing with particular mention of the difficulties encountered in an acceptable simulation of space conditions.

Dr. R. H. BATTIN, the Associate Director of the Charles Stark Draper Labs., provides details on the attitude controls of the APOLLO flights during its various phases, the free flight phase as well as the powered flight phase for re-entry into the atmosphere; this lecture series is therefore concluded by the description of one of the most outstanding achievements of modern stabilization techniques.

STABILISATION D'ATTITUDE DE SATELLITES EN ORBITE

INTRODUCTION

Henri Vigneron
Directeur Technique - SAIT Electronics
Bruxelles.

La stabilisation d'attitude en orbite est certainement un des problèmes les plus délicats que soulève la conception d'un satellite. Ce problème est vaste car les missions des engins spatiaux sont diversifiées et les exigences de précision d'attitude variées. De plus, une procédure parfois très complexe est mise en action entre la phase d'injection sur orbite et la stabilisation finale. En conséquence, les disciplines mises en jeu sont nombreuses; elles font appel aux techniques les plus modernes et il est évident qu'il a fallu restreindre le problème lorsqu'il s'est agi de choisir neuf sujets de conférence à exposer en deux jours. Nous avions d'abord pensé à une subdivision possible entre stabilisation active, passive et semi-active, mais il est apparu qu'une certaine confusion existait entre ces termes et que, de plus, des solutions hybrides étaient couramment employées.

Finalement, le cycle de communications a été limité aux domaines suivants :

- fondements théoriques en insistant sur les problèmes d'actualité et notamment celui de la non-rigidité,
- conception d'une boucle d'asservissement dans le cas d'une stabilisation d'attitude active,
- description des capteurs et des actionneurs couramment employés,
- enfin, quelques exemples typiques de stabilisation de satellites déjà en orbite ou en cours de projet.

Le problème fort intéressant de l'optimisation des commandes ne sera qu'effleuré au cours des conférences.

Pour une compréhension claire des exposés, il était utile d'entamer ce cycle par la synthèse des problèmes mathématiques que pose la stabilisation d'attitude. C'est l'objet de la conférence du Dr M.A. FRIK, Professeur à l'Université de Stuttgart. Le conférencier reprend la notion des angles et des équations d'Euler, l'ellipsoïde de Poinsot, la linéarisation dans le cas des petites déviations. Il décrit l'influence des couples perturbateurs et introduit enfin les équations du mouvement d'un satellite non rigide. Cette dernière partie est reprise en détails par MM. Likins et Willems.

D'un côté, le Professeur Pieter W. LIKINS, de l'Université de Californie, étudie l'influence de la non rigidité d'un engin. Reprenant l'historique de quelques échecs partiels, il attribue des cas d'anomalies de stabilité à une flexibilité dont l'effet s'est manifesté sous forme d'énergie dissipée ou de déformations préjudiciables. Le Professeur P. LIKINS expose l'état de nos connaissances actuelles; il insiste sur le fait que les problèmes soulevés ne relèvent pas d'un pur académisme, mais qu'ils doivent, au contraire, être résolus pour les satellites de grandes dimensions du futur.

Le Professeur P. WILLEMS, de l'Université de Louvain, étudie le problème des satellites à double rotation dans le cas d'une trajectoire en espace libre et dans le cas d'une orbite circulaire autour de la terre; il recherche les positions d'équilibre et de stabilité. Il expose le cas où la jonction entre les deux parties en mouvement est flexible et esquisse un traitement rigoureux de ce problème.

Monsieur W.G. HUGHES de la Royal Aircraft Establishment (R.A.E.) étudie la boucle complète d'asservissement d'un satellite actif. Il décrit rapidement les différents types de moteurs couples employés. Il met en équations un système présentant trois roues d'inertie et donne les conditions qui assurent un intercouplage faible entre axes. Il étudie en détails le cas d'un seul axe, la commande par roue d'inertie en y incluant les méthodes de désaturation, la commande par gyroscope (control moment gyro) et celle par expulsion de gaz. Dans ce dernier cas, l'emploi d'un modèle dynamique de l'engin dans la boucle de contrôle permet d'engendrer des ordres plus appropriés. Il étudie enfin le moyen d'obtenir une référence inertielle pour un engin pointant vers la terre.

Les conférences suivantes ont un but d'ordre plus technologique, ce qui ne diminue en rien leur intérêt, d'autant plus que chacun des problèmes est traité par un spécialiste ayant eu une part très active dans le projet décrit.

Monsieur T.I. HUBER de la "Stabilization and Control Branch" à la NASA a travaillé de nombreuses années sur les problèmes associés au contrôle d'attitude des satellites OAO. Il est d'ailleurs l'ingénieur responsable de ces sous-systèmes. Prenant précisément comme exemple l'OAO (Observatoire Astronomique en Orbite), il décrit les différents senseurs qui permettent finalement de pointer une masse de 4.500 lbs dans toutes les directions du ciel avec une précision meilleure que la minute d'arc. Les senseurs décrits caractérisent l'état de la technique actuelle : senseurs solaires grossiers - senseurs solaires précis - senseurs digitaux - référence inertielle fournissant les informations d'angle et de variation d'angle - systèmes de poursuite d'étoiles - enfin, un magnétomètre de haute précision.

Monsieur Philippe HUGUIER, ingénieur au Centre National des Etudes Spatiales (CNES) décrit les satellites PEOLE et EOLE dont la stabilisation selon deux axes est obtenue au moyen du gradient de gravité; il explique en détails la procédure d'acquisition et notamment le retournement d'un demi-tour du satellite PEOLE lancé en décembre 1970 à partir de la base française de KOUROU, le mât de stabilisation devant être dirigé finalement vers la géocentrique ascendante.

Monsieur W. INDEN, ingénieur de ERNO Raumfahrttechnik Gmbh, étudie en détails le système de propulsion par gaz froid du satellite européen TD. Il insiste tout spécialement sur les méthodes de fabrication et de qualification.

La boucle de commande d'attitude du satellite SIRIO est exposée par Monsieur A. BURATTI, ingénieur de la Compagnia Industriale Aerospaziale (C.I.A.); il décrit les senseurs et les actionneurs de ce vaisseau spatial et explique les manoeuvres à opérer tant en phase de transfert qu'en phase finale. Monsieur BURATTI insiste surtout sur la mesure d'attitude par divers senseurs terrestres et solaires. Il décrit les essais au sol en indiquant notamment les difficultés rencontrées dans une simulation acceptable des conditions spatiales.

Enfin, le Dr R.H. BATTIN, Directeur associé du Charles Stark Draper Labs., nous fournit des détails sur les commandes d'attitude des vols APOLLO au cours de ses phases multiples, c'est-à-dire tant en vol libre, en vol propulsé que pour le retour dans l'atmosphère, ce qui termine cette série de communications par la description d'une des plus brillantes réalisations de la technique moderne.

ROTATIONAL DYNAMICS

by

Martin A. Frik
Associate Professor
Institut A für Mechanik
Universität Stuttgart
7 Stuttgart 1
Keplerstr. 17
Germany

SUMMARY

This paper is concerned with the fundamentals of the rotational dynamics of satellites. After a short introduction into basic geometric and kinematic relations, the Euler equations describing the rotational motion of rigid bodies are derived. The torque free motion of dynamically symmetrical as well as unsymmetrical satellites is investigated, including a stability analysis of permanent rotations about axes of principal moments of inertia. External torques, such as gravity-gradient, magnetic, aerodynamic, and solar radiation torques, which are caused by the interaction of an orbiting satellite with its environment, are discussed. Finally, for some types of non-rigid satellites the equations of motion are considered.

1. INTRODUCTION

One of the most important problems in space technology is the attitude stabilization of satellites. In order to fulfill its mission requirements the satellite must be able to assume and maintain a specified orientation, e.g. with respect to the earth (weather and communication satellites), the sun (solar observatory), or some other reference. The problems associated with the attitude stabilization always require a detailed analysis of the rotational motion of the satellite.

For satellites moving in the gravitational field the rotational and the orbital (translational) motions are coupled. Considering the orbital motion, this coupling is very weak and may usually be neglected. The rotational motion, however, is always considerably influenced by the orbital motion. Since in this paper we are concerned with the rotational motion only, the orbital motion is supposed to be given.

2. COORDINATE SYSTEMS

In order to describe the rotational motion of a satellite, in general three orthogonal, right-handed coordinate systems are used:

1) A body-fixed coordinate system,
2) a reference coordinate system,
3) an inertial coordinate system.

The proper choice of these systems depends upon the particular problem under consideration.

The body-fixed system is assumed to be fixed to the main structure of the satellite. For rigid satellites usually the system of principal axes of inertia is selected, the origin O of which is the satellite's center of mass.

The origin of the reference system be coincident with the origin of the body-fixed system. The reference system is usually chosen so as to characterize the desired attitude of the satellite. Therefore, in order to choose the reference system properly, the knowledge of the satellite's mission is necessary. If, for instance, the satellite is to be oriented with respect to the earth, the earth-pointing reference system (Fig. 1) is appropriate: the x_3-axis points towards the center of the earth and the x_2-axis is perpendicular to the orbital plane and has the opposite direction of the orbital angular velocity $\underline{\Omega}$. The x_1, x_2, x_3 axes are called roll, pitch, and yaw axes, respectively.

Inertial coordinate systems may be defined by elements which are directionally fixed in space, e.g. the ecliptic or the equator.

The orientation of the reference system in inertial space may be assumed to be known as a function of time, since the satellite's orbital motion is supposed to be given. Thus the attitude of the satellite is determined by the orientation of the body-fixed system with respect to the reference system.

The orientation of one coordinate system relative to another one may be described in different ways, e.g. by Euler angles, direction cosines, or quaternion parameters |1|. In this paper Euler angles will be used exclusively; they represent

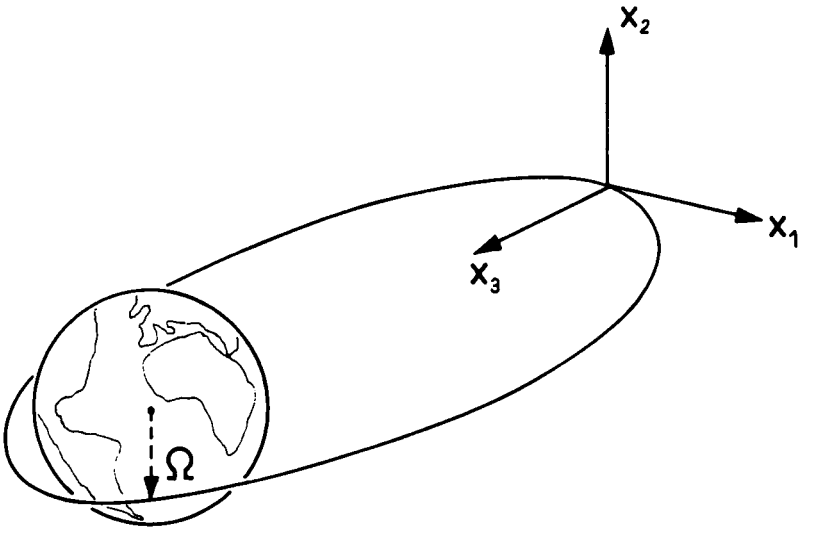

Figure 1. Earth-pointing coordinate system

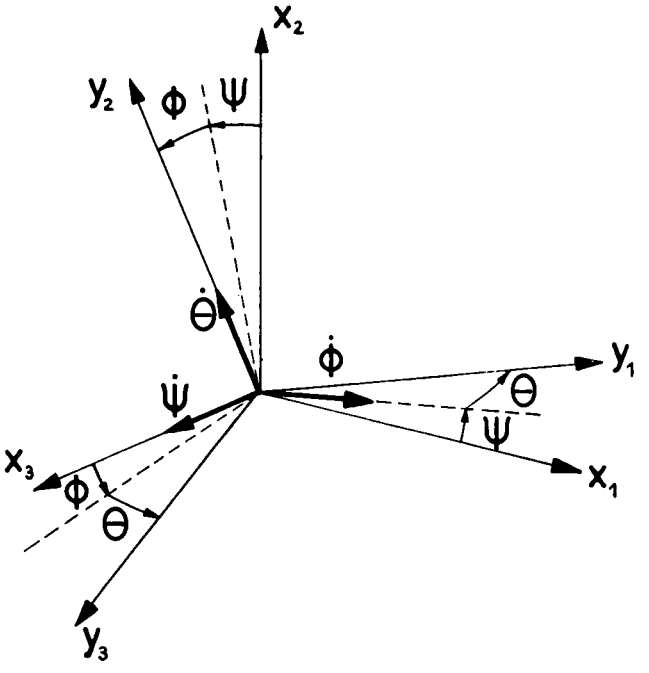

Figure 2. Euler angles

a set of three generalized coordinates according to the three rotational degrees of freedom. It should be mentioned, however, that for particular orientations of the systems (e.g. $\phi=90^{\circ}$) singularities may occur, which could be avoided using direction cosines or quaternion parameters.

In Fig. 2 the Euler angles Ψ,ϕ,θ are used to describe the orientation of the body-fixed y-system relative to the reference x-system. They define a sequence of three finite positive rotations as follows:

1) rotation by the angle Ψ about the x_3-axis,
2) rotation by the angle ϕ about the new 1-axis,
3) rotation by the angle θ about the y_2-axis.

There is no unanimity in literature on the sequence of the three rotations and, consequently, on the definitions of the Euler angles. The definition given above is only one of several possibilities.

Finite rotations can be represented by matrices, relating the components of a fixed vector in the original system to its components in the rotated system. If (ξ_1, ξ_2, ξ_3) and (η_1, η_2, η_3) denote the components in the original and the rotated system, respectively, and if α_i $(i=1,2,3)$ is a positive rotation about the ξ_i-axis, these matrix representations are

axis of rotation		matrix representation
ξ_1	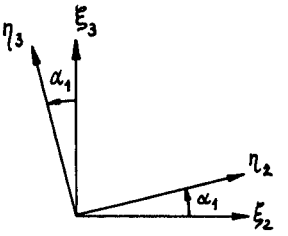	$\begin{bmatrix}\eta_1\\ \eta_2\\ \eta_3\end{bmatrix} = \begin{bmatrix}1 & 0 & 0\\ 0 & c\alpha_1 & s\alpha_1\\ 0 & -s\alpha_1 & c\alpha_1\end{bmatrix} \cdot \begin{bmatrix}\xi_1\\ \xi_2\\ \xi_3\end{bmatrix}$
ξ_2	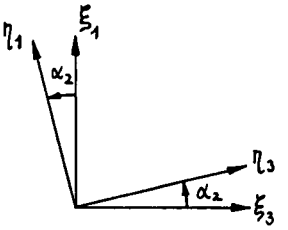	$\begin{bmatrix}\eta_1\\ \eta_2\\ \eta_3\end{bmatrix} = \begin{bmatrix}c\alpha_2 & 0 & -s\alpha_2\\ 0 & 1 & 0\\ s\alpha_2 & 0 & c\alpha_2\end{bmatrix} \cdot \begin{bmatrix}\xi_1\\ \xi_2\\ \xi_3\end{bmatrix}$
ξ_3	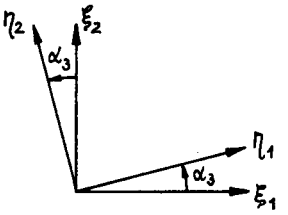	$\begin{bmatrix}\eta_1\\ \eta_2\\ \eta_3\end{bmatrix} = \begin{bmatrix}c\alpha_3 & s\alpha_3 & 0\\ -s\alpha_3 & c\alpha_3 & 0\\ 0 & 0 & 1\end{bmatrix} \cdot \begin{bmatrix}\xi_1\\ \xi_2\\ \xi_3\end{bmatrix}$

with $c\alpha_1 \equiv \cos\alpha_1$, $s\alpha_1 \equiv \sin\alpha_1$, etc.

To represent an arbitrary sequence of finite axis rotations these matrices must be multiplied in the corresponding sequence. Consequently, the rotation matrix T_{yx} between the x- and y-systems pictured in Fig. 2 is:

$$T_{yx} = \begin{bmatrix}c\theta & 0 & -s\theta\\ 0 & 1 & 0\\ s\theta & 0 & c\theta\end{bmatrix} \cdot \begin{bmatrix}1 & 0 & 0\\ 0 & c\phi & s\phi\\ 0 & -s\phi & c\phi\end{bmatrix} \cdot \begin{bmatrix}c\psi & s\psi & 0\\ -s\psi & c\psi & 0\\ 0 & 0 & 1\end{bmatrix}$$

or

$$T_{yx} = \begin{bmatrix}c\psi c\theta - s\phi s\psi s\theta & s\psi c\theta + s\theta c\psi s\phi & -s\theta c\phi\\ -s\psi c\phi & c\phi c\psi & s\phi\\ s\theta c\psi + c\theta s\phi s\psi & s\theta s\psi - c\theta c\psi s\phi & c\phi c\theta\end{bmatrix} . \qquad (1)$$

The components of a vector in the body-fixed y-system are related to the components in the reference x-system by

$$\begin{bmatrix}y_1\\ y_2\\ y_3\end{bmatrix} = T_{yx} \begin{bmatrix}x_1\\ x_2\\ x_3\end{bmatrix} \quad ; \quad \begin{bmatrix}x_1\\ x_2\\ x_3\end{bmatrix} = T'_{yx} \begin{bmatrix}y_1\\ y_2\\ y_3\end{bmatrix} . \qquad (2)$$

The transposed matrix T'_{yx} is equal to the inverse matrix

$$T'_{yx} = T_{yx}^{-1}$$

because T_{yx} represents an orthonormal transformation.

It should be emphasized that a change in the sequence of the rotations will in general result in a different rotation matrix. However, if the angles are small, i.e. if the elements of T_{yx} may be linearized, the sequence of the rotations is without influence. The linearized matrix T_{yx} is

$$T_{yx} = \begin{bmatrix} 1 & \Psi & -\Theta \\ -\Psi & 1 & \Phi \\ \Theta & -\Phi & 1 \end{bmatrix} \tag{3}$$

3. ANGULAR VELOCITIES

The angular velocity $\underline{\omega}$ of the body is composed of its angular velocity relative to the reference system and the angular velocity $\underline{\omega}_R$ of the reference system itself

$$\underline{\omega} = \dot{\underline{\Psi}} + \dot{\underline{\Phi}} + \dot{\underline{\Theta}} + \underline{\omega}_R \ . \tag{4}$$

Regarding Fig. 2 and the previously given transformation relations, $\underline{\omega}$ described by its components in the body-fixed y-system is

$$\underline{\omega}_y = T_{yx} \begin{bmatrix} 0 \\ 0 \\ \dot{\Psi} \end{bmatrix} + \begin{bmatrix} c\Theta & 0 & -s\Theta \\ 0 & 1 & 0 \\ s\Theta & 0 & c\Theta \end{bmatrix} \begin{bmatrix} \dot{\Phi} \\ 0 \\ 0 \end{bmatrix} + \begin{bmatrix} 0 \\ \dot{\Theta} \\ 0 \end{bmatrix} + \underline{\omega}_{Ry} \ . \tag{5}$$

The components of $\underline{\omega}_y$ are

$$\begin{aligned} \omega_{y1} &= -\dot{\Psi}s\Theta c\Phi + \dot{\Phi}c\Theta + \omega_{Ry1} \\ \omega_{y2} &= \dot{\Psi}s\Phi + \dot{\Theta} + \omega_{Ry2} \\ \omega_{y3} &= \dot{\Psi}c\Phi c\Theta + \dot{\Phi}s\Theta + \omega_{Ry3} \ . \end{aligned} \tag{6}$$

If the reference system is chosen to be the earth pointing system shown in Fig. 1, $\underline{\omega}_{Ry}$ becomes

$$\underline{\omega}_{Ry} = T_{yx} \begin{bmatrix} 0 \\ -\Omega \\ 0 \end{bmatrix} \tag{7}$$

and consequently

$$\begin{aligned} \omega_{y1} &= -\dot{\Psi}s\Theta c\Phi + \dot{\Phi}c\Theta - \Omega(s\Psi c\Theta + s\Theta c\Psi s\Phi) \\ \omega_{y2} &= \dot{\Psi}s\Phi + \dot{\Theta} - \Omega c\Phi c\Psi \\ \omega_{y3} &= \dot{\Psi}c\Phi c\Theta + \dot{\Phi}s\Theta - \Omega(s\Theta s\Psi - c\Theta c\Psi s\Phi) \ . \end{aligned} \tag{8}$$

4. EQUATIONS OF MOTION OF RIGID BODIES

The rotational equations of motion are obtained regarding the law that the rate of change of the body's angular momentum $\underline{H}$ equals the total external torque $\underline{L}$ acting on the body

$$\dot{\underline{H}} = \underline{L} \ . \tag{9}$$

Equation (9) refers to an inertially fixed coordinate system (dot denotes here differentiation in the inertial frame). If $\underline{\omega}$ is the angular velocity of the body relative to the inertial frame, $\dot{\underline{H}}$ can be expressed by

$$\dot{\underline{H}} = \left[\frac{d\underline{H}}{dt}\right]_y + \underline{\omega} \times \underline{H} \tag{10}$$

where $(d\underline{H}/dt)_y$ is the time derivative of $\underline{H}$ relative to the body-fixed y-system. The equation of motion referring to the y-system then becomes

$$\left[\frac{d\underline{H}}{dt}\right]_y + \underline{\omega} \times \underline{H} = \underline{L}_y \ . \tag{11}$$

The angular momentum of a rigid body with respect to its center of mass is

$$\underline{H} = J\underline{\omega} \tag{12}$$

with J being the inertia tensor

$$J = \begin{bmatrix} J_{11} & J_{12} & J_{13} \\ J_{21} & J_{22} & J_{23} \\ J_{31} & J_{32} & J_{33} \end{bmatrix} \tag{13}$$

where

$$J_{11} = \int (y_2^2 + y_3^2)dm \; ; \quad J_{22} = \int (y_1^2 + y_3^2)dm \; ; \quad J_{33} = \int (y_1^2 + y_2^2)dm$$

$$J_{12} = J_{21} = -\int y_1 y_2 dm \; ; \quad J_{13} = J_{31} = -\int y_1 y_3 dm \; ; \tag{14}$$

$$J_{23} = J_{32} = -\int y_2 y_3 dm \; .$$

The integrations must be performed over all mass elements of the body.

The diagonal terms in (13) are the moments of inertia, the off-diagonal terms are the moments of deviation (or products of inertia) of the body.

From the theory of second rank tensors it is well known that the y-system can always be chosen so that the moments of deviation become zero, in which case the inertia tensor is a diagonal tensor

$$J = \begin{bmatrix} J_1 & 0 & 0 \\ 0 & J_2 & 0 \\ 0 & 0 & J_3 \end{bmatrix} \; . \tag{15}$$

Then the y-axes are the principal axes of inertia and J_1, J_2, J_3 are the principal moments of inertia.

Inserting (15) into (12) the equations of motion (11) can be expressed in the form

$$\begin{aligned} J_1 \dot{\omega}_{y1} + (J_3 - J_2)\omega_{y2}\omega_{y3} &= L_{y1} \\ J_2 \dot{\omega}_{y2} + (J_1 - J_3)\omega_{y3}\omega_{y1} &= L_{y2} \\ J_3 \dot{\omega}_{y3} + (J_2 - J_1)\omega_{y1}\omega_{y2} &= L_{y3} \end{aligned} \tag{16}$$

where ω_{yi} and L_{yi} $(i = 1,2,3)$ are the components of $\underline{\omega}$ and $\underline{L}$ in the y-system. Equations (16) are called the Euler equations for the rotational motion of a rigid body.

If the external torques L_{y1}, L_{y2}, L_{y3} acting on the satellite are known, Equations (16) and (6) form a set of 6 nonlinear differential equations which must be integrated simultaneously in order to obtain the 6 unknown variables ω_{y1}, ω_{y2}, ω_{y3}, Ψ, Φ, Θ as functions of time. The solution of these equations can be given in closed form only in very few cases.

4.1 Linearized equations of motion

The Euler equations (16) and the kinematic relations (6) and (8) can be considerably simplified if the deviations of the body-fixed y-system with respect to the reference x-system are supposed to be small. Since the reference system is usually chosen so as to coincide with the body system in the satellite's desired orientation, the assumption of small angles Ψ, Φ, Θ means a small deviation from the perfect orientation. This assumption is frequently valid, especially in case of actively controlled satellites.

Assuming the Euler angles and their time derivatives to be quantities which are small of first order, and neglecting all small terms of second and higher order, Equations (6) become

$$\begin{aligned} \omega_{y1} &= \dot{\Phi} + \omega_{Ry1} \\ \omega_{y2} &= \dot{\Theta} + \omega_{Ry2} \\ \omega_{y3} &= \dot{\Psi} + \omega_{Ry3} \; . \end{aligned} \tag{17}$$

If the reference system is the earth-pointing system (Fig. 1), the linearized components of the angular velocity (8) are

$$\begin{aligned} \omega_{y1} &= \dot{\Phi} - \Omega\Psi \\ \omega_{y2} &= \dot{\Theta} - \Omega \\ \omega_{y3} &= \dot{\Psi} + \Omega\Phi \; . \end{aligned} \tag{18}$$

In this case the linearized Euler equations become

$$\begin{aligned} J_1\ddot{\phi} - (J_1 - J_2 + J_3)\Omega\dot{\Psi} + (J_2 - J_3)\Omega^2\phi - J_1\dot{\Omega}\Psi &= L_{y1} \\ J_2\ddot{\theta} - J_2\dot{\Omega} &= L_{y2} \\ J_3\ddot{\Psi} + (J_1 - J_2 + J_3)\Omega\dot{\phi} - (J_1 - J_2)\Omega^2\Psi + J_3\dot{\Omega}\phi &= L_{y3} \end{aligned} \tag{19}$$

where the torques L_{y1}, L_{y2}, L_{y3} are assumed to be linearized also.

If the external torques and the orbital angular velocity Ω are known, the Euler angles ϕ, θ, Ψ can be determined from (19) as functions of time. Equations (19) show that the pitch-motion θ is uncoupled from the roll- and yaw-motions, provided L_{y2} is independent of ϕ and Ψ. This is e.g. the case, if gravitational torques are the only regarded external torques.

If the satellite is in a circular orbit, the orbital angular velocity Ω is constant and we get the equations

$$\begin{aligned} J_1\ddot{\phi} - (J_1 - J_2 + J_3)\Omega\dot{\Psi} + (J_2 - J_3)\Omega^2\phi &= L_{y1} \\ J_2\ddot{\theta} &= L_{y2} \\ J_3\ddot{\Psi} + (J_1 - J_2 + J_3)\Omega\dot{\phi} - (J_1 - J_2)\Omega^2\Psi &= L_{y3} \quad . \end{aligned} \tag{20}$$

Equations (20) can be used also to investigate the dynamic behavior of spin-stabilized satellites, if Ω is interpreted as the desired constant spin rate of the satellite.

In order to obtain the linearized rotational equations of a satellite which is to be stabilized with respect to an inertial reference frame, we must set Ω equal to zero and obtain

$$\begin{aligned} J_1\ddot{\phi} &= L_{y1} \\ J_2\ddot{\theta} &= L_{y2} \\ J_3\ddot{\Psi} &= L_{y3} \quad . \end{aligned} \tag{21}$$

4.2 Free motion of a rigid body

The equations of the torque free motion of a rigid body are obtained setting the right hand sides of the Euler equations (16) equal to zero

$$\begin{aligned} J_1\dot{\omega}_{y1} + (J_3 - J_2)\omega_{y2}\omega_{y3} &= 0 \\ J_2\dot{\omega}_{y2} + (J_1 - J_3)\omega_{y3}\omega_{y1} &= 0 \\ J_3\dot{\omega}_{y3} + (J_2 - J_1)\omega_{y1}\omega_{y2} &= 0 \quad . \end{aligned} \tag{22}$$

Two integrals of motion can easily be determined: Multiplication of the three Equations (22) by ω_{y1}, ω_{y2}, and ω_{y3}, respectively, and subsequent addition yields that the rotational kinetic energy

$$T = \tfrac{1}{2}\left[J_1\omega_{y1}^2 + J_2\omega_{y2}^2 + J_3\omega_{y3}^2\right] \tag{23}$$

remains constant.

The second integral of motion is obtained in a similar way multiplying the three Equations (22) by $J_1\omega_{y1}$, $J_2\omega_{y2}$, and $J_3\omega_{y3}$, respectively, and adding them up. Then we get

$$H^2 = J_1^2\omega_{y1}^2 + J_2^2\omega_{y2}^2 + J_3^2\omega_{y3}^2 = \text{const} \quad , \tag{24}$$

which confirms the fact that without external torques the angular momentum

$$\underline{H} = \begin{bmatrix} J_1\omega_{y1} \\ J_2\omega_{y2} \\ J_3\omega_{y3} \end{bmatrix} \tag{25}$$

is constant.

Using the two integrals of motion (23) and (24) and Equations (22), the angular velocities ω_{y1}, ω_{y2}, ω_{y3} can be obtained as functions of time in terms of elliptic integrals [2]. The torque free motion of an unsymmetrical rigid body may be visualized by Poinsot's geometrical solution:

From (25) and (23) follows

$$\underline{H} \cdot \underline{\omega} = 2T \tag{26}$$

which shows that with $\underline{H}$ and T being constant, the locus of the end of the vector $\underline{\omega}$ is in a plane perpendicular to $\underline{H}$, known as the invariable plane.

If Equation (23) is written in the form

$$\frac{\omega_{y_1}^2}{2T/J_1} + \frac{\omega_{y_2}^2}{2T/J_2} + \frac{\omega_{y_3}^2}{2T/J_3} = 1 \tag{27}$$

it follows that the locus of the end point of $\underline{\omega}$ is a body-fixed ellipsoid, called the Poinsot ellipsoid.

The motion of the body may now be visualized as the rolling of the Poinsot ellipsoid on the invariable plane (Fig. 3) with the distance OP between the center of the ellipsoid and the invariable plane being constant according to Equation (26)

$$OP = \frac{2T}{H} . \tag{28}$$

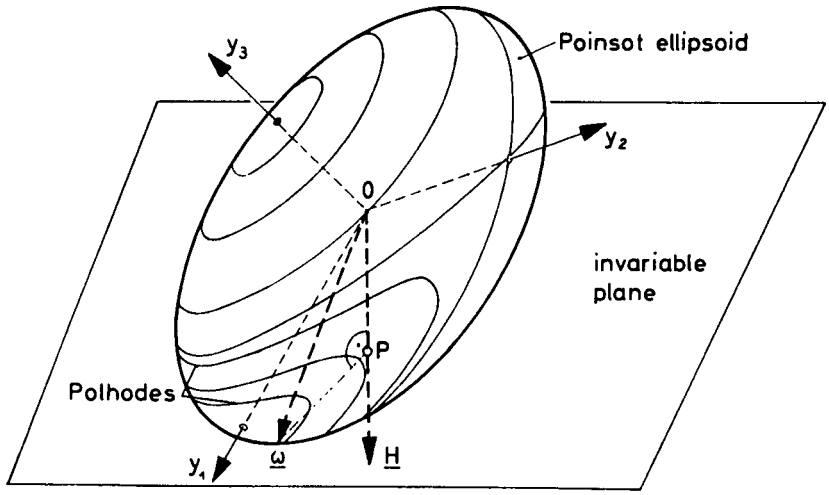

Figure 3. Free motion of an unsymmetrical rigid body, $J_1 < J_2 < J_3$

The curve formed on the Poinsot ellipsoid by the end of the vector $\underline{\omega}$ during the motion is called polhode, and the corresponding curve on the invariable plane herpolhode. The polhodes are closed curves, indicated in Fig. 3 for a body with $J_1<J_2<J_3$. The herpolhodes are in general not closed.

The torque free motions of a rigid body as described above, are known as nutations.

4.3 Stability of rotations about principal axes

It can be easily verified that Equations (22) have the solutions

$$\begin{aligned} &a)\ \omega_{y1} = \omega_{y10} = \text{const}\ ,\quad \omega_{y2} = \omega_{y3} = 0\ ; \\ &b)\ \omega_{y2} = \omega_{y20} = \text{const}\ ,\quad \omega_{y1} = \omega_{y3} = 0\ ; \\ &c)\ \omega_{y3} = \omega_{y30} = \text{const}\ ,\quad \omega_{y1} = \omega_{y2} = 0\ . \end{aligned} \tag{29}$$

According to (29) the body can perform permanent rotations, i.e. rotations with constant angular velocity about each principal axis of inertia. For a body with three different principal axes these are the only possible permanent rotations, which follows from (22) setting $\omega_{yi} = \text{const}$ $(i = 1,2,3)$.

In order to investigate the stability of these rotations we assume small disturbances η_i of the angular velocities ω_{yi}

$$\omega_{y1} = \omega_{y10} + \eta_1$$
$$\omega_{y2} = \eta_2 \qquad (30)$$
$$\omega_{y3} = \eta_3 \ .$$

Inserting (30) into (22) and neglecting small quantities of second order, we get

$$J_1\dot{\eta}_1 = 0$$
$$J_2\dot{\eta}_2 + (J_1-J_3)\eta_3\omega_{y10} = 0 \qquad (31)$$
$$J_3\dot{\eta}_3 + (J_2-J_1)\eta_2\omega_{y10} = 0 \ .$$

The first of these equations gives $\eta_1 = \text{const}$. Consequently, the angular velocity about the y_1- axis is slightly disturbed but still constant. The other two Equations (31) have the characteristic equation

$$s^2J_2J_3 + (J_1-J_3)(J_1-J_2)\omega_{y10}^2 = 0 \qquad (32)$$

which shows that the rotation can be stable only for

$$(J_1-J_3)(J_1-J_2) > 0 \qquad (33)$$

i.e. if J_1 is either the smallest or the largest principal moment of inertia. The rotation about the axis of the intermediate principal moment of inertia is unstable. The stability of permanent rotations about the axes of the smallest and the largest moments of inertia may, strictly speaking, not be concluded from the linearized Equation (31), since in this case the roots of the characteristic equation have zero real parts. However, a rigorous stability investigation using Liapunov techniques gives the result that these rotations are indeed stable.

Remark: This result holds if the rotational energy of the body remains constant. However, in practice always some energy dissipation takes place due to the non-rigidity of the satellite. The energy dissipation (energy sink) causes the satellite to tend towards the minimum energy state. Since for a fixed angular momentum the rotations about the axis of the smallest (largest) moment of inertia correspond to a maximum (minimum) of the rotational energy, only rotations about the axis of the largest moment of inertia are stable.

4.4 Free motion of a symmetrical rigid body

Let us consider next the rotation of a rigid body with two equal principal moments of inertia

$$J_1 = J_2 \neq J_3 \ . \qquad (34)$$

Inserting (34) into (22) we get

$$J_1\dot{\omega}_{y1} + (J_3-J_1)\omega_{y2}\omega_{y3} = 0$$
$$J_1\dot{\omega}_{y2} + (J_1-J_3)\omega_{y3}\omega_{y1} = 0 \qquad (35)$$
$$J_3\dot{\omega}_{y3} = 0 \ .$$

With

$$\omega_{y3} = \omega_{y30} = \text{const} \qquad (36)$$

resulting from the third equation of (35), the first and second equations can be written as

$$\dot{\omega}_{y1} + \nu\omega_{y2} = 0$$
$$\dot{\omega}_{y2} - \nu\omega_{y1} = 0 \qquad (37)$$

where

$$\nu = \frac{J_3-J_1}{J_1}\omega_{y30} \ . \qquad (38)$$

The solution of (37) is

$$\omega_{y1} = N\cos(\nu t+\alpha)$$
$$\omega_{y2} = N\sin(\nu t+\alpha) \qquad (39)$$

where N and ν are amplitude and frequency, respectively, of the nutations.

From (36) and (39) follows that the angular velocity has constant magnitude

$$|\underline{\omega}| = \sqrt{N^2 + \omega_{y30}^2} = \text{const} .$$

The angular momentum vector, which is a constant vector in inertial space, is expressed by its components in the y-system as

$$\underline{H} = \begin{bmatrix} J_1 N\cos(\nu t+\alpha) \\ J_1 N\sin(\nu t+\alpha) \\ J_3\omega_{y30} \end{bmatrix} . \qquad (40)$$

From (40) it can be easily seen that the projection of $\underline{H}$ into the y_1, y_2 plane is parallel to the corresponding projection of $\underline{\omega}$. Hence $\underline{\omega}$, $\underline{H}$, and the y_3-axis are in one plane. Consequently, the plane containing the y_3-axis and $\underline{\omega}$ rotates about the fixed angular momentum vector $\underline{H}$ (Fig. 4a).

The angles δ and γ between the y_3-axis and the vectors $\underline{H}$ and $\underline{\omega}$, respectively, are constant and related by

$$\tan\delta = \frac{J_1}{J_3}\tan\gamma . \qquad (41)$$

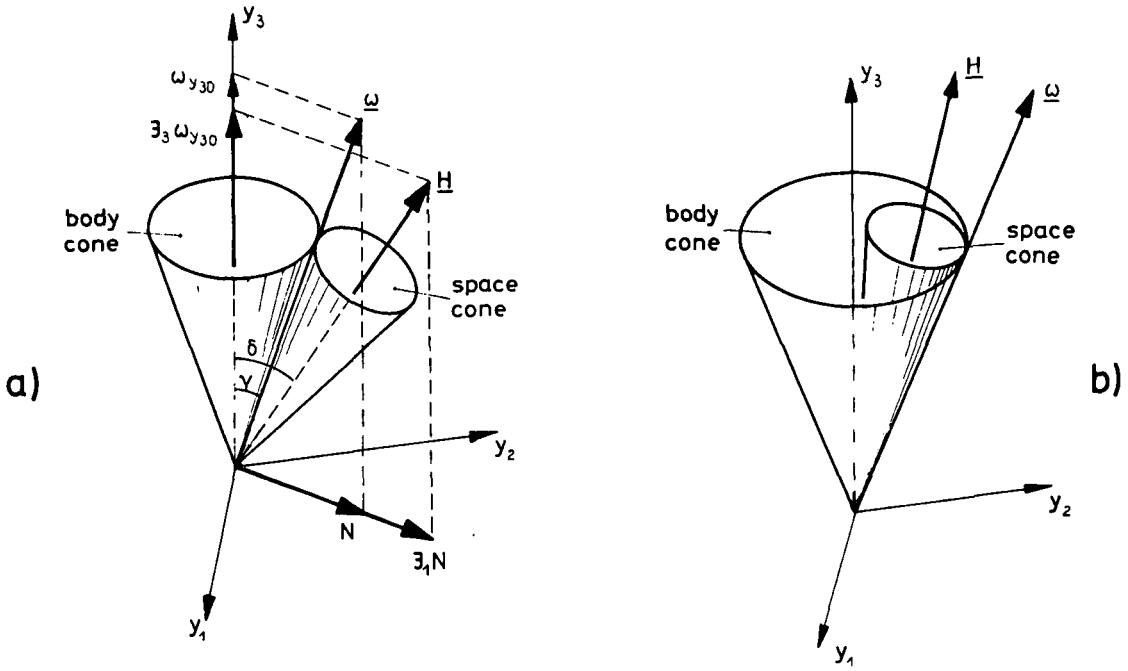

Figure 4. Free motion of a symmetrical rigid body
a) $J_1 = J_2 > J_3$ b) $J_1 = J_2 < J_3$

The vector $\underline{\omega}$ rotating about $\underline{H}$ describes a cone fixed in space, which is called the space cone. Since in the y-system, $\underline{\omega}$ rotates about the y_3-axis, it describes another cone, the body-cone. The motion of the body can now be visualized by a rolling motion of the body cone on the space cone. According to (41) for $J_1>J_3$ the space cone is outside the body cone (Fig. 4a), whereas for $J_3>J_1$ the space cone is inside the body cone (Fig. 4b).

It should be emphasized that Equations (36) and (39) refer to body-fixed axes. In order to obtain the rotational motion with respect to an inertial frame in terms of Euler angles, Equations (36) and (39) must be inserted into (6) setting $\omega_{Ryi\equiv 0}$.

5. EXTERNAL TORQUES

The rotational motion of an orbiting satellite is influenced by various external torques which are caused by the interaction of the satellite with its environment. The most important components of this environment are the gravitational field, the geomagnetic field, the remaining atmosphere, and the solar radiation field.

5.1 Gravity-gradient torque

Let us consider a rigid body in the earth's gravitational field which is approximated by an inverse square field. Then the gravitational force acting on a mass element dm of the body is

$$d\underline{F}_G = -\frac{\Gamma m_E}{r^3}\,\underline{r}\,dm \tag{42}$$

with Γ denoting the gravitational constant, m_E the mass of the earth, and $\underline{r}$ the radius vector from the center of the earth (Fig. 5). The torque applied by the gravitational force with respect to the satellite's center of mass 0 is

$$\underline{L}_G = \int_{(m)} \underline{s}\times d\underline{F}_G \ . \tag{43}$$

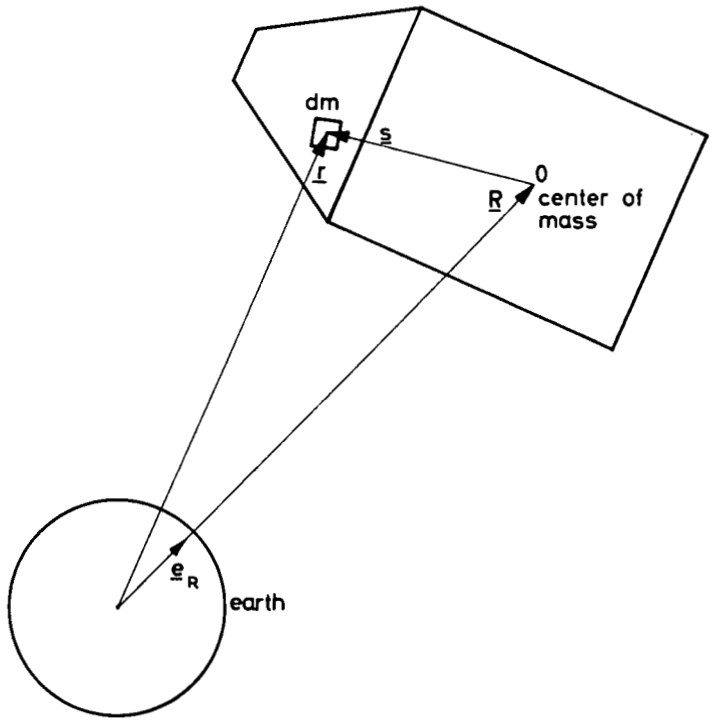

Figure 5. Satellite in the gravitational field

By a power series expansion we obtain with $\underline{r} = \underline{R} + \underline{s}$

$$\frac{1}{r^3} = \frac{1}{|\underline{R}+\underline{s}|^3} = \frac{1}{R^3}\left(1 - 3\,\frac{\underline{s}\,\underline{R}}{R^2} + \ldots\right). \tag{44}$$

Since the dimensions of the satellite are very small compared with its distance from the center of the earth, quadratic and higher order terms in $\left(\frac{s}{R}\right)$ have been neglected in Equation (44). Inserting (44) and (42) into (43) and regarding $\int_{(m)} \underline{s}\,dm = 0$ we get after some simple vector manipulations

$$\underline{L}_G = -\frac{3\Gamma m_E}{R^3}\,\underline{e}_R\times\int_{(m)}(\underline{s}\underline{s}')dm\,\underline{e}_R \tag{45}$$

where $(\underline{s}\underline{s}')$ is a dyadic product and $\underline{e}_R = \frac{\underline{R}}{R}$ denotes the unit vector in the local vertical. If the identically zero term

$$\frac{3\Gamma m_E}{R^3}\,\underline{e}_R\times\int_{(m)} s^2 E\,dm\,\underline{e}_R \equiv 0$$

with E being the unit matrix, is added to Equation (45), we obtain the gravity-gradient torque

$$\underline{L}_G = \frac{3\Gamma m_E}{R^3}\,\underline{e}_R\times J\underline{e}_R \ . \tag{46}$$

In Equation (46) $J = \int(s^2E - \underline{s}\underline{s}')dm$ is the moment of inertia tensor (13). In the principal axes system J is the diagonal tensor (15).

We now want to determine the components of the gravity-gradient torque in the body axes. If the reference x-system is the orbital system (Fig. 1), then $\underline{e}_R$ points

along the negative x_3-axis. Using the transformation matrix (1) we get

$$(\underline{e}_R)_y = \begin{bmatrix} s\theta c\phi \\ -s\phi \\ -c\phi c\theta \end{bmatrix} . \tag{47}$$

Inserting (47) into (46), the components of the gravitational torque in the principal y-axes are obtained

$$\begin{aligned} L_{Gy_1} &= \tfrac{3}{2} \frac{\Gamma m_E}{R^3} (J_3 - J_2)\, c\theta s2\phi \\ L_{Gy_2} &= \tfrac{3}{2} \frac{\Gamma m_E}{R^3} (J_3 - J_1)\, c^2\phi s2\theta \\ L_{Gy_3} &= \tfrac{3}{2} \frac{\Gamma m_E}{R^3} (J_1 - J_2)\, s\theta s2\phi \end{aligned} \tag{48}$$

From (48) follows that the gravity-gradient torque is identically zero for a spherical body. It also vanishes for an unsymmetrical satellite if $\phi = \theta = 0$.

Inserting (48) into (16) the equations describing the rotational motion of a rigid body in an inverse square gravitational field are obtained. If the body moves in a circular orbit the term $\frac{\Gamma m_E}{R^3}$ may be replaced by Ω^2 , where Ω is the constant orbital angular velocity.

5.2 Aerodynamic torque

The aerodynamic torque depends upon the shape of the satellite, its orientation and velocity relative to the atmosphere, the atmospheric density, and the flow mechanics in the upper atmosphere. At altitudes of low orbiting satellites where the influence of the remaining atmosphere must be regarded, a free molecule flow may be assumed, i.e. the mean free path of the molecules is large compared with a characteristic length of the satellite. Then the incident stream of molecules is practically undisturbed by the presence of the satellite and the effect of the incident and the reflected flows may be calculated separately. The interaction of the molecular flux with a surface element is expressed in terms of coefficients which characterize the accomodation of the incident flow to the surface conditions as well as the nature of the reflected stream. For a detailed discussion of the interaction of a free molecule flow with a surface element see Reference |3|. For a given interaction model the pressure $\underline{p}$ and shear stress $\underline{\tau}$ acting upon a surface element dA can be computed. The resulting aerodynamic torque $\underline{L}_A$ relative to the satellite's center of mass is obtained by integration over the satellite's surface A

$$\underline{L}_A = \int_{(A)} \underline{s} \times (\underline{p} + \underline{\tau})\, dA \tag{49}$$

where $\underline{s}$ denotes the radius vector from the center of mass to the surface element.

The aerodynamic torque is usually expressed in terms of three dimensionless torque coefficients c_{Li} $(i = 1,2,3)$

$$\underline{L}_A = \tfrac{1}{2}\rho u^2 A_R \ell_R \begin{bmatrix} c_{L_1} \\ c_{L_2} \\ c_{L_3} \end{bmatrix} \tag{50}$$

where ρ is the atmospheric density, u the velocity of the satellite's center of mass relative to the atmosphere, and A_R and ℓ_R are reference area and length, respectively. The coefficients c_{Li} $(i = 1,2,3)$ are usually computed with respect to a body-fixed geometric coordinate system. These coefficients depend upon the orientation of the geometric system relative to the flow vector, which can be described by two angles. Obviously, c_{Li} $(i = 1,2,3)$ are periodic functions of these two angles and may be approximated by a finite number of terms of a double Fourier series |4|.

It may be mentioned that the satellite's rotational motion relative to the atmosphere produces a damping torque which depends linearly upon the relative angular velocity. However, this torque is very small and may usually be neglected.

5.3 Magnetic torque

The interaction of the earth's magnetic field with the magnetic moment of the satellite produces a torque $\underline{L}_M$ which is described by

$$\underline{L}_M = \underline{M} \times \underline{B} \tag{51}$$

where $\underline{M}$ is the magnetic moment of the satellite and $\underline{B}$ the intensity of the geomagnetic field. There are several factors contributing to the magnetic moment $\underline{M}$, such as permanent magnets and electric current carrying devices in the payload, magnetization of the satellite's hull in the geomagnetic field, and eddy currents which are induced when the satellite rotates in the geomagnetic field. An extensive discussion of these factors can be found for instance in Reference |5|.

In a first approximation the geomagnetic field can be considered as being a magnetic dipole at the earth's center with the dipole axis inclined by about 17° to the earth's axis. The potential function of the dipole is

$$V = - \frac{M_E \sin\beta}{R^2} \tag{52}$$

where M_E is the strength of the dipole, R the distance from the dipole, and β the latitudinal position relative to the magnetic equator. The strength of the magnetic field is

$$\underline{B} = - \operatorname{grad} V = - \frac{M_E}{R^3} \left(2\sin\beta \underline{e}_R - \cos\beta \underline{e}_\beta \right) \tag{53}$$

with $\underline{e}_R$ and $\underline{e}_\beta$ being unit vectors along $\underline{R}$ and normal to $\underline{R}$ in latitudinal direction, respectively. In Equation (53) $\underline{B}$ is given in geomagnetic coordinates. In order to calculate the influence of the magnetic torque on the rotational motion of the satellite using the Euler equations (16), the magnetic torque must be given in body-fixed axes. The transformation matrix relating the components of $\underline{B}$ in the geomagnetic system to those in the body-fixed system has been derived in Reference |6|. The elements of this matrix are in general rather complicated functions of time.

5.4 Solar radiation torque

Solar radiation hitting a surface element of a satellite imposes a pressure $\underline{p}$ and shear stress $\underline{\tau}$ which may be expressed in terms of coefficients characterizing the percentage of absorbed radiation, and the percentages of radiation reflected diffusely and specularly, respectively |7|. The resulting solar radiation torque affecting the satellite can be calculated and expressed in analogy to the aerodynamic torque (5.2).

The magnitude of the various external torques depends upon the satellite's shape, its mass distribution, its magnetic moment, the reflection properties of its surface, its distance from the earth, upon daytime, orbit, etc. Therefore, a quantitative comparison of the external torques is possible only, if all the necessary informations about the orbit and the physical properties of a specific satellite are available.

6. EQUATIONS OF MOTION OF NON-RIGID SATELLITES

The development of the equations of motion of a non-rigid satellite, i.e. a satellite with flexible or movable parts, depends very much upon the nature of non-rigidity. It is beyond the scope of this paper to present the equations of motion for the various models treated in the literature. However, a few types of configurations may be mentioned.

If the satellite has movable parts performing translational motions relative to the satellite in such a way that only the magnitude of the principal moments of inertia is changed but not the principal axes, the equations of motion can very easily be obtained from Equations (11) and (12) regarding the time dependence of the moments of inertia

$$\begin{aligned} J_1\dot{\omega}_{y1} + (J_3 - J_2)\,\omega_{y2}\omega_{y3} + \dot{J}_1\omega_{y1} &= L_{y1} \\ J_2\dot{\omega}_{y2} + (J_1 - J_3)\,\omega_{y3}\omega_{y1} + \dot{J}_2\omega_{y2} &= L_{y2} \\ J_3\dot{\omega}_{y3} + (J_2 - J_1)\,\omega_{y1\,y2} + \dot{J}_3\omega_{y3} &= L_{y3} \,. \end{aligned} \tag{54}$$

Another configuration which is simple with respect to the derivation of the equations of motion, is a satellite consisting of a rigid main body and three equal reaction wheels mounted with their spin axes along the principal axes of the main body (Fig. 6). These reaction wheels may be used to control the satellite's attitude: Control torques on the main body can be produced by acceleration or deceleration of the wheel rotations. The angular momentum of the whole system is in body coordinates

$$\begin{aligned} H_{y1} &= J_1\omega_{y1} + J_r\nu_1 \\ H_{y2} &= J_2\omega_{y2} + J_r\nu_2 \\ H_{y3} &= J_3\omega_{y3} + J_r\nu_3 \end{aligned} \tag{55}$$

where J_1, J_2, J_3 are the principal moments of inertia of the whole system, J_r is the moment of inertia of the reaction wheels with respect to their axis of symmetry, and ν_1, ν_2, ν_3 are the angular velocities of the wheels relative to the satellite. Inserting Equation (55) into (11) we obtain

$$\begin{aligned} J_1\dot{\omega}_{y1} + (J_3 - J_2)\omega_{y2}\omega_{y3} &= J_r\,(\nu_2\omega_{y3} - \nu_3\omega_{y2} - \dot{\nu}_1) + L_{y1} \\ J_2\dot{\omega}_{y2} + (J_1 - J_3)\omega_{y3}\omega_{y1} &= J_r\,(\nu_3\omega_{y1} - \nu_1\omega_{y3} - \dot{\nu}_2) + L_{y2} \\ J_3\dot{\omega}_{y3} + (J_2 - J_1)\omega_{y1}\omega_{y2} &= J_r\,(\nu_1\omega_{y2} - \nu_2\omega_{y1} - \dot{\nu}_3) + L_{y3} \,. \end{aligned} \tag{56}$$

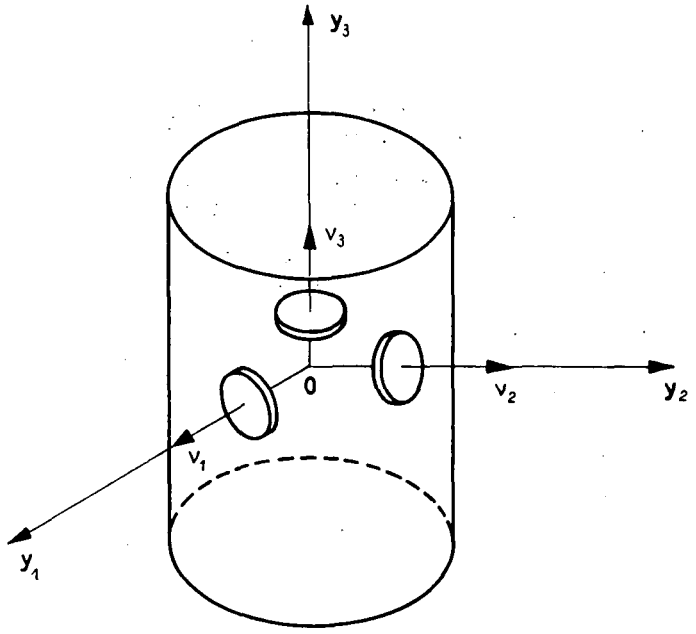

Figure 6. Satellite with reaction wheels

The rotational motion of the reaction wheels is described by

$$J_r\,(\dot{\omega}_{y1} + \dot{\nu}_1) = L_{m1} - k\nu_1$$
$$J_r\,(\dot{\omega}_{y2} + \dot{\nu}_2) = L_{m2} - k\nu_2 \qquad (57)$$
$$J_r\,(\dot{\omega}_{y3} + \dot{\nu}_3) = L_{m3} - k\nu_3$$

with L_{mi} and $k\nu_i$ $(i = 1,2,3)$ being the motor and frictional torques, respectively.

In Reference |8| a satellite consisting of a main rigid body and an arbitrary number of rigid internal moving parts is considered. The equations of motion of the main body are derived assuming that the internal parts perform translations and rotations relative to the main body which are prescribed functions of time.

In Reference |9| a similar model is investigated which in addition contains parts whose motion relative to the main body is not specified as a function of time. These parts are assumed to have a torque interaction with the main body depending on the relative motion.

For the dynamical analysis of satellites which can be idealized as a combination of rigid bodies and flexible appendages, in Reference |10| so called "hybrid"-coordinates are introduced, i.e. position and attitude coordinates for the rigid bodies and modal deformation coordinates for elastic appendages.

In Reference |11| the equations of motion for a system of interconnected rigid bodies moving in a Newtonian gravitational field is derived under the following assumptions: a) The structure of the interconnections form a topological tree, i.e. from any body of the system to any other there is a unique sequence of other bodies; b) Every contiguous part of bodies contains at least one point in common; c) Gravitational torques are the only external torques.

REFERENCES

|1| Whittaker, E.T., Analytical Dynamics, Cambridge University Press, London, 1937

|2| Leimanis, E., The General Problem of the Motion of Coupled Rigid Bodies About a Fixed Point, Springer Verlag, New York, 1965

|3| Schaaf, S.A., Mechanics of Rarefied Gases, Encyclopedia of Physics (editor S. Flügge), Vol. VIII,2, Springer Verlag, Berlin, 1963

|4| Nurre, G.S., Effects of Aerodynamic Torque on an Asymmetric Gravity-Stabilized Satellite, Journal of Spacecraft and Rockets, Vol. 5, 1968, 1046-1050

|5| Beletskij, V.V., Motion of an Artificial Satellite About Its Center of Mass, Israel Program for Scientific Translations, Jerusalem, 1966

|6| McElvain, R.J., Satellite Angular Momentum Removal Utilizing the Earth's Magnetic Field, Torques and Attitude Sensing in Earth Satellites (editor S.F. Singer), Academic Press, New York, 1964

|7| Evans, W.J., Aerodynamic and Radiation Disturbance Torques on Satellites Having Complex Geometry, Torques and Attitude Sensing in Earth Satellites (editor S.F. Singer), Academic Press, New York, 1964

|8| Roberson, R.E., Torques on a Satellite Vehicle From Internal Moving Parts, J. Appl. Mech., Vol. 25, 1958, 196-200

|9| Roberson, R.E., Attitude Control of Satellites and Space Vehicles, Advances in Space Sciences, Vol. 2, 1960, 351-436

|10| Likins, P.W., and Gale, A.H., The Analysis of Interactions Between Attitude Control Systems and Flexible Appendages, IAF AD 29, 19th International Astronautical Congress, New York, 1968

|11| Wittenburg, J., Die Differentialgleichungen der Bewegung für eine Klasse von Systemen starrer Körper im Gravitationsfeld, Ingenieur Archiv, Vol. 37, 1968, 221-242

SPACECRAFT ATTITUDE SENSORS WITH EMPHASIS ON THE ORBITING ASTRONOMICAL OBSERVATORY

by

Thomas E. Huber

Goddard Space Flight Center - NASA
Greenbelt, Maryland 20771

SUMMARY

The OAO spacecraft contains a multiplicity of control system sensors. The sensors range from analog type sun sensors with 5 degree pointing errors to gimbal star trackers where an accuracy of 30 arc seconds is achieved. The OAO control system has many modes of operation, but its major task is to point the 4500 lb spacecraft to any point in the celestial sphere to a pointing accuracy of one arc minute. The OAO control system per se will not be discussed.

The sensors that provide references for the OAO control System are coarse sun sensors, fine sun sensors, Adcole aspect sensors, Rate and Position sensors, inertial reference unit, Boresight tracker, gimbal star trackers, fixed head tracker, and magnetometers. The coarse and fine sun sensors are analog type sensors and are part of the OAO control loop. The aspect sensors are digital type and are used with the magnetometers primarily for attitude determination. The inertial sensors are used to slew or reposition the vehicle and are also used to inertially hold the spacecraft. The gimbal trackers and boresight tracker are used for stellar control holding the vehicle to an attitude accuracy of one arc minute.

1.0 COARSE SUN SENSORS

The coarse sun sensors are silicon cells with an electrical output proportional to the cosine of the angle between the sunline and the center of the field of view (normal to the sun). The field of view of an individual sensor is approximately 180 degrees. To utilize these sensors for spacecraft control, a total of eight sensors are located on a vehicle. Four eyes are used to sense errors about the pitch (Y_c) axis and four eyes are used to sense errors about the yaw (Z_c) axis. Two of the four cells are located on the sun pointing side of the vehicle and two are located on the anti-sun side. The polarity of one cell is reversed with respect to the other cell and the outputs of the two cells are hard wired together and the output currents added algebraically. Figure 1 shows the individual response of a cell and the composite signal used for OAO yaw control.

1.1 ELECTRICAL CHARACTERISTICS

The transfer function of the combined output is linear to within $\pm$ 5 percent of the output for plus or minus 10 degrees from null. The output slope between the $\pm$ 10 degrees is approximately 18 micro amp/degree. The overall accuracy of the coarse sun sensor system is $\pm$ 2 degrees. The main contributor to this error magnitude is earth's albedo.

2.0 FINE SUN SENSORS

The fine sun sensors are also silicon cells. The output of the sensor is proportional to the spacecraft attitude with respect to the sun. However, half of each eye is opaqued reducing the field of view to $\pm$ 15 degrees. The masking of the sensors reduces the albedo effects and the accuracy of the fine eyes, over a -106°F to 161°F temperature range, is $\pm$ 2 arc minutes.

Two fine eyes are used for OAO pitch (Y_c) control and two eyes are used for yaw (Z_c) control. The output of the sensor is 42 micro amp/arc minute over a $\pm$ 25 arc minute range.

3.0 ADCOLE ASPECT DIGITAL SUN SENSOR

The Adcole sun sensor measures the angle of incident sunlight with respect to a reference axis and expresses this angle as a digital number. Figure 2 shows the principle of operation where light, passed through a slit on the top of a quartz block, is screened by a gray-coded pattern on the bottom of the block to either illuminate or not illuminate each of eight photo cells. The angle of incidence determines which photocells are illuminated. The information uniquely describes the sun vector in 0.5 degree increments with an accuracy of 0.25 degree. The eight photocells provide 256 unique combinations of one and zeros which represent 128 degree full coverage ($\pm$ 64°). The sensor also has an indentification bit.

Because of the gray-coded pattern, only one bit changes at a time. If the opaque and clear area on the reticle were arranged in a conventional binary code with simultaneous changes in more than one bit, there could be catastrophic errors in the determination of the angle if the transitions were not perfectly synchronized.

The important mechanical tolerances of the sensor are completely contained within the single block of fused quartz and are held to 0.0003 inches tolerance on the critical reticle dimensions. The

accuracy of the Adcole sensor is dependent on the constant ratio of the thickness to the width of the quartz block which is relatively unaffected by expansion or contraction of the block. The Adcoles are used on OAO spacecraft in conjunction with a magnetometer for 3 axes attitude determination.

3.1 DETERMINATION OF SUN

To determine the sun position using the Adcole sun sensor, the following derivation is given. Figure 3 illustrates a reticle with thickness, T, and index of refraction, n. The sun rays OP, make an angle θ, with the normal OZ, to the reticle and angle ϕ with the y axis. The refracted ray OP' strikes the far side of the reticle at a distance d, from the Z axis. One of the two reticles has a slit parallel to the X axis and measures the y component of d; the other slit is parallel to the Y axis and measures the x component of d. From Snell's law of refraction, the following relationships between θ and ϕ and X and Y can be derived.

$$\theta = \tan^{-1} \frac{n(x^2 + y^2)^{\frac{1}{2}}}{\left(T^2-(n^2-1)(x^2+y^2)\right)^{\frac{1}{2}}}$$

$$\phi = \tan^{-1} \frac{X}{Y}$$

The sun position may also be defined by two angles (a) and (B), which are angles of rotation about X and Y axes. These angles in terms of the distance X and Y measured by two orthogonal reticles are:

$$a = \tan^{-1} \frac{ny}{\left(T^2-(n^2-1)(x^2+y^2)\right)^{\frac{1}{2}}}$$

$$B = \tan^{-1} \frac{nx}{\left(T^2-(n^2-1)(x^2+y^2)\right)^{\frac{1}{2}}}$$

The distance X and Y are quantized by the reticle pattern. In terms of the decimal equivalent of the numbers (nx and ny) read from the two reticles,

$$X = K \pm (nx + 0.5)$$

$$Y = K \pm (ny + 0.5)$$

where K is a constant determined from the geometry of the reticle and 0.5 is added to the number read out to yield the distance to the center of the segment, or the midpoint between two transitions.

4.0 HIGH RESOLUTION ADCOLE SUN SENSOR SYSTEM

The Adcole sensor described in Section 3.0 yield 0.5 degree resolution with 0.25 degree accuracy. OAO-4 will fly a high resolution Adcole sun sensor with resolution of $1/256^{\circ}$ (14 arc seconds) with an accuracy of 1 arc minute. To obtain this high resolution, interpolation between the 0.5 degree transitions is required. The interpolated or fine angles are measured by four columns of patterns arranged successively in space phase quadrature. The output of the four fine photocells behind these columns are chopped by four quadrature square waves derived from a chain of flip-flops counting down from a fixed frequency oscillator. Their outputs are summed and passed through a band-pass filter to yield a sine wave whose phase is an indication of sun angle. This phase angle is measured by counting the number of pulses at the oscillatory frequency that occur between the zero crossing of the phase reference and the zero crossing of the sine wave. Pulses from a master oscillator are gated into a seven stage binary counter. At the end of each cycle of a 25KHz waveform, which is a four phase switching wave form produced by binary diversion from a crystal oscillator, the counter contains a binary number representing the position of the slit image in fractional parts of a degree. The counter's flip-flops are connected as a shift register and the seven bits are shifted out serially upon command, following the five more significant bits obtained during coarse angle measurement. A block diagram is shown in Figure 4. The salient features of the sensor are in Table 1.

Table 1

High Resolution Sun Sensor Characteristics

Field of View (two axis)	- 64° X 64°
Resolution	- $1/256^{\circ}$
Accuracy	- 1 arc minute
Digital Output	- 14 bit natural binary
Weight (Sensor & Electronics)	- 10 lbs
Size (Sensor)	- 3" x 3" x 1"
Power	- 1.9 watts
Analog Transfer Function	- 8.33v/arc sec
(Linear Range)	$\pm$ 20 arc minutes

The OAO sensor has an analog output for controlling the spacecraft via fine reaction wheels. The characteristics of these signals are also contained in Table 1.

5.0 INERTIAL REFERENCE UNIT (IRU)

The IRU is a ultra-precision gyro inertial system. The IRU consists of two packages: an Inertial Package and an Electronic Package. The Inertial Package is a temperature controlled cube 9 inches on a side. It contains three precision rate integrating gyros, the gyro control and readout electronics, a frequency source assembly which provides the precision frequency for the electronics. The gyros are operated with binary pulse restrained torque loop. Torque data from the gyros are processed as rate and rate integrals (i.e., angles) in the electronics and converted to analog signals for use in the OAO control system. A block diagram of the restraint loop is shown in Figure 5. The electronics contain analog, digital and hybrid electronics. There are 17 major electronics blocks including: power supplies, control units, input/output units, logic and conditioning units.

The IRU is operated in three modes (ISTAB, SLEW, and HOLD) that correspond to the three rate levels encountered in the OAO mission. The ISTAB mode is used when high rates are anticipated such as orbital injection. This mode has a rate capability of $\pm$ 2°/sec. The SLEW mode is used on one axis at a time during precision repositioning of the OAO. The rate capability of this mode is 0.13°/sec. The HOLD mode used for precise holding of the OAO spacecraft has a rate capability of $\pm$ .004°/sec.

The salient characteristics of the IRU are contained in Table 2.

TABLE 2

IRU Characteristics

Modes:	Rate Capability	Wheel Frequency	Wheel Speed
ISTAB	- 2°/sec	50 Hz	750 RPM
SLEW	- .13°/sec	800 Hz	12 000 RPM
HOLD	- .004°/sec	800 Hz	12 000 RPM
On-Board - Drift Compensation Capability	- $\pm$ .24°/hr.		
After In-Orbit Calibration: SLEW SCALE FACTOR	- 1 part in 30,000		
After In-Orbit Calibration: SLEW BIAS	- .01°/hr		
After In-Orbit Calibration: HOLD BIAS	- .0015°/hr		
Input Axis Stability	- 5 arc sec		
Angular Momentum	- 1.73 x 10^6 g-cm^2/sec		
Pulse Rebalance Sys.	- 200 pulses/sec		
Quantization Level	- .077 arc sec / pulse		
Power (28v Unregulated)	- 75 watts		
Weight - Inertial Pkg.	- 40 lbs		
Electronics Pkg.	38 lbs		
Gyro Gain (H)/(C)	- 1.9		
Type of Bearing	- Ball Bearing		
Gyro Temp	- 135°F $\pm$ 1°F		

The IRU accepts, decodes, and processes the following programmed command inputs:

1. Selection of one of three operating modes: ISTAB, SLEW and HOLD.
2. Command slew on one of three axis.
3. Position reset: To establish a new inertial reference for the IRU.
4. R Term Update: to null out gyro bias drift.

6.1 GYRO UNIT

The IRU gyro unit consists of a 2FBG-6F-OAO gyroscope, a signal generator end assembly and torque generator end assembly. The three gyro units are used in the IRU inertial package in a "strapdown"

configuration. The "strapdown" configuration is where the gyros are hard mounted to the spacecraft. Signal generator and torque generator end assemblies combine to form a "torque balance loop" with each gyro. Gyro torque, and therefore float rotation, develops about the gyro axis when an angular rate is applied about the gyro input axis. The signal generator senses the angular offset about the gyro output axis. The gyro error signal is amplified and sampled at a fixed frequency. During each sampling period a torque pulse is generated in either the positive or negative winding of the gyro torquer depending on the sign of the error signal. A torque pulse is transmitted as either a "1" state or as a "0" state to circuitry in the electronics. The electronics processes the digital signals and provides both analog and digital rate and angle information to the OAO control system.

6.2 ELECTRONICS

The gyro signal generator generates a phase sensitive suppressed carrier signal (1.6 KHz) proportional to gyro float offset angle, which is amplified by the signal generator pre-amplifier. This signal is amplified further in the torque word generator and synchronously demodulated and filtered. Its phase is sampled at a 200 Hz rate and outputs either a one or zero level to the electronics. The torque word output also provides the control signals for driving the torque generator windings. Rate and angle data are derived from the IRU gyros and their control electronics. Processing of the data is accomplished by six functional sub-units:

1. Synchronizer - This unit is the summing point for all rate information and the converter of two state pulses into two line pulse rates. The two line pulses are added to a carrier frequency (409.6 KHz) and the output is 409.6 + 800 θ (where θ = degree/min) KHz.

2. Rate Integrator - This unit converts rate data to angle data by integration of the rate signal.

3. Phase Logic - This unit performs the angle extraction process. It compares the phase shifted square from the rate integrator with the reference source and an exclusive "OR" yields a logic signal whose width is equal to angle.

4. R-Term Compensation - This unit is used to eliminate constant gyro drift observed in orbit. It can input a total rate change of $\pm$ 0.24°/hr with a most significent bit level of 0.00047°/hr.

5. Error Signal Conditioner - This unit converts the digital error signals to analog error signals which are used by the OAO control system for spacecraft control.

6. Angle Telemetry Selection and Hold Unit - This unit processes the rate integrator signals and outputs them to the OAO as bi-level data for a specific axis.

6.0 RATE AND POSITIVE SENSOR SYSTEM (RAPS)

The RAPS subsystem is another inertial unit but less precise used on the OAO spacecraft for rate and position information. The system consists of basically three packages:

1. Gyro unit
2. Gyro Electronics
3. Gyro Controller

6.1 Gyro Unit

The gyro unit consists of three rate integrating gyroscopes, gyro heaters and thermistors. Each gyro is capable of producing either rate or attitude signals depending whether or not the loop is closed between the gyro pickoff and gyro torquer through the electronics. The gyro torquer loop is strictly analog in nature. The gyro spin motors operate on 3 phase 26V, 400 Hz and the signal generators operate at 800 Hz.

6.2 Electronics

The electronics amplifies the gyro signal generator output through a gyro output amplifier, the signal is then fed through a demodulator, torque amplifier and output filter to the gyro controller. The temperature regulating circuitry for the gyros are also contained in the electronics. The gyros operate at 142°F $\pm$ 2°F. Depending on the position of attitude/rate switch in the electronics, position or rate information is fed on the three output lines. A block diagram of the system is shown in Figure 6. The salient features of the RAPS package is shown in Table 3.

TABLE 3

RAPS Characteristics

Type of Gyro Bearing	Ball Bearing
Torque Rate Capability	$\pm$ 3°/sec
Wheel Momentum	2.27 x 10^5gm-cm^2/sec
Rate Accuracy	$\pm$ .01°/sec
Random Drift	0.02°/hr
Attitude Output Accuracy	1 arc minute

Table 3 (Cont'd)

Torquer Scale Factor	1 PART IN 1,000
Torque Loop	Analog
Wheel Frequency	400 Hz
Power	20 Watts
Weight	25 lbs
No on-board compensation capability	
Rate Output (analog)	60V/degree/sec
Position Output (analog)	6V/degree

6.3 Controller

The controller contains logic and processing electronics which accept the gyro outputs and conditions the signals to drive the reaction wheels and jet system aboard OAO.

7.0 GIMBALLED STAR TRACKER

7.1 General

The OAO gimballed star tracker consists of an integral telescope with a one degree of field of view mounted on a two degree of freedom gimballing system (Figure 7). The device is used for detection, acquisition and tracking of 2.0 magnitude stars in space. The general characteristics are shown in Table 4.

TABLE 4

Star Tracker Characteristics

Tracking Accuracy (Two Axes)	30 arc sec (1 σ)
Field of View	$\pm$ 0.5°
Gimbal Travel (Two Axis)	$\pm$ 43°
Star Recognition Level	2.0 mag
Photo Multiplier Tube	1P21 - S-4 photometric surface
System Weight (Gimbal Electronics, Phasolver)	52 lbs
High Voltage	1000 VDC
System Power	20 watts
Resolution of Encoder	5 arc sec
Command Resolution	10 arc sec

7.2 Optical System

The tracker employs a Cassegrainian reflector type telescope having a beryllium primary mirror of 3.5 inch diameter and 5.0 inch focal length. Individual beams of light reflected from this primary surface are passed back up the telescope barrel where they are again reflected from two beryllium plane mirrors at an angle of 45 degrees to each other. The impinging beam is thereby split into two components at 90 degrees to each other. Each beam is related to one of the gimbal axes. The beams pass back down the telescope barrel and each passes through the square window of a vibrating reed. The vibrating reed assemblies are precision tuned to 350 hertz for the inner gimbal motion and 450 hertz for the outer axis motion. Each reed aperture is rectangular in shape and is 0.087 inches along the reed, which corresponds to 1 degree in the focal plane and 0.036 inches wide in the direction of motion. The 1 degree field of view of the telescope is obtained by vibrating the reed assemblies approximately 0.052 inches, which results in each aperture transversing an area 1 degree by 1 degree.

The modulated light in each channel is then directed by flat mirrors to relay lenses that form an image of each paraboloid segment. An aperture stop corresponding to the size and shape of each image is positioned in the corresponding image plane to prevent stray light from outside the objective area from proceeding to the photomultiplier. Mirrors then direct each modulated light bundle through condenser lenses which in combination with the relay lenses, re-image and superimposes the objective segments in the plane of the photomultiplier cathode.

7.3 Error Detection System

A vibrating reed is included in each telescope channel in order to modulate the star light entering the tracker telescope. The vibrating reed and scanning assembly consists of the following

elements:

a. reed

b. reed base

c. permanent magnet

d. drive coil

e. pickup coil

f. aperture

When the reed drive coil is excited at the resonant frequency of the reed (350 Hz or 450 Hz) the magnetic flux produced by the drive coil current attracts the reed once each cycle, setting the reed in motion. The permanent magnet in the drive coil provides a dc bias, preventing the reed from being attracted twice each cycle.

If the star light is brought into focus at the center of the reed aperture, the light flux is cut twice for each cycle of reed motion. Therefore the light impinging on the photomultiplier tube cathode is a square wave having a predominant frequency which is (2X) reed frequency (2 f_o). This square wave is equivalent to a null condition where the angle between the optical axis and the star line is less than eight minutes of arc. When the star image is brought into focus at a position removed from the center of reed aperture oscillation by half the width of the aperture, the light flux is cut only once for each cycle of reed motion. This results in a square wave having a predominant frequency which is equal to the reed frequency (f_o). The phase of this signal, with respect to the reed pickup coil voltage, depends upon which side off center that the star is brought into focus. These characteristics make (f_o) suitable for the servo position errors as well as star recognition. The second harmonic (2 f_o) is used with (f_o) to determine star recognition or star presence.

7.4 MODES OF OPERATION - COMMAND AND TRACK, (Figure 7-1)

7.4.1 Command Mode

This mode enables the tracker telescope to be pointed by external command signals. In the command mode, the inner and outer gimbal errors are compared to a gimbal angle command produced by a Digitizer Logic Unit (DLU) aboard the spacecraft. The error difference is converted to an analog signal which drives the proper gimbal to null. The increment of command angle is 10 arc seconds.

7.4.2 Track Mode

In the track mode each star tracker telescope channel essentially forms an independent closed loop servo system. The parabolic mirror collects star light for both optical channels. The light in each channel is modulated by respective vibrating reed scanners and superimposed on the cathode of the photomultiplier tube. The outputs of the tube is sent through a pre-amplifier and the signals for each channel are separated into their fundamental components in narrow band amplifiers with the second harmonic also being obtained. The fundamental signal for each channel is converted into a dc signal by a demodulator and routed through a compensation network to a power d.c. amplifier which drives the gimbals via torque motors.

The fundamental signals are also applied to a tracking null detector. This detector provides a tracking signal when the sum of the two axes gimbal angle errors are less than two minutes of arc. The second harmonic signals, along with the fundamental signals, are also applied to signal detectors where they are processed to supply a star presence signal and an automatic gain control signal to control the high voltage level. The high voltage level is varied over the detectable star magnitude range to maintain a relatively constant gain over the operating range of star magnitudes.

7.5 Phasolver System (Figure 8)

A phasolver is a "two speed" capacitively coupled phase-analog angle readout device. This device consists of two discs; one stationary and one rotating with the respective gimbal. The stationary disc is excited with a sine wave and is capacitively coupled to the rotating disc. The phase shift between the coupled signal recovered on the rotating disc and the reference sine wave is a function of angular displacement between the discs. The phasolver system has a driver section which generates sine wave voltages to the stationary disc from (2) pairs of programmer gating signals. The two sine wave voltages (coarse and fine) are 1.5625 KHz for the fine scale and 6.25 KHz for the coarse scale. The coarse angle readout contains a four-cycle pattern, indicating that, for a gimbal displacement of 90 mechanical degrees from a reference, the output sine wave is displacement 360 electrical degrees from the referenced sine wave. The fine angle readout contains a 256 cycle pattern which, for an angular displacement of 1.40625 degrees, gives 360 electrical degrees phase shift in the output sine wave with respect to the referenced sine wave.

The phasolver output circuitry generates stop pulses to indicate negative-going zero crossings of the phase shifted output sine waves. The fine reference and coarse reference signals, together with a 25 KHz sync pulse, are processed to give negative-going zero crossing of the referenced sine waves. The Digitizer Logic Unit (DLU) on the spacecraft converts the time lag between the reference signals and output signals into a usable digital indication of gimbal angle. When the mechanical angle increased by 1.40625 degrees the delay will increase by 2.50 micro seconds. The amplitude of the four sine waves (coarse and fine for inner and outer gimbal) must be equal to within 0.5 per cent to yield required accuracy.

7.6 Sun Shade Shield Assembly

The sun shield, attached to the telescope assembly, protects the optical system from both sun and earth illumination. A razor sharp entrance aperture minimizes specular reflection of the earth and sun impingement by reducing the surface from which reflection occurs to the smallest practical area. The main body of the shield is 8.6 inches and resembles an inverted "minaret" which is a light trap making the most efficient use of the volume available for the shade. All internal surfaces directly or indirectly illuminated by the sun and earth are kept as far as possible from the telescope objective and are formed into the shape which results in the optimum number of absorptive rays bounces from the unwanted illumination. The angle at which the tracker can operate with respect to the sunlit earth and sun are 16^{o} and 30^{o} respectively. Sun and earth sensors, mounted on the shade, trigger a solenoid which operates a protective shutter in the optical path of the tracker when the critical angles (16^{o} and 30^{o}) are exceeded.

8.0 BORESIGHT STAR TRACKER

The OAO boresight tracker is mounted with its optical axis co-incident with the main telescope axis, but is completely independent. The salient features of the tracker are listed in Table 5 and a pictorial diagram of the tube system is shown in Figure 9.

TABLE 5

Boresight Tracker Characteristics

Star Recognition Level	+6 magnitude
Objective Aperture	2.7 inches DIA.
Focal Ratio	f/1.8
Instantaneous field of view	$\pm$ 5 arc min
Offset Capability	$\pm$ 1.5^{o}
Offset Increment	15 arc sec steps to 15 arc minutes and one minute step to 1.5 degrees
Bandwidth	0,5 Hz
Tracking to Sun	45 degrees
Tracking to Sunlit Earth	30 degrees
Detector	Image Dissector (2000v) S-20 photometric surface)
Deflection	Magnetic deflection
Error Gradient	1.0v/arc minute
Tracking Accuracy	2 arc seconds (1σ) tracking a +6 mag star
Weight	25 lbs
Power	8 watts

The boresight tracker is composed of two units: a sensor head and an electronics package. The sensor head contains the front end optics, which is a refractive optical system, an image dissector tube, preamplifier, high voltage supply and a sun shutter solenoid. The electronics package contains the offset logic, sweep generator, binary counter, error generator, null detector and star presence circuitry.

8.1 Operation

The boresight tracker is an electronics scanning device. It has a sixteen stage photomultiplier tube with an operative electrode between the transparent cathode and the first dynode and connected to the first dynode.

This aperture plate contains an aperture hole which can be sized and shaped as desired. The aperture plate hole for the boresight subtends an angle of 10 arc minutes, which is stated as the instantaneous field of view. By deflecting or scanning the parallel beam of electrons caused by starlight impinging on the cathode, the electrons can be made to pass through the aperture hold and be detected. Thus the optical image formed at the photocathode is converted to an electron image and be dissected with an instantaneous viewing aperture.

The external magnetic field produced by the deflection coil moves the electron beam in a star shaped or cruciform pattern. The triangular wave that energizes the pitch and yaw coils is 350 Hz. If the star is centered in the aperture, the output wave will consist of a symmetrical square wave at twice the pattern scan frequency. If the star image is displaced the output will be non-symmetrical and an output current of the fundamental pattern frequency will be generated whose phase is an indication of direction of displacement and the amplitude a function of magnitude of displacement. This signal is

detected by a synchronous detector that develops a dc error (pitch or yaw) which is fed to the OAO control system.

8.2 Offset Capability

The boresight can be electronically offset up to 90 arc minutes about the origin in both pitch and yaw. A pair of reversible, nine stage digital counters with digital to analog conversion matrics are used. The analog voltage is superimposed on the AC deflection signals generating the cruciform pattern, and offset the scan pattern in any desired location. Incremental steps of 15 ● 2 arc seconds can be made out to 15 arc minutes, then one arc minute steps from 15 to 90 arc minutes are employed. The cumulative error of offset is 5 arc seconds out to 15 arc minutes and 20 arc seconds out to 90 arc minutes.

The boresight tracker has been extremely useful in determining OAO sensor misalignments and also for controlling the spacecraft to obtain a low jitter mode (< 3 arc seconds) operation.

9.0 OAO FIXED HEAD TRACKER

The fixed head tracker will fly on OAO-4 and will track stars between 3.5 and -1.0 AO-V magnitude in an 8 degree diameter circular field of view. The star field is imaged in the plane of the photocathode with the optical system. The center of this field is aligned to an optical cube for purposes of alignment. The star position and intensity information are contained on the photocathode in the form of displacements relative to the tube center and brightness, respectively. The phototube contains an electron-lens system, which generates an electronic replica of the photocathode scene. A square aperture is placed in the electron-lens, focal-plane, which serves to sample the current density of the reconstructed scene. Current passing through the aperture is multiplied by a sixteen stage dynode chain. The output current signal is linearly amplified in the video amplifier, where it is clipped to standard logic levels and measured to determine the respective star brightness.

The star field is interrogated by magnetically deflecting the photocathode electrons position. The scene is thus moved around on the aperture; providing the means of electronically modulating the position information. The scene is interrogated in two distinct modes of operation each optimized for its particular application. The search mode raster scans the entire field selecting the brightest star and its approximate position. Useful position information is developed in the track mode where an electron position servo is used to center a small scan on the star image.

The salient features of the tracker are contained in Table 6

TABLE 6

Fixed Head Tracker Characteristics

Field of View	Circular 8^{o} dia
Instantaneous Field of View	40 arc min
Detector	FW 143 Image Dissector (2000 volts)
Optical System	F/0.7
Position Accuracy	1 arc min (1σ)
Star Recognition Level	3.5 or brighter
Detection Protection:	
Sun Sensor	60^{o} to sun
Earth Sensor	25^{o} to earth
Over-current detector	Remove Hi Voltage from Tube
size	6" x 6" x 12"
weight	12 lb
power	10 watts

9.1 Acquisition Mode

In the acquisition mode the star tracker interrogates the photocathode image of the stellar star field. This mode is not used to produce output information, but to internally search the star field and respond to star intensity and position. If a star magnitude above the threshold value is detected, the event is noted and star field is raster scanned four more times beyond the point of detection. After the fourth scan, the deflection is stopped and held at the point where the video pulse is obtained. The total 8 degree diameter field of view is completely interrogated once every 80 milliseconds. The field is scanned by horizontally deflecting the aperture at 16 discrete increments of the vertical. The horizontal scan is a linear function of time being swept at a rate of 96 arc min/ms. The vertical scan is discrete and is incremented 28 arc minutes at the end of each horizontal scan. Thus this process continues until the total field of view is interrogated, at this time the scan direction reverses and retraces itself.

9.2 Track Mode

After the fourth scan, the tracker switches to the track mode. Simultaneous to mode change, a cruciform deflection is about the detected star. The error information obtained from the cruciform demodulator is used in an electronic position-servo-loop to modify the mean deflection such that the centroid of the scan tends to align itself with the star image. Cartesian angular error information with respect to the optical axis is now linearly related to the average deflection required to maintain the scan centered on the star image. As the position changes, the scan centroid will follow, thus providing the capability of generating errors over the entire field of view.

10.0 MAGNETOMETER

A magnetometer is an instrument that measures magnet fields. The OAO has three magnetometers (Figure 10) used to detect earth magnetic field at 500 nautical miles. These outputs are used in conjunction with Adcole sun sensors for attitude determination and as an input to the OAO magnetic unloading system. The magnetometer operates on the flux gate principle. The probe is energized with a 2 KHz signal. The probe output contains even harmonics of 2 KHz whose amplitude is proportional to the vector component of magnetic field aligned along the probe axis. The probe contains a small piece of magnetic material which is the core of a transformer. One winding of the transformer is driven by the 2 KHz sine wave. The presence of the earth's steady field saturates the magnetic material and the resulting ac magnetic field which is sensed by a second winding on the transformer, is distorted and contains a large second harmonics component. The phase of this component to the reference 2 KHz drive signal is a function of earth's field direction. The second harmonic signal is amplified by an amplifier tuned to 4 KHz. The amplifier is fed through a phase sensitive demodulator and a dc voltage is derived.

The dc voltage feeds a current amplifier whose output is fed to a drive coil on the probe transformer which produces a bucking dc field. The system is always being driven towards null. The output of the current amplifier is recovered across a precision resistor and is proportional to earth's field.

The magnetometer is sensitive to the frequency and voltage of the drive excitation. A 4 KHz tuning fork is used for the oscillator, which drives a 2 KHz multivibrator. The voltage has zener regulation. The 2 KHz square wave is filtered and the output is used for probe excitation. The range of the probes is $\pm$ 60,000 gamma, with a linearity of $\bullet$ 3 percent and a drift rate of 5 gamma/hour. The frequency response of the probe is 280 hertz.

REFERENCES

1. Grumman Aerospace Corporation "Spacecraft System Design Manual" Grumman Bethpage, Long Island, New York

2. Massachusetts Institute of Technology Instrumentation Laboratory, "IRU (OAO) System Handbook', Cambridge, Mass. 02139

3. Adcole Corporation, November 1968, "Consideration in the Design of Digital Solar Aspect System", Adcole Corporation, Waltham, Mass.

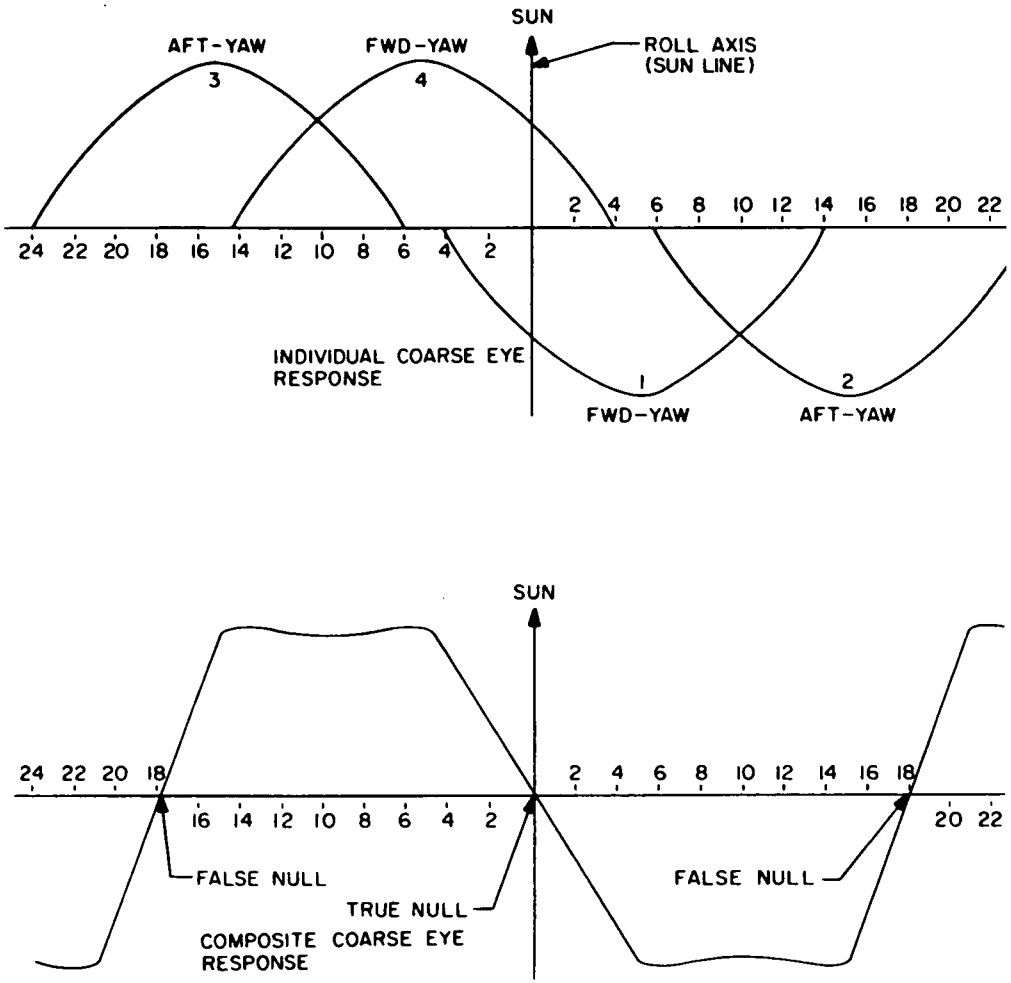

Individual and Composite Responses
Of Coarse Solar Cells
Figure 1

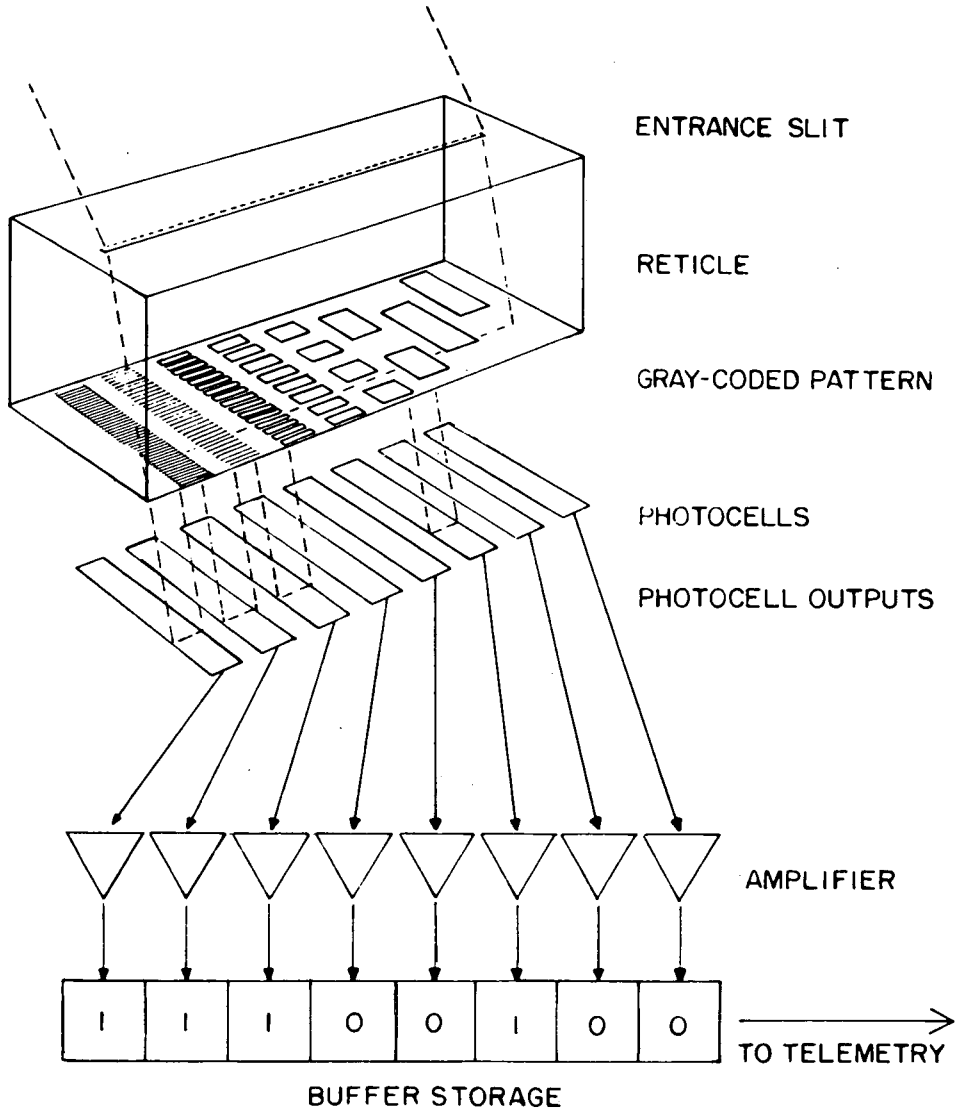

Block Diagram of Adcole Aspect Sensor Operations
Figure 2

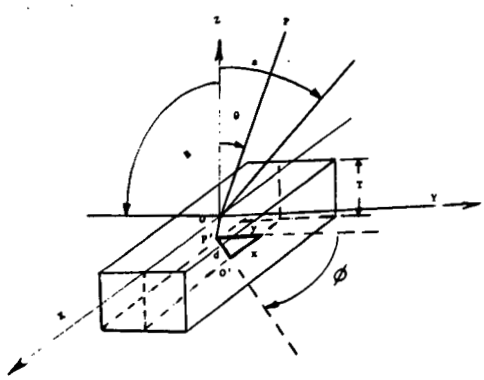

Adcole Aspect Sensor Angle
Determination of the Sun
Figure 3

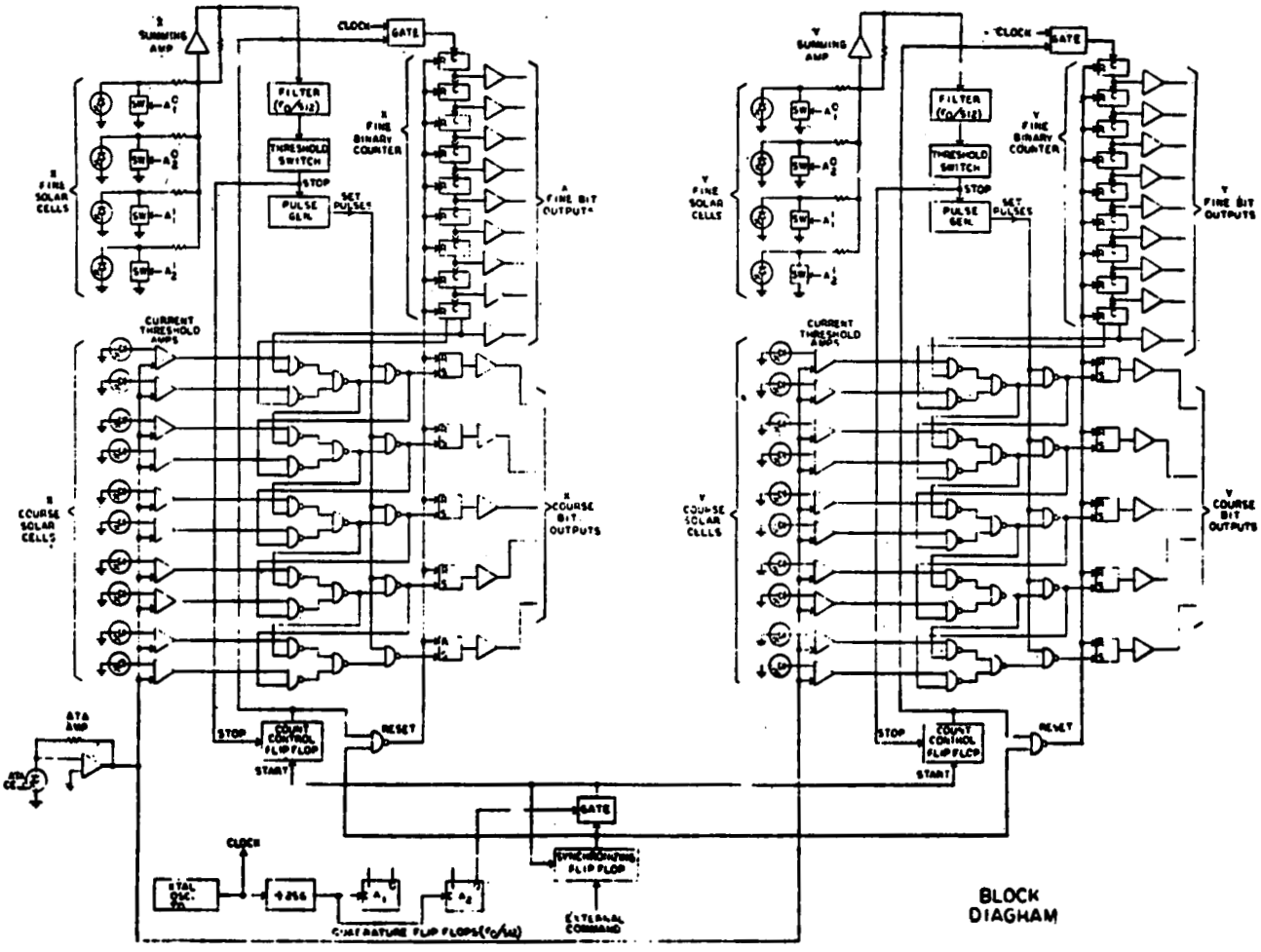

Block Diagram of High Resolution
Adcole Sun Sensor Electronics
Figure 4

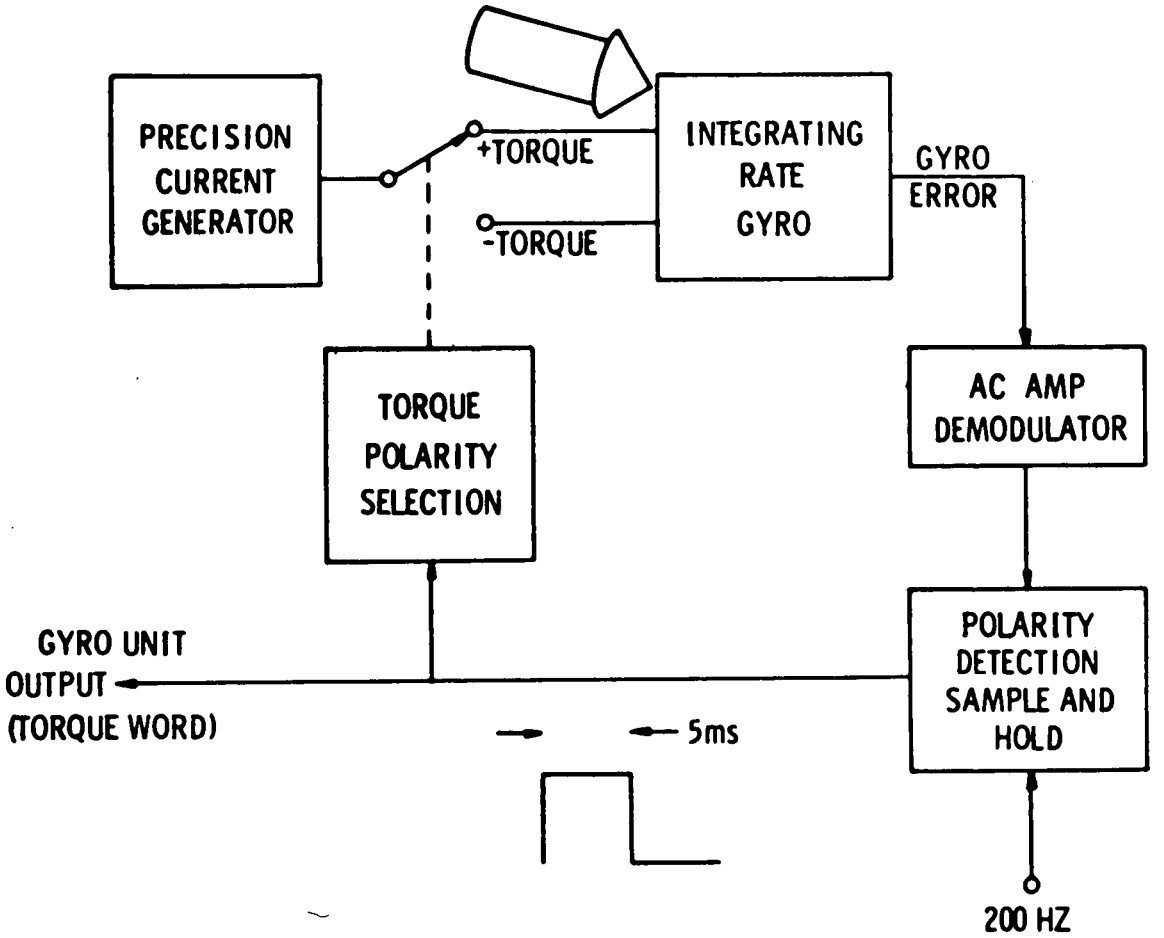

IRU Gyro Restraint Loop
Figure 5

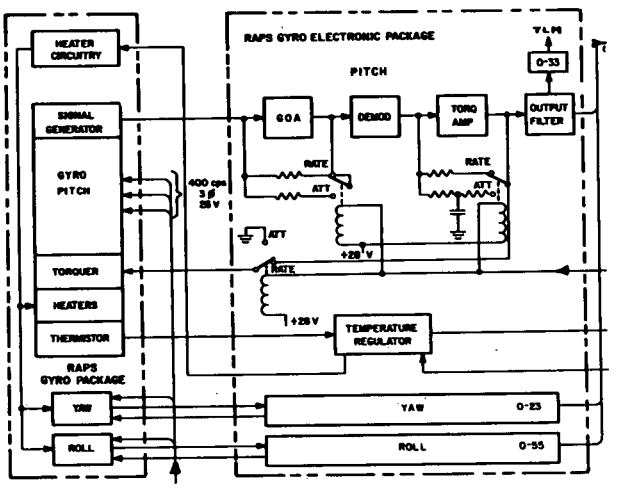

Block Diagram of RAPS Subsystem
Figure 6

AGARD Lecture Series No.45 North Atlantic Treaty Organization, Advisory Group for Aerospace Research and Development ATTITUDE STABILIZATION OF SATELLITES IN ORBIT Published September 1971 156 pages The material in this book has been collected to support a Lecture Series presented by the authors in Brussels (Belgium) and Stuttgart (Germany) on "Attitude Stabilization of Satellites in Orbit". Papers presented review the fundamental equations and various types of stabilization: spin, dual-spin, gravity gradient system and associated dampers, flywheels, P.T.O.	629.783: 629.7.058.47	AGARD Lecture Series No.45 North Atlantic Treaty Organization, Advisory Group for Aerospace Research and Development ATTITUDE STABILIZATION OF SATELLITES IN ORBIT Published September 1971 156 pages The material in this book has been collected to support a Lecture Series presented by the authors in Brussels (Belgium) and Stuttgart (Germany) on "Attitude Stabilization of Satellites in Orbit". Papers presented review the fundamental equations and various types of stabilization: spin, dual-spin, gravity gradient system and associated dampers, flywheels P.T.O.	629.783: 629.7.058.47
AGARD Lecture Series No.45 North Atlantic Treaty Organization, Advisory Group for Aerospace Research and Development ATTITUDE STABILIZATION OF SATELLITES IN ORBIT Published September 1971 156 pages The material in this book has been collected to support a Lecture Series presented by the authors in Brussels (Belgium) and Stuttgart (Germany) on "Attitude Stabilization of Satellites in Orbit". Papers presented review the fundamental equations and various types of stabilization: spin, dual-spin, gravity gradient system and associated dampers, flywheels, P.T.O.	629.783: 629.7.058.47	AGARD Lecture Series No.45 North Atlantic Treaty Organization, Advisory Group for Aerospace Research and Development ATTITUDE STABILIZATION OF SATELLITES IN ORBIT Published September 1971 156 pages The material in this book has been collected to support a Lecture Series presented by the authors in Brussels (Belgium) and Stuttgart (Germany) on "Attitude Stabilization of Satellites in Orbit". Papers presented review the fundamental equations and various types of stabilization: spin, dual-spin, gravity gradient system and associated dampers, flywheels P.T.O.	629.783: 629.7.058.47

magnetic torquers, thrusters, nutation dampers. Various sensors, and complete systems are described: ATS 5, TACSAT 1, Skylab B, Apollo, EOLE, PEOLE, SIRIO, OAO, TD.

The Lecture Series was under the sponsorship of the Guidance and Control Panel and the Consultant and Exchange Programme of AGARD.

magnetic torquers, thrusters, nutation dampers. Various sensors, and complete systems are described: ATS 5, TACSAT 1, Skylab B, Apollo, EOLE, PEOLE, SIRIO, OAO, TD.

The Lecture Series was under the sponsorship of the Guidance and Control Panel and the Consultant and Exchange Programme of AGARD.

magnetic torquers, thrusters, nutation dampers. Various sensors, and complete systems are described: ATS 5, TACSAT 1, Skylab B, Apollo, EOLE, PEOLE, SIRIO, OAO, TD.

The Lecture Series was under the sponsorship of the Guidance and Control Panel and the Consultant and Exchange Programme of AGARD.

magnetic torquers, thrusters, nutation dampers. Various sensors, and complete systems are described: ATS 5, TACSAT 1, Skylab B, Apollo, EOLE, PEOLE, SIRIO, OAO, TD.

The Lecture Series was under the sponsorship of the Guidance and Control Panel and the Consultant and Exchange Programme of AGARD.

AGARD Lecture Series No.45 North Atlantic Treaty Organization, Advisory Group for Aerospace Research and Development ATTITUDE STABILIZATION OF SATELLITES IN ORBIT Published September 1971 156 pages The material in this book has been collected to support a Lecture Series presented by the authors in Brussels (Belgium) and Stuttgart (Germany) on "Attitude Stabilization of Satellites in Orbit". Papers presented review the fundamental equations and various types of stabilization: spin, dual-spin, gravity gradient system and associated dampers, flywheels, P.T.O.	629.783: 629.7.058.47	AGARD Lecture Series No.45 North Atlantic Treaty Organization, Advisory Group for Aerospace Research and Development ATTITUDE STABILIZATION OF SATELLITES IN ORBIT Published September 1971 156 pages The material in this book has been collected to support a Lecture Series presented by the authors in Brussels (Belgium) and Stuttgart (Germany) on "Attitude Stabilization of Satellites in Orbit". Papers presented review the fundamental equations and various types of stabilization: spin, dual-spin, gravity gradient system and associated dampers, flywheels P.T.O.	629.783: 629.7.058.47
AGARD Lecture Series No.45 North Atlantic Treaty Organization, Advisory Group for Aerospace Research and Development ATTITUDE STABILIZATION OF SATELLITES IN ORBIT Published September 1971 156 pages The material in this book has been collected to support a Lecture Series presented by the authors in Brussels (Belgium) and Stuttgart (Germany) on "Attitude Stabilization of Satellites in Orbit". Papers presented review the fundamental equations and various types of stabilization: spin, dual-spin, gravity gradient system and associated dampers, flywheels, P.T.O.	629.783: 629.7.058.47	AGARD Lecture Series No.45 North Atlantic Treaty Organization, Advisory Group for Aerospace Research and Development ATTITUDE STABILIZATION OF SATELLITES IN ORBIT Published September 1971 156 pages The material in this book has been collected to support a Lecture Series presented by the authors in Brussels (Belgium) and Stuttgart (Germany) on "Attitude Stabilization of Satellites in Orbit". Papers presented review the fundamental equations and various types of stabilization: spin, dual-spin, gravity gradient system and associated dampers, flywheels P.T.O.	629.783: 629.7.058.47

magnetic torquers, thrusters, nutation dampers. Various sensors, and complete systems are described: ATS 5, TACSAT 1, Skylab B, Apollo, EOLE, PEOLE, SIRIO, OAO, TD.

The Lecture Series was under the sponsorship of the Guidance and Control Panel and the Consultant and Exchange Programme of AGARD.

magnetic torquers, thrusters, nutation dampers. Various sensors, and complete systems are described: ATS 5, TACSAT 1, Skylab B, Apollo, EOLE, PEOLE, SIRIO, OAO, TD.

The Lecture Series was under the sponsorship of the Guidance and Control Panel and the Consultant and Exchange Programme of AGARD.

magnetic torquers, thrusters, nutation dampers. Various sensors, and complete systems are described: ATS 5, TACSAT 1, Skylab B, Apollo, EOLE, PEOLE, SIRIO, OAO, TD.

The Lecture Series was under the sponsorship of the Guidance and Control Panel and the Consultant and Exchange Programme of AGARD.

magnetic torquers, thrusters, nutation dampers. Various sensors, and complete systems are described: ATS 5, TACSAT 1, Skylab B, Apollo, EOLE, PEOLE, SIRIO, OAO, TD.

The Lecture Series was under the sponsorship of the Guidance and Control Panel and the Consultant and Exchange Programme of AGARD.

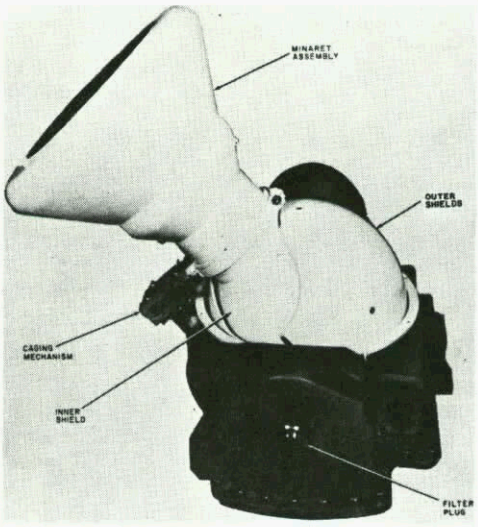

OAO Gimballed Star Tracker
Figure 7

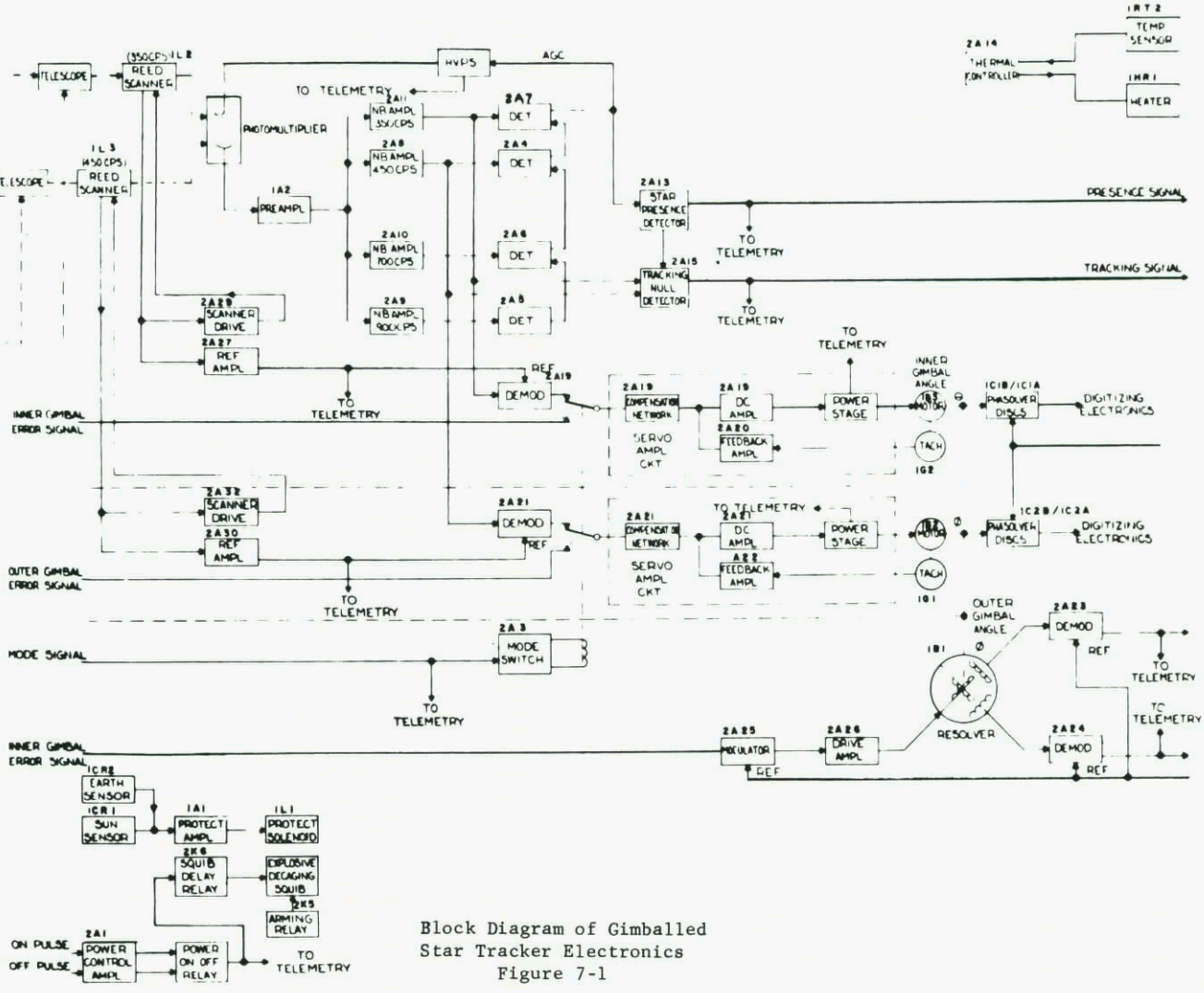

Block Diagram of Gimballed
Star Tracker Electronics
Figure 7-1

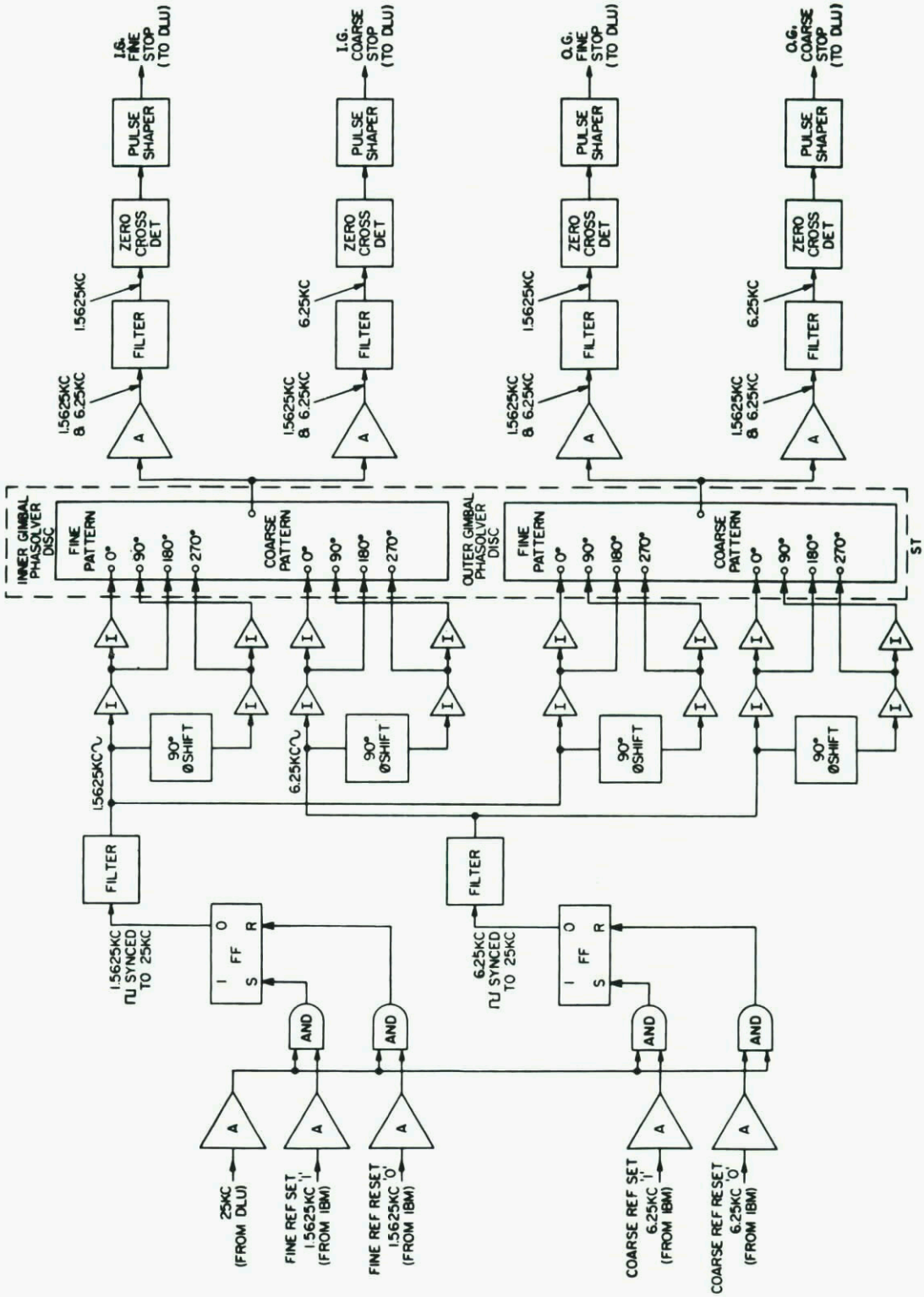

Block Diagram of Phasolver Electronics
For Gimballed Star Tracker
Figure 8

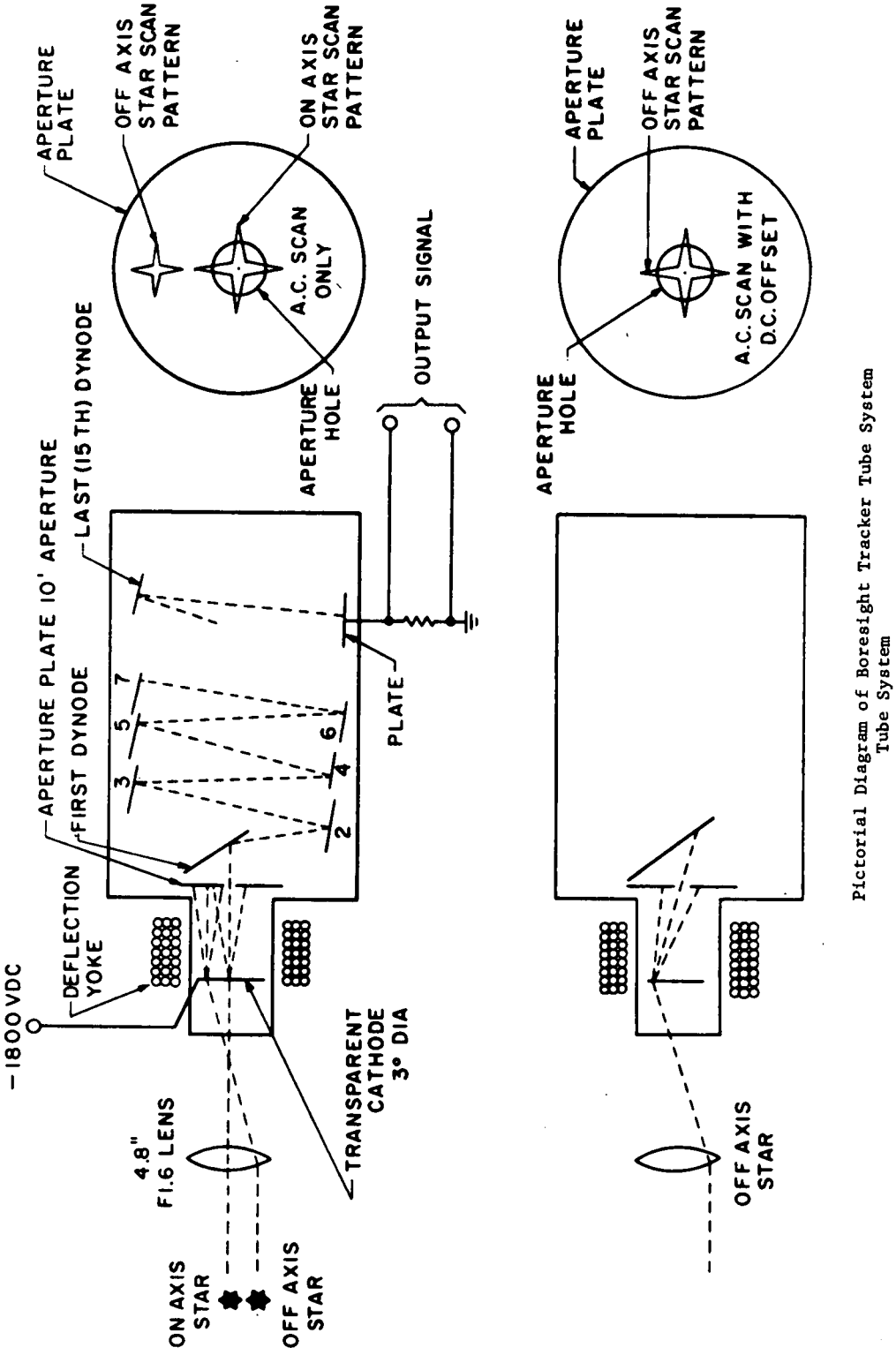

Pictorial Diagram of Boresight Tracker Tube System
Tube System
Figure 9

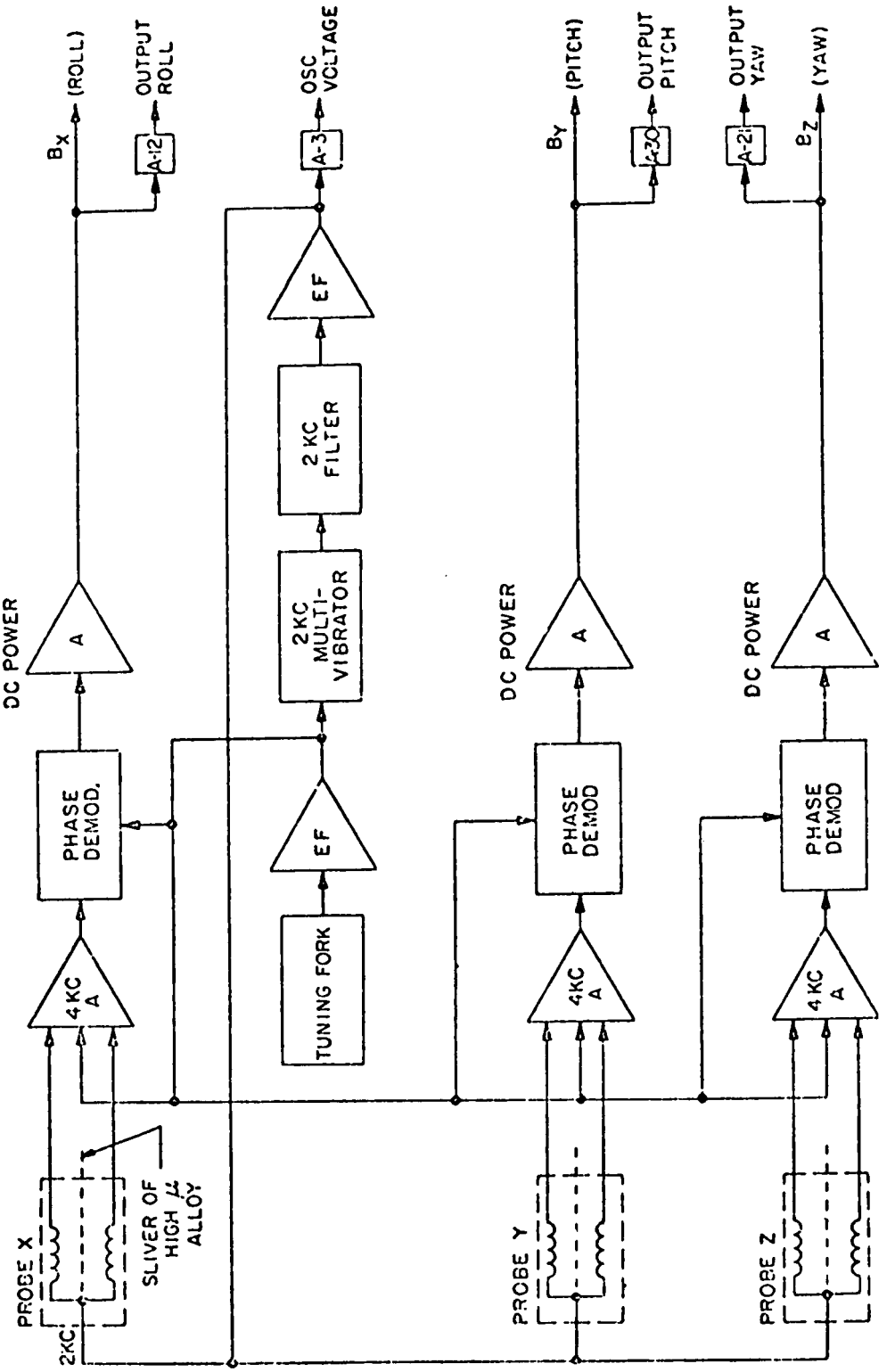

OAO Magnetometer System
Figure 10

PASSIVE AND SEMI-ACTIVE ATTITUDE STABILIZATIONS

by

P.W. Likins and P.Y. Willems

DUAL-SPIN SATELLITES

Pierre Y. Willems
Université de Louvain
Institut de Mécanique
300 Celestijnenlaan
B-3030 Héverlée, Belgium

Summary.

Dual-spin systems find space applications in missions for which the ability to point some instruments or a platform with a good spin stabilization is required. In this paper, the equations of motion of a deformable system including internal momenta are derived. The equilibrium configurations of such a system in free space and in an inverse square field are obtained. The attitude stability of a deformable gyrostat, a convenient idealization of a dual-spin satellite, is investigated. The effect of dissipation in both sections of the system is discussed and a rigorous method permetting the stability determination is set forth.

Introduction.

As only two lectures could be devoted to the problem of passive and semi-active attitude stabilizations of space vehicles in orbit and as a complete survey of the attitude stabilization problems would also have forced to superficiallity, it was decided to focus on developments of the last few years in the two areas of multiple-spin and flexible satellites. The behaviour of the spin stabilized and gravity stabilized vehicles will be investigated together as far as possible.

Systems operating without closed-loop control for the attitude will be considered here as passive (or possibly semi-active) systems. Active satellites can then be considered as passive systems when their controllers are not operating, during mission transfer for instance. For active satellites, the problems of attitude determination and control are of critical importance, but it is clear that for the systems considered here the dynamics play the most important role.

The first problem encountered is the problem of equilibrium with respect to a rotating reference frame. For a gravity stabilized vehicle this reference will be the orbital frame with one axis perpendicular to the plane of the orbit $\hat{\underset{\sim}{a}}_3$ and a second axis aligned with the local vertical, $\hat{\underset{\sim}{a}}_1$ (Fig. 1). For satellites spinning in free-space, the reference frame will have a constant angular velocity equal to the nominal angular velocity of the system $\underset{\sim}{\omega}_o = \omega_o \hat{\underset{\sim}{a}}_3$ (Fig. 2). The second problem which is even more important, is the problem of equilibrium stability.

These problems are well known for rigid bodies and equations of motion can be derived and solved exactly when the system is free space or orbiting on circular orbit in an inverse square field. Some generalizations were obtained for systems on elliptic orbit and when the effects of field harmonics are taken into account.

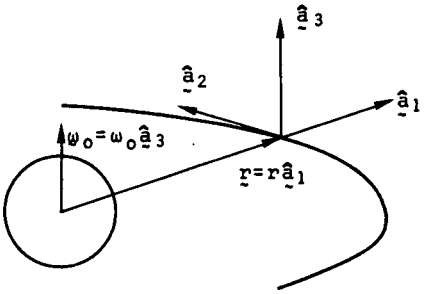

Fig. 1 Reference frame for a satellite on a circular orbit.

Soon it appeared that the description of the motion obtained from rigid body considerations was not sufficient, the effect of energy dissipation being ignored. The energy dissipation can be due to flexibility of the structure in the sense of continuum mechanics or can be obtained from damping mechanisms specially devised to eliminate the nutation. The effect of damping is even more important when the satellite includes an internal angular momentum or when dissipation occurs in sections with different angular rates, as is the case in multiple-spin vehicles.

These kind of satellites find application in missions for which the ability to point some instruments or a platform and to obtain large gyroscopic stability is required. For instance, dual-spin satellites are made up of two parts which are connected by a bearing permitting relative rotation. The slowly rotating part is usually named the platform, while the fast rotating part is termed the rotor. Such a configuration has been

used for Intelsat IV and TACSAT, the U.S. tactical communication satellite and was proposed for the ESRO-EBU television satellites. Dual-spin vehicles have also been used for scientific missions in the sun-pointing OSO series, were proposed for Ionospheric satellites and may have a large number of applications. These satellites permit the use of techniques and hardware that are similar to those of pure spinners and as it will be seen, permit passive stabilization for satellites with large length to diameter ratios. This has real advantages for the launching operation and could not be achieved with classical satellites.

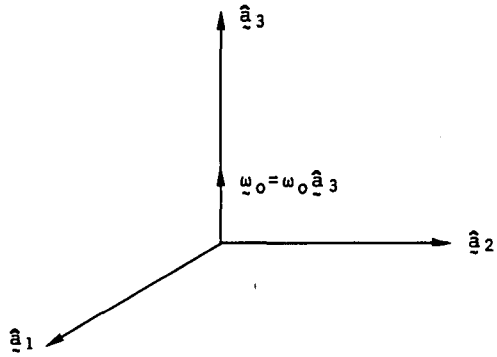

Fig. 2 Reference frame for a free spinning satellites.

The rotor is generally devised to have an axis of symmetry parallel to the bearing axis. A dual-spin satellite can then be idealized as a rigid gyrostat, i.e. a body with constant inertia configuration which includes some constant internal angular momentum. A further step is to consider the system as a flexible gyrostat if it is supposed that deformations take place in one part only. With this assumption, general analytical results can be obtained but they do not permit a complete description of the behaviour of the system.

Another difficult problem with dual-spin satellites is the bearing assembly which has to transfer power and signals, must operate almost without friction and resist mechanical loads. The flexibility of the bearing was the reason of the coning motion of TACSAT, although this motion remained within specification.

We will now show how to derive the equations of motion for a system which includes deformation, find the equilibrium configurations, show what can be concluded from the study of the deformable gyrostat, give some intuitive idea of the effect of energy dissipation in both sections of a dual-spin system and present a numerical method which permits a rather simple but rigorous way to solve the stability problem of a dual-spin system composed of two deformable sections.

Equations of motion and equilibrium.

Most papers treating the problem of interconnected bodies present the equations under the form of the Euler equations for each separate body [1], [2]. The number of equations can then exceed the total number of degrees of freedom and connection constraints have to be introduced [3], as it will be seen in the second part of this paper. Here the system is considered as one body which can have internal motion described by some deformation variables and the Euler-Liouville equations of the system are obtained. The additional equations are derived from the Lagrangian expressed in terms of the internal variables ; when all these variables have a determined motion or are cyclic (ignorable) the three rotational equations are sufficient to describe the motion.

Concerning the equilibrium, the system will be said in equilibrium with respect to the reference frame when all the non cyclic internal variables are equal to zero and when some "body-fixed" frame has the same angular velocity as the reference frame [4], [5].

The time derivative of the total angular momentum of the body with respect to some point is equal to the total torque applied about this point, when the point under consideration is fixed in inertial space or coincides with the centre of mass of the body (this relation is also exact in other very specific circumstances). When the reference point is the centre of mass, we have the vectorial relation,

$$\dot{\underset{\sim}{H}} = \underset{\sim}{L} \ , \qquad (1)$$

where $\underset{\sim}{H}$ is the total angular momentum with respect to the centre of mass,
$\underset{\sim}{L}$ is the resultant of external torques applied about the centre of mass.
By definition, $\underset{\sim}{H}$ is the integral over all the elements (dm) of the moment of momentum, or,

$$\underset{\sim}{H} = \int_{mt} \underset{\sim}{\rho} \times \dot{\underset{\sim}{\rho}} \, dm \ ,$$

$\underset{\sim}{\rho}$ being the position vector of dm with respect to the centre of mass (Fig. 3). The operator $(\dot{})$ applied to a vector means time derivative (with respect to some inertial space), mt is the set of elements of mass. The mass is considered as a measure and the formulation remains valid if the system is composed of continuous media, point masses, rigid parts or any of their combinaisons.

The vectors will be expressed in the "body-fixed" frame $\{\hat{\underset{\sim}{X}}_\alpha\}$ which will coincide with the reference frame at equilibrium. Then,

$$\underset{\sim}{H} = [\hat{\underset{\sim}{X}}_\alpha]^T H \ , \quad \underset{\sim}{\rho} = [\hat{\underset{\sim}{X}}_\alpha]^T \rho \ ,$$

where for operational purpose one defines a vector array or matrix $[\hat{\underset{\sim}{X}}_\alpha] \equiv [\hat{\underset{\sim}{X}}_1 \ \hat{\underset{\sim}{X}}_2 \ \hat{\underset{\sim}{X}}_3]^T$ with vector elements. The elements of the matrices H and ρ are then the components of $\underset{\sim}{H}$ and $\underset{\sim}{\rho}$ in the vector basis $\{\hat{\underset{\sim}{X}}_\alpha\}$.

The time derivative of $\underset{\sim}{\rho}$ will be

$$\dot{\underset{\sim}{\rho}} = \frac{d}{dt}\,\underset{\sim}{\rho} = \frac{d}{dt}\,[\hat{\underset{\sim}{X}}_\alpha]^T\rho + [\hat{\underset{\sim}{X}}_\alpha]^T \frac{d}{dt}\,\rho \ . \tag{2}$$

The velocity of a reference vector is due to its rotation and if the angular velocity of the vector frame is $\underset{\sim}{\omega}$, expressed as

$$\underset{\sim}{\omega} = [\hat{\underset{\sim}{X}}_\alpha]^T\,\omega \ ,$$

one has

$$\frac{d}{dt}\,[\hat{\underset{\sim}{X}}_\alpha]^T = \underset{\sim}{\omega} \times [\hat{\underset{\sim}{X}}_\alpha]^T = [\hat{\underset{\sim}{X}}_\alpha]^T\,\tilde{\omega} \ ,$$

where the 3×3 matrix $\tilde{\omega}$ is defined from the elements of the 3×1 matrix ω as,

$$\tilde{\omega} = \begin{bmatrix} 0 & -\omega_3 & \omega_2 \\ \omega_3 & 0 & -\omega_1 \\ -\omega_2 & \omega_1 & 0 \end{bmatrix} \ ,$$

the relation (2) can then be written

$$\underset{\sim}{\rho} = [\hat{\underset{\sim}{X}}_\alpha]^T\,(\tilde{\omega}\rho + \dot{\rho}) \ ,$$

the operator $(\dot{})$ applied to a matrix refers to the matrix with elements equal to the time derivation of the corresponding elements in the original matrix. This relation in written in vectorial notation in the well known form

$$\dot{\underset{\sim}{\rho}} = \underset{\sim}{\omega} \times \underset{\sim}{\rho} + \overset{\circ}{\underset{\sim}{\rho}} \ , \tag{3}$$

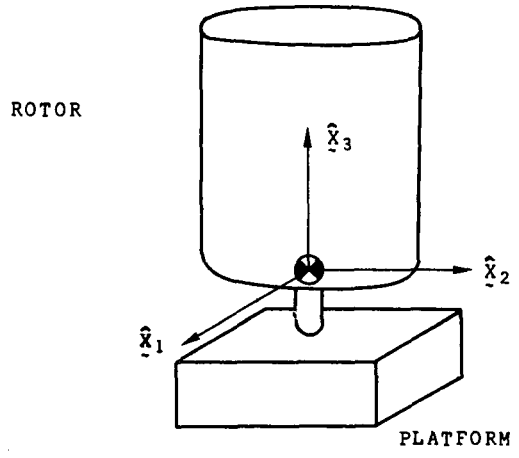

Fig. 3 Dual-spin vehicle

where the vector $\overset{\circ}{\underset{\sim}{\rho}}$ is defined as the vector with components equal to the time derivative of the elements of the matrix ρ or

$$\overset{\circ}{\underset{\sim}{\rho}} = [\hat{\underset{\sim}{X}}_\alpha]^T\,\dot{\rho} \ ,$$

this vector is referred as the "relative velocity" vector of $\underset{\sim}{\rho}$ with respect to the frame $\{\hat{\underset{\sim}{X}}_\alpha\}$.

The angular momentum vector can then be written,

$$\underset{\sim}{H} = \int \underset{\sim}{\rho} \times \overset{\circ}{\underset{\sim}{\rho}}\ dm + \int \underset{\sim}{\rho} \times \underset{\sim}{\omega} \times \underset{\sim}{\rho}\ dm \ .$$

One defines the inertia tensor of the body as

$$\underset{\sim}{J} = \int (\underset{\sim}{\rho}\cdot\underset{\sim}{\rho})E - \underset{\sim}{\rho}\underset{\sim}{\rho}\ dm \quad \text{or} \quad \underset{\sim}{J} = [\hat{\underset{\sim}{X}}_\alpha]^T\,J[\hat{\underset{\sim}{X}}_\alpha] \ , \tag{4}$$

where $\underset{\sim}{E}$ is a unit tensor and J is the inertia matrix of the system (with respect to the centre of mass) expressed in the $\{\hat{\underset{\sim}{X}}_\alpha\}$ basis and the internal angular momentum vector $\underset{\sim}{h}$ is defined as

$$\underset{\sim}{h} = [\hat{\underset{\sim}{X}}_\alpha]^T\,h = \int \underset{\sim}{\rho} \times \overset{\circ}{\underset{\sim}{\rho}}\ dm \ . \tag{5}$$

The internal angular momentum may include the angular momentum of rotors spinning at constant rates, with respect to the main structure. When the rotors are symmetric and are spinning with relative angular velocity $\underset{\sim}{\Omega}$ about the axis of symmetry, the corresponding internal angular momentum is equal to

$$\underset{\sim}{h}_r = I'\underset{\sim}{\Omega} = [\hat{\underset{\sim}{X}}_\alpha]^T\,h_r \ ,$$

where I' is the moment of inertia about the axis of symmetry and the norm of $\underset{\sim}{\Omega}$ is a constant. The angular velocity becomes then

$$\underset{\sim}{H} = \underset{\sim}{J}\cdot\underset{\sim}{\omega} + \underset{\sim}{h} \quad \text{or} \quad \underset{\sim}{H} = [\hat{\underset{\sim}{X}}_\alpha]^T\,(J\omega+h) = [\hat{\underset{\sim}{X}}_\alpha]^T\,H \ .$$

With

$$\underset{\sim}{L} = [\hat{\underset{\sim}{X}}_\alpha]^T\,L \ ,$$

the basic relation (1) becomes,

$$L = \dot{H} + \tilde{\omega}H \quad \text{or} \quad L = J\dot{\omega} + \tilde{\omega}J\omega + \tilde{\omega}h + \dot{J}\omega + \dot{h} \ . \tag{6}$$

This can also be written,

$$\underset{\sim}{L} = \underset{\sim}{J}\cdot\dot{\underset{\sim}{\omega}} + \underset{\sim}{\omega} \times \underset{\sim}{J}\cdot\underset{\sim}{\omega} + \underset{\sim}{\omega} \times \underset{\sim}{h} + \overset{\circ}{\underset{\sim}{J}}\cdot\underset{\sim}{\omega} + \overset{\circ}{\underset{\sim}{h}} \ . \tag{7}$$

Here too, the external torques can be considered as a vectorial measure or the torque distribution can be considered as a measurable function of the set of mass elements.

The gravitational torque in an inverse square field for a satellite on a circular orbit is equal to

$$\underset{\sim}{L} = 3\omega_0^2 \, \underset{\sim}{\hat{a}}_1 \times \underset{\sim}{J} \cdot \underset{\sim}{\hat{a}}_1 \ ,$$

where ω_0 is the orbital angular velocity,
$\underset{\sim}{\hat{a}}_1$ is the unit vector aligned with the local vertical.

If θ_{11}, θ_{12} and θ_{13} are the components of $\underset{\sim}{\hat{a}}_1$ in the frame $\{\underset{\sim}{\hat{a}}_\alpha\}$ and if, $\theta_1 = [\theta_{11} \ \theta_{12} \ \theta_{13}]^T$, the corresponding matrix L is

$$L = 3\omega_0^2 \, \tilde{\theta}_1 \, J \, \theta_1 \ .$$

We can already give the rigid body equilibrium conditions, as when all the internal variables are identically equal to zero and when the angular rate of the body is equal to the angular rate of the reference frame $\underset{\sim}{\omega}_0 = \omega_0 \, \underset{\sim}{\hat{a}}_3$ the rotational equations (7) are

$$\underset{\sim}{L} = \omega_0^2 \, \underset{\sim}{\hat{a}}_3 \times \underset{\sim}{J} \cdot \underset{\sim}{\hat{a}}_3 + \omega_0 \, \underset{\sim}{\hat{a}}_3 \times \underset{\sim}{h}_r \ . \tag{8}$$

The tensors $\underset{\sim}{h}_r$ and $\underset{\sim}{J}$ can be expressed in the $\{\underset{\sim}{\hat{a}}_\alpha\}$-frame as

$$\underset{\sim}{h}_r = \omega_0 \, J_\alpha \, \underset{\sim}{\hat{a}}_\alpha \quad , \quad \underset{\sim}{J} = J_{\alpha\beta} \, \underset{\sim}{\hat{a}}_\alpha \, \underset{\sim}{\hat{a}}_\beta = [\underset{\sim}{\hat{a}}_\alpha]^T \, I [\underset{\sim}{\hat{a}}_\alpha] \ .$$

For spinning systems in free space $\underset{\sim}{L} = 0$ and in the gravitational field $\underset{\sim}{L} = 3\omega_0^2 \, \underset{\sim}{\hat{a}}_1 \times \underset{\sim}{I} \cdot \underset{\sim}{\hat{a}}_1$. The relation (8) then implies that,

$$I_{12} = \alpha \quad , \quad I_{23} = -J_2 \quad , \quad I_{13} = -\alpha' J_1 \ ,$$

with $\alpha' = 1$ in free space and $\alpha' = 1/4$ in the gravitational field [6]. On orbit α must be equal to zero and in free space α can be set equal to zero without lacking generality. The inertia matrix is then

$$I = \begin{bmatrix} I_{11} & 0 & -\alpha J_1 \\ 0 & I_{22} & -J_2 \\ -\alpha J_1 & -J_2 & I_{33} \end{bmatrix} \ . \tag{9}$$

In general, dual-spin satellites will be designed to have $J_1 = J_2 = 0$ and then at equilibrium the reference axes will be the principal axes of the system. Nevertheless, it is important to note that other equilibria are possible as real systems will not be perfectly designed. The stability of these equilibrium configurations were discussed by various authors for rigid gyrostats [14], [15], [16] and also for deformable systems [8], [9].

The equations of deformation are derived from the Lagrange equation in the non cyclic variables β_ν :

$$\frac{d}{dt} \frac{\partial R}{\partial \dot{\beta}_\nu} - \frac{\partial R}{\partial \beta_\nu} + \frac{\partial W}{\partial \dot{\beta}_\nu} = Q_\nu \qquad (\nu = 1 \ldots n) \ , \tag{10}$$

where R is the Routhian function,
W the Rayleigh dissipation function,
Q_ν the generalized force for the variable β_ν.

The kinetic energy of rotation of the system (when there is no coupling between translation and rotation) is a scalar defined as

$$T = \frac{1}{2} \int \dot{\underset{\sim}{\rho}} \cdot \dot{\underset{\sim}{\rho}} \, dm \ .$$

Using (3) and the definitions (4) and (5), this energy can be written,

$$T = \frac{1}{2} \int \overset{\circ}{\underset{\sim}{\rho}} \cdot \overset{\circ}{\underset{\sim}{\rho}} \, dm + \underset{\sim}{\omega} \cdot \underset{\sim}{h} + \frac{1}{2} \, \underset{\sim}{\omega} \cdot \underset{\sim}{J} \cdot \underset{\sim}{\omega} \quad \text{or} \quad T = \frac{1}{2} \int \dot{\rho}^T \dot{\rho} \, dm + \omega^T h + \frac{1}{2} \, \omega^T J \omega \ .$$

The potential energy in the inverse square field is

$$V = -\frac{k}{r} \, m - \omega_0^2 \int \underset{\sim}{\rho} \cdot \underset{\sim}{\rho} \, dm + \frac{3}{2} \, \omega_0^2 \, \underset{\sim}{\hat{a}}_1 \cdot \underset{\sim}{J} \cdot \underset{\sim}{\hat{a}}_1 \ ,$$

or in matrix form,

$$V = -\frac{k}{r} \, m - \frac{1}{2} \, \omega_0^2 \, \mathrm{tr} J + \frac{3}{2} \, \omega_0^2 \, \theta_1^T \, J \, \theta_1 \ ,$$

where k is the gravitational constant,
m is the mass of the system,
tr meaning "trace of".

We already said that the body-fixed frame will coincide with the reference frame at equilibrium. In fact, we still have to define this frame with respect to the body itself. For systems of rigid bodies, it may be easier to fix the reference frame to one particular body referred to as the main body, then the reference point will not always coincide with the general centre of mass and additional terms should be added to the equations. This formalism permits the description of systems with large deformations but always relies on a particular configuration. One can also follow the actual principal axes of the system or axes such that the internal momentum vector $\underset{\sim}{h}$ is always equal to zero (Tisserand axes). But the orientation of these axes is defined by rather impracti-

cal equations. When deformations can be described by normal modes, one could take as reference the frame which follows the rigid modes, i.e. which is normal to the modes of deformation [7], but this implies that the deformations are small and that the system can be linearized. Systems composed of interconnected rigid bodies can not be described by this method.

Another "body fixed" frame, convenient for the determination of the attitude stability of deformable satellites and gyrostats, by the use of linearized equations, is a frame centered at the centre of mass, which is aligned, at equilibrium, with the desired orientation of the reference frame with respect to the body, and which is defined, during the motion, by the following conditions,

$$\int \underset{\sim}{u}\, dm = 0 \quad , \quad \int \underset{\sim}{x} \times \underset{\sim}{u}\, dm = 0 \quad , \tag{11}$$

where $\underset{\sim}{x}$ is the position vector of dm in undeformed configuration,
$\underset{\sim}{u}$ is the deformation vector,
the above vectors being determined when the rotors do not spin with respect to the body (Fig. 4), [8], [9]. The deformations can be expressed in terms of a set of n independant variables which are equal to zero at equilibrium. It should be noted that the deformations described by n arbitrarly chosen variables will not necessarily satisfy the relations (11). It is then sufficient to add six additional variables and consider (11) as a set of six constraints between the (n+6) variables. As it is assured that the variables are equal to zero at equilibrium, constant generalized forces will not appear in the equations and the Lagrange multipliers introduced will be of the order of the others variables. Consequently, the linearized system will be equivalent if the constraint equations are linearized. These constraints can then be integrated, six variables can be eliminated and the deformation can be expressed in terms of the n remaining variables β_ν.

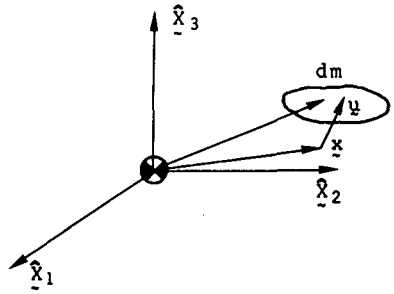

Fig. 4 Position vectors in body frame.

In order to simplify somewhat the formalism and to decrease the number of definitions, we will consider a system with one internal variable and which includes a single rotor. As only linear systems are considered, we have to keep quadratic terms in the variables in the expressions of the kinetic and potential energies. The inertia matrix will then have to be developped up to quadratic terms and will be written,

$$J = I + 2\Lambda\beta + \Pi\beta^2 \quad ,$$

where I is the inertia matrix of the system at equilibrium given by (9),
Λ and Π are 3×3 constant matrices functions of the shape of the deformations.

The components of the rotor angular momentum expressed in the frame $\{\hat{\underset{\sim}{X}}_\alpha\}$ will be written,

$$h_r = \omega_o[E + \tilde{\psi}\beta - \Psi\beta^2] \begin{bmatrix} J_1 \\ J_2 \\ J_3 \end{bmatrix} \quad \text{with} \quad \tilde{\psi} = \begin{bmatrix} 0 & -\psi_3 & \psi_2 \\ \psi_3 & 0 & -\psi_1 \\ -\psi_2 & \psi_1 & 0 \end{bmatrix}$$

where the 3×1 matrix ψ corresponding to $\tilde{\psi}$ and the 3×3 matrix Ψ are constant matrices.

It will be assumed that the dissipation function is a quadratic in $\dot{\beta}$, $W = 1/2\ Z\dot{\beta}^2$, and that the potential energy of deformation has the form,

$$U_d = \frac{1}{2} k\beta^2 + F\beta \quad .$$

At equilibrium, the dynamical potential has to be minimum and the equilibrium does not necessarily correspond to the equilibrium of the system outside the gravitational field with zero angular momentum.

The attitude of the frame $\{\hat{\underset{\sim}{X}}_\alpha\}$ with respect to the reference frame $\{\hat{\underset{\sim}{a}}_\alpha\}$ will be described by the rotation angles $\theta_1\theta_2\theta_3$, about 1, 2 and 3 axes respectively (Fig. 5). The angular velocity of $\{\hat{\underset{\sim}{X}}_\alpha\}$ can then be expressed in terms of the angular velocity of the reference frame and of the angles θ_α and their time derivatives.

If one defines the vector x as the vector array

$$x = [\theta_1\ \theta_2\ \theta_3\ \beta]^T \quad ,$$

the linearized equations (6) and (10) can be written in matrix form as

$$M\ddot{x} + G\dot{x} + Kx = -D\dot{x} \quad , \tag{12}$$

where M, K and D are symmetric matrices,
G is a skew-symmetric matrix.
Further an additional equilibrium condition is obtained.

The matrices M and D are

$$M = \begin{bmatrix} I & 0 \\ 0 & m \end{bmatrix} \qquad D = \omega_o \begin{bmatrix} 0 & 0 \\ 0 & Z \end{bmatrix} ,$$

where m is the generalized mass associated with β. When $J_1 = J_2 = 0$, the matrix G is equal to

$$G = \omega_o \begin{bmatrix} 0 & -(I_{11}+I_{22}-I_{33}-J_3) & 0 & 2\Lambda_{13}+J_3\psi_2 \\ I_{11}+I_{22}-I_{33}-J_3 & 0 & 0 & 2\Lambda_{23}-J_3\psi_1 \\ 0 & 0 & 0 & 2\Lambda_{33} \\ -(2\Lambda_{13}+J_3\psi_2) & -(2\Lambda_{23}-J_3\psi_1) & -2\Lambda_{33} & 0 \end{bmatrix} ,$$

and K is given by

$$K = \omega_o^2 \begin{bmatrix} I_{33}-I_{22}+J_3 & 0 & 0 & -(2\Lambda_{23}-J_3\psi_1) \\ 0 & a(I_{33}-I_{11})+J_3 & 0 & 2a\Lambda_{13}+J_3\psi_2 \\ 0 & 0 & b(I_{22}-I_{11}) & -2b\Lambda_{21} \\ -(2\Lambda_{23}-J_3\psi_1) & 2a\Lambda_{13}+J_3\psi_2 & -2b\Lambda_{21} & \Pi \end{bmatrix} ,$$

where for a free spinning system,

$$a = 1 \quad , \quad b = 0 \quad , \quad \Pi = \frac{K}{\omega_o^2} - \Pi_{33} + 2J_3\Psi_{33} ,$$

and for gravity stabilized satellite,

$$a = 4 \quad , \quad b = 3 \quad , \quad \Pi = \frac{K}{\omega_o^2} + 2\Pi_{11} - 2\Pi_{33} - \Pi_{22} + 2J_3\Psi_{33} .$$

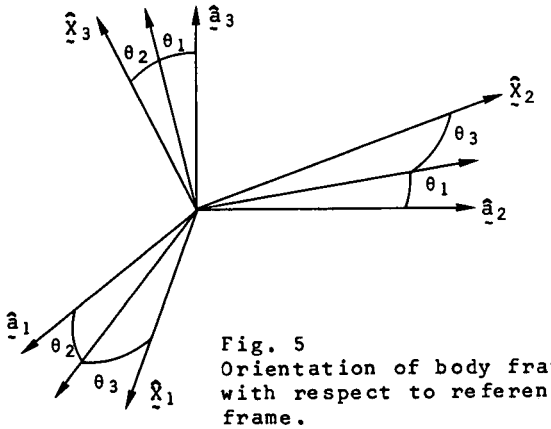

Fig. 5
Orientation of body frame with respect to reference frame.

The additional equilibrium condition is
- for a free spinning system : $\Lambda_{33} - F = 0$,
- for a gravity stabilized system : $-2\Lambda_{11} + \Lambda_{22} + 2\Lambda_{33} - F = 0$.

These conditions, together with the rigid gyrostat equilibrium conditions, can be considered as a set of algebraic relations between the system parameters. They can then be used to determine the equilibria. A system of two rigid bodies connected by a line hinge was investigated. Once the equilibrium is determined the matrices $\Lambda\ \Pi\ \psi\ \Psi$ can be derived and the stability can be obtained. Systems of several interconnected gyrostats could also be analyzed by this method.

Stability analysis.

The stability can be determined by the Liapunov method. The Hamiltonian of the system described by the system (12) is equal to,

$$H = \dot{x}^T M \dot{x} + x^T K x . \qquad (13)$$

Using (12), the time derivative along a trajectory of this quadratic function is

$$\dot{H} = - \dot{x}^T D \dot{x} .$$

The Hamiltonian can be used as a Liapunov function. The matrix D being semi definite positive, the positive definiteness of the Hamiltonian is a necessary and sufficient condition for stability when the damping is complete and a sufficient condition only, when damping is not complete [10], [11], [12]. Damping is said complete when there is no trajectory (in state space) different from a trivial solution $x \equiv 0$, along which the energy dissipation is identically equal to zero.

The stability of the linear system is obtained, and the stability of the corresponding nonlinear system can be derived from a theorem given by Liapunov which states that the system described by the equation

$$\dot{x} = Ax + f(x) ,$$

where $f(x)$ is a nonlinear function of x, such that,

$$\lim_{|x| \to 0} \frac{|f(x)|}{|x|} = 0$$

is asymptotically stable if the linearized system is asymptotically stable,
is unstable if the linearized system is unstable.
The stability of this system is determined by the nonlinear terms, only when the lineari-

zed system is neutrally stable.

The matrix M is positive definite by definition, the Hamiltonian will be positive definite when the matrix K is positive definite. From Sylvester's criterion, the determinants of all the principal minors of K have to be positive to have stability. For gravity stabilized systems, the damping is complete when all the variables are coupled to the variable β. The stability conditions are then as $\omega_o \neq 0$

$$I_{33} - I_{22} + J_3 > 0 \quad , \quad 4(I_{33}-I_{11}) + J_3 > 0 \quad , \quad I_{22} > I_{11} \quad , \quad |K| > 0 \ .$$

The first three conditions are sufficient conditions for an equivalent rigid gyrostat [13], [14], [15], [16]. For systems with complete damping they also become necessary [9]. The last condition depends on the deformations and is a function of the stiffness of the system. It must be noted that the value of the damping coefficient does modify the stability, for any positive value of this parameter the gyroscopic stability of the equivalent rigid gyrostat is destroyed. When J_3 is positive (internal angular momentum aligned with the orbital angular velocity) the presence of the rotor increases the stability.

It may be instructive to look at the stability conditions when the body degenerates to a single rigid rotor, i.e. when $I_1 = I_2$ and $J_3 = I_3 R$, where R is the normalized angular velocity of the satellite.

The first two conditions are then,

$$(1-K)R - K > 0 \quad , \quad (1-K)R - 4K > 0 \ ,$$

where $K = \dfrac{I_1-I_3}{I_1}$.

The damping is not complete in this case. Further, the third condition is not satisfied, only sufficient conditions are then obtained. These conditions are obtained in the literature [17], [18] for a spinning satellite.

For spin stabilized systems, the damping is not complete. In fact, if initial conditions modify the total angular momentum, the satellite will be in equilibrium for some constant values of θ_1 θ_2 and θ_3. The positive definiteness of K provides only sufficient conditions. If $\Lambda_{33} = 0$, the system will be only partially stable in θ_1 θ_2 β as K will be only semi-definite, this can be understood as a drift can occur for the variable θ_3, the equation in θ_3 being uncoupled to the others. In this case the equilibrium for the variable β is the same as the equilibrium for the non spinning system.

The sufficient stability conditions are

$$\omega_o^2(I_{33}-I_{22}+J_3) > 0 \quad , \quad \omega_o^2(I_{33}-I_{11}+J_3) > 0 \quad , \quad |K| > 0 \ .$$

If necessary conditions have to be obtained, one must constrain the system to keep its total angular momentum [19], [20]. These constraints must hold for initial conditions and then also for every point on the trajectory. Their introduction permits the elimination of some variables and new (necessary and sufficient) stability criteria are obtained.

The angular momentum must remain constant in the $\{\hat{\underset{\sim}{a}}_\alpha\}$-frame. As $\hat{\underset{\sim}{a}}_3$ is aligned with the nominal value of $\underset{\sim}{H}$, the components along $\hat{\underset{\sim}{a}}_1$ and $\hat{\underset{\sim}{a}}_2$ must be identically equal to zero.

In linear approximation these conditions are

$$H_1 + \theta_2 H_3 = 0 \quad , \quad H_1 - \theta_1 H_3 = 0 \ ,$$

or

$$\begin{aligned} I_{11}\dot{\theta}_1 + (I_{33}-I_{11}+J_3)\omega_o\theta_1 + (2\Lambda_{13}+J_3\psi_2)\omega_o\beta = 0 \ , \\ I_{22}\dot{\theta}_2 - (I_{33}-I_{11}+J_3)\omega_o\theta_1 + (2\Lambda_{23}-J_3\psi_1)\omega_o\beta = 0 \ . \end{aligned} \qquad (14)$$

The variables $\dot{\theta}_1$ and $\dot{\theta}_2$ can be eliminated and the Hamiltonian (13) can be expressed in terms of θ_1 θ_2 β (and $\dot{\beta}$). The positive definiteness of H will then be a necessary and sufficient condition for stability.

Let us now specialize to a system composed of two symmetrical rotors spinning about their common axis of symmetry with different angular rates (such a system is completely symmetric) with $I_{11} = I_{22} = I$. If one defines

$$\Lambda = \frac{I_{33}-I+J_3}{I} \quad , \quad A = \frac{2\Lambda_{13}+J_3\psi_2}{I} \quad , \quad B = \frac{2\Lambda_{23}-J_3\psi_1}{I} \ ,$$

$$\mu = \frac{m}{I\omega_o^2} \quad , \quad \xi = \frac{Z}{I\omega_o^2} \quad , \quad \kappa = \frac{\pi}{I} \ . \qquad (15)$$

The sufficient conditions for stability (K definite positive) are,

$$\omega_o^2\Lambda > 0 \quad , \quad \omega_o^2(\kappa\Lambda - A^2 - B^2) > 0 \ .$$

The constraints can be written,

$$\dot{\theta}_1 = -\Lambda\omega_o\theta_2 - A\omega_o\beta \quad , \quad \dot{\theta}_2 = +\Lambda\omega_o\theta_1 - B\omega_o\beta \ .$$

The Hamiltonian expressed in terms of, θ_1 θ_2 β and $\dot{\beta}$, can be written as :

$$H = x'^T K' x' \ ,$$

with $x'^T = [\theta_1 \ \theta_2 \ \beta \ \dot{\beta}]$, and

$$K' = \omega_o^2 \begin{bmatrix} \Lambda(1+\Lambda) & 0 & -B(1+\Lambda) & 0 \\ 0 & \Lambda(1+\Lambda) & A(1+\Lambda) & 0 \\ -B(1+\Lambda) & A(1+\Lambda) & \kappa+A^2+B^2 & 0 \\ 0 & 0 & 0 & \mu \end{bmatrix} .$$

The necessary and sufficient stability conditions are now

$$\omega_o^2\mu > 0 \quad , \quad \omega_o^2\xi > 0 \quad , \quad \omega_o^2\Lambda(1+\Lambda) > 0 \quad , \quad \omega_o^2\Lambda(\Lambda\kappa-A^2-B^2) > 0 \ . \tag{16}$$

The first condition is always satisfied μ being a generalized mass. The second is obvious for mechanically damped systems. The third condition depends only on the equivalent rigid system parameters and the fourth can be considered as a condition on the stiffness necessary to maintain "internal stability". The condition $\Lambda(\Lambda+1) > 0$ can then be considered as the critical stability condition. Recalling the definitions (15) and that of J_3 this condition can be written,

$$\omega_o^2\left(\frac{I_{33}}{I} + \frac{I'}{I}\frac{\Omega}{\omega_o}\right)\left(\frac{I_{33}}{I} + \frac{I'}{I}\frac{\Omega}{\omega_o} - 1\right) > 0 \ . \tag{17}$$

When the platform does not spin ($\omega_o = 0$), the system is always stable, if the internal stiffness is sufficient and if there is some damping device on the platform and no energy dissipation in the rotor.

For such a system one could be interested in the stability with respect to the variables ω_1 ω_2 and β and not with respect to a fixed orientation. This is the case if the system includes some active controllers which restore the orientation if some change in angular momentum occurs.

The rotational equations become with the above assumptions and definitions :

$$\dot{\omega}_1 + \Lambda\omega_o\omega_2 + A\omega_o\dot{\beta} - B\omega_o^2\beta = 0 \quad , \quad \dot{\omega}_2 - \Lambda\omega_o\omega_1 + B\omega_o\dot{\beta} + A\omega_o^2\beta = 0 \quad ,$$
$$\mu\ddot{\beta} + \xi\dot{\beta} + \kappa\beta - A\frac{\omega_1}{\omega_o} - B\frac{\omega_2}{\omega_o} = 0 \ .$$

The characteristic equation of this system is

$$\mu s^4 + \xi s^3 + (\kappa+A^2+B^2+\mu\omega_o^2\Lambda^2)s^2 + \Lambda^2\xi\omega_o^2 s + \omega_o^2\Lambda(\Lambda\kappa-A^2-B^2) = 0 \ .$$

The necessary and sufficient stability conditions for this linear system are given by the Routh-Hurwitz rule and are,

$$\mu > 0 \quad , \quad \zeta > 0 \quad , \quad \kappa + A^2 + B^2 > 0 \quad , \quad \omega_o^2\Lambda(\Lambda+1) > 0 \quad , \quad \omega_o^2\Lambda(\Lambda\kappa-A^2-B^2) \quad 0 \ .$$

The condition $\kappa+A^2+B^2 > 0$ will always be satisfied, when the others are satisfied and, as could be expected, the stability conditions are the same as the onesprovided by the Liapunov method for completely damped systems. The conditions are equivalent to those obtained for particular cases in [21], [22].

Now let us recall that for the symmetrical system under consideration, we arbitrarily took one body as the platform, the other being the rotor. If we now choose the second body as the deformable platform, derive the equations and obtain their stability, we shall obtain the stability of a dual-spin satellite with energy dissipation in the rotor only. Such changes of definition involve the substitution of $\omega_{30} + \Omega$ for ω_{30}, $-\Omega$ for Ω, $I_{33} - I'$ for I', but the parameters describing the shape of deformation of the two cases can be unrelated as we will assume that in both cases the stiffness is sufficient to maintain "internal stability".

The modified stability condition becomes, when the rotor has some inertial angular velocity,

$$\left(\frac{I_{33}}{I}\omega_o + \frac{I'}{I}\Omega\right)\left[\left(\frac{I_{33}}{I} - 1\right)\omega_o + \left(\frac{I'}{I} - 1\right)\Omega\right] > 0 \ . \tag{18}$$

This condition differs from (17) and it can be concluded that systems which are stable when damping is associated to the platform only, can be unstable when damping occurs in the rotor only. When the platform remains inertially fixed, the condition (18) reduces to

$$\Omega^2\frac{I'}{I}\left(\frac{I'}{I} - 1\right) > 0 \ .$$

The system will be stable if $I'/I > 1$ or

$$I' > I \ , \tag{19}$$

unstable if $I'/I < 1$, i.e. when the moment of inertia of the rotating part is smaller than the transverse moment of inertia of the total system.

In space applications, dual-spin systems have an almost non spinning platform (one revolution per day for geostationary communication satellites, one revolution per year for a solar cells package) and have a large length to diameter ratio (such that $I' < I$). For such systems a damping device on the platform will have a stabilizing effect and damping

in the rotor will tend to destabilize the system. Unfortunately, there is always energy dissipation in the rotor, due to structure flexibility, bearing bending or due to the presence of fuel containers. The effect of the energy dissipation must then be compensated by the effect of a platform damper. The above stability criteria do not provide the time constants involved in the problem.

Only particular systems may be analyzed from the theory of linear equations with constant coefficients if damping exists in both sections. Probably, the most instructive example is provided by a symmetric dual-spin system with a flexible bearing assembly. In this system, it is assumed that the inertia configuration of both sections remains constant (in the considered body frame) (Fig. 6). If the relative orientation of the bearing axis in the rotor and in the platform is described by two angles $\beta_1\beta_2$, it can be seen that the Rayleigh function associated with the dissipation in the platform has the form

$$R_c = \frac{1}{2} c(\dot{\beta}_1^2 + \dot{\beta}_2^2) ,$$

where c is the corresponding damping coefficient. Dissipation can exist in the rotor even when the angles β_1 and β_2 remain constant as the part of the bearing associated with the rotor spins with relative angular velocity Ω. The corresponding deformation ratios are then equal to $-\Omega\beta_1$ and $\Omega\beta_2$, and the Rayleigh function associated with the rotor part of the bearing will have the form

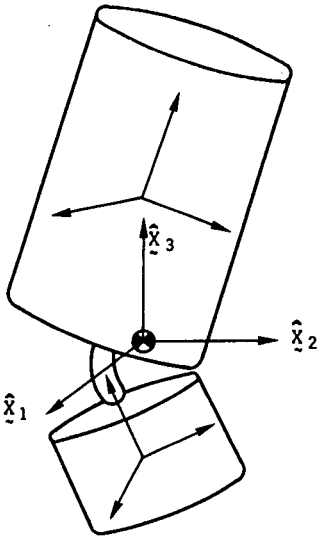

Fig. 6 Dual-spin system with flexible bearing.

$$R_{c'} = \frac{1}{2} c' [(\dot{\beta}_1+\Omega\beta_2)^2 + (\dot{\beta}_2-\Omega\beta_1)^2] ,$$

where c' is the corresponding damping coefficient.

If a proper "body-fixed" frame is chosen, the equations of motion will have a form similar to (12), but additional terms due to "constraint damping forces" derived from $R_{c'}$ will now be present. The system can then be written under the form [20], [25],

$$M\ddot{x} + G\dot{x} + Kx + Fx = -D\dot{x} ,$$

where, as previously, M and K are symmetrical matrices, G is a skew symmetric matrix but where the "constraint damping" matrix F is skew-symmetric.

The Hamiltonian is not a suitable Liapunov function and a modified function can be used as test function [20]. If the constant angular momentum constraint is introduced necessary and sufficient stability conditions can be obtained. These conditions are now functions of the damping coefficients c and c'. For a system with inertial platform with sufficient internal stiffness, the stability condition then reduces to,

$$I' - \frac{c'}{c+c'} I > 0 .$$

It must be noted that when $c = 0$ (no damper in the platform) this condition reduces to the condition obtained previously for the gyrostat with dissipation in the rotor (19). The condition is always satisfied when $c' = 0$, this was expected from gyrostat considerations.

When the rotor also has some deformation, the equations of motion will not necessarily have constant coefficients. For instance, the inertia tensor of the rotor expressed in the body frame will vary during the rotation if the rotor does not remain symmetric. If one assumes that the relative angular velocity of the rotor is constant, and this can be achieved by some control even within the scope of "passive" stabilization, the time varying coefficient will be periodic. The linearized system which provides the information on the stability will then have the form of a system of coupled Hill's equations. The stability of this system can be determined by the Floquet analysis [22] and we will now show how this method can be used practically.

By a proper choice of reference axes and after some linear transformations, the system can be written under the form

$$\dot{X} = A(t)X , \qquad (20)$$

where X is a m vector,
$A(t)$ is a periodic matrix of period T, with $A(t+T) = A(t)$. The matrix equation

$$\dot{Z} = A(t)Z , \qquad (21)$$

where Z is a m × m matrix, is associated to (20).

If $\Phi(t)$ is the fundamental matrix of (21), such that $\Phi(0) = E$ one has $Z(t) = \Phi(t)Z_0$. The matrix $\Phi(t+T)$ is also a fundamental matrix and

$$\Phi(t+T) = \Phi(t)\,\Phi(T) \ ,$$

where the matrix $\Phi(T)$ is a non singular constant matrix which can be written under the form

$$\Phi(T) = e^{RT} \ .$$

It is then shown that the matrix $P(t) = \Phi(t)e^{-Rt}$ is periodic with period T as $P(t+T) = P(t)$ and the solution $\Phi(t)$ can be written as $\Phi(t) = P(t)e^{Rt}$.

It is then sufficient to determine the value of the principal fundamental matrix over one period of time. Then $\Phi(T)$ is know and the matrix R can be computed. The function $P(t)$ is then determined over the period, and as $P(t)$ is periodic, the complete behaviour of $\Phi(t)$ is known.

If λ are the eigenvalues of $\Phi(T)$, such that $(\Phi(T) - \lambda E)\bar{x} = 0$, the eigenvectors $\bar{x}$ will have the property

$$\bar{x}(t+T) = \lambda\bar{x}(t) \ .$$

As the vectors $\bar{x}(0)$ form a base for the solution of the system, it is clear that the norm of the λ must be smaller than one to have stability. If the equations are integrated over one period and if the eigenvalues of the principal fundamental matrix are obtained, the stability problem is solved. This considerably simplify the solution of the problem with computers as only a reduced number of integration steps is required.

It is clear that an idea of the stability of system (20) can be obtained from approximate methods. Particular dual-spin problems were investigated by use of averaging method [25], [26], by the infinite determinant method [27] or an analytical method derived from the Floquet analysis [28], [29].

To complete the review of dual-spin attitude stability, one must mention the "energy-sink" method which helped a lot in the acceptance of the dual-spin concept. This method is based on the fact that a system with constant angular momentum will tend to dissipate energy until it reaches a state of minimal kinetic energy. This method is familiar to people working in physics and was applied in astronomical problems and for gyroscope design. V. Landon was the first to apply the method to space vehicles even before the first artificial satellite was launched but published his results in 1964 only, in a paper on the stability of axi-symmetric body containing a rotor. The method was also used by Iorillo [26]. A nice interpretation of this analysis is provided in [30] where the effect of the bearing motor is also considered.

Using this method, it is concluded that a symmetrical dual-spin satellite will be stable in free space when

$$\frac{P_p}{A\omega_o} + \frac{P_r}{A\omega_o - \Omega} < 0 \ ,$$

where P_p and P_r are equal to the time average of the energy dissipation rate in the platform and rotor respectively. This criterion is quite satisfactory when the internal stiffness is sufficient to maintain stability and when the presence of deformation do not sensibly modify the natural frequency of the system.

Conclusion.

The attitude stability of dual-spin satellites has been widely investigated and the feasibility of the system has been proved. Nevertheless, a large number of problems remains to be solved.

For instance, the motion of fuel in cavities included in the rotor is described by partial differential equations and, considering some integrals of motion, one could obtain partial stability conditions for the attitude variables.

One can achieved an attitude control by use of an intentionally off-set platform. The rotational equations about the spin axes are then coupled with the attitude equations and the spin controllers could achieve attitude stabilization.

The methods presented here could easily be applied to multiple-spin systems and in particular to triple-spin satellites. Such a configuration has some advantages if one likes to use the pure spinners technology with earth oriented platform and an oriented solar cells package.

The study of flexible bearings can be extended to cases where the bearing stiffness is nonlinear or piecewise linear.

One should also investigate more deeply the behaviour of the system during despin or spin-up operations and also during the active part of orbit transfer when the mass of the system may not be considered as constant.

These studies are a difficult mathematical challenge but are of immediate practical applications.

References.

[1] Hooker, W.W. and G. Margulies, "The Dynamical Attitude Equations for an n-Body Satellite", *J. Astronaut. Sci.*, 12, 1965.

[2] Roberson, R.E. and J. Wittenburg, "A Dynamical Formalism for an Arbitrary Number of Interconnected Rigid Bodies, with Reference to the Problem of Satellite Attitude Control", *Proc. of the 3d Int. Cong. of Automatic Control*, (London, 1966), Butterworths and Co, London, 1967.

[3] Hooker, W.W., "A Set of r Dynamical Attitude Equations for an Arbitrary n-Body Satellite having r Rotational Degrees of Freedom", *AIAA J.*, 8, 1970.

[4] Likins, P.W. and R.E. Roberson, "Uniqueness of Equilibrium Attitudes for Earth-Pointing Satellites", *J. of Astronaut. Sci.*, 13, 1966.

[5] Willems, P.Y., "Attitude Stability of Deformable Satellites", in *"Attitudes Changes and Stabilization of Satellites"*, (Proc. of CNES Int. Conf., Paris, 8-11 Oct. 1968), Paris, 1968.

[6] Roberson, R.E. and W.W. Hooker, "Gravitational Equilibria of a Rigid Body Containing Symmetric Rotors", *Proc. of the 17th Cong. Int. Astronaut. Fed.*, (Madrid, 1966), Paris, 1967.

[7] Buckens, F., "The Influence of the Elasticity of Components on the Attitude Stability of a Satellite", *Proc. of the 5th Int. Symp. on Space Techn. and Sci.*, Tokyo, 1963.

[8] Willems, P.Y., "Dual-Spin Satellites considered as Deformable Gyrostats", *Proc. of the 8th Int. Symp. on Space Techn. and Sci.*, Tokyo, Aug. 1969.

[9] Willems, P.Y., "Stability of Deformable Gyrostats on a Circular Orbit", *J. of Astronaut. Sci.*, 18, 1970.

[10] Zajac, E.E., "The Kelvin-Tait-Chetaev Theorem and Extensions", *J. of Astronaut. Sci.*, 11, 1964.

[11] Zajac, E.E., "Comments on Stability of Damped Mechanical Systems and Further Extensions", *AIAA J.*, 3, 1965.

[12] Pringle, R., Jr, "On the Stability of a Body with Connected Moving Parts", *AIAA J.*, 4, 1966.

[13] Anchev, A.A., "Fly Wheel Stabilization of Relative Equilibrium of a Satellite", *Kosmicheskie Issledovaniya*, 4, 1966.

[14] Rumiantsev, V.V., "On the Stability of Stationary Motion of a Satellite with a Rotor and Cavity Containing Fluid", *Kosmicheskie Issledovaniya*, 5, 1967.

[15] Rumiantsev, V.V., "On Stability of Stationary Motions of the Gyrostat-Satellite", *Proc. of the 18th Cong. Int. Astronaut. Fed.*, Beograd, 1967.

[16] Roberson, R.E., "Stability of Orbiting Gyrostats in the Elementary Cases", *Ing. Archiv.*, 39, 1970.

[17] Thomson, W.T., "Spin Stabilization of Attitude against Gravity Torque", *J. of Astronaut. Sci.*, 9, 1962.

[18] Kane, T.R., E.L. March and W.G. Wilson, "Letter to the Editor", *J. of Astronaut. Sci.*, 9, 1962.

[19] Pringle, R., Jr, "Stability of the Force Free Motions of a Dual-Spin Spacecraft", *AIAA J.*, 7, 1969.

[20] Mingori, D.L., "Stability of Linear Systems with Constraint Damping and Integrals of the Motion", *Proc. of the 21st Cong. Int. Astronaut. Fed.*, 1970.

[21] Likins, P.W., "Attitude Stability Criteria for Dual-Spin Spacecraft", *J. of Spacecraft and Rockets*, 4, 1967.

[22] Mingori, D.L., "Attitude Stability of Dual-Spin Satellites", *AIAA J.*, 7, 1969.

[23] Likins, P.W., "Stability Analysis of Mechanical Systems with Constraint Damping", *AIAA J.*, 5, 1967.

[24] Willems, P.Y., "Effect of Bearing Flexibility on Dual-Spin Attitude Stability", to appear.

[25] Iorillo, A.J., "Nutation Damping", *Hughes Aircraft Co*, Doc. I.D.C. 2230, 14/69, 1964.

[26] Iorillo, A.J., "Nutation Damping Dynamics of Axisymmetric Rotor Stabilized Satellites", *ASME Ann. Winter Meeting*, Chicago, 1965.

[27] Lingh, K. and P.W. Likins, "Infinite Determinant Method for Stability Analysis of Periodic Coefficient-Differential Equations", *AIAA J.*, 8, 1970.

[28] Willems, P.Y., "Attitude Stability of Dual-Spin Satellites", *ESRO CR*, to appear.

[29] Cloutier, G., "Nutation Damper Instability on Spin Stabilized Spacecraft", *AIAA J.*, 7, 1969.

[30] Brewer, M., R. Bushell, J. Holt and N. Swift, "A Study of Dual-Spin Stability", *ESRO CR*, 24, 1970.

PASSIVE AND SEMI-ACTIVE ATTITUDE STABILIZATIONS – FLEXIBLE SPACECRAFT

by

Dr. Peter W. Likins
Associate Professor
4731 Boelter Hall
University of California, Los Angeles
Los Angeles, California
USA 90024

Summary

The influence of spacecraft nonrigidity is identified as the pre-eminent current problem in attitude stabilization of passive and semi-active spacecraft. Attitude control anomalies in the flight histories of eight satellites are attributed to nonrigidity, manifested either as unexpected internal energy dissipation or unanticipated structural deformations. Recent progress in the development of methods for analysis of flexible spacecraft is surveyed, with attention to discrete coordinate methods, vehicle normal coordinate methods, and hybrid coordinate methods. New results are provided for each of these analytical procedures, and the utility of these results is discussed in the context of anticipated future spacecraft.

Introduction

In the early days of space exploration, the classification of a satellite by its attitude stabilization scheme was not a difficult matter; a satellite was actively stabilized if the control system utilized an energy source, sensors, and artificial feedback control, and it was passively stabilized if it had none of these features. There was little need for additional categories of classification. Passive vehicles were either spin-stabilized or gravity-stabilized, and in either case the satellite was almost invariably idealized for dynamic analysis as a rigid primary body with a viscoelastically connected secondary body for internal damping. We were able to accomplish much of our analysis literally, without numerical computations, and we learned a great deal about the behavior of highly idealized spacecraft.

Today we must function in a much more complicated technological environment. The distinction between active and passive control systems has been blurred by the introduction of semi-passive systems (which require energy but lack artificial closed-loop control) and semi-active systems (which utilize energy-consuming, closed-loop control about one or two axes but not all three). These labels are not used uniformly by all, but even if they were universally adopted the ambiguities would not disappear. Virtually all spin-stabilized spacecraft today have the capability of occasional periods of active control for angular momentum reorientation, and many gravity-stabilized spacecraft include active controllers for periods of high pointing accuracy. Where does one draw the line between a "passive" vehicle subject to occasional active control and an "active" spacecraft with an on-off controller, when the only difference is in the frequency of actuation of the active controllers? Moreover, what has happened to the old distinction between spin-stabilized and gravity-stabilized satellites? What distinguishes a "spin-stabilized" satellite with an earth-pointing despun platform of a configuration with a stabilizing gravity torque from a "gravity-stabilized" satellite with a rotor along the pitch axis? Either vehicle might be called a dual-spin satellite with an earth-pointing platform, and although this configuration has a significant role for today and tomorrow, it simply does not fit into any of the simple classifications of yesterday.

We must not get trapped into a pre-occupation with labels, but must get on with the business of solving the problems posed by modern spacecraft. In preparing these lectures, Dr. Willems and I therefore resolved to shed the artificial constraints presented by the original lecture titles, so that we could focus sharply on what we consider to be the crucial problems of the day.

I have no hesitation in identifying the influence of spacecraft nonrigidity as the spacecraft attitude control problem receiving the greatest attention in the United States today. This then becomes the central topic of this lecture, which will trace the past, describe the present, and project the future of the problem of attitude stabilization of nonrigid spacecraft, with emphasis on those vehicles traditionally considered passive or semi-active.

The lessons of experience

The influence of spacecraft nonrigidity on attitude control takes two rather distinct forms: i) internal energy dissipation, and ii) structural flexibility. Although both elements are present in all spacecraft, and separation of these two aspects of the problem is only an analytical convenience, it appears to simplify our understanding to consider these phenomena separately.

The problem of attitude instability due to vehicle nonrigidity is as old as our space program. As you are all aware, the first U. S. satellite, Explorer I, shown in Fig. 1, did not persist in the intended state of spin about its symmetry axis, but soon tumbled end over end. The explanation (1) for this anomalous behavior lay in the flexibility of the small wire turnstile antennas shown protruding from the cylindrical housing of the vehicle; the mass of these antennas is so small that the instability could not be explained in terms of elastic antenna vibrations alone, but only as a consequence of the ensuing energy dissipation.

The list of satellites that exhibited some degree of anomalous attitude behavior due to dissipativity and/or flexibility (2) covers the entire time span of our space program. Beginning with Explorer I in 1958, the list includes Alouette I (Ref. 3) in 1962, 1963-22A (Ref. 4) in 1963, Explorer XX (Ref. 3) in 1964, OGO III (Ref. 5) in 1966, OV1-10 (Ref. 6) in 1966, Tacsat 1 (Ref. 7) in 1969, ATS 5 in 1969, and probably others as well (see Figs. 1-8). Some of these vehicles maintained attitude within mission specifications (e. g. Tacsat 1 and 1963-22A), and in other cases some mission objectives were met despite the unexpected loss of attitude control. In every case, however, post-flight analysis and/or test revealed a probable explanation of attitude anomalies in terms of vehicle nonrigidity (see Table 1).

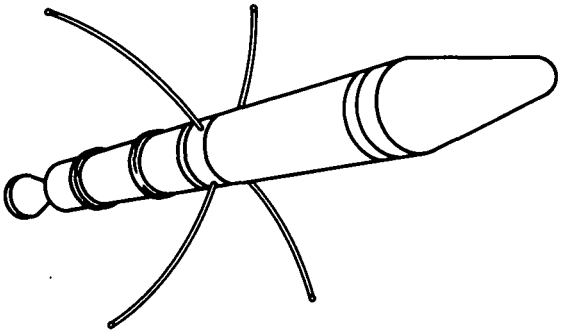

Fig. 1. Explorer I

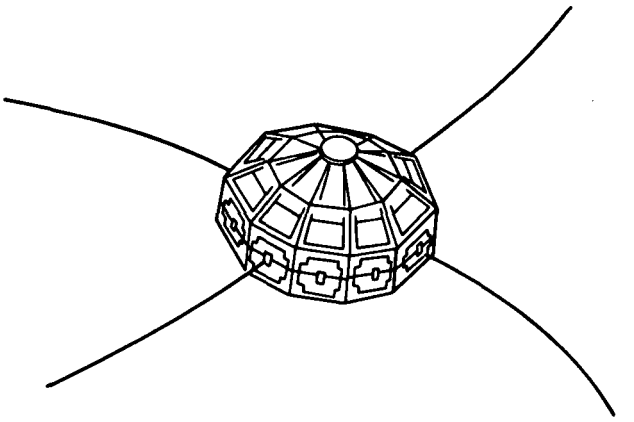

Fig. 2. Alouette I

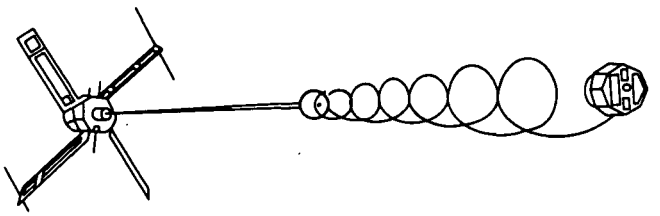

Fig. 3. 1963-22A

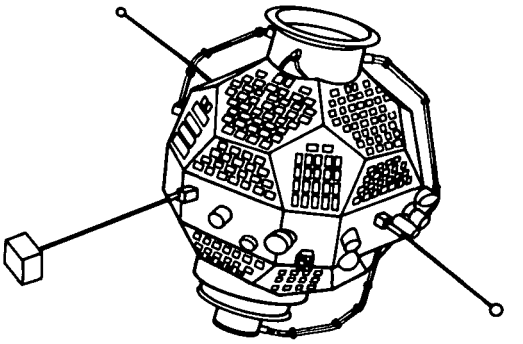

Fig. 4. Explorer XX

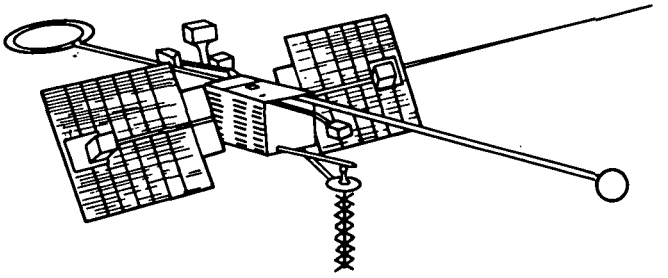

Fig. 5. Orbiting Geophysical Observatory III

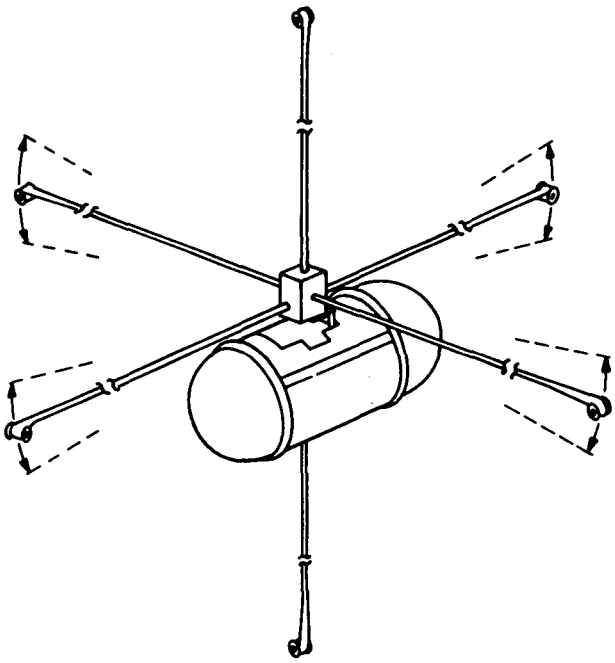

Fig. 6. OV1-10

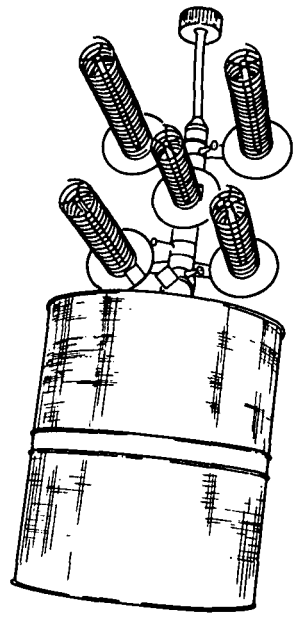

Fig. 7. Tactical Communications Satellite 1

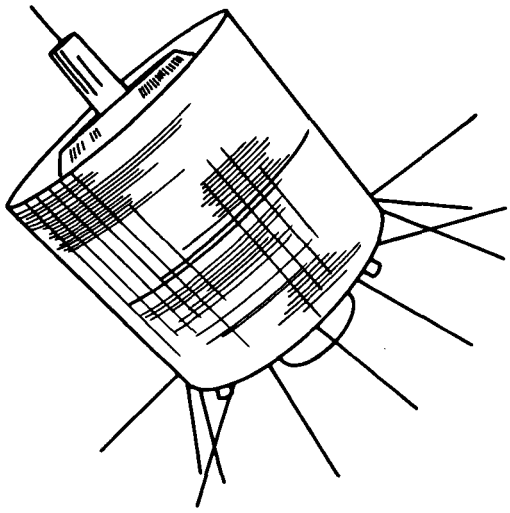

Fig. 8. Advanced Technology Satellite 5

Sometimes painful experience tells us that, even if tomorrow's spacecraft were quite similar to those already launched, we would have to expand our preflight evaluation program in order to avoid occasional attitude anomalies due to the influence of vehicle nonrigidity. In fact, the spacecraft now on the drawing boards promise to be much more troublesome in this regard than past vehicles. In anticipation of the challenges posed by future spacecraft, we are embarked on a program of substantial improvement in our pre-flight programs of analysis and test.

The state of the art

Separation of problems due to vehicle nonrigidity into vehicle dissipativity problems and vehicle flexibility problems is a practice which proves convenient not only in the description of past flight histories but also in the discussion of our present program of developing methods of analysis and testing of modern spacecraft. Indeed, the possibly deleterious influence of energy dissipation on attitude stability is confined to spin-stabilized or multi-spin spacecraft, and Dr. Willems has in the preceding lecture given substantial attention to this problem. I will therefore confine my own remarks in this area to the observation that our understanding of the behavior of a given mathematical model of a dual-spin spacecraft has in the past few years improved immensely, but that this leaves us still struggling with the substantial problems of devising reliable mathematical models of such spacecraft. Resolution of these questions requires an extensive program of experimental determination of vehicle properties, with particular attention to sources of energy dissipation such as bearings and containers of fluids. Although a very limited number of publications can be found today in this area (7, 8), there are in progress in the United States today numerous experimental programs for the evaluation of the influence of energy dissipation on attitude stability, and further meaningful progress with this problem can be anticipated.

Leaving aside the influence of internal energy dissipation, we can still expect vehicle flexibility to play a potentially significant role in spacecraft attitude stabilization, particularly so in view of the extreme flexibility of portions of spacecraft presently conceived for the future. In anticipation of the requirement for dynamic analysis of increasingly complex mathematical models of spacecraft, new approaches to formulating equations for accurate and efficient analysis have been developed in recent years, and progress in this area is still accelerating. In describing the "state of the art" of flexible vehicle control today, I will concentrate on these developing methods of analysis.

Table 1. The lessons of the past

Year	Satellite	Control technique	Performance	Probable explanation
1958	Explorer I	Spin-stabilized	Unstable	Energy dissipation in whip antennas[1]
1962	Alouette I	Spin-stabilized	Rapid spin-decay	Solar torque on thermally deformed vehicle[3]
1963	1963-22A	Gravity-stabilized	Librations excessive, but within specifications	Boom bending due to solar heating[4]
1964	Explorer XX	Spin-stabilized	Rapid spin-decay	Solar torque on thermally deformed vehicle[3]
1966	OGO III	Reaction wheel control	Excessive oscillations in attitude	Control system interaction with flexible booms[5]
1966	OV1-10	Gravity-stabilized	Unstable	Reaction torques due to thermally induced boom bending[6]
1969	TACSAT 1	Dual-spin control	Unexpected limit cycle within error specifications	Energy dissipation in bearing assembly[7]
1969	ATS 5	Spin-stabilized with active nutation damper[a]	Unstable	Energy dissipation in heat pipes

[a] For orbit injection only; satellite is gravity-stabilized after orbit is achieved.

In the era when a gravity-stabilized satellite could be idealized as a pair of viscoelastically interconnected rigid bodies with a common point, the general equations of motion of such a system were contained in a publication (9) by Fletcher, Rongved, and Yu. In 1965, these vector-dyadic equations were generalized by Hooker and Margulies (10) to characterize an arbitrary number of point-connected rigid bodies in a topological tree (no closed loops of bodies), and Roberson and Wittenburg (11) soon thereafter provided an independently derived matrix formulation of these equations. The pressing need in the space industry for the capability of simulating complex spacecraft resulted in substantial interest in these two papers, and on the basis of these and a variety of independent formulations several organizations developed numerical integration programs which could predict vehicle performance given only initial conditions and the physical parameters of an n-body model of the vehicle.

Both the Hooker-Margulies equations and the Roberson-Wittenburg equations were complicated by their retention of internal constraint torques between bodies, and several of the subsequent formulations involved some procedure for the elimination of these generally unwanted unknowns. Perhaps the best of the strategies for constraint torque elimination was suggested by Hooker in 1970. Because Hooker's brief note (12) provides no more than a description of the conceptually significant operations required to accomplish the elimination of constraint torques from the Hooker-Margulies vector-dyadic equations, I shall outline today the Hooker procedure and in the spirit of the Roberson-Wittenburg paper provide an explicit matrix equation which is equivalent conceptually to Hooker's more symbolic result.

The Hooker-Margulies equations are presented in the form

$$\underline{\underline{\Phi}}^{*}_{\lambda} \cdot \dot{\underline{\omega}}_{\lambda} + \underline{\omega}_{\lambda} \times \underline{\underline{\Phi}}^{*}_{\lambda} \cdot \underline{\omega}_{\lambda} = \underline{T}_{\lambda} + \sum_{j \in J_{\lambda}} \underline{T}^{H}_{\lambda j} + \underline{D}_{\lambda} \times \underline{F}_{\lambda} + \sum_{\mu \neq \lambda} \underline{D}_{\lambda\mu} \times (\underline{F}_{\mu} + m\ddot{\underline{D}}_{\mu\lambda}) \qquad (1)$$

for a typical body b_λ of an n-body set. Here a single underscore denotes a (Gibbsian) vector, a double underscore denotes a dyadic, and overdots indicate inertial differentiation with respect to time. The symbols $\underline{\omega}_\lambda$, $\underline{F}_\lambda$, and $\underline{T}_\lambda$ represent respectively the inertial angular velocity of b_λ, the resultant for b_λ of forces external to the system of bodies, and the resultant torque about the mass center of b_λ. The total system mass is m, the set J_λ includes the indices of all of the connection points between b_λ and other bodies of the system, and $\underline{T}^{H}_{\lambda j}$ is the torque applied to b_λ at the j^{th} connection point. The remaining symbols in Eq. (1) represent properties of the "augmented bodies" of the system, which are defined as follows: Augmented body b'_λ consists of b_λ with at each connection point an attached particle whose mass equals that of all bodies connected directly or indirectly to b_λ at that point. Thus the mass of each augmented body is m, the total mass. Furthermore, the inertia dyadic of b'_λ about its mass center

(called the barycenter) is Φ^*_λ, and the vector from the barycenter of b^*_λ to the connection point leading to b_μ is $\underline{D}_{\lambda\mu}$.

If the connection to b_λ at point j does not permit three degrees of rotational freedom, absolute constraints must be imposed on the relative motion of the two bodies sharing point j; this would be the case for example if the connection at j were a line hinge, permitting only a simple planar relative rotation of the two bodies. Those components of $T^H_{\lambda j}$ which enforce the absolute constraints (e. g. those normal to a line hinge) are unknown and generally unwanted constraint torques. To eliminate the constraint torques from Eq. (1), Hooker recommended a procedure which can be implemented as follows.

Idealize the system (see Fig. 9) as a collection of N+1 hinge-connected bodies, so that a single degree of freedom is associated with each connection; since a two degree of freedom joint between two bodies can be represented as two single degree of freedom joints connecting those bodies to a massless intermediate body (in Fig. 9, body b_{10} has two degrees of freedom relative to b_8), and similarly for a three degree of freedom joint, there is no loss of generality in the assumption of line hinges.

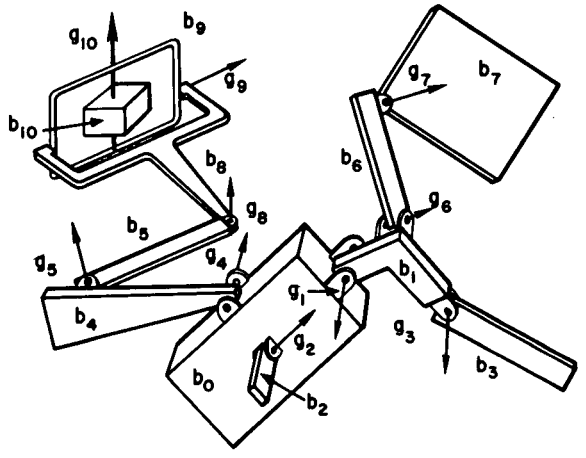

Fig. 9. Typical System of Hinge-Connected Bodies

Assign labels $b_0, b_1, \ldots, b_N$ to the N+1 bodies so ordered that for all bodies b_k between b_0 and b_i the inequality $0<k<i$ is satisfied. Assign $\gamma_1, \ldots, \gamma_N$ to the N angles of relative motion between the bodies, and $\underline{g}_1, \ldots, \underline{g}_N$ to unit vectors paralleling the corresponding hinge axes, with $\dot{\gamma}_i \underline{g}_i$ describing the ancular velocity of b_i with respect to the attached body b_k for some $k<i$; let τ_i be the scalar component along $\underline{g}_i$ of the hinge torque $\underline{T}^H_{ik}$ applied to b_i by b_k, $k<i$. Imbed the dextral, orthogonal unit vectors $\underline{b}^i_1, \underline{b}^i_2, \underline{b}^i_3$ in body b^i, and let C^{ij} be the direction cosine matrix such that $\{\underline{b}^i\} = C^{ij}\{\underline{b}^j\}$, where $\{\underline{b}^i\} = \{\underline{b}^i_1\ \underline{b}^i_2\ \underline{b}^i_3\}^T$, etc. for $\{\underline{b}^j\}$. Define the operator Δ_{ijk} to equal unity when either $k = j$ or b_j lies between b_i and b_k, otherwise being zero.

Substitute $\underline{\omega}_\lambda = \underline{\omega}_o + \sum_{k\epsilon P} \Delta_{0k\lambda}\, \dot{\gamma}_k \underline{g}_k$ into Eq. (1), with P representing the set of integers $1, 2, \ldots, N$, and sum over the set of N+1 bodies to obtain an equation which by virtue of Newton's third law involves no constraint torques. For each $\lambda\epsilon P$, sum over b_λ and all bodies b_i for which b_λ lies on a direct chain between b_0 and b_i, and dot multiply the result by $\underline{g}_\lambda$, to obtain N more equations free of constraint torques. The indicated 3+N scalar equations can be written as the matrix equation

$$\begin{bmatrix} a^{00} & a^{01} & a^{02} & \cdots & a^{0N} \\ a^{10} & a_{11} & a_{12} & \cdots & a_{1N} \\ a^{20} & a_{21} & a_{22} & \cdots & a_{2N} \\ \cdot\cdot & \cdot & \cdot & \cdot & \\ \cdot & \cdot & \cdot & \cdot & \\ \cdot & \cdot & \cdot & \cdot & \\ a^{N0} & a_{N1} & a_{N2} & \cdots & a_{NN} \end{bmatrix} \begin{bmatrix} \dot{\omega}^o \\ \ddot{\gamma}_1 \\ \ddot{\gamma}_2 \\ \cdot \\ \cdot \\ \cdot \\ \ddot{\gamma}_N \end{bmatrix} = \begin{bmatrix} \sum_{i\epsilon B} C^{0i} A^i \\ g^{1T} \sum_{i\epsilon B} \Delta_{01i} C^{1i} A^i + \tau_1 \\ g^{2T} \sum_{i\epsilon B} \Delta_{02i} C^{2i} A^i + \tau_2 \\ \cdot \\ \cdot \\ \cdot \\ g^{NT} \sum_{i\epsilon B} \Delta_{0Ni} C^{Ni} A^i + \tau_N \end{bmatrix} \qquad (2)$$

with the set B containing all body indices, $\omega^i \triangleq \{\underline{b}^i\} \cdot \underline{\omega}_i$, $g^{iT} \triangleq \underline{g}_i \cdot \{\underline{b}^i\}^T$, and all superscripted and subscripted quantities representing respectively matrix and scalar functions of system parameters and $\gamma_1, \gamma_2, \ldots, \gamma_N$. These functions are given explicitly by

$$A^i \triangleq T^i + \tilde{D}^{ii} F^i - \tilde{\omega}^i \Phi^{ii} \omega^i + \sum_{j\neq i} \tilde{D}^{ij} C^{ij} (F^j + \tilde{\omega}^j \tilde{\omega}^j D^{ji})$$

$$- \sum_{j\epsilon B} C^{ij} \Phi^{ij} \sum_{k\epsilon P} \Delta_{0kj}\, \dot{\gamma}_k \left[C^{i0} \tilde{\omega}^o C^{0k} + \sum_{m\epsilon P} \Delta_{0mk}\, \dot{\gamma}_m C^{im} \tilde{g}^m C^{mk} \right] g^k$$

$$a^{00} \triangleq \sum_{i\epsilon B} \sum_{j\epsilon B} C^{0j}\, \Phi^{ij} C^{i0}$$

$$a^{0k} \triangleq \sum_{i\epsilon B} \sum_{j\epsilon B} \Delta_{0kj}\, C^{0j}\, \Phi^{ij} C^{ik} g^{k}$$

$$a^{k0} \triangleq (a^{0k})^{T}$$

$$a_{km} \triangleq g^{k^{T}} \sum_{j\epsilon B} \sum_{i\epsilon B} \Delta_{0kj} \Delta_{0mi}\, C^{ki} \Phi^{ji} C^{jm} g^{m}$$

where $T^{i} \triangleq \{b^{i}\} \cdot \underline{T}_{i}$, $F^{i} \triangleq \{b^{i}\} \cdot \underline{F}_{i}$, $D^{ij} \triangleq \{b^{i}\} \cdot \underline{D}_{ij}$

(with $\underline{D}_{ii}$ the vector from the barycenter of $b_i^!$ to the mass center of b_i), and where $\Phi^{ij} \triangleq \{b^{j}\} \cdot \underline{\Phi}_{ij} \cdot \{b^{i}\}^{T}$ (with $\Phi_{ii} \triangleq \Phi_{i}^{*}$ and, for $j \neq i$, $\underline{\Phi}_{ij} \triangleq -m\,[\underline{D}_{ji} \cdot \underline{D}_{ij}\, U - \underline{D}_{ji} \underline{D}_{ij}]$, U being the unity matrix). The tilde operator transforms any 3x1 matrix x into a skew-symmetric 3x3 matrix, $\tilde{x}$, such that the elements of the matrix $\tilde{x}$ are given by $\tilde{x}_{\alpha\beta} = \epsilon_{\alpha\gamma\beta} x_{\gamma}$, where $\epsilon_{\alpha\gamma b} = \frac{1}{2}(\alpha-\gamma)(\gamma-\beta)(\beta-\alpha)$ for $\alpha, \beta, \gamma = 1, 2, 3$.

Finally, the direction cosine matrix relating arbitrary bodies b_i and b_j can be expressed in terms of direction cosine matrices relating connected bodies with the product

$$C^{ij} = \prod_{k\epsilon P} C^{[k-\Delta_{ikj}(k-N_{ki})],\,k}$$

where N_{ki} is the index of the body connected to b_k on the path to b_i, and Π implies a product of matrices so arranged that $C^{ij} = C^{im} C^{mn} C^{no} \ldots C^{pq} C^{qj}$.

The coefficient matrix on the left of Eq. (2) is symmetric, and the equations have the minimum dimension consistent with the number of degrees of freedom in the system, so it would seem that equations having this general form represent the optimum set for the given mathematical model. Explicit expressions for a^{ij}, a_{ij}, and A^{i} are not derived here, nor can this derivation be found in the published literature, but since they are readily obtained from the Hooker-Margulies equations (10) by following Hooker's procedure (12) and adopting the matrix formulation precedent of Roberson and Wittenburg (11), it may be expected that they will soon become widely used for complex spacecraft simulations.

After a decade of evolution, the equations of motion of a set of rigid bodies in a topological tree seems to have reached its zenith of simplicity and efficiency, but even in this form it would appear that computer capacity, accuracy, and operating costs will prescribe severe limits on the utility of this method of spacecraft simulation. The largest n-body equation numerical integration programs now operative for unrestricted angular motions permit the simulation of dynamical systems with about thirty degrees of freedom. When Eq. (2) is programmed for computation, somewhat larger systems will be simulated at an acceptable cost; but this is not an acceptable approach at present if the spacecraft mathematical model has hundreds of degrees of freedom.

Many spacecraft under development today simply cannot be modeled adequately as a collection of rigid bodies with less than one hundred degrees of freedom. On the other hand, it is never necessary to permit large relative motions between all portions of a spacecraft portrayed as a system with hundreds of degrees of freedom. It is quite generally satisfactory to permit a few coordinates to experience large changes in magnitude, while assuming that all others remain small. If the dynamical equations are linearized in the latter set of coordinates (and their derivatives), one might hope to gain some of the advantages of linear equations from at least a subset of the total system of differential equations.

The procedure of partial linearization of system variables could be applied to Eq. (2), but historically this procedure has developed quite independently of the n-body equations, deriving instead from the equations of structural dynamics. There is of course a well-established tradition in structural dynamics of idealizing a structure as linearly elastic or viscoelastic and subject to small deformations, so as to obtain linearized differential equations. It is further customary to characterize the structure as having a large but finite number of degrees of freedom; this practice involves subdividing the structure into a grid system whose intersection points are called nodes, and then defining the system behavior in terms of translations and rotations at the nodes. Motions of internodal points are then established on the basis of interpolation functions introduced in advance of dynamic analysis. The mass of the structure may be concentrated either as particles or as rigid bodies at the nodes, or it may be distributed throughout the finite elements which interconnect the nodes.

If an entire spacecraft is idealized as a viscoelastic structure whose node points experience only small deviations from a nominal motion defined by the time history of a reference frame in which the nominal locations of the nodes are fixed, and if $q \triangleq [q_1 q_2 \ldots q_{6n}]^{T}$ is the matrix of unknown displacements

(linear and angular) of the n nodes with respect to this reference frame, then the deformational equations of motion take the form (13)

$$M\ddot{q} + D\dot{q} + G\dot{q} + Kq + Aq = L \tag{3}$$

where M, D, and K are symmetric, and G and A are skew-symmetric. If the nominal motion reference frame deviates only slightly from a state of constant spin about an inertially fixed axis, then the coefficient matrices in Eq. (3) are constant. If that spin rate is zero, then A and G are zero. If internal energy dissipation is ignored, then D is zero. These special cases are of particular interest because they permit special kinds of useful coordinate transformations (13), but even in the most general constant coefficient case one can restructure Eq. (3) so as to permit simplification through coordinate transformation.

Eq. (3) appears in first order form as

$$B\dot{Q} + CQ = F \tag{4}$$

where in terms of matrix partitions, $Q \triangleq [q^T \mid \dot{q}^T]^T$, $F \triangleq [0^T \mid L^T]^T$, and

$$B \triangleq \begin{bmatrix} K+A & 0 \\ 0 & M \end{bmatrix} \qquad C \triangleq \begin{bmatrix} 0 & -K-A \\ K+A & D+G \end{bmatrix}$$

If Φ is the 12n x 12n matrix of eigenvectors of Eq. (4), and Φ' is the corresponding matrix of eigenvectors of the homogeneous adjoint equation

$$B^T\dot{Q}' + C^TQ' = 0$$

then the transformation to distributed or modal coordinates

$$Q = \Phi Y$$

followed by premultiplication by Φ'^T produces

$$\Phi'^T B\Phi\dot{Y} + \Phi'^T C\Phi Y = \Phi'^T F$$

The coefficient matrices of $\dot{Y}$ and Y are diagonal, permitting inversion of the former by inspection. Let Λ be the 12n x 12n diagonal matrix of eigenvalues, so that multiplication of the preceding equation by $(\Phi'^T B\Phi)^{-1}$ must furnish

$$\dot{Y} + \Lambda Y = (\Phi'^T B\Phi)^{-1}\Phi'^T F \tag{5}$$

Eq. (5) is equivalent to Eq. (3), but of more convenient form, since the former consists of 12n uncoupled scalar first order equations in $Y_1, \ldots, Y_{12n}$. After conceptually solving each of these independently, one will find in general that not all of them are significant to the vehicle response, so that many can safely be ignored. If one collects the significant variables into a 2N x 1 matrix $\bar{Y}$, and forms similarly truncated versions of Λ, Φ, and Φ', one obtains

$$\dot{\bar{Y}} + \bar{\Lambda}\bar{Y} = (\Phi'^T B\Phi)^{-1}\Phi'^T F \tag{6}$$

In the special case of Eq. (3) for which A = D = 0, the corresponding Eq. (4) involves a symmetric matrix B and a skew-symmetric matric C, so that Φ' is obtained simply as the complex conjugate of Φ.

Since in the present context the total spacecraft is being treated as a flexible structure, the boundaries are free, and one must expect twelve of the eigenvalues to be zero. The coordinates associated with these eigenvalues represent small rigid body motions of the structure with respect to the reference frame previously introduced. Since the precise motion of this frame has not yet been defined, one must either prescribe that motion or else specify that the rigid body motion with respect to that reference frame is zero, allowing the reference frame to follow the mean motion (14) of the structure. This can be accomplished by eliminating the zero-eigenvalue modes in the truncation from Eq. (5) to Eq. (6), and augmenting Eq. (6) with the two vector equations $\underline{F} = m\underline{a}$ and $\underline{T} = \dot{\underline{H}}$, where for the total spacecraft $\underline{F}$ is the resultant force, m is the mass, $\underline{a}$ is the mass center (CM) inertial acceleration, $\underline{T}$ is the resultant external torque about CM, and $\underline{H}$ is the inertial time derivative of angular momentum about CM.

Eq. (6), when augmented by $\underline{T} = \dot{\underline{H}}$ and compared to the general equations of motion of a set of coupled rigid bodies (Eq. 2), offers obvious advantages. Although the mathematical model which led ultimately to Eq. (6) may have hundreds of degrees of freedom (or perhaps, using techniques of structural modularization not discussed here, even thousands), the result finally obtained as Eq. (6) has as few or as many coordinates as the analyst deems appropriate for the task at hand. By truncating the generally irrelevant high frequency responses, the analyst obtains equations more readily amenable to digital computer numerical integration. The linear structure of Eq. (6) permits the use of transfer functions and frequency response studies.

The difficulty with Eq. (6), of course, is that its initial restriction to linearly elastic or viscoelastic spacecraft undergoing small deformations eliminates a good many of the spacecraft configurations

of vital interest today. Eq. (6) would be directly applicable to a passive gravity-stabilized satellite experiencing small librations about an earth-pointing attitude (producing a significant spin at orbital rate), while its libration damper and its deployed booms oscillate at small amplitude. It would apply equally well to a passive spin-stabilized satellite. The introduction of an actively controlled rotor along the pitch axis of the gravity-stabilized satellite, or the introduction of an actively controlled despun platform to the spin-stabilized satellite, transforms the passive vehicle into a semi-active dual-spin satellite, and violates the premises underlying Eq. (6).

The challenges posed by the dual-spin vehicle and other modern spacecraft have stimulated the development of methods which preserve the generality of the discrete coordinate formulation of Eq. (2) wherever necessary and secure the computational efficiency of the distributed coordinate formulation of Eq. (6) wherever possible; such methods, combining discrete and distributed coordinates, are called hybrid coordinate formulations (15, 16).

The basic rationale of the hybrid coordinate approach is to separate the spacecraft into a number of substructures, some being idealized as elastic or visoelastic and others as rigid, but with large relative motions permitted between interconnected substructures. The flexible substructures are then modeled as grids of finite elements interconnected at nodes, and mass is either concentrated at the nodes or distributed throughout the element. As noted previously in discussing the fully elastic vehicle, interpolation functions express deformations of finite elements in terms of nodal body translations and rotations, so only these nodal coordinates appear as unknowns. The equations of motion again have the form of Eq. (3), differing only in the presence of some constrained boundary conditions on the flexible substructure.

The mathematical operations introduced in the context of flexible vehicle analysis are equally applicable to the flexible appendage, so that a first order modal equation such as Eq. (6) can be written for each flexible substructure in the composite vehicle. In many cases of practical interest, some of the coefficient matrices in Eq. (3) will be zero, and coordinate transformations less general than those leading to Eq. (6) will be more useful. A special case of this sort will be illustrated in an example to follow.

It is always the objective of the hybrid coordinate formulation to obtain a set of inhomogeneous equations in terms of truncated modal coordinates for each flexible substructure which experiences large motions or nonlinearly controlled motions relative to a connected substructure. The substructure modal oscillations characterized by these equations will be driven not only by externally applied forces and torques, but also by the deviations of attached bodies from their nominal motions. It is of course necessary to combine each of the flexible substructure equations with additional equations written for the total vehicle, and for as many mixed groups containing both rigid and flexible substructures as required by the number of degrees of freedom in the system. When the original mathematical model incorporates flexible substructures only as appendages attached to individual rigid bodies, which in turn are attached to other rigid bodies in a tree topology, one can formulate the equations so as to involve no interbody constraint forces or torques, utilizing the strategy described in the development of Eq. (2) for systems of rigid bodies. When it becomes necessary to interconnect flexible substructures, the satisfaction of constraints is a more complicated job (particularly if they vary with time as prescribed by a nonlinear control system), and analytical progress is still quite limited.

In order to establish a clear conception of the hybrid coordinate approach and to show that its utility is not limited to digital simulation programs, I will apply this method to the problem of a spin-stabilized satellite consisting of a rigid central body with an attached flexible appendage, and obtain literal attitude stability criteria for special cases of interest. This problem has been examined in different ways by many researchers (17-20), and even the flexible dual-spin spacecraft has been analyzed (21-22), but the stability analysis to be outlined here is the work of Dr. F.J. Barbera in his very recent UCLA Ph.D. dissertation.

For conceptual and analytical convenience, the flexible appendage is here idealized as a collection of n elastically interconnected particles. (The structure of the equations to follow would be unchanged if a distributed-mass finite element model were used, but these equations would have a slightly different form if arbitrary rigid bodies were used instead of particles.) Moreover, it is assumed that for the nominal motion the vehicle spins as a rigid body at rate Ω_0 about an inertially stationary axis which for the vehicle mass center is a principal axis, both of the central rigid body and of the total vehicle, with the appendage node points lying in a plane perpendicular to this axis and passing through the vehicle mass center. See Fig. 10 for a typical configuration. Let 0 be the point of the central rigid body b which coincides with the center of mass CM in the nominal state; let $\underline{X}$ locate CM from an inertially fixed point and let $\underline{c}$ locate 0 from CM; let $\underline{\Gamma}^\alpha$ locate the α^{th} node P_α in b in the nominal state, and let $\underline{u}^\alpha$ be the small displacement of P_α from its nominal location at P'_α. Then, if $\underline{\Omega}$ is the inertial angular velocity of b, the inertial acceleration of P_α is given by

$$\underline{A}^\alpha = \ddot{\underline{X}} + \dot{\underline{\Omega}} \times (\underline{c} + \underline{\Gamma}^\alpha + \underline{u}^\alpha) + \underline{\Omega} \times [\underline{\Omega} \times (\underline{c} + \underline{\Gamma}^\alpha + \underline{u}^\alpha)]$$

$$+ 2\underline{\Omega} \times (\dot{\underline{c}} + \dot{\underline{u}}^\alpha) + \ddot{\underline{c}} + \ddot{\underline{u}}^\alpha$$

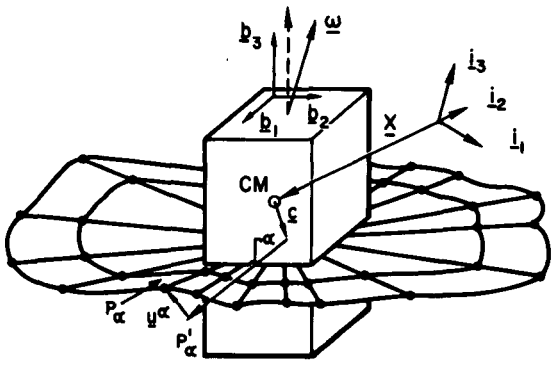

Fig. 10. Spinning Spacecraft with Planar Flexible Appendage

where overdot denotes inertial differentiation with respect to time and over-circle denotes time differentiation in the frame of b. The vector $\underline{c}$ is available from the mass center definition as $\underline{c} = -\Sigma m_\eta \underline{u}^\eta/m$, where m is the total vehicle mass and Σ indicates summation over all n nodes.

Writing $\underline{F}^\alpha = m_\alpha \underline{A}^\alpha$ in the vector basis $\{b\} \triangleq \{\underline{b}_1\ \underline{b}_2\ \underline{b}_3\}^T$ fixed in b then furnishes

$$F^\alpha = m_\alpha [\circledcirc \ddot{X} + (\dot{\tilde{\Omega}} + \tilde{\Omega}\tilde{\Omega})(\Gamma^\alpha + u^\alpha - \Sigma u^\eta m_\eta/m) + 2\tilde{\Omega}(\dot{u}^\alpha - \Sigma \dot{u}^\eta m_\eta/m) + \ddot{u}^\alpha - \Sigma \ddot{u}^\eta m_\eta/m] \qquad (7)$$

where in terms of the inertially fixed vector basis $\{i\} \triangleq \{\underline{i}_1\ \underline{i}_2\ \underline{i}_3\}^T$ the definitions $\underline{X} \triangleq \{i\}^T X$ and $\{b\} \triangleq \Theta\{i\}$ have been introduced, and the tilde convention has been adopted (see text following Eq. (2).

In addition to Eq. (7) for each of the appendage nodal particles, the differential equations $\underline{F} = m\ddot{\underline{X}}$ and $\underline{T} = \dot{\underline{H}}$ for the total vehicle may be appended to obtain a complete set. Here $\underline{F}$ is the resultant force on the vehicle, $\underline{T}$ is the external torque about the vehicle mass center, and $\underline{H}$ is the system angular momentum about CM. If $\underline{F}$ and $\underline{T}$ are resolved into basis $\{b\}$, the vehicle translation equation becomes

$$F = m \circledcirc \ddot{X} \qquad (8)$$

and the rotational equation becomes

$$T = I\dot{\Omega} + \tilde{\Omega} I\Omega + \dot{I}\Omega + \tilde{\Omega} h + \dot{h} - m\tilde{c}[\ddot{c} + 2\tilde{\Omega}\dot{c} + (\dot{\tilde{\Omega}} + \tilde{\Omega}\tilde{\Omega})c] \qquad (9)$$

where I is the instantaneous inertia matrix in basis $\{b\}$ of the angular momentum with respect to point 0, and where h is the matrix in basis $\{b\}$ of the angular momentum with respect to point 0 and frame b of the nodal particles. In explicit terms h becomes

$$h = \Sigma(\tilde{\Gamma}^\eta + \tilde{u}^\eta) m_\eta \dot{u}^\eta \qquad (10)$$

In the absence of external force F and torque T, Eqs. (7-9) admit the solution $u^\alpha \equiv 0$ ($\alpha = 1, \ldots, n$), $\ddot{X} \equiv 0$, and $\Omega = [0\ 0\ \Omega_0]^T \triangleq \bar{\Omega}$, with Ω_0 constant. The goal is to establish necessary and sufficient conditions for the asymptotic stability of this solution. Although more than one method of stability analysis can be applied this problem, it will suffice for present purposes to linearize the coupled Eqs. (7) and (9) in the variational coordinates contained in the matrices $\omega \triangleq \Omega - \bar{\Omega}$ and $u^\alpha (\alpha = 1, \ldots, n)$.

Linearization of Eq. (7) and substitution of $\ddot{X} = 0$ produces

$$F^\alpha = m_\alpha [(\dot{\tilde{\omega}} + \tilde{\bar{\Omega}}\tilde{\bar{\Omega}} + \tilde{\bar{\Omega}}\tilde{\omega} + \tilde{\omega}\tilde{\bar{\Omega}})\Gamma^\alpha + \tilde{\bar{\Omega}}\tilde{\bar{\Omega}}(u^\alpha - \Sigma u^\eta m_\eta/m) + 2\tilde{\bar{\Omega}}(\dot{u}^\alpha - \Sigma \dot{u}^\eta m_\eta/m) + \ddot{u}^\alpha - \Sigma \ddot{u}^\eta m_\eta/m] \qquad (11)$$

Collection of all n such equations as a single matrix equation can be accomplished by defining $u \triangleq \left[u^{1T}\ u^{2T}\ \ldots\ u^{nT}\right]^T$ and writing (for F = 0)

$$M'\ddot{u} + G'\dot{u} + K'u = M[\tilde{\Gamma}\hat{U}\dot{\omega} + (\hat{U}\bar{\Omega})^{\sim}\tilde{\Gamma}\omega - (\tilde{\Gamma}\hat{U}\bar{\Omega})^{\sim}\hat{U}\omega] \qquad (12)$$

where $\hat{U} \triangleq [U\ U\ \ldots U]^T$, a 3nx 3 matrix whose 3x3 partitions are unit matrices, $\tilde{\Gamma}$ is a 3nx3n matrix null except for the 3x3 partitions $\tilde{\Gamma}^1, \ldots \tilde{\Gamma}^n$ along the diagonal, and the tilde operator on a 3nxi matrix is a 3nx3n skew-symmetric matrix whose diagonal 3x3 partitions are obtained with the tilde operation on the 3xi partitions of the 3nxi matrix. The matrix M is diagonal, with 3x3 elements m_α U along the diagonal, $\alpha = 1, \ldots, n$. The symmetric matrix K' is the elastic stiffness matrix modified by a matrix with the 3x3 partitions $m_\alpha \tilde{\bar{\Omega}}\tilde{\bar{\Omega}} (\alpha = 1, \ldots, n)$ along the main diagonal and the 3x3 element $-m_\alpha m_\beta \tilde{\bar{\Omega}}\tilde{\bar{\Omega}}/m$ in the α, β partition ($\alpha, \beta = 1, \ldots, n$). The skew-symmetric matrix G' contains the 3x3 elements $2m_\alpha \tilde{\bar{\Omega}}$ along the main diagonal and the 3x3 element $-2m_\alpha m_\beta \bar{\Omega}/m$ ($\alpha, \beta = 1, \ldots, n$) in the α, β partition. The matrix M' is M with the addition of the element $-m_\alpha m_\beta U/m$ in the α, β partition ($\alpha, \beta = 1, \ldots, n$).

Eq. (12) for the appendage vibration is a special case of Eq. (3). This equation must be augmented by Eq. (9) to provide a complete set. Although one could apply to Eq. (12) a coordinate transformation

of the class that provided Eq. (6) from Eq. (3), in this special case of the planar appendage the equations are partially uncoupled, and simpler transformations can be used. Specifically, if the three scalar equations implied by Eq. (11) are recorded (mindful of the restriction $\Gamma^\alpha = [\Gamma_1^\alpha \; \Gamma_2^\alpha \; 0]^T$, representing the nominally planar appendage in Fig. 10), one finds for $\alpha = 1, \ldots, n$

$$F_1^\alpha = m_\alpha[-\Gamma_2^\alpha \dot{\omega}_3 - 2\Omega_o \omega_3 \Gamma_1^\alpha - \Omega_o^2(\Gamma_1^\alpha + u_1^\alpha - \Sigma u_1^\eta m_\eta/m) - 2\Omega_o(\dot{u}_2^\alpha - \Sigma \dot{u}_2^\eta m_\eta/m) + \ddot{u}_1^\alpha - \Sigma \ddot{u}_1 m_\eta/m] \tag{13a}$$

$$F_2^\alpha = m_\alpha[\Gamma_1^\alpha \dot{\omega}_3 - 2\Omega_o \Gamma_2^\alpha \omega_3 - \Omega_o^2(\Gamma_2^\alpha + u_2^\alpha - \Sigma u_2^\eta m_\eta/m) + 2\Omega_o(\dot{u}_1^\alpha - \Sigma \dot{u}_1^\eta m_\eta/m) + \ddot{u}_2^\alpha - \Sigma \ddot{u}_2^\eta m_\eta/m \tag{13b}$$

$$F_3^\alpha = m_\alpha[\Gamma_2^\alpha \dot{\omega}_1 - \Gamma_1^\alpha \dot{\omega}_2 + \Omega_o(\Gamma_1^\alpha \omega_1 + \Gamma_2^\alpha \omega_2) + \ddot{u}_3^\alpha - \Sigma \ddot{u}_3^\eta m_\eta/m] \tag{13c}$$

The apparent uncoupling of these equations is also evident in Eq. (9), which in linearized scalar form becomes

$$A\dot{\omega}_1 + (C-B)\Omega_o \omega_2 + \Omega_o^2 \Sigma m_\eta \Gamma_2^\eta u_3^\eta + \Sigma m_\eta \Gamma_2^\eta \ddot{u}_3^\eta = 0 \tag{14a}$$

$$B\dot{\omega}_2 + (A-C)\Omega_o \omega_1 - \Omega_o^2 \Sigma m_\eta \Gamma_1^\eta u_3^\eta - \Sigma m_\eta \Gamma_1^\eta \ddot{u}_3^\eta = 0 \tag{14b}$$

$$C\dot{\omega}_3 + 2\Sigma m_\eta(\Gamma_1^\eta \dot{u}_1^\eta + \Gamma_2^\eta \dot{u}_2^\eta) + \Sigma m_\eta(\Gamma_1^\eta \ddot{u}_2^\eta - \Gamma_2^\eta \ddot{u}_1^\eta) = 0 \tag{14c}$$

where A, B, and C are for point 0 the moments of inertia of the vehicle in its nominal state for axes parallel to $\underline{b}_1$, $\underline{b}_2$, and $\underline{b}_3$, assumed principal.

The n scalar equations represented by Eq. (13c) couple only with Eqs. (14a) and (14b), while the remaining 2n+1 scalar equations are an independent internally coupled set. Stability analysis can therefore be accomplished by dealing with these coupled sets independently. The number of equations makes a literal stability analysis quite infeasible at this stage of the derivation, but, after transforming to modal coordinates for appendage vibrations and restricting the vibratory response to a single mode, one can obtain attitude stability results directly.

The coordinate transformation required to obtain vibratory motions involving out-of plane motion is obtained from the n equations defined by Eq. (13c). In terms of the nx1 matrix variable $\underline{\underline{q}} \triangleq [u_3^1 \; u_3^2 \ldots u_3^n]^T$, these equations have for an (undamped) elastic appendage the form

$$\mu' \ddot{q} + \kappa' q = \mu[\Gamma^1(\dot{\omega}_2 - \Omega_o \omega_1) - \Gamma^2(\dot{\omega}_1 + \Omega_o \omega_2)] \tag{15}$$

where for i = 1, 2, $\underline{\underline{\Gamma_i}} \triangleq [\Gamma_i^1 \ldots \Gamma_i^n]^T$; μ is a diagonal matrix with nonzero elements $m_1, \ldots, m_n$; μ' is μ plus a matrix with $-m_\alpha m_\beta/m$ in the α, β element ($\alpha, \beta = 1, \ldots, n$); and κ' is the appendage stiffness matrix κ (assumed free of coupling with u_1^α and u_2^α), with the added terms $-\Omega_o^2 m_\alpha$ on the diagonal and the added term $\Omega^2 m_\alpha m_\beta/m$ in the α, β element ($\alpha, \beta = 1, \ldots, n$). In contrast to the general form of Eq. (3), or even the special form of Eq. (12), one can for Eq. (15) introduce the transformation $q = \phi\eta$, where ϕ is the nxn matrix of eigenvectors of Eq. (15), and after premultiplication by ϕ^T obtain

$$\ddot{\eta} + \sigma^2 \eta = \phi^T \mu \Gamma^1(\dot{\omega}_2 - \Omega_o \omega_1) - \phi^T \mu \Gamma^2(\dot{\omega}_1 + \Omega_o \omega_2) \tag{16a}$$

where σ^2 is a diagonal matrix with elements $\sigma_1^2, \sigma_2^2, \ldots, \sigma_n^2$, the negative squares of the imaginary eigenvalues of Eq. (15).

In terms of the modal coordinate matrix η, the coupled vehicle equations (Eqs. 14a, b) become

$$A\dot{\omega}_1 + (C-B)\Omega_0 \omega_2 + \Gamma^{2T} \mu^T (\Omega_0^2 \eta + \ddot{\eta}) = 0 \tag{16b}$$

$$B\dot{\omega}_2 + (A-C)\Omega_0 \omega_1 - \Gamma^{1T} \mu^T \phi(\Omega_0^2 \eta + \ddot{\eta}) = 0 \tag{16c}$$

With the definitions of the nx1 matrices $\underline{\underline{\rho^1}} \triangleq \phi^T \mu \Gamma^1$ and $\underline{\underline{\rho^2}} \triangleq \phi^T \mu \Gamma^2$, Eqs. (16) take a more convenient form. In conformity with standard practice in structural dynamics, one can truncate the matrices $\eta, \phi, \sigma, \rho^1$, and ρ^2 to the matrices $\bar{\eta}, \bar{\phi}, \bar{\sigma}, \bar{\rho}^1$, and $\bar{\rho}^2$, reducing the dimension n to N, and simultaneously insert a diagonal modal damping term (with the modal damping ratios $\zeta_1, \ldots, \zeta_N$ filling the diagonal elements of the otherwise null matrix ξ), to obtain the final equations

$$\ddot{\bar{\eta}} + 2\bar{\zeta}\bar{\sigma}\dot{\bar{\eta}} + \bar{\sigma}^2\bar{\eta} - \bar{\rho}^{-1}(\dot{\omega}_2 - \Omega_o\omega_1) + \bar{\rho}^{-2}(\dot{\omega}_1 + \Omega_o\omega_2) = 0 \tag{17a}$$

$$A\dot{\omega}_1 + (C-B)\,\Omega_o\omega_2 + \bar{\rho}^{-2T}(\Omega_o^2\bar{\eta} + \ddot{\bar{\eta}}) = 0 \tag{17b}$$

$$B\dot{\omega}_2 + (A-C)\Omega_o\omega_1 - \bar{\rho}^{-1T}(\Omega_o^2\bar{\eta} + \ddot{\bar{\eta}}) = 0 \tag{17c}$$

With sufficiently severe truncation, Eqs. (17) can be analyzed for stability of the null solution by means of Routh's criteria. If only a single out-of-plane mode of appendage vibration is preserved in truncation, the characteristic equation obtained from Eq. (17) is only of fourth order, and Routh's criteria provide the following necessary and sufficient conditions for asymptotic stability:

$$\text{i)}\ C > A \qquad \text{ii)}\ C > B \qquad \text{iii)}\ \zeta_i > 0$$

$$\text{iv)}\ \frac{\sigma_i^2}{\Omega_0^2} > \frac{(C-B)(\rho_i^1)^2 + (C-A)(\rho_i^2)^2}{(C-A)(C-B)} \tag{18}$$

where the index i identifies the mode retained in truncation. The first and second of these criteria express the familiar requirement that the vehicle must spin about its principal axis of maximum inertia; this is a result that would be expected as a consequence of internal energy dissipation even if the appendage had inconsequential mass. The third criterion merely expresses the physically obvious fact that energy must be diminished (and not increased) by the damping. The last of these criteria is the new and significant one, since it establishes a lower limit on the i^{th} natural frequency of the appendage in its spinning state, expressed in terms of inertia differences of the total vehicle and the effective inertia contributions of the appendage, when vibrating in its i^{th} mode.

Eq. (18) is not the most general set of stability criteria obtained by Dr. Barbera, but it illustrates quite forcibly the possibilities of closed form attitude stability analysis of passive spacecraft. Predictions of vehicle flight performance would of course be based on digital computer simulations of the dynamics of more complex spacecraft models, but such literal criteria have a substantial utility in preliminary design.

In describing the state of the art of flexible spacecraft attitude stabilization, I have concentrated on the most recent analytical progress in this field. One could devote substantial time as well to the behavior of grossly flexible satellites presently in orbit (the Radio Astronomy Explorer is a dramatic example which has been extensively studied[21]). The specific analytical results recorded here are too new to have found application to current spacecraft, but they may be expected to have many applications to the spacecraft of the next decade.

Future problems

It requires no more than a glance at the conceptual designs being proposed today to appreciate the nature of future problems of attitude stabilization. Fig. 11 illustrates a hypothetical modification of the Skylab which has balance masses extended on very flexible booms in order to permit spin about a vehicle principal axis of maximum inertia (satisfying criteria i) and ii) of Eq. (18)). The feasibility of passive or semi-active spin-stabilization of this vehicle for gravity simulation depends critically on the influence of the flexibility of these booms, and that of solar cell arrays as well. Fig. 12 portrays a hypothetical space station, whose articulated flexible solar panels pose special problems both during periods of active control and during periods of possible semi-passive spin-stabilization. Fig. 13 is a highly speculative portrayal of a dual-spin space base, which almost certainly would pose problems of flexibility in virtually all of its parts. Finally, Fig. 14 illustrates what may be the communications satellite of tomorrow. This tri-spin spacecraft poses all of the problems which Dr. Willems and I have discussed today, and perhaps offers a symbolic justification of our selection of topics for this lecture series.

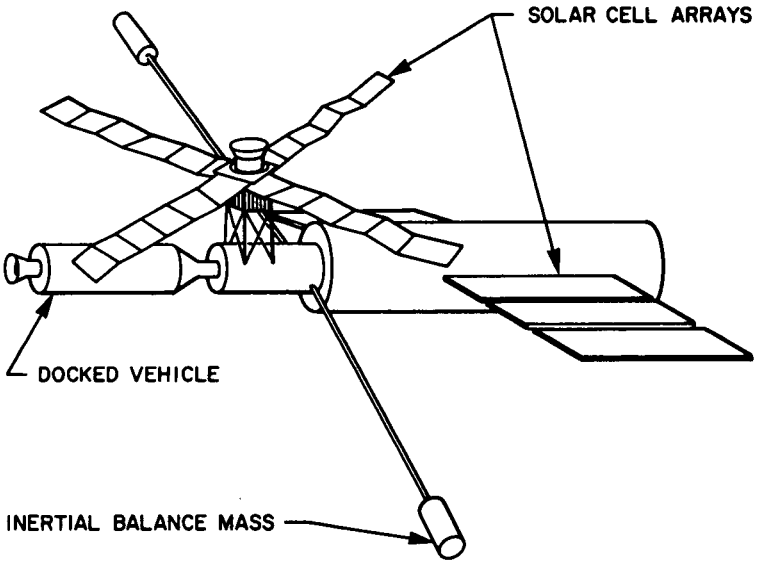

Fig. 11. Hypothetical Spinning Skylab

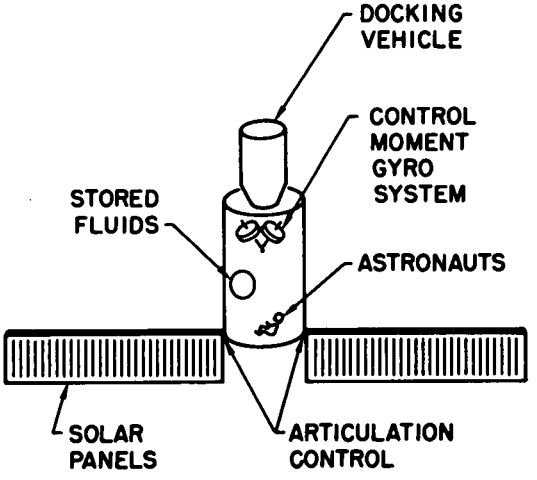

Fig. 12. Hypothetical Space Station

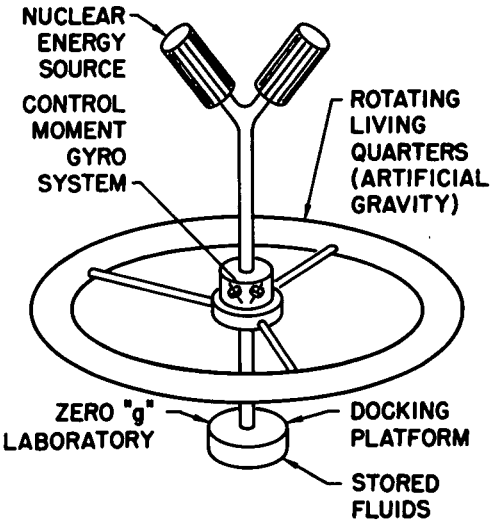

Fig. 13. Hypothetical Space Base

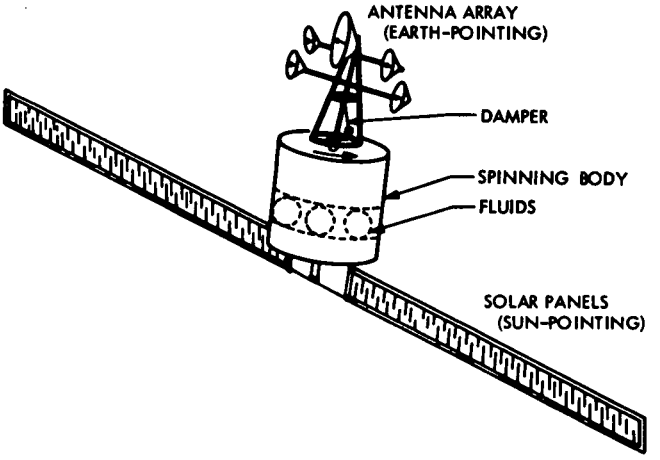

Fig. 14. Hypothetical Tri-spin Communications Satellite

References

1. W. C. Pilkington, "Vehicle Motions as Inferred from Radio Signal Strength Records," Ext. Pub. No. 551, Jet Propulsion Lab., Sept. 1958.

2. P. W. Likins and H. K. Bouvier, "Attitude Control of Nonrigid Spacecraft," Astronautics and Aeronautics, Vol. 9, 1971, pp. 64-71.

3. B. Etkin and P. C. Hughes, "Explanation of the Anomalous Spin Behavior of Satellites with Long, Flexible Antennae," J. Spacecraft and Rockets, Vol. 4, 1967, pp. 1139-1145.

4. R. E. Fischell and F. F. Mobley, "A System for Passive Gravity-Gradient Stabilization of Earth Satellites," TG 514, Johns Hopkins Applied Physics Lab., Aug. 1963.

5. K. J. McKenna, "The OGO Attitude Control Subsystem Redesign as a Result of OGO-III Experience," System Analysis and Design Studies, Vol. 1, Rept. 67.7231, TRW Systems Group, June 1967, pp. 7-116.

6. G. M. Connell and V. Chobotov, "Possible Effects of Boom Flutter on the Attitude Dynamics of the OV1-10 satellite," J. Spacecraft and Rockets, Vol. 6, 1969, pp. 90-92.

7. C. R. Johnson, "Tacsat 1 Nutation Dynamics," AIAA Preprint No. 70-455, presented at AIAA 3rd Communications Satellite Systems Conf., Los Angeles, April 1970.

8. J. P. Vanyo and P. W. Likins, "Measurement of Energy Dissipation in a Liquid-Filled, Precessing Spherical Cavity," to appear in J. Applied Mech. (paper No. 71-APM-4).

9. H. J. Fletcher, L. Rongved, and E. Y. Yu, "Dynamics Analysis of a Two-Body Gravitationally Oriented Satellite," Bell System Tech. J. Vol. 42, 1963, pp. 2239-2266.

10. W. W. Hooker and G. Margulies, "The Dynamical Attitude Equations for an n-Body Satellite," J. Astronaut. Sci., Vol. 12, 1965, pp. 123-128.

11. R. E. Roberson and J. Wittenburg, "A Dynamical Formalism for an Arbitrary Number of Interconnected Rigid Bodies, with Reference to the Problem of Satellite Attitude Control, Proc. of the 3rd International Congress of Automatic Control, (London, 1966), Butterworth and Co., London, 1967, pp. 46D.1-46D.8.

12. W. W. Hooker, "A Set of r Dynamic Attitude Equations for an Arbitrary n-Body Satellite Having r Rotational Degrees of Freedom," AIAA J., Vol. 8, 1970, pp. 1205-1207.

13. P. W. Likins, "Dynamics and Control of Flexible Space Vehicles," TR 32-1329, Jet Propulsion Lab., 1970.

14. R. D. Milne, "Some Remarks of the Dynamics of Deformable Bodies," AIAA J., Vol. 6, 1968, pp. 556-558.

15. P. W. Likins and P. H. Wirsching, "Use of Synthetic Modes in Hybrid Coordinate Dynamic Analysis," AIAA J., Vol. 6, 1968, pp. 1867-1872.

16. P. W. Likins and A. H. Gale, "Analysis of Interactions Between Attitude Control Systems and Flexible Appendages," Proc. of the 19th International Astronautical Congress, (Belgrade, 1968) Vol. 2, Pergamon Press, 1970, pp. 67-90.

17. F. Buckens, "On the Influence of the Elasticity of Components in a Spinning Satellite on the Stability of Its Motion," Proc. of the 16th International Astronautical Congress, (Athens, 1965).

18. F. R. Vigneron, "Stability of a Freely Spinning Satellite of Crossed-Dipole Configuration," Canadian Aeronautics and Space Institute Trans., Vol. 3, March 1970, pp. 8-19.

19. T. W. Flatley, "Attitude Stability of a Class of Partially Flexible Spinning Satellites," NASA TN D-5268, 1969.

20. J. E. Rakowsky and M. L. Renard, "A Study of the Nutational Behavior of a Flexible Spinning Satellite Using Natural Frequencies and Modes of the Rotating Structure," AIAA Paper No. 70-1046, presented at AAS/AIAA Astrodynamics Conf., Santa Barbara, Calif., Aug. 1970.

21. A. H. Gale and P. W. Likins, "Influence of Flexible Appendages on Dual-Spin Spacecraft Dynamics and Control," J. Spacecraft and Rockets, Vol. 7, 1970, pp. 1049-1056.

22. P. Y. Willems, "Stability of Deformable Gyrostats on a Circular Orbit" J. of the Astronautical Sciences, September-October 1970, XVIII-2, pp. 65-85.

23. J. L. Farrell and J. K. Newton, "Continuous and Discrete RAE Models," J. Spacecraft and Rockets, Vol. 6, 1969, pp. 414-423.

ACTIVE STABILIZATION*

by

W. G. Hughes
Ministry of Defence (Aviation Supply), Space Department,
Royal Aircraft Establishment, Farnborough, Hampshire, UK.

SUMMARY

A survey is given of the principal devices available for the generation of control torque, covering mass expulsion systems (cold gas, hot gas, electric), momentum exchange systems (reaction wheels, control moment gyros) and magnetic torquers.

Study of reaction wheel systems commences with presentation of the complete linearized equations of motion in three axes, with commentary on the effect of inter-axis couplings. Control in a single axis is considered in detail. Discussion is given of mass expulsion and magnetic techniques for momentum unloading.

Control moment gyro systems are discussed briefly.

Pure jet systems are studied from the viewpoint of achieving high precision while preserving economy in the use of jet fuel. Difficulties arising from jet delay and sensor delay and noise are seen to be minimized by the use of a signal processing technique which incorporates a model of the spacecraft dynamics.

Finally, the special properties of inertially referenced systems are considered, together with an examination of the gyrocompassing technique for use in earth-pointing spacecraft.

1 INTRODUCTION

Though most people working in the field have a fair idea of what is meant, it is not always completely clear where the dividing lines should be drawn between the classes of spacecraft attitude control system known as PASSIVE, SEMI-PASSIVE, SEMI-ACTIVE and ACTIVE. For a system to be classed as ACTIVE it is necessary that it should contain attitude sensing instruments, and that control of the orientation of the spacecraft should be accomplished through operating torque producing devices by signals derived from the outputs of these instruments. However, for the purpose of this paper, specific exclusion is made of systems which, while having these features, depend for their operation upon the overall dynamic system containing a non-zero total angular momentum vector. Such systems have been used extensively in past and present geostationary communications satellites (Syncom through Intelsat IV) and may well be so used in the future. They make use of the essentially PASSIVE feature that environmental torques can produce only slow changes in the direction of this angular momentum vector, which can therefore be used as the basis for short-term control about appropriate axes.

While it is a simple matter to envisage a system which is entirely PASSIVE (e.g. a gravity-gradient system employing eddy-current damping between booms which have some freedom of relative motion), it is worth noting that no system is entirely free of PASSIVE features. The very inertia of a spacecraft provides a PASSIVE opposition to disturbing torques. In its function of resisting disturbing torques, a single degree-of-freedom control moment gyroscope acts in a SEMI-PASSIVE manner (SEMI- since power is required to maintain the gyro rotor speed). Hardly more PASSIVE could be the feature of simple geometry which permits 'gyrocompassing' control in the roll (along orbit) and yaw (local vertical) axes of an earth-pointing satellite, when attitude position information is available only in roll.

The paper commences with a brief survey of the various devices available for the generation of control torque. This is followed by a more detailed study of the two main classes of ACTIVE control system, viz. the angular momentum exchange systems (reaction wheel and control moment gyro) and the pure jet systems. Jet and magnetic procedures will be described for unloading the momentum exchange systems. A brief review will then be given of systems (of either of the above classes) which employ an inertial attitude reference, including the mechanization of the 'gyrocompassing' control scheme.

2 METHODS FOR PRODUCING CONTROL TORQUE

2.1 Mass Expulsion Systems

Control torque can be provided by the ejection of a fluid from the spacecraft, along a path which has a suitable lever arm relative to the mass-centre of the vehicle. The thrust F produced by the device is given by

$$F = \dot{m}v \tag{1}$$

where $\dot{m}$ is the mass ejection rate and v is the mean ejection velocity. Clearly economical use of fuel mass requires that v be as large as possible.

Current spacecraft systems eject some type of gas or plasma. The systems differ in the method used to store or impart the energy of ejection, the main classes being:-

---

(1) Cold gas jets.

(2) Hot gas jets.

(3) Electric thrusters.

Each of the classes may be subdivided, the whole range being as shown in Fig.1.

The simplest cold gas systems use an inert gas, such as nitrogen or argon, stored in a conventional high pressure bottle with an initial pressure up to about 400 atmospheres. Normally the gas is passed through one or more pressure regulators before reaching the expulsion control valve, which therefore operates at nearly constant pressure and produces similarly constant thrust. Exhaust velocities in the range 500 to 1000 m/s are normally obtained, with thrusts in the range 0.05 N to 25 N. Efficient operation can be achieved with pulse durations less than 10 ms. Due to the very high storage pressure, the mass of the bottle may be as much as twice that of the contained gas.

If the working fluid is a gas which can be stored as a liquid at a relatively low pressure, e.g. propane, ammonia or freon, the mass of the bottle may be reduced to 10 to 20% of its contents. Depending on the mode of use, this advantage may be offset by the penalty that a source of heat has to be provided to vaporize the liquid before it can be used in the jet. One convenient method for achieving this is shown in Fig.2, in which a boiler coil, wrapped round the tank, draws on the sensible heat of tank and contents to provide the latent heat of vaporization. This process tends to cool the tank, but its temperature is maintained at a satisfactory level by conduction and radiation from surrounding parts of the spacecraft.

It is possible for the working fluid to be stored as a subliming solid, e.g. ammonium hydrosulphide. This is released to the jets as a vapour, as required, by application of heat to the container.

The systems using liquid and solid storage have similar levels of performance to that using gaseous storage, though the effective performance may be two to three times better, due to the much lower mass of the storage vessel. However they are limited to the lower end of the thrust range by the problem of readily providing adequate heat.

The exhaust velocities of many of the gases usable in cold gas systems may be increased to the region of 1500 to 3000 m/s by externally heating the gas on its way to the thrust nozzle. Such systems are usually classed as resisto-jets, although the additional energy does not necessarily have to be provided by resistive heating; radio-active isotopes can be used. Resisto-jets can be a very useful class of system since the advantages of low thrust levels can be retained while achieving the economy which results from the high exhaust velocity.

Fig.3 illustrates the principle of dissociating monopropellent systems, which use working fluids such as HTP or hydrazine. The fuel flow is controlled by a fairly conventional valve, after which it is passed through a catalyst pack on its way to the thrust nozzle. The catalyst for HTP is usually silver plated nickel gauze, which causes the fuel to dissociate into steam and oxygen at about 600°C. For hydrazine the catalyst is in the form of iridium coated alumina pellets, a mixture of ammonia and nitrogen being produced at about 1000°C. Exhaust velocities up to about 2500 m/s are obtainable with such systems. Disadvantages in some applications are that it is difficult to produce low thrust efficiently, the limit probably being at about 1N, and that the catalytic process imposes time delays on the build-up of thrust. Pulse durations shorter than about 50 ms would be very inefficient, and substantially longer ON times (perhaps provided cumulatively by a train of pulses) are necessary to heat the catalyst pack and thereby to realize the full potential for high exhaust velocity.

Due to their complexity, hypergolic bi-propellent systems (e.g UDMH and nitrogen tetroxide) have not so far found much favour in relation to spacecraft attitude control.

Some electrical thruster systems have already been flown in experimental capacities. There are several fundamentally different types of thruster, using greatly different fuels and acceleration processes. Currently most advanced (at least for attitude control purposes) is probably the pulsed plasma rail gun (Fig.4). In this the fuel may be mercury, a wax, a metal or even PTFE. A very small amount of fuel is vaporized and ionized by discharge of a capacitor. The ionized material is then situated between a pair of rail electrodes connected to a large capacitor charged to a few kilovolts. The resulting current and associated electromagnetic field causes the ionized material to be accelerated along the electrodes to achieve an exhaust velocity in the region of 20 km/s. This pulsed process can be repeated several times a second to provide a mean thrust of a few millinewtons. At present the efficiency of these systems is very low, a few per cent, but they are potentially useful for long-life spacecraft, in which the economy which results from the high exhaust velocity can offset the rather high system mass.

2.2 Angular Momentum Exchange Devices

By varying the state of motion or configuration of rotating masses carried in a spacecraft, the vector $\underline{h}$ of the total angular momentum contained in these masses can be altered. As a result a reaction torque vector $\underline{g}$ is applied to the remainder of the spacecraft where

$$\underline{g} = - d\underline{h}/dt \quad , \tag{2}$$

the time derivative being computed relative to an inertially fixed reference. The attitude control system will be organized to produce the required value of $\underline{g}$ in order that the spacecraft may manoeuvre and resist disturbing torques.

In a given system, physical considerations will determine an envelope in angular momentum space such that interior points only are available for values of $\underline{h}$. The angular momentum exchange system can then satisfy all requirements for control torque as long as the vector

$$\underline{h}(0) - \int_0^t dt\underline{g}(t) \qquad (3)$$

remains within the envelope. The integral will remain within finite bounds in respect of the control action required to provide manoeuvres, to counter disturbances due to motions of on-board equipment and to resist certain often significant components of environmental torques. A momentum exchange system is therefore capable, on its own, of providing the appropriate service, avoiding the need to carry the corresponding mass of propellent which a mass expulsion torquing system would use. However, environmental torques normally contain components which will cause the magnitude of $\int_0^t dt\underline{g}(t)$ to exceed any realistic bound. Eventually it will be necessary for the spacecraft to unload angular momentum, use of a mass expulsion system being the most obvious technique. Alternatively, appropriate environmental torques may be created: magnetic torquing may often be practicable and, in principle, the gravity-gradient, solar pressure and aerodynamic effects could be used.

If a comparison is made on the sole ground of torquing system mass, between a pure mass-expulsion system and a momentum exchange system with provision for unloading, it is clear from the above discussion that the preference for a momentum exchange system will increase with increasing mission duration, when the 'dead-weight' of the exchange devices becomes more than offset by the saving in mass of jet fuel.

It will be seen in section 3.4 that in order to make economical use of jet fuel, a 'dead-band' of attitude error must be provided, within which jet torquing is not permitted. This magnitude of attitude error has therefore to be tolerated. No such provision is necessary if use is made of a momentum exchange system, which may therefore be preferred on the ground of improved precision of control.

(a) Reaction Wheels

A reaction wheel assembly consists of an electric motor with a wheel mounted directly on its rotor, enclosed in a hermetically sealed container so that the optimum atmosphere may be provided, taking account of bearing survival and windage losses. Control torque is provided about the axis of rotation and is equal to the algebraic sum of the torques produced by motor, and bearing and aerodynamic drag.

For ease of control system design it is desirable that a reaction wheel should be a linear device, i.e. the control torque g produced should be a linear function of the driving signal e and of the contained angular momentum h (here h is evaluated relative to the wheel mount rather than to an inertial reference). In practice this aim is realized only approximately: actual torque-speed characteristics might have the form shown in Fig.5. Among other non-linearities, a step change in torque occurs as a result of the change in bearing drag when the wheel speed changes sign. In general g may be expressed as $g = g(e,h)$. Selecting a particular working point (e,h) and regarding the variables g, e, h now as small departures from that working point, the relation may be written:-

$$g = \frac{\partial g}{\partial e} e + \frac{\partial g}{\partial h} h$$

$$= k_r e + \omega_r h \qquad (4)$$

having defined $k_r = \partial g/\partial e$, $\omega_r = 1/T_r = \partial g/\partial h$.

If the wheel mount has zero inertial angular velocity, then

$$h = -\int_0^t dtg \quad , \qquad (5)$$

and (4) may be re-written in the familiar operational form

$$g = k_r \frac{p}{\omega_r + p} e \qquad (6)$$

where p is the Laplace operator. k_r and ω_r may then be regarded as parameters which vary with the working point. As long as this variation is not too great, it will usually be possible to design the control system using suitable mean values of k_r and ω_r. However, for assessment of attitude error at very low frequencies, it will often be necessary to refer directly to the torque-speed characteristics. Also more detailed consideration will be necessary to determine the transient error which will occur when the wheel speed changes sign.

Since the function of the wheel (as distinct from the motor) is to absorb angular momentum while maintaining moderation in its mass and speed requirements, it will normally be constructed with the mass concentrated in the rim, as far as is possible.

The motors for the reaction wheels used in spacecraft such as OAO, OGO and Nimbus[1] have all been two-phase ac induction motors. Such motors, when designed for most efficient power conversion, have torque-speed characteristics which are highly non-linear. In order to achieve reasonable linearity, substantial reductions in efficiency had to be tolerated. The much more desirable characteristics of dc motors could not be used due to the unreliability of brush commutation. More recently, with the development of brushless commutation techniques, motors having greatly improved efficiency and linearity have

been developed[2]. With constant current drive, a close approach may be made to the ideal condition of $\omega_r = 0$ (torque independent of speed).

(b) Control Moment Gyros

A control moment gyro (CMG) is basically similar to an instrument gyro in that it has a constant speed rotor suspended in a one or two degree-of-freedom gimbal system. However, since its function is to absorb angular momentum (by appropriate gimbal motions in two or more such gyros), the spin angular momentum will normally be substantially larger than would be used in an instrument gyro. Further, in order to transmit the comparatively large torques between casing and rotor and perhaps to monitor the gimbal angular velocities, the gimbal torquing arrangements may be very different.

Since the rotor runs at constant speed, its drive motor can be designed for most efficient operation at that speed. Similarly the gimbal torquers can be designed for efficient operation at near zero rates. It would therefore be not unexpected that if compared with a reaction wheel having similar torque and momentum capability, the CMG would emerge as substantially the more efficient. This is certainly the case if ac driven reaction wheels are considered. However, the issue may be much less clear-cut when the comparison is made with dc driven wheels, particularly if account is taken of the complexity of the control computing which may need to be associated with CMGs, in view of the high degree of inter-axis coupling which may occur.

Let $\underline{h}$ be the spin angular momentum of a CMG rotor, and let the casing containing the rotor have an angular velocity $\underline{\omega}$ relative to an inertially fixed reference. Then the control torque experienced by the spacecraft is

$$\underline{g} = -\underline{\omega} \times \underline{h} \quad . \tag{7}$$

Consider a single degree of freedom CMG carried in a spacecraft which is stabilized to have essentially zero inertial angular velocity (Fig.6). Suppose that at some instant, the rotor angular momentum $\underline{h}$ is perpendicular to some nominated control axis of the spacecraft and that the gimbal angular velocity is $\underline{\omega}$, as shown. Then the spacecraft will experience the control torque $\underline{g}$ about this control axis, this torque being presumed to be countering an appropriate disturbance torque. The point to be made is that this control torque is transmitted to the spacecraft via side-loads in the gimbal bearings and that it is not necessary for the gyro torquer to be sized to transmit such, possibly large, torques. In fact the torquer needs to supply only the torque necessary to cancel the gimbal bearing drag. This property has sometimes been erroneously referred to as 'torque amplification', but is actually a purely SEMI-PASSIVE response of the gyro to the situation considered. Clearly, as the gimbal rotates, the axis about which the control torque is produced rotates correspondingly, remaining perpendicular to $\underline{h}$. However, by provision of three suitably oriented single degree-of-freedom CMGs, this SEMI-PASSIVE property can be maintained continuously in three axes[3,4,5]. In principle, this would seem to be an ideal system for a manned spacecraft, in which crew movement would generate frequent requirements for large control torques, but with zero secular component.

Clearly, as mentioned earlier, the use of CMGs potentially involves a high degree of inter-axis coupling. This could be avoided to a large extent by permitting only small gimbal rotations, but this would imply poor utilization of the stored angular momentum. Suggestions have been made[4,5] that single degree-of-freedom gyros should be coupled mechanically (or perhaps electrically?) in pairs as shown in Fig.7. The total angular momentum vector of a pair then remains directed along a selected axis. The simple gyroscopic coupling due to this total vector remains (an identical effect occurs with reaction wheels) but its effect may not be unduly troublesome.

A restriction to the use of single degree-of-freedom CMGs clearly places a limitation on flexibility for utilizing the contained angular momentum in the most effective manner. Some benefit has been shown to derive from the use of four such CMGs in a tetrahedral arrangement[3]. Clearly full flexibility requires the use of two degree-of-freedom devices. An immediate penalty is that the SEMI-PASSIVE action is lost, and the torquers have to be designed to transmit the full control torques. However, an ingenious method has been suggested[4] for coupling the inner gimbals in pairs, as described above for the single degree-of-freedom case: in addition to alleviating the inter-axis coupling problem, the SEMI-PASSIVE facility is restored. A full assessment of the balance of advantage between one and two degree-of-freedom devices and between coupled and uncoupled devices is clearly a very complicated matter. The system proposed for the Apollo Telescope Mount[5,6] contains three separate two degree-of-freedom CMGs.

2.3 Magnetic Torquers

If a spacecraft carries a vector magnetic moment $\underline{m}$ and the environmental magnetic flux density vector is $\underline{B}$, the spacecraft will experience a torque $\underline{g}$ where

$$\underline{g} = \underline{m} \times \underline{B} \quad . \tag{8}$$

For $\underline{g}$ to be expressed in N m, the unit A m^2 (or A-turn m^2) must be used for $\underline{m}$ and the unit T (tesla, or Wb/m^2) for $\underline{B}$ (1 tesla = 10^4 gauss). Clearly the torque produced has zero component along the instantaneous direction of $\underline{B}$.

(a) 'Coreless' Torques

If materials within the 'range of influence' of a coil have permeabilities not significantly different from that of free space, it is found that to minimize the product of the power and mass allocations required to generate a given magnetic moment, the best design involves a flat coil having the maximum practicable cross-section area. Design formulae are readily derivable[7]. Minimization of the

power-mass product is achieved by constructing the coil from wire having the smallest practicable product of resistivity and density. This will normally imply that aluminium wire be used.

(b) Torquers with Ferromagnetic Cores

The use of a ferromagnetic core in association with a coil results, for many applications, in lower mass and power requirements than for the 'coreless' type, in order to generate a given magnetic moment.

By contrast with the 'coreless' variety, the optimum design is found to consist of a long thin solenoid coil surrounding the core material. Design considerations are relatively complex[8,9]. For some applications a disadvantage of this type of torquer is that, having provided a required magnetic moment, some degree of magnetization remains when the energizing current is removed. This effect is more pronounced, the greater the length/diameter ratio, since such a configuration weakens the demagnetizing effect of the free poles at the ends of the core. A possible solution, if this effect constitutes a problem, is to reduce the energizing current in an oscillatory 'de-perming' fashion.

3 OVERALL SYSTEM DESIGN

In the detailed discussion of systems which follows, the assumption will be made that the system in question can be provided with initial conditions which permit satisfactory convergence to the 'small error' regime. How far outside this regime such conditions can be will vary considerably, depending on the characteristics of the attitude sensing, torquing and data conditioning systems. One or more preliminary modes of control could be necessary, each handing on to the next a progressively reduced set of initial errors.

3.1 Definitions

Consideration will be limited to the case in which the spacecraft is a single rigid body. A mutually orthogonal right-handed set of axes V_1, V_2, V_3 is defined which are fixed relative to this body. These will be the axes about which individual devices exert control torque and about which attitude sensors provide attitude error information (it being assumed that any necessary axis transformation of the raw sensor outputs is provided). Relative to the V-axes the spacecraft has the moment of inertia tensor $\underline{\underline{J}}$ (referred to the spacecraft mass-centre) where

$$\underline{\underline{J}} = \begin{bmatrix} J_1 & -J_{12} & -J_{31} \\ -J_{12} & J_2 & -J_{23} \\ -J_{31} & -J_{23} & J_3 \end{bmatrix} \tag{9}$$

In $\underline{\underline{J}}$ the diagonal elements are the moments of inertia and the off-diagonal elements are the products of inertia.

A set of reference axes R_1, R_2, R_3 is defined with which the corresponding V-axes will coincide when the spacecraft has its desired attitude. For many applications, the R-axes may be regarded as having a fixed orientation in inertial space. However, to cover the case of an earth-pointing vehicle in a circular orbit, the more general situation will be considered initially, in which the R-axes have a constant angular velocity relative to inertial space, of magnitude ω_0, directed along the negative R_2 axis.

Starting from coincidence of the V- and R-axes, the actual attitude of the spacecraft is obtained by rotations of the V system relative to the R system through angles θ_1, θ_2, θ_3 about the corresponding axes. Since only small attitude errors will be considered, the order in which these rotations are made is not significant.

The inertial angular velocity vector $\underline{\omega}$ of the spacecraft has components, expressed in V-axes:-

$$\underline{\omega} = \begin{bmatrix} \omega_1 \\ \omega_2 \\ \omega_3 \end{bmatrix} = \begin{bmatrix} \dot{\theta}_1 - \omega_0\theta_3 \\ \dot{\theta}_2 - \omega_0 \\ \dot{\theta}_3 + \omega_0\theta_1 \end{bmatrix} \tag{10}$$

3.2 Reaction Wheel Systems

(a) Equations of Motion

The equation of motion of the spacecraft is

$$\underline{\underline{J}} \cdot \dot{\underline{\omega}} + \underline{\omega} \times \underline{\underline{J}} \cdot \underline{\omega} = \underline{g} \quad , \tag{11}$$

where $\underline{g}$ is the vector of the total torque applied to the body. The time derivative of $\underline{\omega}$ is to be evaluated relative to V-axes.

If a reaction wheel has moment of inertia tensor $\underline{\underline{J}}^r$ (relative to its own mass-centre) and angular velocity $\underline{\omega}^r$ relative to the spacecraft, then its equation of motion is

$$\underline{\underline{J}}^r \cdot (\dot{\underline{\omega}}^r + \dot{\underline{\omega}}) + \underline{\omega} \times \underline{\underline{J}}^r \cdot (\underline{\omega}^r + \underline{\omega}) = -\underline{g}^r \quad , \tag{12}$$

where $\underline{g}^r$ is the vector of the torque reaction on the spacecraft due to the wheel. Time derivatives again are relative to V-axes.

The spacecraft is assumed to contain three identical reaction wheels, with axes of rotation aligned with each of the V-axes. The wheels are axially symmetric, with moment of inertia I about the axis of rotation.

Define, for $i = 1,2,3$

v_i : the wheel speeds relative to the spacecraft

$h_i = Iv_i$: the wheel angular momenta relative to the spacecraft

g_i^c : the control torques exerted by the wheels on the spacecraft (i.e. the components of the $\underline{g}^r$ in the directions of the wheel axes of rotation)

g_i^e : the components relative to V-axes of the disturbing torque acting on the spacecraft.

Assuming that the θ_i, $\dot{\theta}_i$ are small quantities and retaining only first order small quantities, use of the above definitions and Eqs (9) to (12) permits the equations of motion to be expressed in the linearized form:-

$$\begin{aligned} J_1\ddot{\theta}_1 = {} & g_1^e + g_1^c + J_{23}\omega_0^2 + \omega_0 h_3(t) + J_{12}\ddot{\theta}_2 + J_{31}\ddot{\theta}_3 \\ & - (h_3(t) + 2J_{23}\omega_0)\dot{\theta}_2 + \{h_2(t) + (J_1 - J_2 + J_3)\omega_0\}\dot{\theta}_3 \\ & + \{h_2(t) + (J_3 - J_2)\omega_0\}\omega_0\theta_1 + J_{31}\omega_0^2\theta_3 \end{aligned} \tag{13}$$

$$\begin{aligned} J_2\ddot{\theta}_2 = {} & g_2^e + g_2^c + J_{23}\ddot{\theta}_3 + J_{12}\ddot{\theta}_1 \\ & - (h_1(t) + 2J_{12}\omega_0)\dot{\theta}_3 + (h_3(t) + 2J_{23}\omega_0)\dot{\theta}_1 \\ & - (h_3(t) + J_{23}\omega_0)\omega_0\theta_3 - (h_1(t) + J_{12}\omega_0)\omega_0\theta_1 \end{aligned} \tag{14}$$

$$\begin{aligned} J_3\ddot{\theta}_3 = {} & g_3^e + g_3^c - J_{12}\omega_0^2 - \omega_0 h_1(t) + J_{31}\ddot{\theta}_1 + J_{23}\ddot{\theta}_2 \\ & - \{h_2(t) + (J_1 - J_2 + J_3)\omega_0\}\dot{\theta}_1 + (h_1(t) + 2J_{12}\omega_0)\dot{\theta}_2 \\ & + \{h_2(t) + (J_1 - J_2)\omega_0\}\omega_0\theta_3 + J_{31}\omega_0^2\theta_1 \end{aligned} \tag{15}$$

$$h_1(t) = -\int dt g_1^c - I(\dot{\theta}_1 - \omega_0\theta_3) \tag{16}$$

$$h_2(t) = -\int dt g_2^c - I(\dot{\theta}_2 - \omega_0) \tag{17}$$

$$h_3(t) = -\int dt g_3^c - I(\dot{\theta}_3 + \omega_0\theta_1) \quad . \tag{18}$$

Apart from the small error approximation, the above equations are exact provided that the wheels are included when evaluating the spacecraft moments of inertia, but with the exclusion, for each wheel, of its moment of inertia about its own axis of rotation. This exclusion is in fact of little consequence, since the wheel moments will normally be smaller than those of the spacecraft by a factor of at least 10^3.

To complete the system equations of motion it remains to specify the means by which the g_i^c shall be generated as functions of the attitude error information.

(b) Commentary on Inter-axis Coupling

In any likely application, the right-hand side terms in Eqs (16) to (18), apart from the integrals, can safely be ignored. Eqs (13) to (15) are then a highly coupled set of linear equations with several time-varying coefficients which depend on the $h_i(t)$. System synthesis using the full equations is not normally practicable but it is important that they should be examined initially in order to ensure that important terms are not ignored. The g_i^e and g_i^c terms will always be significant. Of the remainder some may be clearly negligible. Some terms may be of a 'borderline' nature, judged small enough to ignore for preliminary synthesis but requiring evaluation of their effects as perturbations (i.e. regarding them as additional components of the g_i^e) on the system designed in their absence[10].

A substantial simplification of Eqs (13) to (15) would result if the V-axes were principal axes of inertia of the spacecraft, in which case the product of inertia terms would disappear. Spacecraft are normally designed in this way unless good reasons exist for not doing so. In practice residual non-zero products of inertia will exist and their effects through the $\dot{\theta}$ terms may be assessed on the basis indicated above.

The importance of the remaining terms may often be assessed by comparing them with like terms in the g_i^c. Slowly varying terms (such as $\omega_0 h_3(t)$ in (13)) or slowly varying components of other terms should be compared with the zero frequency stiffness term in the relevant g_i^c term (if integral control is employed this stiffness will differ from the stiffness in the neighbourhood of the system natural frequency). For assessment of the importance of the θ and $\dot{\theta}$ terms, it may often be satisfactory to assume g_i^c has the form

$$g_i^c = -J_i(2\omega_n\dot{\theta}_i + \omega_n^2\theta_i) \tag{19}$$

where ω_n is the natural frequency of the control system, assumed critically damped. If it can be assumed that similar attitude errors and natural frequencies are present in all three axes then, for example, terms of the type $h_3(t)\dot{\theta}_2$ (in (13)) will not be important if

$$h_{max} \ll 2J\omega_n \quad , \tag{20}$$

where J is a 'typical' movement of inertia of the spacecraft. h_{max} will normally be chosen so that the wheel can absorb cyclic components of disturbing torque without calling in an unloading system (see 2.2). Given this value of h_{max}, and if there is no conflict with other requirements (e.g. avoidance of undue sensitivity of attitude to sensor noise), it could be elected to make ω_n large enough for appropriately strong satisfaction of (20).

Another approach toward the avoidance of difficulty due to the coupling terms in Eqs (13) to (15) lies in the use of 'decoupling' signals. For instance if measurements are available, of suitable quality, of the h_i and $\dot{\theta}_i$ variables, signals can be added to the g_i^c which will cancel terms of the form $h_i\dot{\theta}_j$.

Further study of reaction wheel systems will be limited to the basic synthesis phase in which, in Eqs (13) to (15), all right-hand side terms will be ignored, with the exception of the g_i^e and g_i^c terms. The forms of the equations are then identical for all three axes: control in a single axis only will therefore be considered.

(c) Detailed Design of a Single-axis Reaction Wheel System

It will be assumed that the only attitude information available is provided by a sensor of attitude position error θ, whose output may be contaminated by a noise signal n. Using the form (6) for the reaction wheel transfer function, a single-axis reaction wheel control system can be constructed in accordance with the block diagram of Fig.8. System damping is provided in the conventional manner by use of the derived rate network having transfer function $(1 + \alpha Tp)/(1 + Tp)$, where $\alpha > 1$. If this were the only frequency dependent transfer function between sensor and wheel, it is possible that the noise level on e could be undesirably high even though that on θ were acceptable. Since e is an electrical signal having a limited working range, the performance of the system could be affected if the noise caused e to run into saturation for a significant proportion of the total time. Accordingly it is desirable to insert a sensor filter as shown (the sensor transfer characteristic is assumed to be otherwise independent of frequency) having a transfer function $1/(1 + T_s p)$. T_s should be as large as is possible while avoiding significant interference with the action of the derived-rate network.

The loop transfer function of the system is

$$L(p) = \frac{kk_r(1 + \alpha Tp)}{Jp(\omega_r + p)(1 + T_s p)(1 + Tp)} \quad . \tag{21}$$

The asymptotic behaviour of $\log |L(i\omega)|$ as a function of $\log \omega$ is illustrated in Fig.9, k having been chosen so that an adequate phase margin exists at the frequency Ω for which $|L(i\omega)| = 1$. On the assumption that ω_r is very much smaller than Ω and that, given Ω, reasonable values are chosen for the remaining parameters, the performance of the system is largely determined by the value of Ω. Though minor improvements might be obtained by other choices, for most purposes satisfactory performance will result from use of the parameter values

$$T = 1/3\Omega \ , \ \alpha = 9 \ , \ T_s = 1/6\Omega \ , \ k = J\Omega^2/3k_r \quad .$$

Then

$$L(p) = \frac{6\Omega^3(3p + \Omega)}{p(p + \omega_m)(p + 3\Omega)(p + 6\Omega)} \quad . \tag{22}$$

The important overall responses are then given by the operational relations

$$\theta = P_n(p)n \tag{23}$$

$$\theta = P_g(p)g^e \tag{24}$$

$$e = Q(p)n \tag{25}$$

where

$$P_n(p) = \frac{6\Omega^3(3p + \Omega)}{C(p)} \tag{26}$$

$$P_g(p) = \frac{(p + \omega_m)(p + 3\Omega)(p + 6\Omega)}{JpC(p)} \tag{27}$$

$$Q(p) = \frac{6J\Omega^3 p(p + \omega_m)(3p + \Omega)}{k_r C(p)} \tag{28}$$

and

$$C(p) = 6\Omega^3(3p + \Omega) + p(p + \omega_m)(p + 3\Omega)(p + 6\Omega) \tag{29}$$

$C(p)$, the characteristic polynomial of the system may be expressed in the form

$$C(p) = (p + a_1)(p + a_2)(p^2 + 2\zeta\omega_n p + \omega_n^2) \quad . \tag{30}$$

Values of a_1, a_2, ω_n and ζ have been computed for certain values of ω_r:-

ω_r/Ω	a_1/Ω	a_2/Ω	ω_n/Ω	ζ
0.1	0.47	6.7	1.39	0.70
0.05	0.51	6.7	1.32	0.70
0	0.58	6.7	1.25	0.69

If the noise signal n has a frequency independent spectral density N $(\text{rad})^2/\text{rad/s}$, use of (23) and (25) permits evaluation of the mean-square noise levels σ_θ^2 and σ_e^2 on θ and e respectively:-

$$\sigma_\theta^2 = 0.90\pi\Omega N \qquad (\text{rad})^2 \tag{31}$$

$$\sigma_e^2 = 21\pi J^2\Omega^5 N/k_r^2 \qquad (\text{rad})^2 \quad . \tag{32}$$

These formulae are approximate, but with error not exceeding 10% if $\omega_r \leqslant 0.05\Omega$.

It is recalled that if the reaction wheel characteristics are significantly non-linear, it may be necessary to take account of the variations of k_r and ω_r with working point. If the variations are severe, the above design may need modification to assure adequate performance under all conditions. Direct reference to the wheel characteristics may be necessary to evaluate the attitude error due to essentially zero frequency components of disturbing torque. Special attention may also be necessary to cover the transient situation which arises as the wheel speed passes through zero.

(d) Unloading of Reaction Wheel Systems

Unloading is necessary to prevent the speeds of the reaction wheels exceeding their design limits, largely as a result of the action of secular components of disturbing torque.

The most obvious means for unloading is through the use of a mass expulsion system. This system would be energized, in a given axis, when the speed of the corresponding wheel exceeded a preset threshold. There are two principal methods of mechanizing such an operation:-

(i) The appropriate jet is commanded ON and remains ON until the wheel speed falls below a lower threshold. The reduction of wheel speed is accomplished through the normal action of the wheel control loop, which treats the jet torque as a disturbing torque. If the jet torque exceeds the torque capability of the wheel, it will be necessary to operate the jet in a pulsing mode, to reduce the mean jet torque.

(ii) A change of control mode is initiated, the new mode controlling the attitude of the spacecraft purely by use of jet torque. Simultaneously, maximum deceleration torque is applied to the wheel. When the wheel speed falls below an appropriate threshold, the normal control mode is re-enabled.

In the detailed design of the unloading system, account must be taken of the extent to which it may be necessary to limit attitude error during the unloading process.

Systems as described above, using preset wheel speed thresholds, may not be optimally economic in use of jet system fuel, unless the threshold which disables unloading is set only a small amount below the enabling threshold. This latter course could be undesirable in view of the resulting relatively high frequency of unloading operations and therefore of occasions on which the attitude error might be larger than is tolerable for normal operation. Recently proposals have been made[11] for unloading systems which make use of knowledge or estimation of disturbing torque time variations in order to operate both economically and with minimum frequency.

Reaction wheel unloading may also be accomplished through the use of magnetic torquing. The spacecraft must carry a set of three mutually perpendicular torquers so that a magnetic moment $\underline{m}$ can be generated in any required direction. Also needed is a three-axis magnetometer to measure the ambient magnetic flux density $\underline{B}$. Care may be needed to ensure that the measured value of $\underline{B}$ is not contaminated by fields generated by the spacecraft. The magnetic moment which the torquers must provide is computed according to

$$\underline{m} = k(\underline{h} \times \underline{B}) \tag{33}$$

where $\underline{h}$ is the total angular momentum contained in the wheels. The unloading torque experienced by the spacecraft is then

$$\begin{aligned} \underline{g} &= \underline{m} \times \underline{B} \\ &= -kB^2(\underline{\underline{I}} - \underline{u}_B\underline{u}_B) \cdot \underline{h} \end{aligned} \tag{34}$$

where $\underline{\underline{I}}$ is the unit tensor and $\underline{u}_B$ is the unit vector in the direction of $\underline{B}$. The unloading torque therefore acts against the component of $\underline{h}$ which is perpendicular to $\underline{B}$. Obviously it is not possible to generate torque in the direction of $\underline{B}$. However, unless the spacecraft has an orbit which lies close to the geomagnetic equator, the direction of $\underline{B}$ will vary substantially as the orbital motion proceeds. As long as the wheels have adequate momentum capacity, it is then possible to unload in all axes during the course of an orbit.

The magnetic unloading method has the obvious advantage that it avoids consumption of fuel mass. The power requirements for energizing the torquers are normally quite small. Also, since unloading proceeds continuously, the unloading torque will have an order of magnitude similar to that of the disturbing torques, avoiding the likelihood of significant increase in attitude error during unloading.

3.3 Control Moment Gyro Systems

In view of the complexity which arises from inter-axis coupling, only a brief discussion of CMG systems can be given in this paper.

Early suggestions[3] for the design of the overall control system employed what may be termed the 'direct' approach. After necessary processing to take account of coupling, signals from the attitude error sensors were used directly to command currents to flow in appropriate gyro torquers, in such a way that reaction torques were produced which would reduce the attitude errors. More recently, an 'indirect' method appears to have been preferred[5] on the grounds of minimizing difficulties due to coupling and of ease of implementation of unloading procedures. The principle of this method is outlined below.

Referring to Fig.10, the error information from the sensors is processed conventionally (e.g. by use of derived rate networks as shown in Fig.8 for a reaction wheel system) to produce, in the three spacecraft control axes, the components of a demanded control torque vector $\underline{g}_d^c$. These components are integrated with respect to time to yield a demanded angular momentum content $\underline{h}_d^c$ of the CMG array. The actual content $\underline{h}^c$ of the array is computed, via appropriate axis transformations, from the gimbal position information. The difference $\underline{\varepsilon} = \underline{h}_d^c - \underline{h}^c$ is processed to obtain signals which drive the gimbal servos in a manner which causes the magnitude of $\underline{\varepsilon}$ to be reduced. As time proceeds $\underline{h}^c$ will follow $\underline{h}_d^c$ in a way which absorbs the effect of the disturbing torque $\underline{g}^e$, and, in varying, will generate the actual control torque $\underline{g}^c$.

3.4 Pure Jet Systems

Under the assumption that no significant inter-axis coupling effects are present, discussion of pure jet systems will be limited to the study of control in a single axis. It will also be assumed that it is required to achieve the highest practicable precision of control while maintaining economy in the use of jet fuel.

The requirement that jet fuel be used economically implies that jets should thrust only in opposition to the instantaneous disturbing torque whenever the magnitude of this torque exceeds a small fraction (0.1, say) of its maximum value. Gas-dynamic considerations in the nozzle and electro-mechanical considerations in the control valve lead to the imposition of lower limits on the thrust F and pulse duration δ which can be provided efficiently. For a cold gas jet, these limits are in the region of 0.05 N thrust and 5 ms ON time. Efficient production of torque requires that the length of the jet lever arm be reasonably large. Thus, in a given spacecraft with lever arm ℓ and moment of inertia J, the control acceleration will be $a_c = F\ell/J$. If a nominal pulse duration δ is chosen (bearing in mind that somewhat shorter pulses may be required as the system converges to its steady-state operation), the nominal angular velocity increment from a jet pulse will be $a_c\delta$. If $(g_e)_{min}$ is the value of disturbing torque for which it is required that the jets should thrust only in opposition to the disturbing torque, then the highest precision of control which is achievable is that given by the state of motion ('limit-cycle') illustrated in the phase-plane diagram of Fig.11. $(a_e)_{min} = (g_e)_{min}/J$ is the disturbance acceleration corresponding to $(g_e)_{min}$. Clearly it is necessary to provide a 'dead-band' $\pm\theta_d$ of attitude error, where

$$\theta_d = a_c^2\delta^2/16(a_e)_{min} \quad . \tag{35}$$

Within this dead-band control action is inhibited, and it is necessary to tolerate attitude position and rate errors of magnitudes θ_d and $a_c\delta/2$ respectively. The aim of the designer is then to produce a system which will converge to the state motion shown in Fig.11.

If θ and $\dot{\theta}$ information of sufficient quality is available, and if the jet responds virtually instantaneously to ON and OFF commands, this objective can be achieved by use of a jet switching logic system corresponding to the switching boundaries shown in Fig.12, together with a typical rapid convergence to the limit cycle. A less satisfactory form of logic is illustrated in Fig.13; it suffers[12] from relatively poor convergence once the attitude rate has been reduced to below the magnitude $a_c\delta$, with the result that to avoid jet pulsing at both boundaries of the dead-band it may be necessary to use a value of θ_d up to four times larger than that determined by the ideal limit-cycle. Though reasonable quality θ information may be readily available, it is comparatively rare that the same can be said for $\dot{\theta}$ information. The additional circuit complexity required for realization of the Fig.12 logic (compared with that for the Fig.13 logic) is unlikely to be justified by improved performance if the $\dot{\theta}$ information is of poor quality.

Since nominal jet pulse durations of less than 10 ms are being considered, and if it required to approach the ideal behaviour illustrated in Fig.12, it is clear that it is not possible to tolerate pulse duration errors exceeding about 1 ms. If, having commanded the jet ON, generation of the following OFF command is contingent upon direct observation of sensor measurements, three types of difficulty arise. First, delays in the control valve and nozzle may cause the termination of the actual jet pulse to occur several milliseconds later than generation of the electrical OFF command. Second, many sensors exhibit response delays: in some cases these can be as long as some hundreds of milliseconds. Third, sensor output signals may be contaminated with noise, either inherently or as a result of transient structural vibration caused by the jet pulse.

These difficulties have been recognized for nearly a decade. In practice it was usually the case that their effect on the quality of the $\dot{\theta}$ information was far more serious than on that of the θ information. This led to the proposal[13,14] of systems of the type illustrated in Fig.14. No attempt is made to derive rate information from a sensor signal. Instead, a quasi-rate signal $k\omega_q$ was obtained by passing the noise-free jet command signals through the transfer function $K/(1 + T_f p)$, on the intuitive basis that the jet command signals approximately represented spacecraft angular acceleration and that the transfer function provided an approximate integration. Though avoiding all the difficulties mentioned earlier, this rate signal clearly contains errors which could make it unsuitable for use in driving logic of the type shown in Fig.12. The Fig.13 logic was in fact used. The delay of the actual jet pulse relative to the command signal is of little consequence, since this error is detected by the sensor and used to correct the system state information in preparation for the next pulse.

A result of the intuitive and approximative thinking which generated the system of Fig.14 is that a complete theoretical analysis of its behaviour does not appear to be practicable. Further, if the basic system falls short of meeting a specification, it is difficult to see how to apply techniques familiar in the design of linear systems for obtaining a good compromise between the conflicting aims of low sensitivity to sensor noise and low sensitivity to disturbing torque. A number of variants of the system have been proposed but none avoid the intuitive basic approach.

A closer examination of the system of Fig.14 reveals that, as long as it is operating fairly close to the nominal limit-cycle, the feedback loop around the switching logic is designed to produce a pulse duration equal to that required in this nominal cycle. The input from the sensor acts primarily as a trigger for this pulse, and has little effect on its duration. In other words, given knowledge of the

dynamic properties of the spacecraft, a crude 'model' of the relevant part of the dynamics is implicitly incorporated in the system. It is the behaviour of this model, rather than that of the actual spacecraft, which determines the pulse duration. This observation led the author to investigate systems making explicit use of a comprehensive model of the spacecraft dynamics[12,15].

This comprehensive model appears as part of Fig.15. The spacecraft carries two electronic integrators which, from the sum of modelled versions of the control acceleration (f_{cm}) (generated by the jet switching logic) and disturbance acceleration (f_{em}), produce modelled versions of the spacecraft attitude rate (ω_m) and attitude position (θ_m). The ω_m and θ_m signals drive the jet logic avoiding any delays due to sensors. So far, these signals are free from noise. The f_{cm} signal also drives the real jets. Clearly the model is incomplete in that it has no means of generating f_{em}, of setting the integrator initial conditions to conform with the actual state of the spacecraft and of ensuring that integrator drifts and errors in parameters do not cause the state of the model to diverge from the spacecraft state. These shortcomings are remedied by use of a follow-up servo, represented by the box 'linear processing' in Fig.15. This servo may take various forms. One possibility is shown in Fig.16, it being assumed that the servo speed of response is sufficiently slow that any frequency dependence in the sensor may be ignored. The servo incorporates integral control and the various gains have been selected to provide simple forms in the transfer functions to be discussed below. Minor improvements in performance might be obtainable through the use of somewhat different values.

To assess the performance of the system it is necessary to evaluate the noise levels on the modelled variables which result from noise on the sensor output θ_s. For this purpose the transfer functions $F(p:q,\theta_s)$ are derived, which determine the response of variable q to a signal imposed at the point θ_s, with f_{cm} held equal to zero. It is also necessary to determine the values of the error quantities:-

$$\delta\omega_m \equiv \omega_m - \dot{\theta}_s \; ; \quad \delta\dot{\theta}_m \equiv \dot{\theta}_m - \dot{\theta}_s \; ; \quad \delta\theta_m \equiv \theta_m - \theta_s \tag{36}$$

in response to the variable f_e, with f_{cm} and f_c held equal to zero. The transfer functions $F(p:r,f_e)$ provide the necessary information, where r may be any one of the above error quantities (36). The transfer functions for the system of Fig.16 are:-

$$\left.\begin{aligned} F(p:f_{em},\theta_s) &= \frac{(1+3\tau p)p^2}{(1+\tau p)^3}, \quad F(p:\omega_m,\theta_s) = \frac{(1+3\tau p)p}{(1+\tau p)^3} \\ F(p:\dot{\theta}_m,\theta_s) &= \frac{(1+3\tau p+3\tau^2p^2)p}{(1+\tau p)^3}, \quad F(p:\theta_m,\theta_s) = \frac{1+3\tau p+3\tau^2p^2}{(1+\tau p)^3} \\ F(p:\delta\omega_m,f_e) &= -\frac{\tau^2(3+\tau p)p}{(1+\tau p)^3}, \quad F(p:\delta\dot{\theta}_m,f_e) = -\frac{\tau^3p^2}{(1+\tau p)^3}, \quad F(p:\delta\theta_m,f_e) = -\frac{\tau^3p}{(1+\tau p)^3}. \end{aligned}\right\} \tag{37}$$

Both ω_m and θ_m have the features that they contain only a 'low-pass filtered' version of noise on θ_s and that they have zero error in response to a constant value of disturbing acceleration f_e.

The value of τ will be chosen to minimize the total errors in ω_m and θ_m, due to sensor noise and to changing disturbing acceleration. If ω_m is then of sufficient quality, logic of the type illustrated in Fig.12 may be used, being driven by ω_m and θ_m. Even if the quality is relatively poor, so that there is little point in using other than the Fig.13 logic, the overall performance may well be substantially better than that achievable using the system of Fig.14.

3.5 Inertially Referenced Systems: Gyrocompassing

Instead of using a sensor of attitude position relative to some 'material' object (e.g. the sun or the earth), a control system can be designed to operate in response to error relative to an inertial position reference provided by a system of gyroscopes. In spacecraft such a reference is most commonly provided by a set of three strap-down rate-integrating gyros. A single-axis control system of this type is illustrated in Fig.17. For the present, ignore the input to the gyro torquer. The system for applying control torque to the spacecraft could be of any convenient type, the processing of the gyro output signal θ_g being chosen appropriately. For instance, it could embody the modelling technique discussed in 3.4 in relation to pure jet systems. The system will then control the attitude of the spacecraft to a reference which is nominally fixed in inertial space, but in practice will drift in accordance with the gyro drift rate $\dot{\theta}_d$. In a spacecraft which has no significant linear acceleration (other than that due to gravity), a high quality gyro can have a very stable drift rate, varying by less than $0.01^\circ/h$ in any hour. Therefore, if it is possible to make an initial compensation for any comparatively large constant component of drift rate, the unaided inertially referenced system can hold a fairly precise attitude for usefully long periods of time. Also by application of an accurately determined current to the gyro torquer, it is often possible to slew a spacecraft through a large angle with little error. Such a facility could be useful when transferring control from one reference object to another, using sensors having limited fields of view.

If it is required to control relative to some reference object, the appropriate sensor can be connected to bias the gyro, via its torquer, as shown in Fig.17. It is desirable to subtract the gyro output θ_g from the sensor output θ_s before applying the result to the gyro torquer, in order to ensure that the position sensor signal is correcting the error in the implicit inertial reference, rather than this error plus error relative to the inertial reference. This point could be of some significance in the case of a jet system with its relatively large dead-band error. If the gain constant k were sufficiently large, failure to decouple in this way could lead to significantly non-nominal operation of the jet system. As shown, an integration path will often be provided in parallel with the direct path to the gyro torquer. The main function of this is to hold the compensation for steady component of gyro drift rate which would otherwise have to be provided by a steady error signal from the position sensor.

If the gyro is of high quality, adequate performance can often be obtained using small values of the gain constants k and ℓ. This implies that precision control to the position reference may be achievable even if the output from the sensor is very noisy or intermittently available or both. Of course, if the sole purpose of the attitude control system is to maintain orientation relative to an object in respect of which a very high quality error signal is available, nothing is gained through the additional presence of an inertial reference system.

If it can be assumed that the natural periods of the system for correction of the inertial reference are long compared with those of the system controlling the spacecraft attitude relative to the inertial reference, the behaviour of the former system can be analysed independently of the latter. Regarding the input to the gyro torquer as scaled in accordance with the angular velocity it represents, the equation of motion of the correction system is

$$\dot{\theta} - \dot{\theta}_d = -\left(k + \ell \int dt\right)(\theta - \delta) \tag{38}$$

where δ is the noise signal generated by the sensor.

In operational form (38) becomes

$$(p^2 + kp + \ell)\theta = p\dot{\theta}_d + (kp + \ell)\delta \quad . \tag{39}$$

If, in the high quality gyro, $p\dot{\theta}_d$ is a sufficiently small quantity, ℓ can be correspondingly small in order to maintain the resulting error in θ below a given level. With selection of a suitable value for k (probably to provide a system with near unity damping ratio), the noise δ is subjected to correspondingly narrow bandwidth filtering before it appears on θ.

A number of applications exist for spacecraft which require stabilization relative to a reference axis system defined by the local vertical and the orbit normal. The R-axes system introduced in section 3.1 is then defined such that R_3 has the direction of the downward local vertical from the spacecraft and R_2 has the direction opposite to that of the orbital angular velocity vector $\underline{\omega}_0$. Through the use of earth horizon sensors, attitude error information for such a spacecraft is readily available about R_1 (θ_1:roll) and R_2 (θ_2:pitch). Except in special cases, error information about the local vertical R_3 (θ_3:yaw) may not be obtainable in a convenient way. However, if the spacecraft had an inertially constant attitude, an error in yaw at one instant would appear as the same error in roll, one quarter of an orbital period later, and *vice versa*. Therefore if the spacecraft is provided with a suitable inertial 'memory', it is possible to achieve control about all three axes even though, at any instant, error information is available about two axes only. This mode of operation is known as 'gyrocompassing'. A number of methods are available for its realization[16]. Explanation is simplest if the spacecraft is assumed to carry a full three-axis inertial reference system: in this paper attention will be restricted to such a system.

The three-axis system configuration is illustrated in Fig.18. The basic control system in each axis is the inertially referenced system of Fig.17. In pitch, a bias rate ω_0 is applied to the gyro torquer. As discussed above, it will be assumed that the natural periods associated with these systems are sufficiently shorter than those of the 'outer loops' which correct the inertial reference, for the latter to be analysable independently of the former.

The inertial angular velocity of the implicit inertial reference is now expressible in terms of the attitude error variables according to relation (10). A circular orbit will be assumed, so that ω_0 is constant. The equations of motion of the inertial reference correction system are then

$$\dot{\theta}_1 - \omega_0\theta_3 = -k_1\theta_1 + \dot{\theta}_{d_1} \tag{40}$$

$$\dot{\theta}_2 - \omega_0 = -\omega_0 - \left(k_2 + \ell_2 \int dt\right)\theta_2 + \dot{\theta}_{d_2} \tag{41}$$

$$\dot{\theta}_3 + \omega_0\theta_1 = -\left(k_3 + \ell_3 \int dt\right)\theta_1 + \dot{\theta}_{d_3} \tag{42}$$

where the $\dot{\theta}_{d_i}$ are the drift rates of the three gyros. The behaviour in pitch (Eq (41)) is identical to that of the single-axis system considered earlier. The coupled roll-yaw system has the characteristic polynomial:-

$$p^3 + k_1 p^2 + \omega_0(k_3 + \omega_0)p + \omega_0 \ell_3 \tag{43}$$

and the following steady-state errors (it has been assumed that the gyro drift rates are constant):-

$$[\theta_1]_{ss} = 0 \tag{44}$$

$$\left[\int^t dt\theta_1\right]_{ss} = \dot{\theta}_{d_3}/\ell_3 \tag{45}$$

$$[\theta_3]_{ss} = \dot{\theta}_{d_1}/\omega_0 \quad . \tag{46}$$

The gains k_1, k_3 and ℓ_3 can be selected to give the characteristic polynomial (43) desired features and to optimize the design in respect of errors due to sensor noise. Note that the natural periods in (43) may be made much shorter than $1/\omega_0$ (unless this conflicts with noise considerations), so that the system can settle in a small fraction of an orbital period.

Note that a separate integrator in the input to the roll gyro must not be used. Its output could settle to an arbitrary value and represent a (possibly large) drift rate of the roll gyro which would (through (46)) lead to an additional yaw error. Nothing would be gained by using the integrator input to the yaw gyro also as an input to the roll gyro.

Eq (46) shows that a yaw error must be tolerated, proportional to the roll gyro drift rate. If it is not possible to compensate this drift rate to the required extent before launch, a useful procedure could be to enter a sun-pointing mode (V_2 sun-pointing). A separate roll gyro bias integrator could then be adjusted to compensate for $\dot{\theta}_{d_1}$, and then be switched into a 'hold' state before entering the earth pointing mode.

REFERENCES

1 Various design data documents issued by Bendix Corporation, Teterboro, New Jersey, USA

2 G.F. Auclair. Advanced Reaction Wheel Controller for Spacecraft Attitude Control. AIAA Guidance, Control and Flight Mechanics Conference, Princeton, New Jersey, USA, August 1969, Paper No.69-855

3 R.C. Wells. Gyroscopic Low Power Attitude Control for Space Vehicles. USAF Report No. ASD-TDR-62-580, September 1962

4 A.D. Jacot and D.J. Liska. Control Moment Gyros in Attitude Control. J. Spacecr. Rockets, Vol.3, No.9, September 1966, 1313-1320

5 B.J. O'Connor and L.A. Morine. A Description of the CMG and Its Application to Space Vehicle Control. J. Spacecr. Rockets, Vol.6, No.3, March 1969, 225-231

6 W.B. Chubb, D.N. Schultz and S.M. Seltzer. Attitude Control and Precision Pointing of Apollo Telescope Mount. J. Spacecr. Rockets, Vol.5, No.8, August 1968, 896-903

7 W.G. Hughes. Space Technology, Vol.2 : Control and Stabilization. ESRO SP-10, July 1966, Lecture No.12

8 J. Braumiller. Magnetic Torquers for Space Vehicle Control. USAF Report No. ASD-TDR-63-74, January 1963

9 M.S. Glass. Principles of Design of Magnetic Devices for Attitude Control of Satellites. Bell Syst. tech. J. Vol.46, No.5, May-June 1967, 893-912

10 W.G. Hughes and G.J. Davison. Reaction Wheel Systems for Coarse and Fine Star-referenced Attitude Control of a Stellar Observatory Satellite. RAE Technical Report 67056, March 1967

11 C.D. Johnson and R.E. Skelton. Optimal Desaturation of Momentum Exchange Control Systems. J. AIAA, Vol.9, No.1, January 1971, 12-22

12 W.G. Hughes. Design for High Precision in Spacecraft Jet Attitude Control Systems. RAE Technical Report 71089, April 1971

REFERENCES (Contd.)

13 J.C. Nicklas and H.C. Vivian. Derived-rate Increment Stabilization: Its Application to the Attitude Control Problem. J. bas. Engng. Vol.84, 1962, 54-60

14 A.P. MacLaren. Design of a Gas-jet Attitude Control System for use in Satellites. RAE Technical Note Space 54, 1964

15 W.G. Hughes. Improved Design Procedures for Precision Attitude Control of a Spacecraft using Pure-jet Control Torquing. Paper proposed for presentation at 4th IFAC Symposium on Automatic Control in Space, Dubrovnik, Yugoslavia, September 1971

16 J.L. Bowers, J.J. Rodden, E.D. Scott and D.B. DeBra. Orbital Gyrocompassing Heading Reference. J. Spacecr. Rockets, Vol.5, No.8, August 1968, 903-910

Acknowledgement

Section 2.1 of this paper was contributed by the author's colleague A.G. Earl.

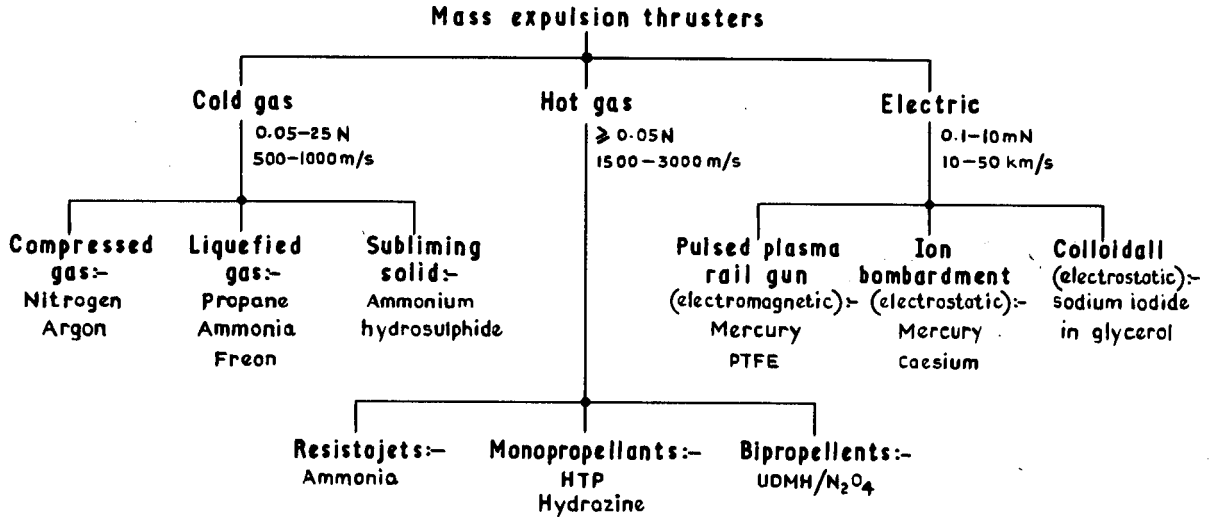

Fig.1 Chart of mass expulsion thrusters

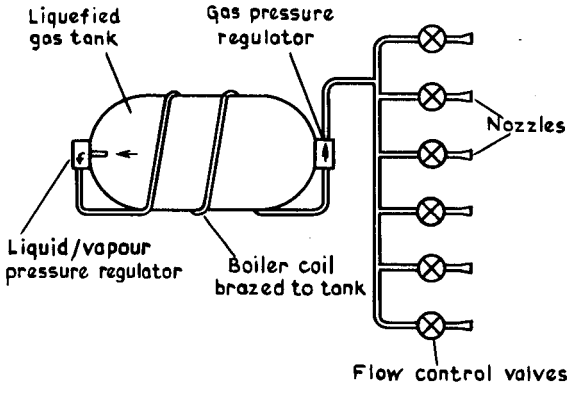

Fig.2 Liquefied gas system

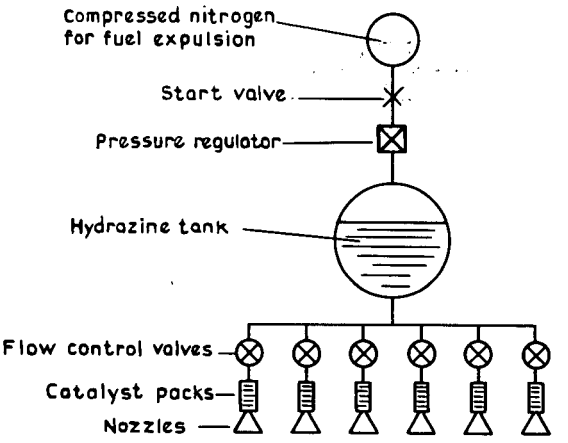

Fig.3 Basic monopropellant hot gas system

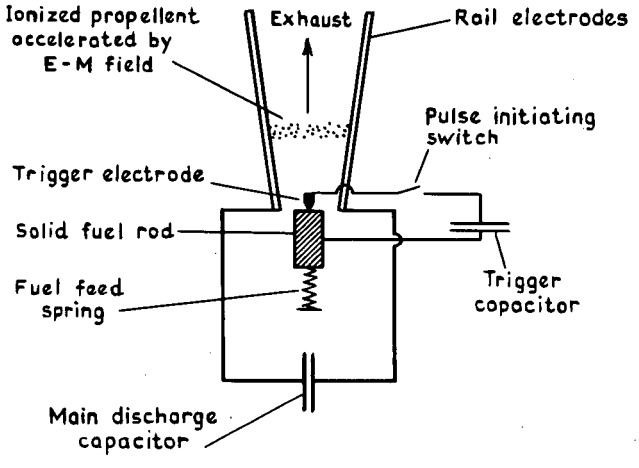

Fig.4 Basic pulsed plasma rail gun

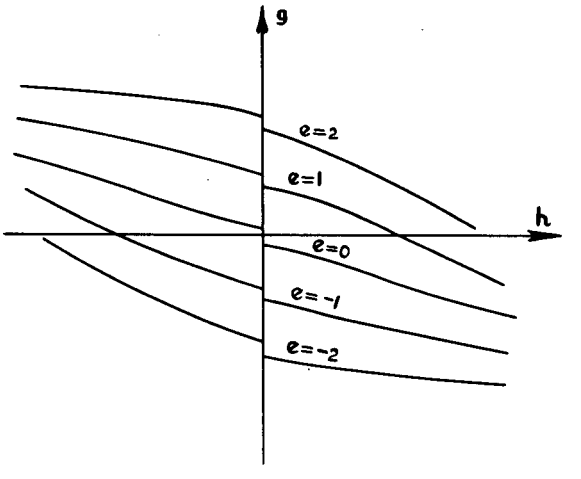

Fig.5 Possible reaction-wheel torque-speed characteristics

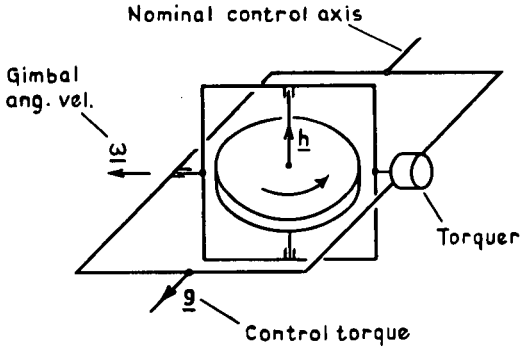

Fig.6 Single degree-of-freedom CMG

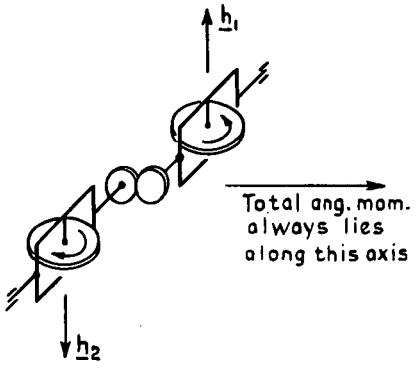

Fig.7 Coupled pair of single degree-of-freedom CMGs

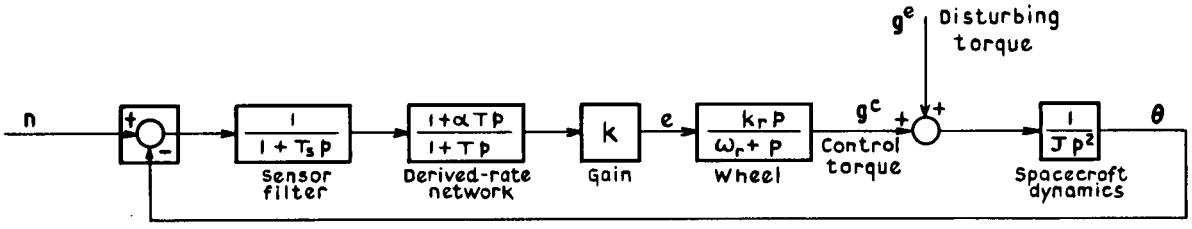

Fig.8 Single-axis reaction wheel control system

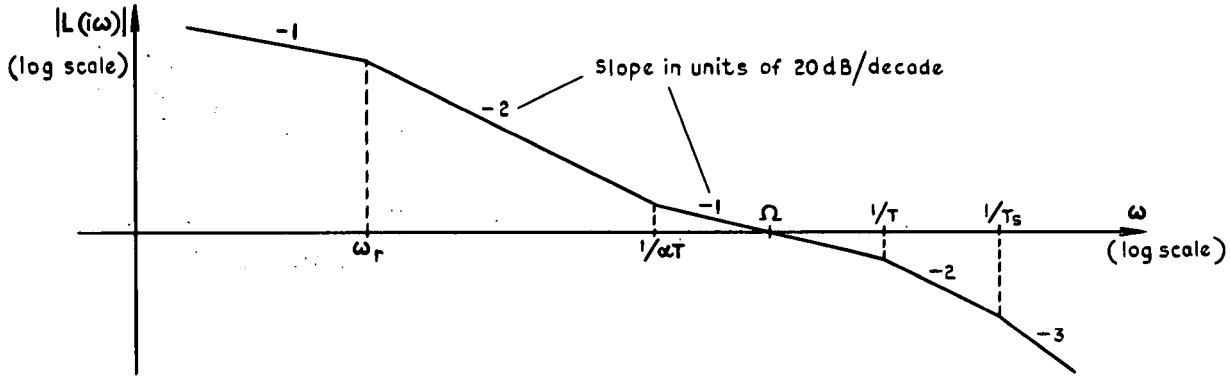

Fig.9 Asymptotic frequency dependence of reaction-wheel system loop transfer function

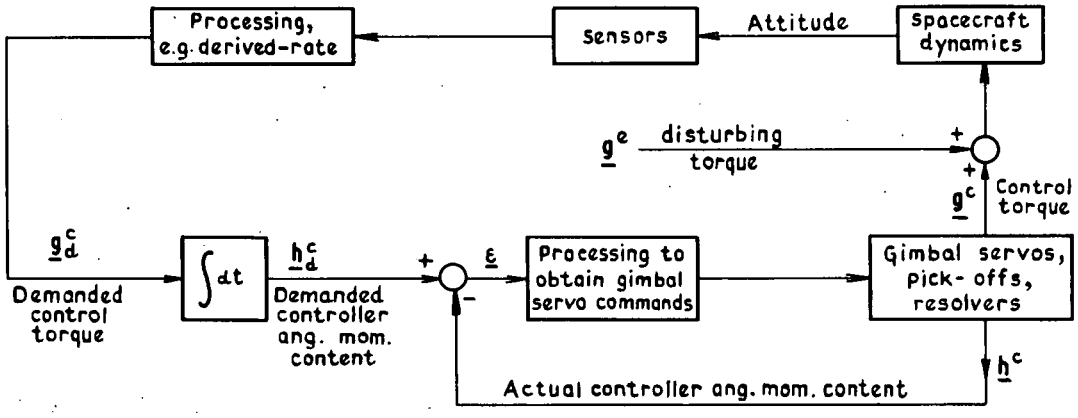

Fig.10 Outline of possible overall CMG system

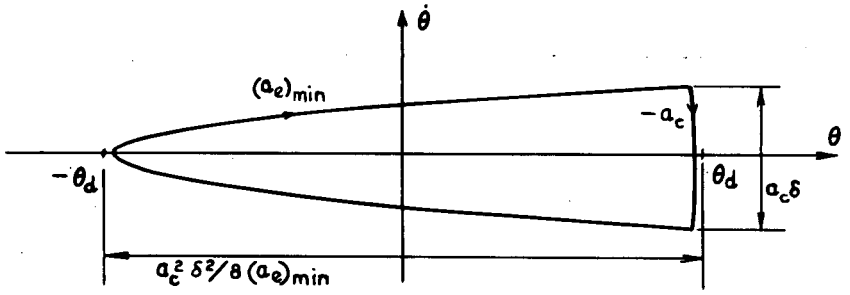

Fig.11 Pure jet system : ideal limit cycle

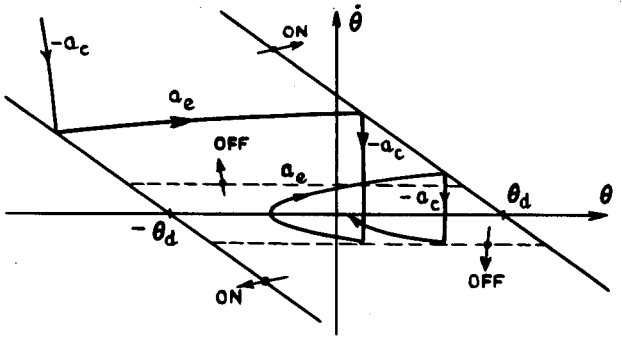

Fig.12 Jet logic providing rapid convergence to limit-cycle

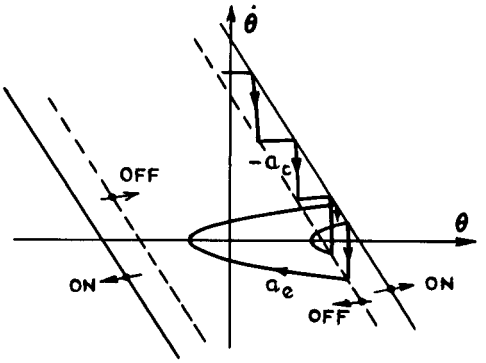

Fig.13 Alternative jet logic

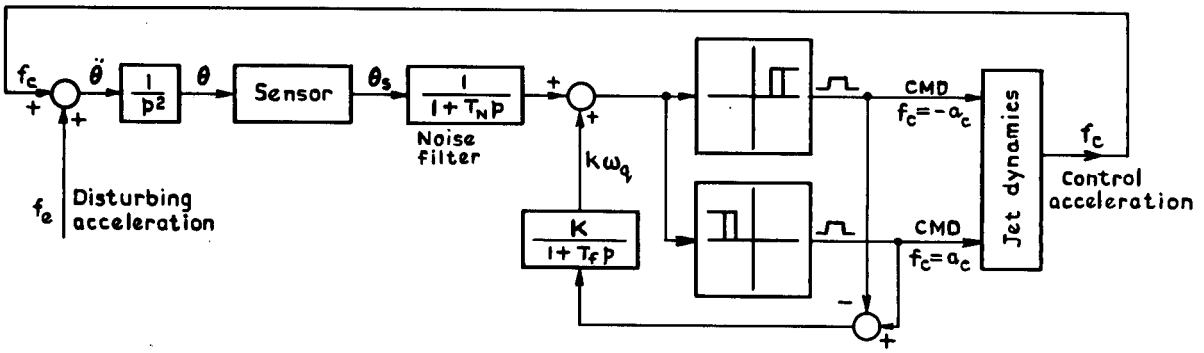

Fig.14 System deriving a quasi-rate signal from the jet command signals

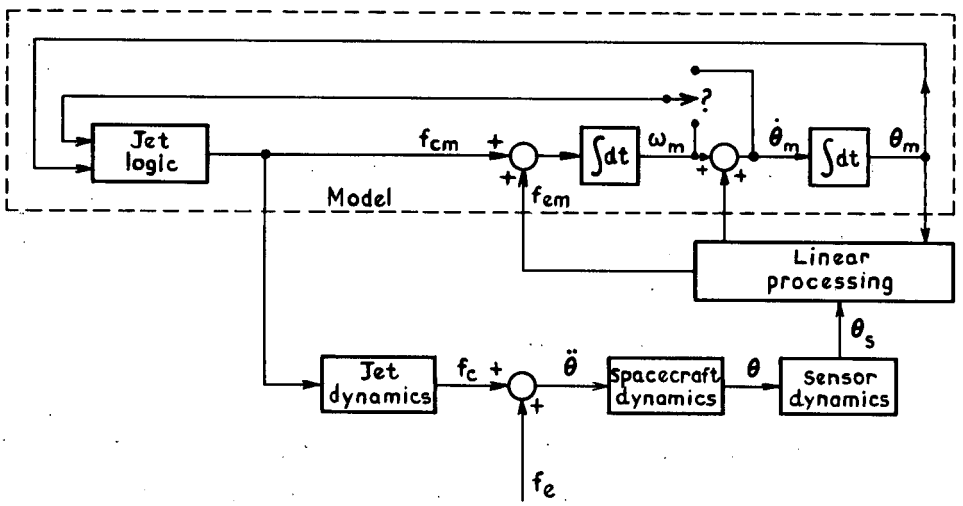

Fig.15 Jet system incorporating model of the ideal control system

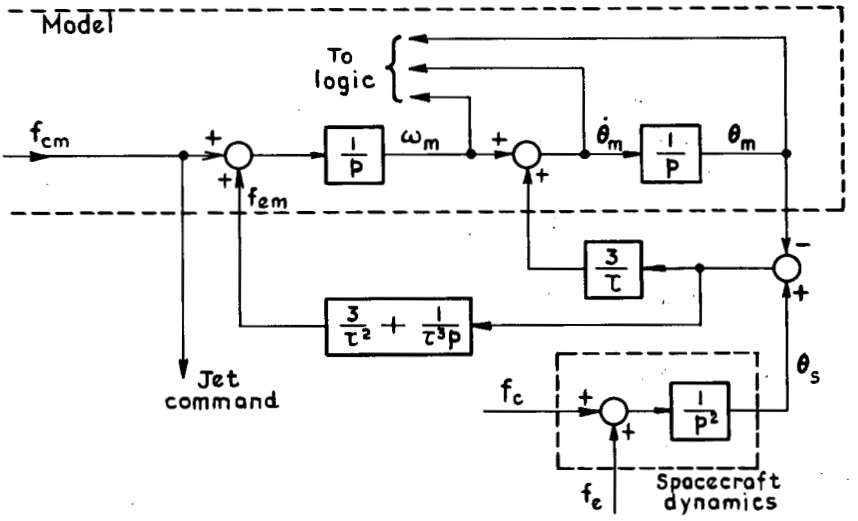

Fig.16 A form of servo for slaving the model to the sensor information

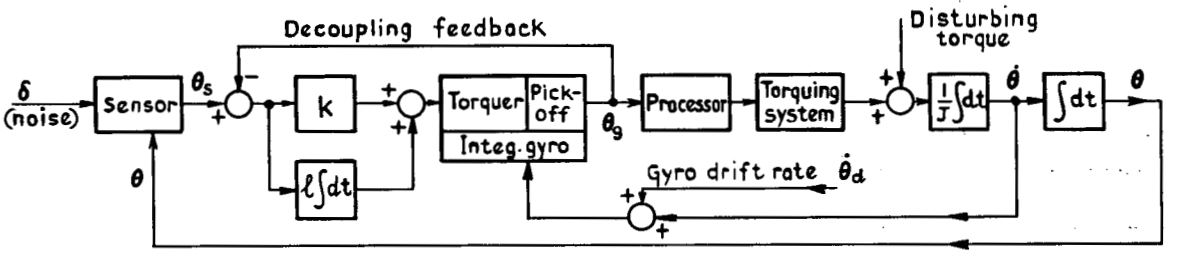

Fig.17 Inertially referenced system with up-dating from a position sensor

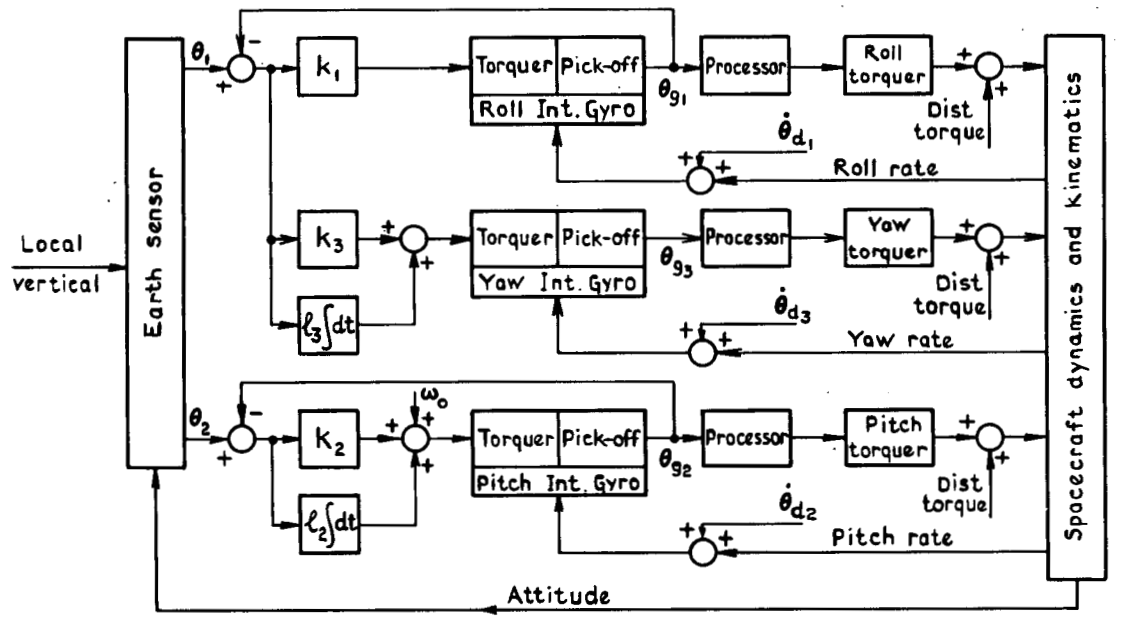

Fig.18 Gyrocompassing technique for stabilization to local vertical and orbit normal

STABILISATION DES SATELLITES EOLE ET PEOLE

Par Philippe HUGUIER, Ingénieur
CENTRE NATIONAL D'ETUDES SPATIALES
B.P. n° 4 - BRETIGNY S/ORGE (91)

Les satellites EOLE et PEOLE utilisent un système de stabilisation passive par gradient de gravité.

La précision recherchée du pointage sur la géocentrique est de 15°. Le système comprend un mât déployable d'une dizaine de mètres de long, comportant une masse d' extrémité de 3 kilogrammes. La stabilisation est "2 axes", c'est-à-dire que la position des satellites autour de la géocentrique est indifférente.

Le système amortisseur est constitué par des barreaux magnétiques en anhyster D S, qui dissipent l'énergie cinétique d'oscillation grâce à leur interaction avec le champ magnétique terrestre.

L'hystérésis magnétique de ces barreaux est utilisée pour remplir cette fonction.

Les barreaux sont disposés suivant les 3 axes principaux du satellite. Ils ont 52 centimètres de long et 2,2 mm de diamètre.

EOLE, dont l'orbite est à 47° d'inclinaison, comporte 12 barreaux.
PEOLE en comporte 18, son orbite étant quasi équatoriale.

La restitution d'attitude est assurée par le soleil et le champ magnétique terrestre, à l'aide de 17 senseurs solaires analogiques et un magnétomètre à trois axes sensibles.

L'acquisition se fait de la façon suivante :

Pour EOLE, une stabilisation temporaire sur le champ magnétique terrestre permet de favoriser le sens de la capture au moment de la sortie du mât déployable.

Pour PEOLE, dont l'orbite ne permet pas une telle procédure, une restitution d'attitude instantanée permet, grâce à un calcul de prédiction, de savoir qu'elles seraient l'énergie et l'orientation du satellite si le mât était déployé à chaque passage au dessus de la station. L'instant de sortie du mât est choisi lorsque les conditions sont favorables.

Un retournement du satellite en vol est envisagé en cas d'échec de la procédure no - minale.

1- Historique

En 1966, le Comité des Programmes Scientifiques du C.N.E.S. donnait son accord pour la mise en route du programme EOLE. Le système spatial prévu consiste en une flotille de ballons destinée à donner des informations sur la vitesse des vents dans l'hémisphère Sud. Les ballons sont intérrogés par un satellite qui transmet les informations au sol lorsqu'il se trouve en visibilité des stations.

Des études préliminaires entreprises au Groupe Technique de Cannes par SUD-AVIATION, sous l'égide de la Direction des Programmes du C.N.E.S., avaient abouti à la " faisabilité " d'une stabilisation par gradient de gravité pour un pointage géocentrique de l'ordre de 15°, sur une orbite quasi circulaire entre 650 et 1200 Km si l'amortisseur utilisé consistait en des barreaux à hystérisis magnétique, d'ailleurs utilisé pour la stabilisation magnétique de DIC.

Les spécifications imposées au pointage géocentrique du satellite EOLE viennent de la compatibilité entre les liaisons radio-électriques entre le satellite et les ballons, et l'orientation de l' antenne. Ces liaisons et la couverture nécessaire sur la terre imposent également une orbite de 900 Km , d'excentricité quasi-nulle.

C'est pourquoi au début du projet EOLE, il fut décidé que le satellite aurait une stabilisation passive par gradient de gravité et un amortisseur constitué par des barreaux à hystérésis magnétique.

La définition du système de stabilisation consiste alors à celle des couples stabilisateurs, du dispositif amortisseur, et par la suite à la minimisation des couples perturbateurs par un choix approprié de la longueur du mât et du lest d'extrémité.

En 1969, il a été proposé de profiter du 2ème tir de qualification du lanceur DIAMANT B pour mettre en orbite un satellite technologique. Le choix s'est fait pour des expériences en vol, préliminaires à EOLE, d'ou le nom de PEOLE.

Parmi plusieurs expériences embarquées, ce satellite devait montrer la validité du système de stabilisation adapté à sa masse, ses paramètre d'inertie et surtout à ses caractéristiques d'orbite.

Ce satellite a été réalisé en 2 ans et mis en orbite le 12 Decembre 1970.

2 - Ressemblances et différences entre les 2 satellites

Les spécifications de pointage géocentrique sont les mêmes : l'angle entre l'axe longitudinal du satellite et la verticale locale doit rester inférieur à 15°.

La structure du satellite est la même : un prisme octogonal de dimensions indiquées figure 1.
une antenne tronconique devant viser le point terrestre sous orbital.
Huit panneaux solaires déployés à 125° du corps du satellite.
Le temps necessaire pour atteindre le régime permanent est d'une dizaine de jours.

L'orbite de PEOLE, prévue initialement, a une excentricité de 0,8 %, pour un périgée à 750 km; Son inclinaison est de 15°.

Celle d'EOLE est nominalement prévue à 900 km circulaire. Son inclinaison est de 47°.

C'est, en fait, la différence d'inclinaison d'orbite qui cause la différence la plus importante entre les systèmes amortisseurs d'une part et ceux d'acquisition d'autre part, des deux satellites.

PEOLE est mis en orbite par le lanceur DIAMANT, à partir de KOUROU, en Guyane Française.

EOLE doit être satellisé par une fusée SCOUT, à partir de WALLOPS Island, sur la côte orientale des ETATS UNIS.

Le diagramme d'antenne impose d'autre part de ne pas déployer de mât de stabilisation vers la géocentrique descendante, ni, d'ailleurs, transversalement au satellite. Par conséquent, le système de stabilisation comporte, à priori, un seul mât longitudinal, déployé dans la direction de la verticale ascendante lorsque le satellite a atteint la phase stabilisée.

La figure 1 montre la configuration extérieure de PEOLE. Celle d'EOLE est la même, à ceci près qu'il n'y a pas de réflecteurs Laser et que les côtés du corps du satellite sont couverts de cellules du générateur solaire, car la puissance électrique demandée est plus importante.

3 - Etude de la phase stabilisée

3.1.- Définitions

Pour l'étude de la stabilisation géocentrique, et en raison des mouvements du satellite, il est naturel de prendre pour référence le trièdre orbital local.

Son centre coïncide avec le centre de masse du satellite, et se déplace donc avec le satellite lors du mouvement orbital.

L'axe OX est défini par la géocentrique ascendante, l'axe OZ est la normale à l'orbite.

L'axe OY complète le trièdre direct XYZ. Cet axe est confondu avec la tangente à l'orbite dans le sens du déplacement dans le cas où celle ci est circulaire ou lorsque le satellite passe au périgée ou à l'apogée.

Le trièdre satellite est défini par ses axes principaux d'inertie. Ox est l'axe longitudinal. Oy et Oz sont les axes transverses; en fait ils sont définis arbitrairement par des axes géométriques de la structure puisque de façon nominale, les moments d'inertie autour de Oy et Oz sont égaux.

On appelle A, B, C les moments d'inertie autour de Ox, Oy, Oz. On a en principe B = C.

Pour repérer l'attitude du satellite, on peut définir le passage du trièdre orbital local O X Y Z du trièdre satellite O x y z de plusieurs façons.

Nous avons choisi les rotations qui semblent les mieux adaptées étant donné la nature des mouvements (voir figure 2)

A partir O X Y Z, on effectue une rotation θ_3 autour de la normale à l'orbite OZ :

$$O \begin{bmatrix} X \\ Y \\ Z \end{bmatrix} \xrightarrow{\mathcal{R}\,\theta_3/Z} \begin{cases} O \\ X_1 \\ Y_1 \\ Z \end{cases}$$

puis une rotation θ_2 autour de Y_1

$$O \begin{bmatrix} X_1 \\ Y_1 \\ Z \end{bmatrix} \xrightarrow{\mathcal{R}\,\theta_2/Y_1} \begin{cases} O \\ X_2 \\ Y_1 \\ Z_2 \end{cases}$$

enfin une rotation θ_1 autour de X_2

$$O \begin{bmatrix} X_2 \\ Y_1 \\ Z_2 \end{bmatrix} \xrightarrow{\mathcal{R}\,\theta_1/X_2} \begin{cases} O \\ X_2 = x \\ y \\ z \end{cases}$$

Dans ces conditions, on voit, en ce qui concerne la position de l'axe x du satellite, axe destiné à pointer la géocentrique, que :

- θ_3 est la composante du déplacement de Ox dans le plan de l'orbite
- θ_2 est la composante du déplacement hors du plan de l'orbite
- θ_1 n'intervient pas pour définir la précision de la stabilisation de Ox.

On appelle θ_3, θ_2, θ_1 les angles de tangage, roulis, lacet, pour la raison suivante : Autour de la position d'équilibre, le tangage correspond à des mouvements autour de l'horizontale perpendiculaire à la trajectoire.

Le roulis correspond à des mouvements autour de la tangente à la trajectoire.

Le lacet correspond à des mouvements autour de la verticale locale.

Par extension, nous conserverons ces appellations même aux grands angles, bien qu' elles ne correspondent plus à une réalité physique, et dépendent de rotations successives envisagées.

3.2.- Rappel sur l'existence des couples de gradient de gravité

On sait que le gradient de gravité exerce un couple efficace lorsque la différence entre les moments principaux d'inertie est grande devant le plus petit moment d'inertie; On sait aussi que lorsque les deux plus grands moments d'inertie sont égaux la position d'équilibre stable correspond à l'alignement de l'axe de moindre moment sur la géocentrique; La position de cet axe autour de la géocentrique reste indifférente.

Les couples stabilisateurs, dans notre cas, sont créés par une différence des moments d'inertie qui se trouve réalisée par le déploiement du mât selon l'axe longitudinal du satellite. Ce mât a une longueur de 10 mètres et est muni d'un lest d'extrémité des trois kilogrammes.

Ainsi, on a les valeurs approximatives des moments d'inertie :

A = 6,5 m2 kg
B = C= 300 m2 kg

Au couple de gradient de gravité s'ajoute le couple dû à la force centrifuge dans le mouvement orbital. Les couples extérieurs auquel est soumis le satellite sont alors :

$\Gamma_T = \frac{3}{2}\,\omega_0^2\,(B-A)\,\sin 2\,\theta_3$ pour un dépointage en tangage

$\Gamma_R = 2\,\omega_0^2\,(C-A)\,\sin 2\,\theta_2$ pour un dépointage en roulis

$\Gamma_L = \frac{1}{2}\,\omega_0^2\,(B-C)\,\sin 2\,\theta_1$ pour un dépointage en lacet

ω_o représente la pulsation d'orbite
Pour une orbite d'altitude 800 à 1000 km, la période est de 100 minutes environ, donc vaut 10^{-3} rad/sec.
Les couples valent donc :

$\Gamma_L = 0$ puisque B = C
$\Gamma_R = 2.10^{-5}$ N.m par degré aux petits angles
Sa valeur maximale est 6.10^{-4} N.m pour $\theta 2 = 45°$
$\Gamma_T = 1,5.10^{-5}$ N.m par degré aux petits angles
Sa valeur maximale est $4,5.10^{-4}$ N.m pour $\theta 3 = 45°$

3.3.- Définition du système stabilisateur d'EOLE

Le problème posé est celui-ci :
Etant donné un satellite sur une orbite circulaire ou légèrement elleptique, d'altitude 800 à 900 km et d'inclinaison environ 48°, comment définir le dispositif créant les couples stabilisateur et celui servant à amortir les mouvements de libration.
On impose :
- un seul mât longitudinal
- une masse de 80 à 100 kg
- une structure prismatique octogonale à la partie supérieure avec 8 panneaux solaires et un cône d'antenne à la partie supérieure
- des moments d'inertie du corps du satellite entre 6 et 8 m2 kg, panneaux déployés.

On désire :
- une précision de pointage de 15°
- une attente maximale d'une dizaine de jours pour atteindre la phase stabilisée
- un sens déterminé du pointage.

On dispose :
- des résultats d'études préliminaires montrant que la stabilisation est possible avec des barreaux amortisseurs à hystérésis pour ce genre d'orbite.

On cherche à définir :
- la longueur du mât de stabilisation
- la masse d'un lest inerte à fixer à l'extrémité du mât
- les barreaux à hystérésis: nombre, longueur, diamètre et disposition à l'intérieur du satellite.

Il en résultera :
- la procédure pour atteindre la phase stabilisée
- le système de restitution d'attitude

En résumé, il faut assurer la compatibilité entre :
- le satellite lui-même : forme, dimensions, masse et moments d'inertie
- les spécifications imposées à la stabilisation
- l'orbite et son environnement
- le réseau de poursuite
- les détecteurs d'attitude possibles
- le traitement d'information au sol
- la masse totale satellisable.

En fin de compte, des simulations doivent fournir la preuve du bien fondé de la définition du système et permettre d'avoir une estimation valable des performances attendues en vol.

3.4.- Dimensionnement du système

Le dimensionnement consiste à définir l'ensemble couples stabilisateurs - couples amortisseurs en présence des perturbations auxquel le satellite est soumis en phase stabilisée.
Les perturbations sont dues essentiellement aux causes suivantes :
- couples aérodynamiques
- couples de pression de radiation solaire
- couples dus au dipole magnétique résiduel du satellite
- couples causés par l'intéraction du champ magnétique terrestre et des barreaux à hystérésis
- couples équivalents à l'influence de la déformée du mât de stabilisation.
- couple équivalent à l'effet de l'excentricité de l'orbite.

Dans un premier temps, on calcule séparément l'effet de chacune de ces perturbations en déterminant le couple statique causé par la perturbation en le comparant au couple stabilisateur crée lors d'un dépointage faible.

Exemple : Couples aérodynamiques

On calcule la force appliquée sur chaque surface élémentaire du satellite, en supposant le satellite stabilisée et par conséquent le vecteur vitesse orbitale perpendiculaire à l'axe longitudinal du satellite. On paramètre en fonction de la longueur du mât et de la masse d'extrémité.
On détermine pour chacune des valeurs de ces paramètres la position du centre de masse (CM) du satellite, mât sorti et les moments principaux d'inertie.
Les forces appliquées sont calculées à partir de modèles disponibles dans la littérature prenant en compte la théorie de l'écoulement moléculaire libre.
Les modèles d'atmosphère terrestre à ces altitudes sont également disponibles dans la littérature.
On doit effectuer des hypothèses pessimistes sur la température du corps, sur la nature de la réflexion des modécules à la surface du corps et sur l'état de surface.
On doit également prendre en compte une valeur maximale de la densité atmosphérique (heure, saison, altitude) que l'on peut rencontrer sur orbite.
On trouve donc une valeur $C_{aéro}$ de ce couple perturbateur, fonction de 2 paramètres (l,m)

l = longueur du mât
m = masse d'extrémité

On procéde de façon analogue pour les autres perturbations; en faisant la somme de leurs influences, on en déduit les couples de valeur l, m rendant possible la stabilisation. On étudie ensuite la compatibilité des moments d'inertie qui en résultent avec le dispositif amortisseur, puis avec l'acquisition. Le choix final résulte d'un compromis entre tous ces impératifs.

3.5.- Description sommaire du système

3.5.1.- Couples stabilisateurs

Ils sont créés, pour les deux satellites, par un mât déployable et rétractable de 10mètres de long et portant une masse d'extrémité de 3 kilogrammes. C'est une stabilisation "2 axes"; il n'y a pas de rappel autour de l'axe de lacet.

3.5.2.- Couples amortisseurs

Ils sont créés par des barreaux à hystérésis magnétiques en anhyster DS de 52 cm de long et 2 mm de diamètre, disposés suivant les 3 axes du satellite.
Sur EOLE il y a 4 barreaux par direction, soit 12 au total;
Sur PEOLE il y a 6 barreaux par direction, soit 18 au total;
Cette différence est une conséquence de la différence d'inclinaison d'orbite (fig 3)

3.5.3.- Capteurs d'attitude

17 senseurs solaires sur chaque satellite, répartis par paires sur chacun des 8 panneaux solaires, et en extrémité d'antenne.
1 magnétomètre triaxial; les sondes sont à l'intérieur du corps pour PEOLE, dans les panneaux pour EOLE (fig 4)

3.6.- Restitution d'attitude

Elle est obtenue à partir de deux références :
- le champ magnétique terrestre
- le soleil

Les capteurs sont disposés comme indiqué sur la figure 4.
Les magnétomètres ont une disposition différente pour chacun des deux satellites.
Pour PEOLE, un magnétomètre à trois axes orthogonaux était disponible: c'était l'un des modèles étudiés pour FR 1. Il était nécessaire de le disposer à l'intérieur du satellite.
Pour EOLE, il était indispensable de placer les sondes hors du corps du satellite afin d'obtenir des mesures valables lors de la préacquisition magnétique. Elles sont disposées dans les panneaux solaires; On remarque qu'elles ne forment pas un trièdre orthogonal.
Un calcul simple par une matrice appropriée permet de passer des mesures obtenues sur les sondes aux composantes du champ sur les axes principaux du satellite.
Les senseurs solaires sont identiques sur les deux satellites. Ils sont constitués par une plaque plane comportant 3 rangées de 7 cellules au silicium branchées en série, de façon à obtenir en plein éclairement solaire une tension de sortie voisine, mais inférieure à 5 volts, ce qui correspond à la saturation de l'entrée du codeur de télémesure. On évite ainsi l'usage d'un amplificateur.
Les senseurs sont au nombre de 17 : 16 sont placés aux extrémités des panneaux solaires, 1 se trouve au sommet de l'antenne 400 MHZ, de façon à ne viser que la terre en phase stabilisée; c'est pourquoi on l'appelle senseur d'albédo, bien qu'il soit technologiquement identique aux autres.
Le choix de l'emplacement de ces senseurs résulte des considérations suivantes :

1°- chaque senseur ayant un champ de 2π stéradians, il est possible d'avoir tout l'espace avec deux senseurs parallèles et de sens opposés.
2°- chaque senseur est éclairé par le soleil et par l'albédo:pour avoir la mesure complète de ces deux sources, il faut éviter les ombres portées du satellite : d'où le choix de l'extrémité des panneaux comme emplacement, et l'inclinaison à 61°30' de la normale à la surface sensible par rapport à l'axe longitudinal du satellite.

Ainsi, les couples de senseurs parallèles et opposés sont : S1 et S 10; S2 et S9 etc...
Le problème posé par la mesure de la direction solaire est la diminution de l'erreur apportée par l'albédo de la terre(fig.5)
Un senseur donne un courant proportionnel au flux solaire reçu.En mesurant la tension sur une résidence de charge appropriée, c'est-à-dire de l'ordre de 10 Kn, on obtient une valeur proportionnelle à ce flux.
Dans ces conditions, pour une source unique, on a : $V = k\ E \cos \Theta$ où E est l'éclairement de la surface sensible sous incidence normale.
Si l'on utilise 2 senseurs opposés et parallèles, et que l'on fasse la différence des tensions, on obtient une sortie $V1 - V2 = k\ E \cos \Theta$, Θ pouvant varier de 0 à 180°
Θ étant l'angle entre la direction de la source et la normale N1
Si maintenant plusieurs sources ponctuelles illuminent la surface sensible, on a :

$$V1 - V2 = k \sum_i Ei \cos \Theta i$$

$\sum_i Ei \cos \Theta i$ définit une source ponctuelle, appelée bary-centre énergique des différentes sources; elle ne dépend pas de la position de la surface sensible.
En effet, sa direction et son intensité sont définis par la somme vectorielle de vecteurs issus de la surface sensible, dirigés vers chaque source et de module proportionnel à l'éclairement sous incidence normale.
On peut alors définir le soleil apparent comme étant une source lumineuse définie par

$$Ea \cos \Theta a = Ev \cos \Theta v + \int_{TERRE} d\ E_T \cos \Theta_T$$

où EV est l'éclairement de la surface sensible sous incidence normale dû au soleil vrai et Θv son incidence réelle. ET est l'éclairement sous incidence normale dû à une surface élémentaire à la surface de la terre et Θ_T son incidence réelle.
Si l'on connait, par rapport à un trièdre fixe, mais centré sur le satellite, d'une part la direction du soleil vrai et son incidence, et d'autre part la valeur de l'albédo et la direction de son bary centre énergétique, on peut calculer les paramètres définissant le soleil apparent.

Le soleil vrai est connu en module; sa direction peut-être calculée par rapport au trièdre orbital dès l'instant où l'on connait avec précision les paramètres de la trajectoire orbitale et le temps.
De même, l'albédo peut-être calculée à l'aide d'un modèle d'albédo, des données orbitales et le temps.
On peut ainsi calculer l'intensité du soleil apparent et sa direction dans le trièdre orbital. Le résultat définit le soleil apparent théorique.
Un modèle de champ magnétique, les données orbitales et l'heure permet également de calculer les composantes du soleil champ dans les axes orbitaux locaux. Une identification du soleil apparent théorique avec le solleil apparent mesuré, du champ apparent avec le champ mesuré, permet de restituer l'attitude du trièdre satellite par rapport au trièdre orbital local.
Ceci a été réalisé à l'aide d'un programme TRT (Traitement des Références Théoriques).
Les entrées sont donc:
- les modèles de champ et d'albédo et les éphémérides du satellite

Les sorties sont fournies à des intervalles de temps donnés :
- 1 fois par seconde pour PEOLE, et par 0,625 pour EOLE

Le programme de restitution d'attitude choisit parmi les 8 couples de senseurs solaires ceux qui se prêtent le mieux au calcul, c'est-à-dire ceux dont les cellules ne voient pas le soleil sous incidence voisine de la normale ou sous incidence voisine de 90°.
Une identification permet de savoir si des cellules ne voient que l'albédo. Il est alors possible de faire une itération pour effectuer une correction du modèle d'albédo. C'est le cas en particulier du traitement en phase stabilisée, où le 17° senseur est pointé sur la géocentrique.
Le programme RASP (Restitution d'Attitude du Satellite Peole) permet ensuite le calcul des angles de roulis lacet tangage et les vitesses de rotation.
Le programme PREVIS permet le calcul de l'énergie dans le cas d'une prédiction ou dans le cas de mât entièrement sorti :
Lorsque le mât n'est pas entièrement sorti, PREVIS calcule l'énergie qu'aurait le satellite à la fin du déploiement, si un ordre de télécommande d'extension était donné.
Il prend comme conditions initiales les attitudes et vitesses de RASP, il intégre le mouvement du satellite, en prend en compte la loi de variation de longueur du mât, connue d'après des mesures faites au sol, la longueur du mât réellement sortie étant fournie par la télémesure.
Lorsque le mât est entièrement sorti, le calcul se fait directement.(sans intégration)

4- Capture

On dit qu'il y a 'capture' lorsque le niveau d'énergie du satellite est tel que, lors des mouvements, l'angle satellite géocentrique ne dépasse jamais 90°.Dans ces conditions, le satellite oscille autour de la géocentrique à la manière d'une pendule à deux degrés de liberté : on décompose la rotation en 2 mouvements, celui dans le plan de l'orbite et celui en dehors du plan de l'orbite.

4.1. Définition et calcul de l'énergie

Le calcul de l'énergie totale considère l'energie du satellite dans son mouvement orbital en présence du champ de gravitation. On ne considère donc pas l'effet des perturbations extérieures.
L'écriture des équations de Lagrange de la façon la plus classique s'écrit :

$$\frac{d}{dt}\left(\frac{\partial \mathcal{E}}{\partial \dot{q}_k}\right) - \frac{\partial \mathcal{E}}{\partial q_k} = Q_k$$

où les q_k sont les coordonnées généralisées, Q_k les forces généralisées et $\mathcal{E}$ la force vive. Q_k dérive du potentiel de gravitation terrestre.
Sur orbite circulaire, ce potentiel ne contient pas le temps. $\mathcal{E}$ le contient de façon implicite - On aboutit après multiplication par q'_k et sommation, à une forme intégrable, dite équation de Painlevé; l'intégrale de Painlevé se met sous la forme : $\mathcal{E}_0 - \mathcal{E}_2 + V = C^{te}$
$\mathcal{E}_0$ ne contient pas les dérivés des paramètres q'_k
$\mathcal{E}_2$ est une forme quadratique de ces paramètres
Le calcul complet de $\mathcal{E}$ permet d'identifier $\mathcal{E}_0$ et $\mathcal{E}_2$. V se calcule par la sommation

$$V = -\mathcal{V} \frac{\Sigma m_i}{\rho_i}$$

Tous les calculs faits, pour le cas du satellite, il vient pour le calcul de l'énergie:

$$E = \frac{1}{2}\left[Ap^2 + Bq^2 + Cr^2\right] + \frac{\omega_0^2}{2}\left[C - A\left(\vec{Z}\cdot\vec{x}\right)^2 - B\left(\vec{Z}\cdot\vec{y}\right)^2 - C\left(\vec{Z}\cdot\vec{z}\right)^2\right] + \frac{3}{2}\omega_0^2\left[A\left(\vec{X}\cdot\vec{x}\right)^2 + B\left(\vec{X}\cdot\vec{y}\right)^2 + C\left(\vec{X}\cdot\vec{z}\right)^2 - A\right]$$

où p, q, r sont les vitesses relatives du corps par rapport au trièdre local.
Cette énergie est connue à une constante près. On a défini l'énergie nulle comme étant celle du satellite parfaitement stabilisé, toutes vitesses relatives nulles.
Cette expression comprend 3 termes :
- le 1er est l'énergie cinétique relative
- le 2ème comprend les produits scalaires de l'axe Z, normale à l'orbite qui porte le vecteur $\vec{\omega}_0$, avec les axes satellites, c'est l'énergie d'entrainement.
- le 3ème terme comporte les produits scalaires de l'axe géocentrique avec les axes satellite. C'est l'énergie potentielle de gradient de gravité.

Si on exprime les produits scalaires en fonction des angles, et dans notre cas où B = C on trouve : $E = \frac{1}{2}\left[Ap^2 + B\left(q^2 + r^2\right)\right] + \frac{3}{2}\omega_0^2(B-A)\sin^2\theta + \frac{1}{2}\omega_0^2(B-A)$

θ est l'angle satellite géocentrique

Dans son mouvement, le satellite échange l'énergie cinétique et les deux autres énergies suivant le sens des couples. Cet échange est analogue à celui que subit un pendule simple dans le champ de pesanteur: $E = \frac{1}{2} m\left[\ell^2\theta'^2 + g\ell(1-\cos\theta)\right]$

Au passage à la position d'équilibre $\theta = 0$ et $E = \frac{1}{2} m\ell^2\theta_0'^2$
au passage au sommet de l'amplitude $\theta' = 0$ et $\theta = \theta_{max}$

Si l'énergie du pendule est inférieure à mgl, θ est toujours compris entre -180° et +180° Dans ces conditions il oscille autour de la verticale sans jamais passer par la position d'équilibre instable.
De même pour le satellite : si son energie est inférieure à $\frac{3}{2}\omega_o^2 (B-A)$, θ reste inférieur à 90°.
Le cas limite correspond à une énergie cinétique nulle, un dépointage en roulis nul et un dépointage en tangage égal à 90°. On appelle donc énergie de capture cette valeur limite. Si l'énergie du satellite est inférieure à $\frac{3}{2}\omega_o^2 (B-A) = Ec$ il oscille autour de la géocentrique sans dépasser 90°.
Autrement dit, $E < Ec$ est une condition suffisante mais non nécessaire pour que $\theta < 90°$.
On vérifie que Ec correspond au travail du couple de gradient de gravité entre 0 et 90°:

$$T = \int_0^{90°} \frac{3}{2}\omega_o^2 (B-A) \sin 2\theta \, d\theta$$

Dans le mouvement hors du plan de l'orbite, on peut calculer l'angle limite θ_L qui correspond à la limite d'énergie :

$$\int_0^{\theta_L} 2\omega_o^2 (B-A) \sin 2\theta \, d\theta = \frac{3}{2}\omega_o^2 (B-A)$$

Le calcul donne 60°. Dans ce mouvement $\theta = \theta_2$: toute la désorientation est hors du plan de l'orbite.
On remarque les sens possibles de la capture :
Si $\theta \rightarrow \theta + \eta$, l'énergie potentielle est inchangée; l'oscillation se fait autour de la 2ème position d'équilibre stable.
La figure 6 montre deux cas particuliers où l'on trouve une relation liant les paramètres d'attitude et de vitesse pour une énergie égale à l'énergie de capture.

1) si toutes les vitesses relatives du satellite par rapport au trièdre orbital local sont nulles, l'écriture de l'égalité de l'énergie a sa valeur limite de capture conduit à:
$$\sqrt{3} \cos\theta_3 = \operatorname{tg}\theta_2$$
La courbe qui en résulte montre que la valeur limite du tangage est 90° pour toutes les autres valeurs nulles, et celle du roulis est 60°.
On retrouve ces valeurs en écrivant que le travail des couples de tangage de 0 à 90° ou de roulis de 0 à 60° est égal à l'énergie de capture :
$$\int_0^{\frac{\pi}{2}} \frac{9}{2}\omega_o^2 (B-A) \sin 2\theta_3 \, d\theta_3 = \int_0^{\frac{\pi}{3}} \frac{4}{2}\omega_o^2 (B-A) \sin 2\theta_2 \, d\theta_2 = \frac{3}{2}\omega_o^2 (B-A)$$

2) Si toutes les vitesses absolues du satellite sont nulles, on trouve : $\cos\theta_3 \cos\theta_2 = \frac{1}{\sqrt{3}}$
Ceci est un cas intéressant, puisqu'après la sortie du mât les vitesses absolues se trouvent pratiquement annulées par suite de la multiplication des moments d'inertie.
Cela montre qu'il est necessaire pour assurer la capture, d'obtenir un dépointage, mât sorti, inférieur à 54° en effet : $\cos\theta_3 \cos\theta_2 = \cos$ (Sat. Géoc).

4.2.- Acquisition de la capture

Cette acquisition consiste :
1) à amener le satellite à un niveau d'énergie inférieur à celui de la capture
2) à une orientation compatible avec la mission c'est-à-dire suivant l'une des deux positions d'équilibre stable qui correspond au pointage de l'antenne sur la géocentrique descendante.

Plusieurs méthodes sont possibles, dans le cas général; elles peuvent faire intervenir un dispositif annexe éventuel, et un choix judicieux de l'instant où le mât est déployé.

4.2.1.- Cas EOLE

L'orbite d'EOLE est inclinée à 47° par rapport à l'équateur. Au point le plus au Nord de l'orbite, l'inclinaison magnétique est telle que le champ géomagnétique est incliné de 35° par rapport à la verticale locale. D'où l'idée de favoriser l'orientation en alignant au préalable le satellite sur le champ magnétique terrestre et de sortir le mât lorsque le satellite passe au point le plus au Nord de son orbite,qui se trouve d'ailleurs à la latitude de Brétigny.
On en déduit les phases essentielles de l'acquisition après l'injection sur orbite (fig 7)

1- Phase passive - après séparation de la case d'équipement freinage par yoyo, déploiement des panneaux solaires, le satellite est soumis à des vitesses résiduelles de l'ordre du tour par minute, soit 10^{-1} rad/sec.
Les barreaux à hystérésis assurent l'amortissement jusqu'à un niveau compris entre 10^{-3} et 10^{-2} rad/sec.

2- Phase active - lorsque l'on a constaté que le niveau des vitesses est convenable, et que le satellite est en vue d'une station, on télécommande la mise sous tension des bobines qui produisent un moment magnétique de 9 A m2.

3- Phase passive - stabilisation sur le champ magnétique. Le satellite est soumis à des couples magnétique qui font osciller son axe longitudinal autour du champ. Les barreaux magnétiques perpendiculaires au moment magnétique amortissent ces mouvements jusqu'à des amplitudes angulaires inférieures à 10°

4- Phase active - lorsque le satellite a suffisamment amorti ses mouvements d'oscillation autour du champ, ses vitesses par rapport au trièdre orbital local sont faibles, de l'ordre de 2 ou 3.10^{-3} rad/sec.
Dans ces conditions, au dessus de Brétigny, la capture est possible : l'énergie cinétique sera faible après déploiement du mât.
L'énergie potentielle correspondra à un dépointage de 40° environ.
La capture sera d'autre part assurée du bon côté.
A un passage au dessus de Brétigny, on opère de la façon suivante, par télécommande :

a) vérification de la qualité de la stabilisation magnétique, et par consequent, des conditions de capture
b) ordre de sortie du mât

c) ordre arrêt de l'alimentation des bobines
d) arrêt automatique du mât à sa longueur finale.

5- Phase passive - le mât déployé, les couples de gradient de gravité rappellent le satellite sur la géocentrique. On se trouve donc en phase d'amortissement des mouvements de libration de satellite autour de la géocentrique

6- Phase passive : régime stabilisé
Lorsque le dépointage atteint une valeur d'une dizaine à une quinzaine de degrés, les perturbations équilibrent les couples stabilisateurs et amortisseurs. Le régime est dit "permanent".

4.2.2.- Simulation EOLE

L'étude de l'acquisition de la stabilisation d'EOLE a fait l'objet de simulations sur ordinateur, avec visualisation sur console graphique et changements de programme commandés par l'opérateur afin de simuler les différentes phases actives ou passives de la stabilisation du satellite.
Ainsi, il est possible d'alimenter ou non la bobine de préacquisition, de sortir ou de rétracter le mât. Les conditions initiales d'attitude et de vitesse de rotation, les paramètres de l'orbite, la loi de sortie et de rétraction du mât, la valeur, le volume et le nombre de barreaux à hystérésis, le moment magnétique de la bobine d'acquisition, la masse et les inerties peuvent être introduits avant chaque cas.
Ainsi il est possible de simuler non seulement EOLE ou PEOLE, mais n'importe quel satellite subissant l'effet du gradient de gravité et du champ magnétique terrestre.
Les figures 8 à 19 montrent le résultat d'un cas de simulation EOLE sur orbite circulaire 900 km.
Ces événements sont les suivants :
t = 0 mât rentré; bobine non alimentée; panneaux solaires déployés. Les trois angles d'attitude sont $\theta_1 = 0$ $\theta_2 = -22°$ $\theta_3 = 186°$
Les 3 composantes de la rotation sont 0, 35.10^{-2} sur les 3 axes
L'attitude choisie correspond à l'angle satellite-champ magnétique égal à 0.
t = 625 secondes la bobine est alimentée
t = 51.660 secondes la bobine n'est plus alimentée
t = 51.875 secondes le mât est déployé
Les courbes fournies par la simulation sont :
C1, C2, C3 : les vitesses p, q, r du satellite, projetées sur les axes satellite.
C4 : le module de la vitesse
C5, C6, C7 : les angles de lacet, roulis, tangage
C8 : le moment cinétique
C9 : l'angle satellite géocentrique
C 10 : l'angle satellite champ
C 11 : l'angle géocentrique champ
C 12 : le rapport $\frac{E}{Ec}$ Rapport de l'énergie prédite à l'énergie de capture
Sur chaque courbe, on lit Xo : origine des abcisses
XM : abcisse maximale
Dans le cas présenté ici, les abcisses sont le temps, de 0 seconde à 100.000 secondes
YO : origine des ordonnées
YM : ordonnée maximale
Les grandeurs sont exprimées en degrés pour les angles et en radians par secondes pour les vitesses de rotation.
On constate que lors de la stabilisation sur le champ, après la phase d'amortissement, l'angle $(X \hat{S} H)$ ne dépasse jamais 20°. (figure 16)
La capture du gradient de gravité a été réussie puisque l'angle satellite géocentrique est inférieur à 90°; l'amplitude de son oscillation diminue au cours du temps ainsi que le rapport d'énergie.
On constate l'effet des couples de gradient de gravité sur le moment cinétique, une fois le mât sorti. (figure 15)

4.2.3.- Cas PEOLE

La stabilisation préliminaire sur le champ magnétique ne présente aucun intérêt puisqu'en raison de l'inclinaison de l'orbite, le champ magnétique vu par le satellite le long de sa trajectoire présente une inclinaison beaucoup trop faible et ne permet donc pas de favoriser le sens de la capture.
La procédure envisagée consiste alors à attendre des conditions favorables pour la sortie, avec éventuellement la possibilité d'effectuer le retournement du satellite si la capture s'est effectuée du mauvais sens, si les conditions favorables n'ont pu être obtenues (fig. 20).
Les conditions favorables sont les suivantes :
1) amortissement de la rotation à une valeur relativement faible pour avoir une énergie cinétique faible. Grâce aux barreaux amortisseurs, cette condition est obtenue au bout d'un certain temps.
2) orientation du satellite, à l'instant de la sortie du mât, telle que l'énergie totale qu'aurait le satellite, après extension, soit inférieure à l'énergie de capture, et ceci avec le sens correct de capture.

Cette deuxième condition impose donc : une restitution immédiate de l'attitude et un calcul de l'énergie qu'aurait le satellite si le mât était déployé.
Cette procédure a été effectuée depuis Kourou, seule station du réseau CNES réunissant les conditions suivantes :
- visibilité du satellite à chaque orbite
- équipements sol permettant la télémesure, le traitement d'information nécessaire pour prendre les décisions, et l'envoi immédiat d'ordres de télécommande.

La procédure envisagée est alors la suivante :
1) Phase passive, identique à celle d'EOLE: après despin par yoyo, séparation de la case d'équipements et déploiement des panneaux, les barreaux à hystérésis amortissant la rotation résiduelle du satellite.

2) Surveillance en temps réel du comportement du satellite- Cette surveillance consiste à chaque passage en visibilité de Kourou, à restituer l'attitude du satellite et calculer à chaque instant l'énergie totale qu'il aurait si l'on décidait de déployer le mât.(énergie prédite).

3) Phase active : déploiement du mât.
La télécommande de sortie de mat est effectuée lorsque les conditions citées précédemment sont remplies.
Cependant, si au bout de plusieurs passages, c'est-à-dire d'une dizaine à une vingtaine, on n'obtient pas de conditions favorables, la décision de sortir le mât doit être prise de toutes façons.
En effet, il est apparu, lors des simulations des mouvements d'attitude effectuées à Brétigny, que, parfois, il pouvait y avoir pendant plusieurs orbites, capture d'une des directions de barreaux magnétiques par le champ géomagnétique.
Si c'est la direction longitudinale qui est captée, le satellite est grosso-modo aligné sur la normale à l'orbite et dans ces conditions l'énergie est voisine de celle de la capture, et le sens dans lequel elle se produira est aléatoire.

4) Phase passive : identique à celle d'EOLE : amortissement des librations autour de la géocentrique et atteinte du régime permanent.

En cas d'échec de capture dans le sens désiré :

4') Phase passive identique à 4, mais avec l'orientation inverse.

5') Phase active : retournement du satellite :
Lorsque la surveillance, identique à celle opérée en 2), montre que le régime permanent est atteint, on procède de la façon suivante, au cours du même passage :
a) vérification au début du passage que les conditions sont toujours favorables
b) télécommande de rétraction du mât
c) arrêt du mât. Cet arret peut se produire soit automatiquement si le mât est rentré entièrement, soit par télécommande si l'évolution en mouvement du corps montre qu'il est préférable de l'arrêter en cours de rentrée
d) attente pendant le basculement
e) télécommande de la sortie du mât
f) arrêt automatique du mât

6') Phase passive : identique à 4

4.3.- Retournement

On appelle "retournement" l'opération qui consiste à inverser le sens de capture lorsqu'elle s'est produite du côté défavorable.
Cette opération se déroule en vue d'un passage au dessus d'une station. Elle consiste, une fois le satellite stabilisé et amorti, à opérer une rétraction de mât suivie d'une extension quelques instans après (fig 21)

4.3.1.- Principe: Le satellite est stabilisé en position inverse autour de la géocentrique
Son vecteur rotation absolue est celui de l'entrainement du trièdre orbital dans le mouvement orbital. Il est donc porté par la normale à l'orbite et vaut ω_0, pulsation de l'orbite supposée circulaire.
Son mouvement d'inertie par rapport à un axe porté par la normale à l'orbite vaut $I = I_0 + m\ell^2$, en 1ère approximation.
I_0 = Mt d'inertie du corps
m = masse d'extrémité
ℓ = longueur du mât.
Le mât est rétracté à une longueur l_1.
On a alors $I = I_0 + m\ell_1^2$
Si pendant le mouvement, le moment cinétique se conserve, on a :
$$(I_0 + m\ell^2)\,\omega_0 = (I_0 + m\ell_1^2)\,\omega_1$$
Le satellite tourne dans le plan de l'orbite à une vitesse supérieure à la pulsation d'orbite. Lorsqu'il a parcouru un angle de 180° par rapport à la géocentrique, on déploie à nouveau le mât à la longueur ℓ. La rotation du satellite vaut ω_0 et il se trouve donc stabilisé dans le bon sens.
Le problème posé par la détermination de la procédure doit, en fait, tenir compte des diverses conditions initiales, puisque la stabilisation inversée n'est pas parfaite, et donc le vecteur rotation n'est pas comme il a été défini plus haut.
La vitesse de rentrée et de sortie du mât doit être prise en compte. Enfin le moment cinétique ne se conserve pas puisque le couple de gradient de gravité rappelle le satellite sur la géocentrique en le freinant dans la première moitié de la manoeuvre et en l'accélérant dans la 2ème moitié. Enfin il faut assurer la compatibilité du temps de manoeuvre avec le temps de visibilité au dessus de la station.

4.3.2.- Longueur minimale théorique
Lorsque la longueur du mât passe de la valeur ℓ_0, à une valeur plus courte ℓ_1, il est nécessaire que pour la nouvelle configuration, l'énergie totale du satellite soit supérieure à l'énergie de capture afin de lui faire "franchir " la position 90°.

a) si le satellite est parfaitement stabilisé en position inversée: la rotation initiale absolue est ω_0 ; après diminution du moment d'inertie transverse à $B_1 = \frac{B}{2}$ la rotation absolue vaut $m\omega_0$, donc la rotation relative est $(m-1)\omega_0$.
L'énergie cinétique relative vaut: $\frac{1}{2} B_1 (m-1)^2 \omega_0^2$

On veut qu'elle soit inférieure à l'énergie de capture, soit : $\frac{3}{2}\omega_0^2 (B-A)$

On obtient une bonne approximation en considérant A petit devant B1, ce qui est valable si on trouve en fin de calcul une longueur de mât encore relativement importante.
La condition impose : $m > 1+\sqrt{3}$
Si on pose $B1 = I_0 + m\ell_1^2$
On a : $\ell_1^2 < \frac{m\ell^2 - \sqrt{3} I_0}{m(1+\sqrt{3})}$; en première approximation $\ell_1 < \frac{\ell}{\sqrt{1+\sqrt{3}}}$
Pour les données d'EOLE et de PEOLE on trouve
$\ell_1 < 6$ mètres

b) si le satellite oscille de 15° autour de la géocentrique.
On peut encore considérer l'amplitude comme petite, ce qui fait que le mouvement dans le plan de tangage s'écrit : $\theta_3 = \theta_{3MAX} \sin(\sqrt{3}\omega_0 t + \varphi)$
θ_3 étant l'angle de tangage

$\theta_3' = \sqrt{3}\,\omega_0\,\theta_{3\,max}\cos(\sqrt{3}\omega_0 t + \varphi)$

θ_3 max vaut environ $\frac{1}{4}$ de radians
d'où la vitesse de rotation absolue $\theta' + \omega_0$ dont la valeur minimale est: $\omega_0\left(1 - \frac{\sqrt{3}}{4}\right)$

Pour cette valeur, on conçoit bien qu'il est nécessaire de rétracter davantage le mât que dans le cas précédent pour que l'énergie cinétique dépasse la valeur de l'énergie de capture.
La vitesse relative après rétraction est : $\omega_0\left[n-1-n\frac{\sqrt{3}}{4}\right]$
La condition d'énergie s'écrit : $\frac{1}{2} m \ell_1^2 \omega_0^2 \left(n-1-n\frac{\sqrt{3}}{4}\right)^2 > \frac{3}{2}\omega_0^2 m \ell_1^2$
On en déduit $\ell_1 < \frac{\ell}{2}\sqrt{\frac{4-\sqrt{3}}{1+\sqrt{3}}}$

dans notre cas où l = 10 m

$\ell_1 < 4{,}5$ mètres

Si la condition n'est pas respectée, et si le mât est rétracté au passage à la position d'équilibre dans le sens défavorable, le satellite continuera à osciller autour de la géocentrique, mais avec une amplitude plus importante; le couple de gradient de gravité dans le plan de tangage le rappellera sur la géocentrique, avec la même orientation que précédemment.

4.3.3.- Prise en compte de la vitesse de déroulement du mât

Les calculs précédents servent à déterminer les ordres de grandeurs de temps et de longueur de mât compatibles avec la mission. En fait, il faut prendre en compte le temps nécessaire pour déployer et rétracter le mât et l'influence des conditions initiales diverses : mouvement de roulis et lacet.
Le procédé utilisé est le suivant:
a) écriture des équations du mouvement dans le plan de tangage :
- équations d'Euler avec moment d'inertie variable dû à la variation de longueur de mât dont on prend un modèle mathématique pour la rentrée et la sortie.
- couple de gradient de gravité à inertie variable
- simulation de la procédure avec diverses conditions initiales en angle et vitesse de tangage
- rétraction du mât à une longueur finale
- attente d'un temps "Ta" dit temps d'attente
- extension complète - on arrive à un angle final θ_f que l'on veut être égal à π
- réitération de la procédure avec un temps d'attente différent si l'on n'a pas obtenu $\theta_f < \pi$
- on arrive ainsi à un diagramme, pour ℓ_f donné, à 3 dimensions : θ' et θ initiaux, et temps total de manoeuvre. Les figures 22 et 23 donnent deux exemples de ces diagrammes.

Si le diagramme n'englobe pas les 3 paramètres de façon réaliste, on recommence avec une longueur de mât différente, plus courte ou plus longue suivant le cas:
Si la vitesse de rétraction du mât est trop lente, le satellite risque de faire un tour complet pendant la manoeuvre; il est alors nécessaire d'arrêter le mât à une longueur relativement importante, mais inférieure à la limite précédemment définie.
Si la vitesse de pivotement, mât partiellement rentré, est trop lente et incompatible avec le temps de visibilité, il est nécessaire de le rentrer davantage.
D'où la nécéssité de rechercher un compromis entre ces trois impératifs :
1) le satellite doit tourner d'un demi tour seulement
2) le temps de manoeuvre doit être compatible avec le temps de visibilité
3) les conditions initiales de manoeuvres doivent être réalistes.

4.3.4.- Influence des mouvements résiduels sur les autres axes

Les diagrammes 22 et 23 ont été tracés pour un angle final de 180°, le mouvement s'effectuant dans le plan de l'orbite.
Il est nécessaire de connaître l'erreur totale lorsque s'ajoutent des vitesses de roulis et de lacet, et un dépointage en roulis; on utilise la procédure définie précédemment en ajoutant des conditions initiales en roulis et en lacet.
Ces conditions initiales ont pour effet que le satellite ne se trouve pas à 180° de la géocentrique dans le sens initial, mais à un angle différent.
La figure 24 montre que la vitesse de lacet à une influence négligeable.
L'angle de roulis peut se traduire par un dépointage d'une dizaine de degrés; la vitesse de roulis par un dépointage d'une vingtaine de degrés.
Il est donc necessaire pour opérer le retournement, que les mouvements de roulis soient relativement amortis.

5-Opération de retournement de PEOLE en vol à KOUROU le 31 Decembre 1970.

5.1.- Installation

La figure 25 donne le schéma général de l'installation du Centre Spatial Guyanais qui a servi à la mise en oeuvre du retournement en temps réel.
La station de poursuite du réseau CNES reçoit la télémesure PAM-FM et l'envoit au centre technique où elle est démodulée.
Un premier traitement sur 1800 permet, à chaque format de durée 1 seconde, de faire le tri des paramètres intéressants la stabilisation: information des capteurs et longueur du mât; Les corrections de température sont effectuées et les valeurs sont envoyées, en données physiques, à l'ordinateur 360/44.
D'autre part, le calcul des références théoriques a préalablement été éffectué sur bande, pour chaque orbite, en connaissant les prevision de passage et les données d'orbite.

Les références théoriques donnent à chaque seconde le champ, le soleil et l'albédo dans les axes orbitaux locaux.
Une synchronisation temps est assurée par l'horloge du centre.
Le 44 calcule les vitesses de rotation, les angles et l'énergie; l'énergie est l'énergie réelle si la longueur du mât est 10 mètres.
C'est l'énergie prédite si elle est inférieure à 10 mètres: on suppose qu'à chaque instant on sortirait le mât complétement, et on obtient l'énergie en fin de manoeuvre.
La salle de contrôle comporte 4 tables traçantes; elles sont commandées par le 44 et enregistrent avec une seconde de retard (temps de calcul), les fonctions désirées:
Angle satellite géocentrique
Rapport d'énergie E/Ec E = énergie (réelle ou prédite)
Ec = énergie de capture, mât sorti
Angle et vitesse de tangage
On peut également tracer le mouvement de roulis ou de lacet.
Un interphone permet aux responsables de manoeuvres, au vu des courbes obtenues sur tables traçantes de demander directement à la station d'exécuter instantanément les ordres suivants :
- armer la commande du mât
- sortir le mât
- arrêter le mât
- rentrer le mât
- désarmer la commande de mât.

5.2.- Résultats obtenus en vol (fig 26)

Après le déploiement des panneaux solaires, le 12 Decembre 1970, le satellite avait une vitesse de rotation bien supérieure à celle que l'on attendait : 10,5 T/minute; cet excès de rotation a sans doute été causé par une sous-estimation du moment d'inertie du corps à despinner par le yoyo qui, en tant que mécanisme, a parfaitement fonctionné.
Il appartenait alors aux barreaux à hystérésis de réduire la rotation pour l'amener à un niveau compatible avec la procédure envisagée.
Or, à l'orbite 118, à Kourou, le 21 Décembre, on constate que le mât est déployé. On ne connait pas l'origine de cette télécommande, probablement due à des parasites et la sensibilité excessive du récepteur de télécommande "2 tons"du satellite.
L'amortissement est donné sur la figure 27.On voit donc que le mât est sorti lorsque la vitesse résiduelle était de l'ordre de 2 T/minute pour assurer la capture.
Après la sortie inopinée du mât, la rotation du satellite est de l'ordre de $\frac{1}{20}$ de tour par minute et par conséquent trop importante pour assurer la capture.
Les barreaux à hystérésis continuent à amortir la rotation jusqu'au moment où l'on a constaté que l'orientation du satellite, à partir du 24 Decembre, reste comprise entre 90 et 180°. La capture s'est effectuée en position inverse et il est nécessaire d'attendre l'amortissement des oscillations autour de la géocentrique pour opérer le retournement.
La figure 28 montre les dépointages enregistrés à Kourou du 23 au 31 Decembre 1970.
On décide d'opérer le 31 Decembre à l'orbite 282.
On s'était fixé comme condition pour opérer : $\theta_o' > -6.10^{-4}$ rad/sec, au vu des résultats de simulation.
Cette condition étant remplie au début du passage, l'ordre de rétraction du mât est télécommandée et opérée entièrement.
On attend l'instant favorable pour donner l'ordre de sortie.
A 0,80 m le mât se bloque et le satellite disparait à l'horizon, mât bloqué, malgré des tentatives infructueuses de nouvelle extension.
A l'orbite 283, on opère la rétraction des 0,8 m dès l'arrivée de la télémesure. On attend l'instant favorable d'extension pour sortir à nouveau le mât. La télécommande est opérée et le mât se déploie, cette fois-ci sans blocage.
La capture est assurée à mieux que 20°.
L'origine du blocage est probablement imputable à un foisonnement du ruban à l'intérieur du dérouleur: en principe le ruban est coincé entre un rouleau et un contre-rouleau en face du guide de sortie. Pour assurer la tension du ruban entre le rouleau et le tambour sur lequel celui-ci est enroulé, le rouleau, pendant le déroulement, tourne plus rapidement que le tambour. Il semble que la mise en rotation du déroulement ait été défectueuse, d'où le foisonnement qui a été "récupéré" lors de l'enroulement à l'orbite 283.
Les enregistrements ont montré la phase stabilisée après le 31 Décembre: ils sont reportés figure 29.

Conclusion

Il n'a pas été question de décrire ici toutes les études et simulations effectuées pour la définition du système, car cela nous entrainerait bien au delà de ce que l'on peut dire dans le cadre d'une communication.
Cependant, l'on peut dire que le critère d'énergie nous a semblé d'un intérêt particulier pour les manoeuvres d'acquisition.
La comparaison des résultats en vol et des simulations au sol ont montré la validité des modèles mathématiques pris en compte pour s'assurer des performances dans le domaine de pointage espéré.
Il est judicieux d'estimer que la stabilisation par gradient de gravité apporte une solution satisfaisante au pointage géocentrique pour des orbites faiblement elliptiques d'altitude supérieure à 600 km.
L'amortissement par barreaux à hystérésis magnétique est valable pour des orbites d'altitude 600 à 1100 ou 1200 km et d'inclinaison quelconque.
L'amélioration de performances peut-être obtenu par l'utilisation d'amortisseurs différents tels que ancrage magnétique ou bras articulés, par l'utilisation d'une configuration symétrique en déployant un mât " vers le bas", par u e stabilisation de l'axe de lacet pour éviter le couplage avec le roulis; D'autres améliorations pourraient être apportées par le couplage avec un système actif, comme une roue d'inertie dans le plan de tangage. L'avenir de ce type de stabilisation dépend, en fait, des missions futures qui seront proposées.
Le gradient de gravité apporte une solution pour un certain type de missions, mais d'autres systèmes seront souvent préférés pour une stabilisation géocentrique, si des corrections d'orbite sont nécessaire et si la précision de pointage est grande.
Cependant, le type de système que nous avons réalisé présente l'avantage d'être entièrement passif et ne pose pas de problème de durée de vie.

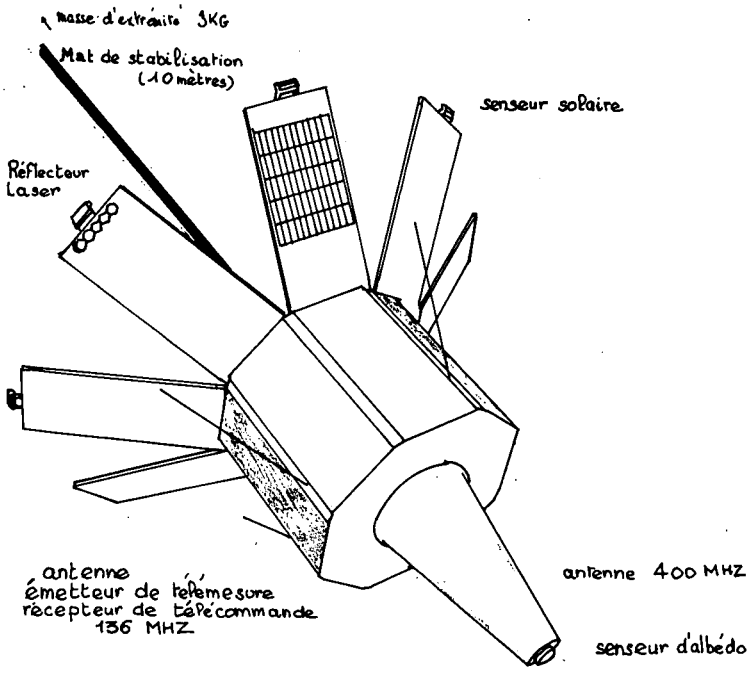

Masse : 60Kg.

Longueur du corps	550 mm
Largeur entre faces	662 mm
entre arêtes	704 mm
Angle panneau - face du corps	125°
Longueur corps + antenne	1081 mm
Diamètre base antenne	300 mm
Angle antenne	20°

Fig.1 PEOLE

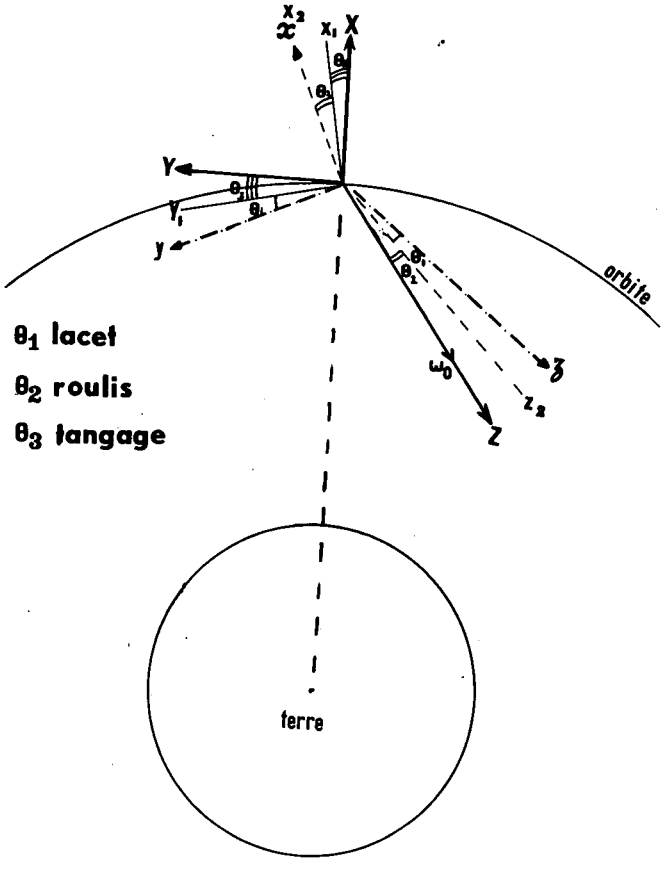

Figure 2

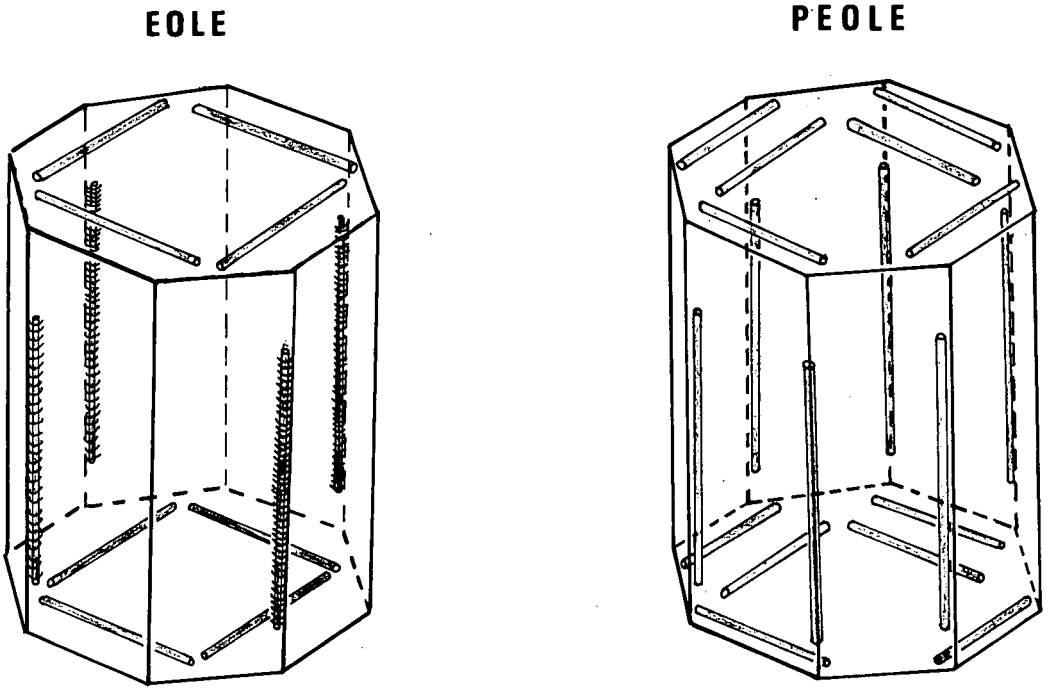

Fig.3 Intégration des barreaux à hystérésis

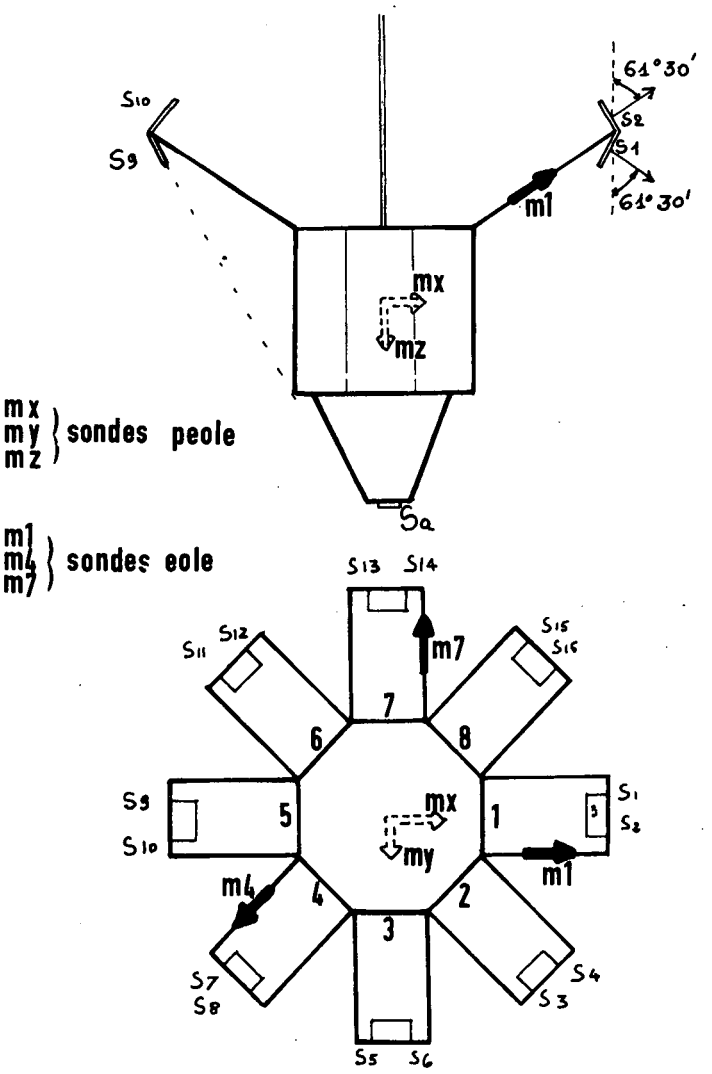

Fig.4 Senseurs solaires et magnétomètres

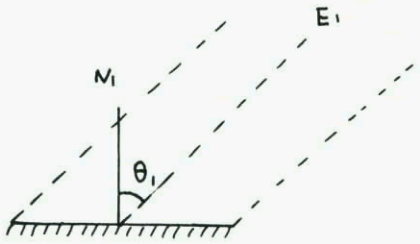

$$V_1 = k\, E_1 \cos\theta_1$$

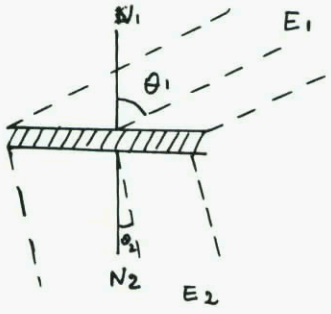

$$V_1 - V_2 = k\left(E_1 \cos\theta_1 - E_2 \cos\theta_2\right)$$

$$= k\left(E_1 \cos\theta_1 + E_2 \cos\pi + \theta_2\right)$$

$$= k\left[E_1 \cos(\hat{\rho_1}, \hat{N_1}) + E_2 \cos(\hat{\rho_2}, \hat{N_2})\right]$$

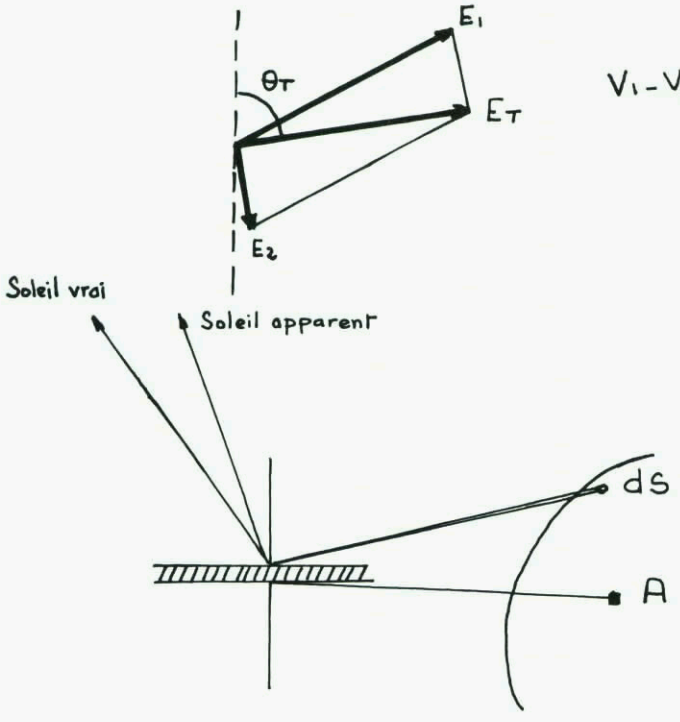

$$V_1 - V_2 = k\, E_T \cos\theta_T$$

Fig.5 Principe de la mesure solaire

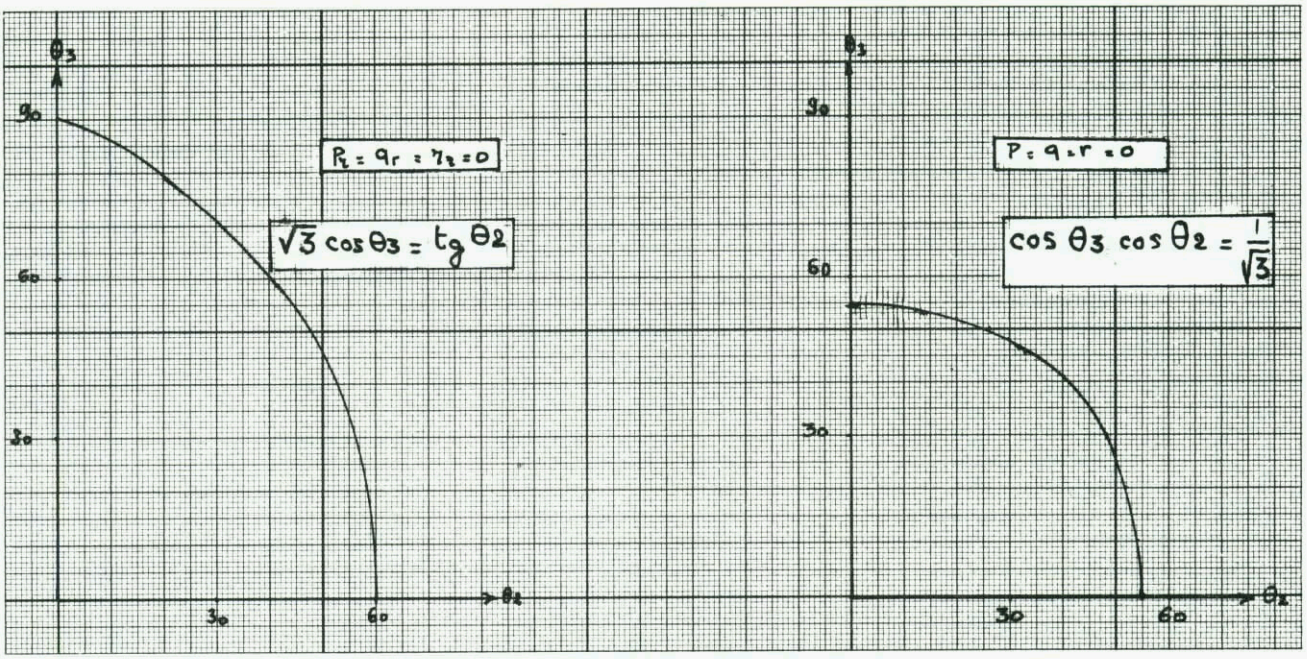

Fig.6 Volume de capture

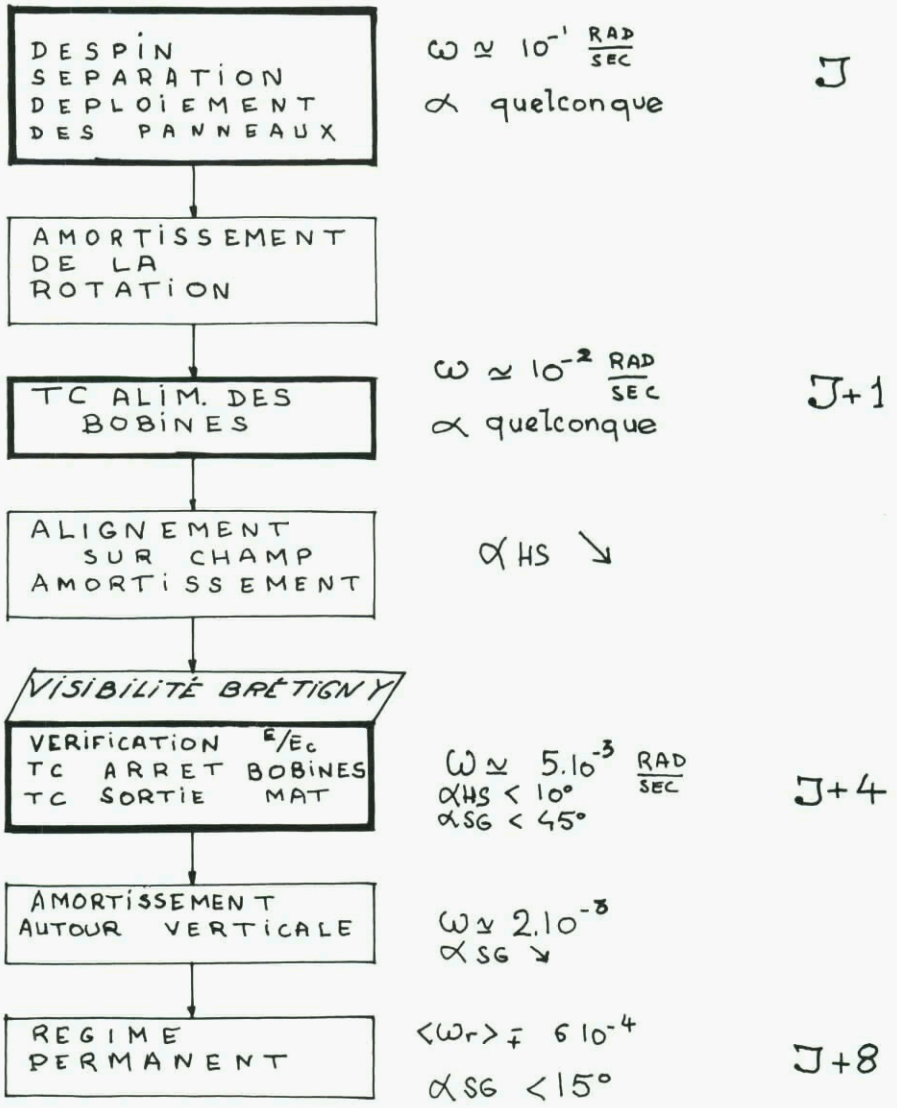

Fig.7 EOLE: capture

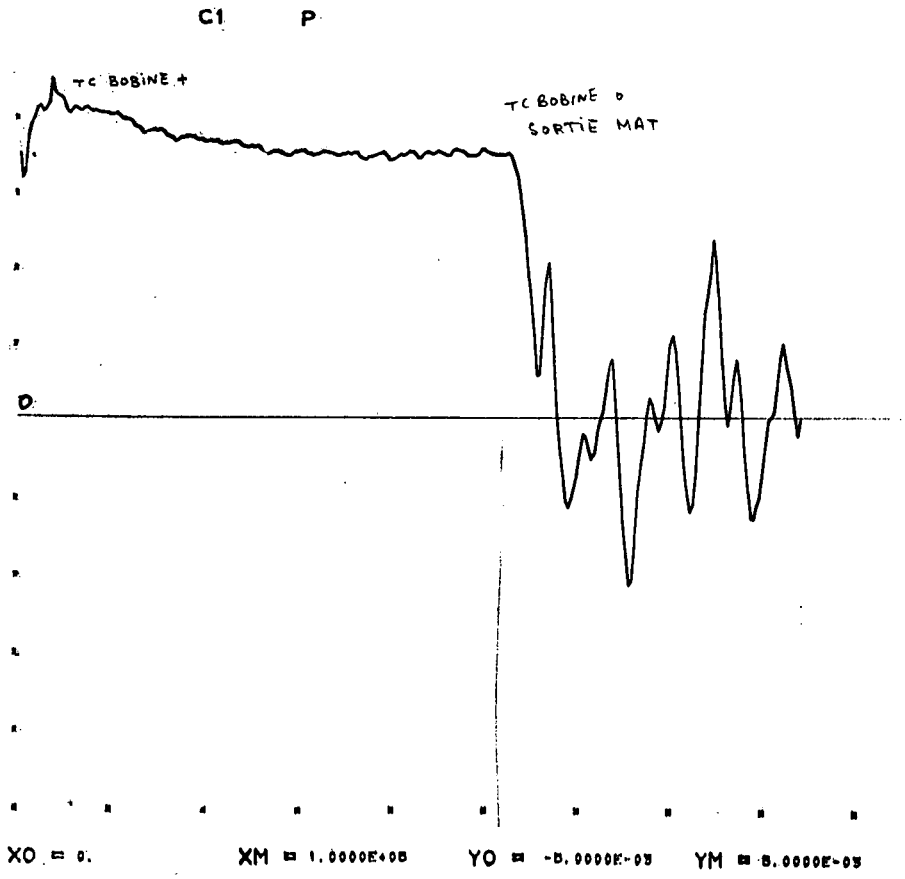

Figure 8

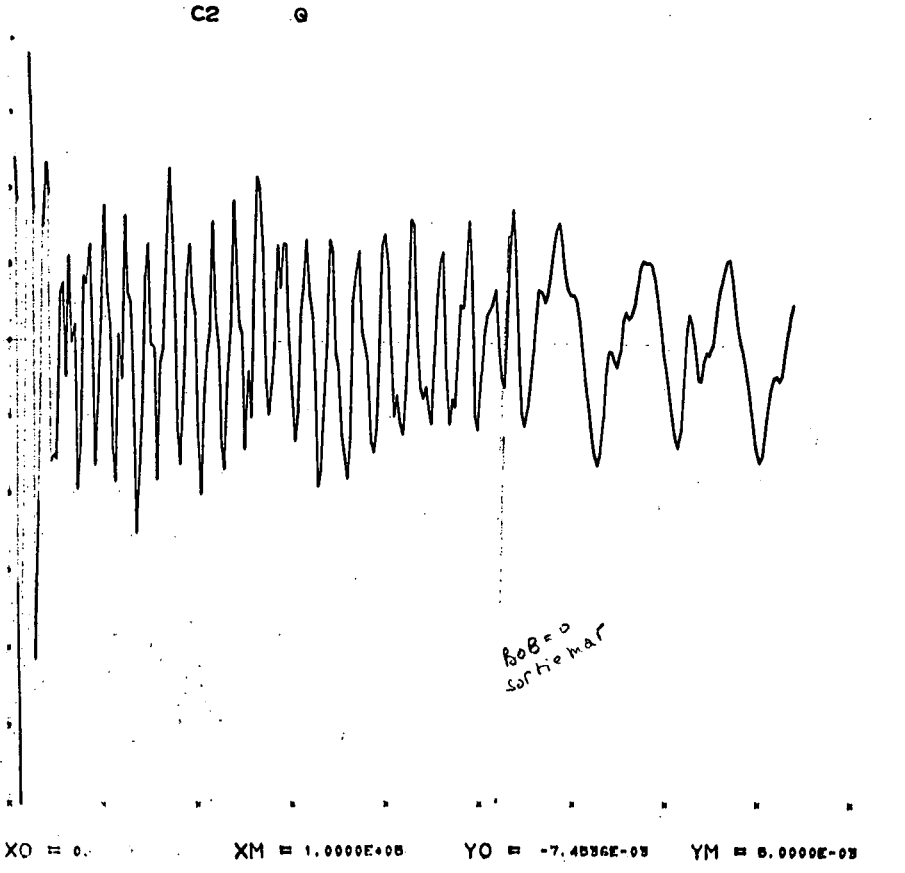

Figure 9

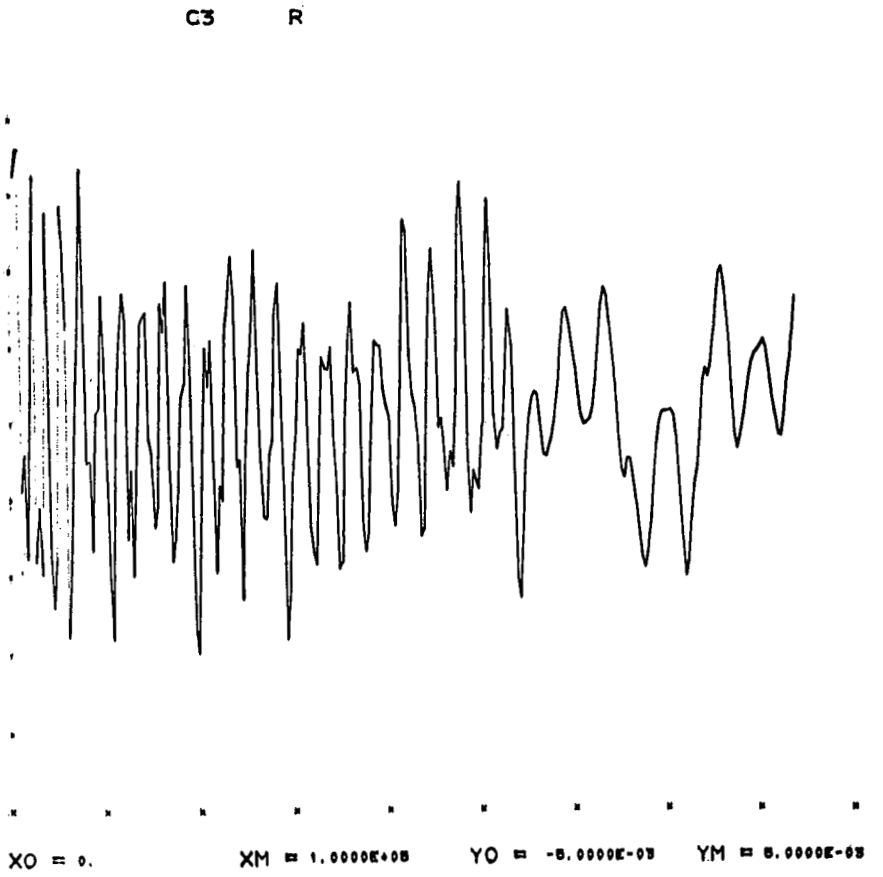

Figure 10

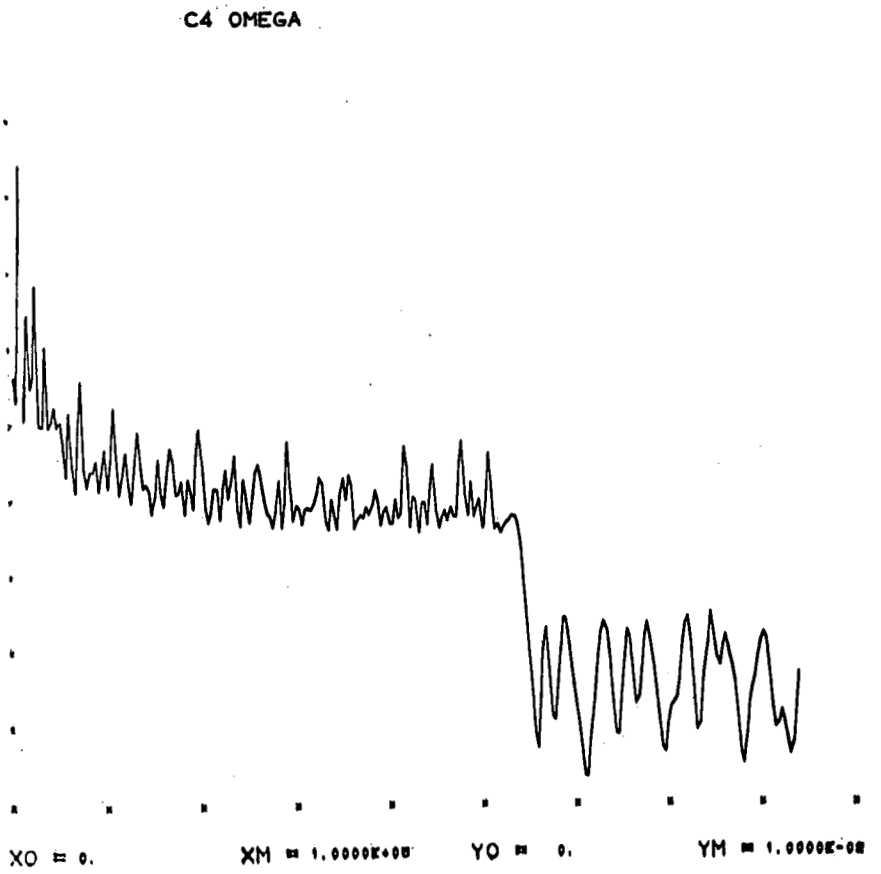

Figure 11

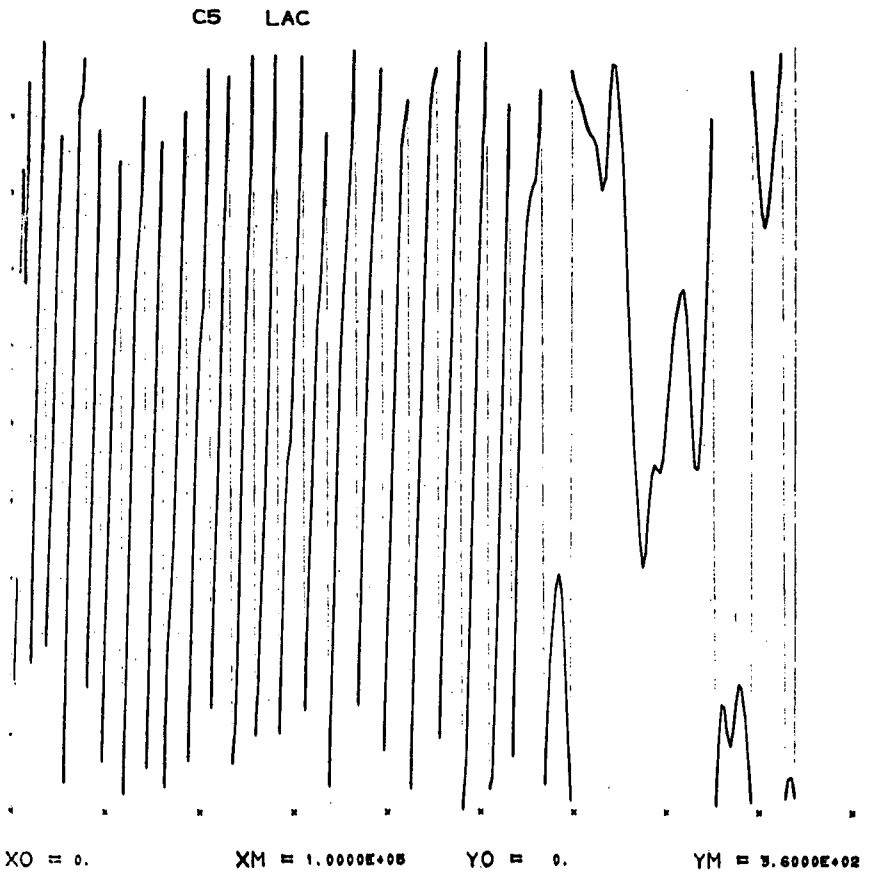

Figure 12

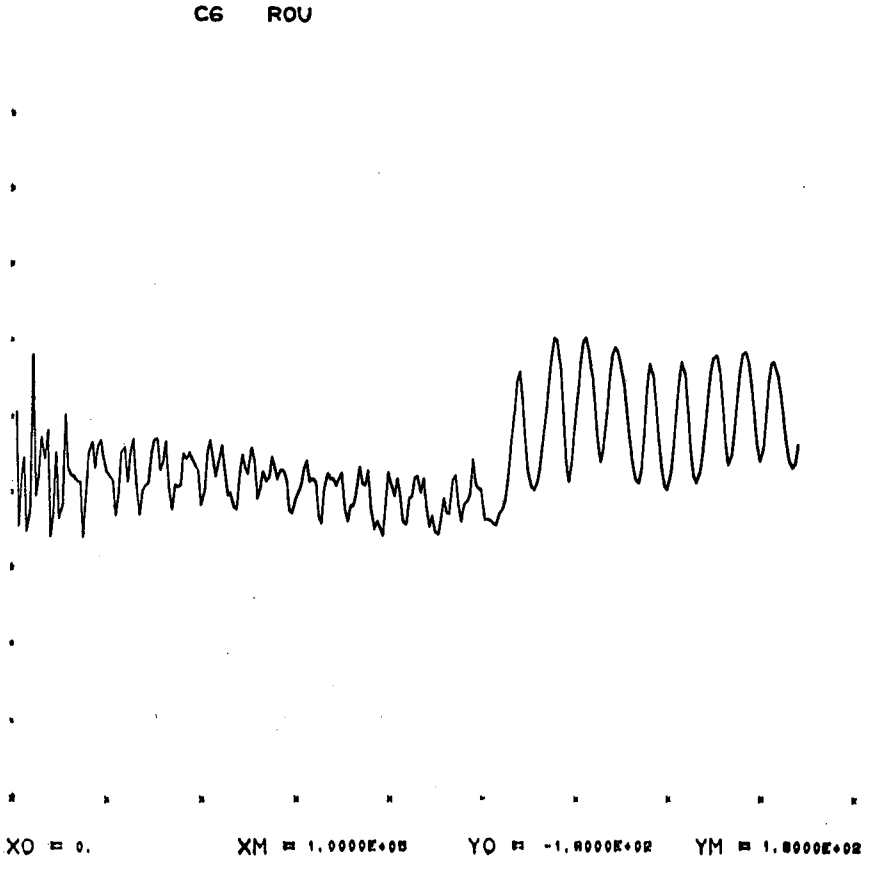

Figure 13

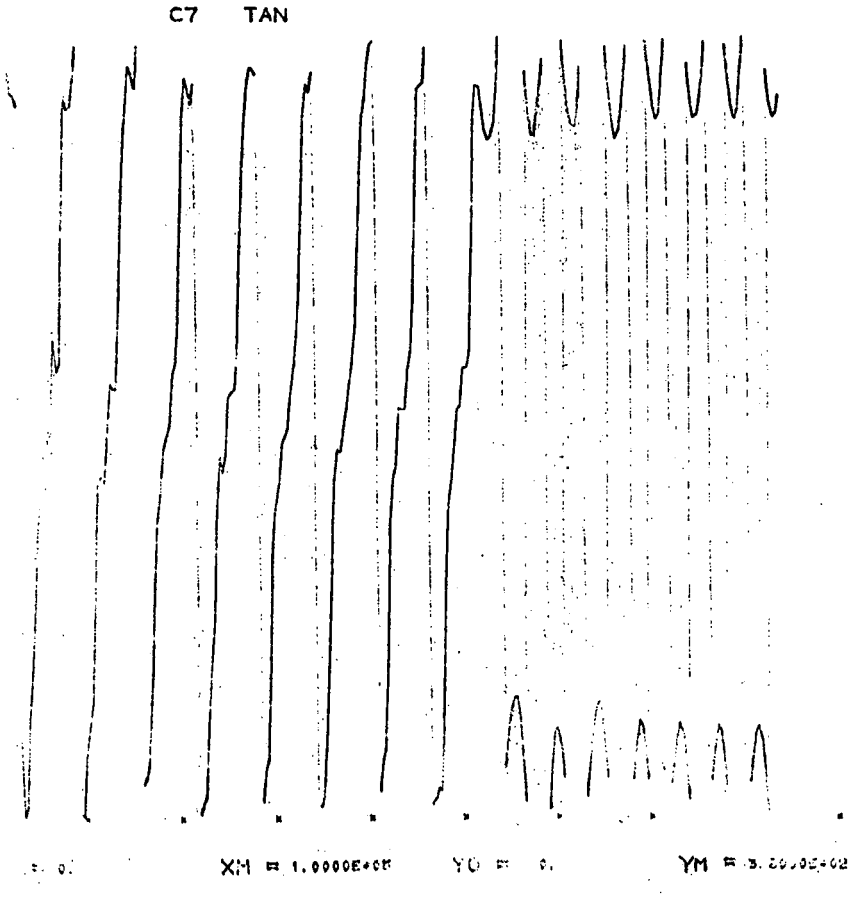

Figure 14

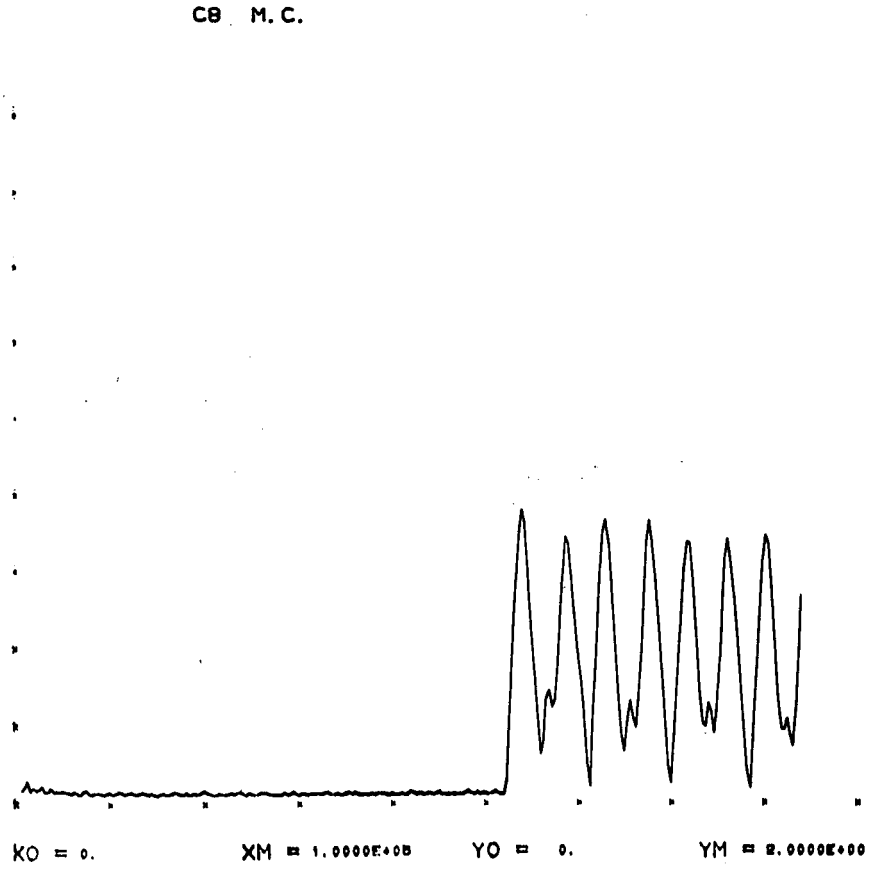

Figure 15

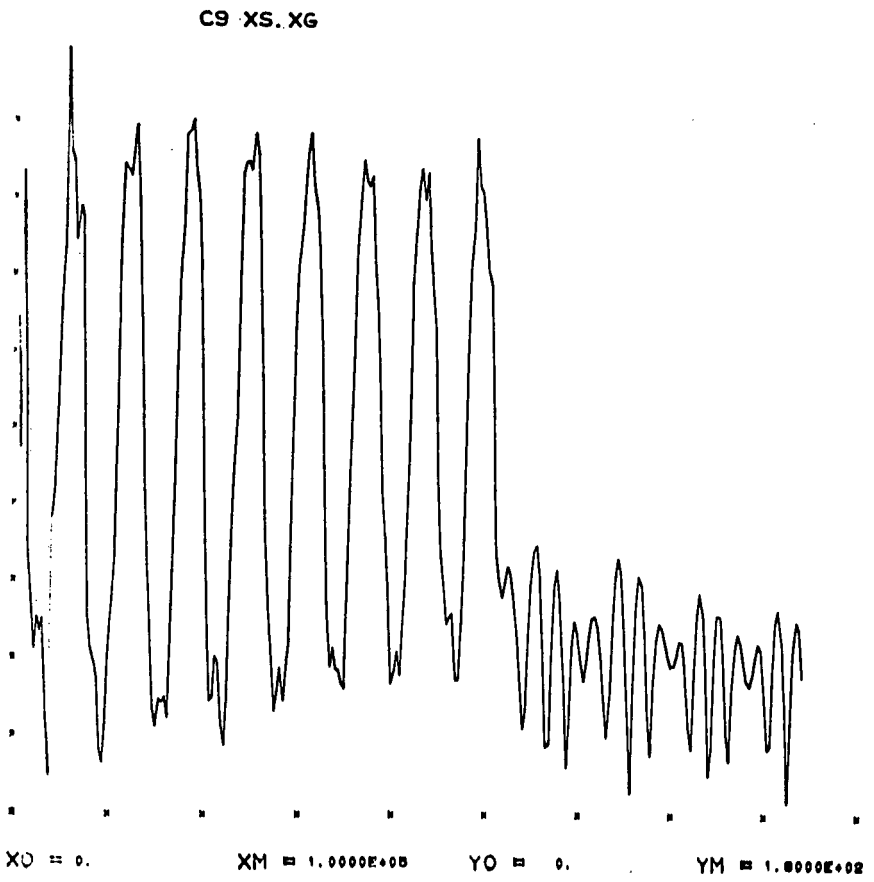

Figure 16

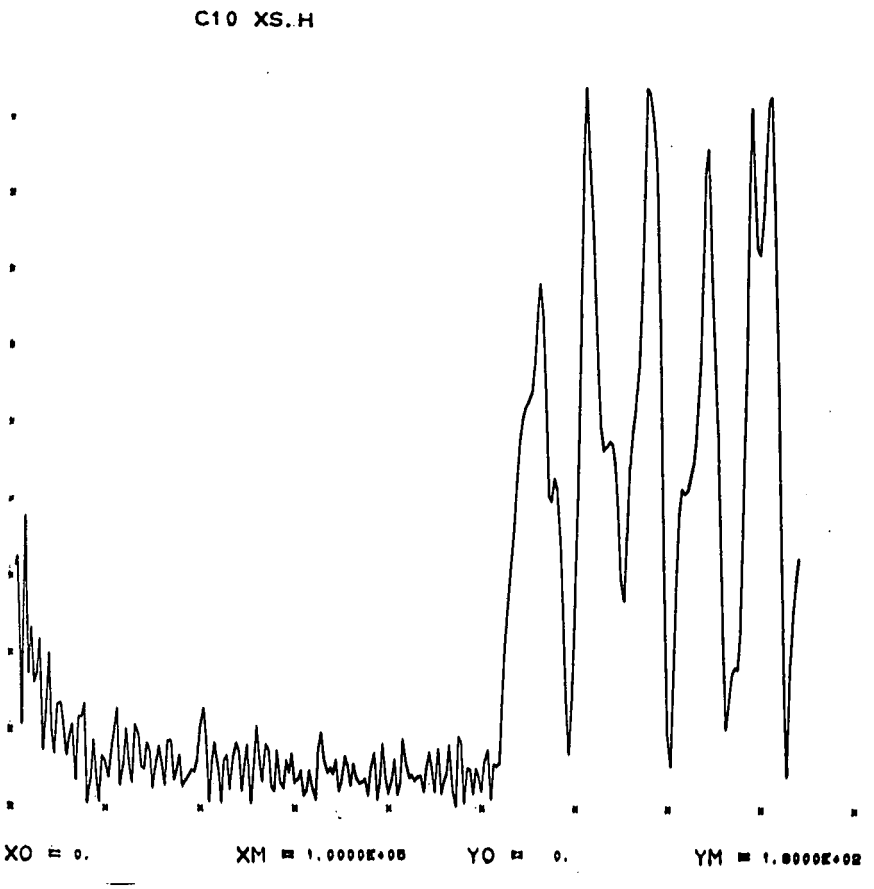

Figure 17

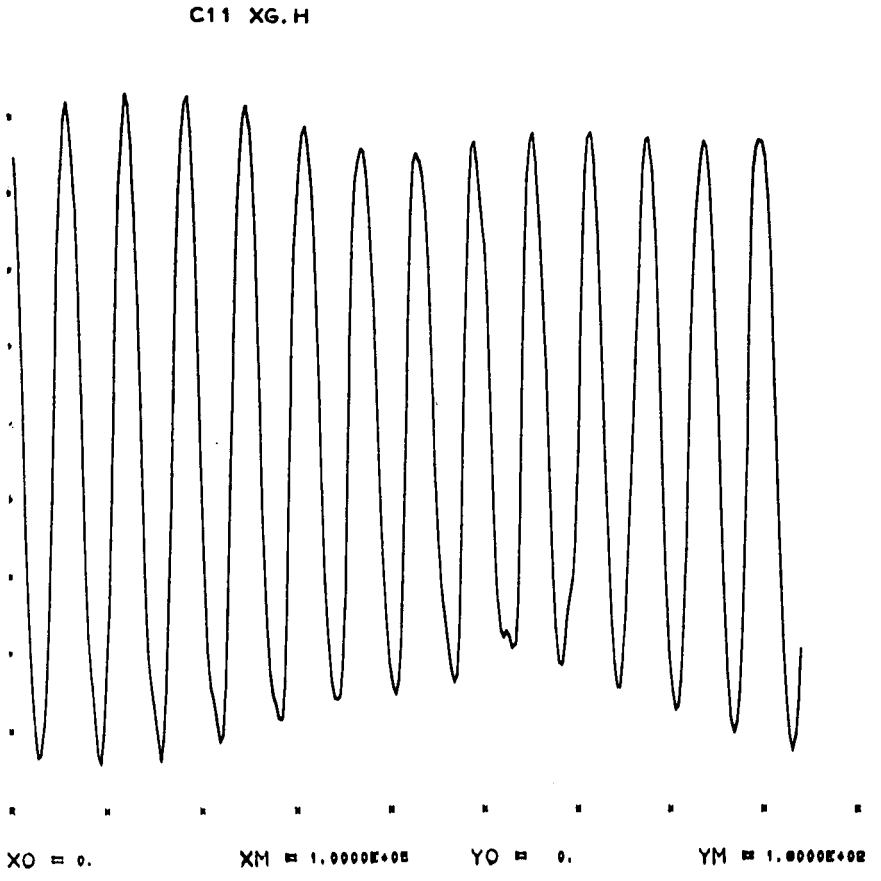

Figure 18

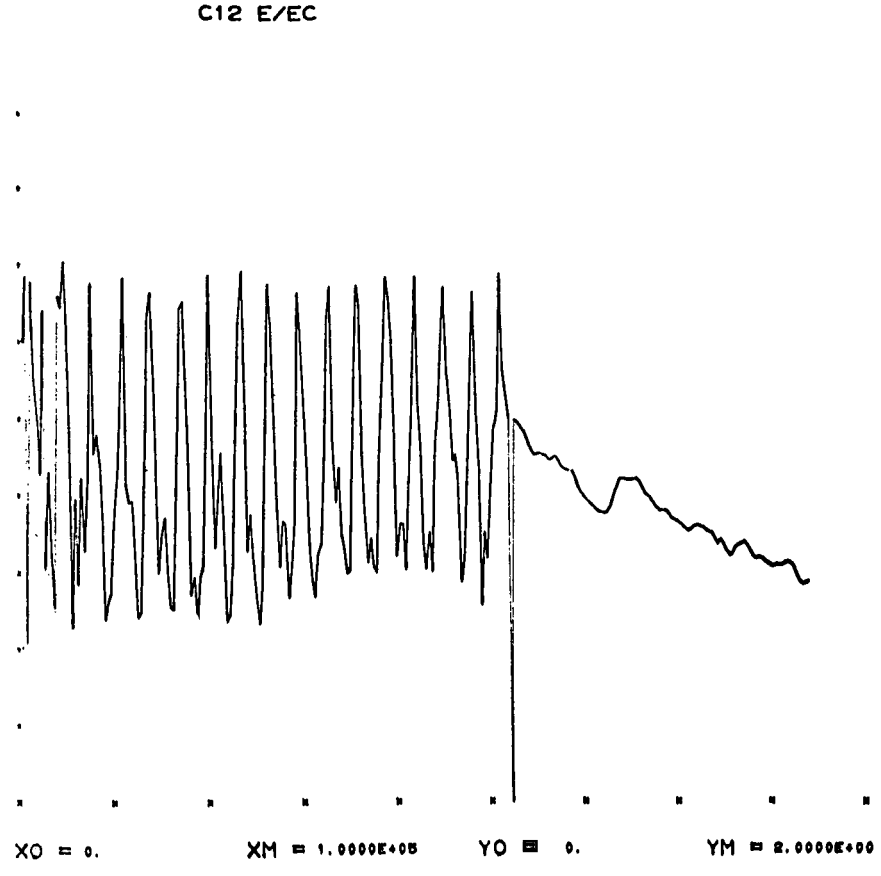

Figure 19

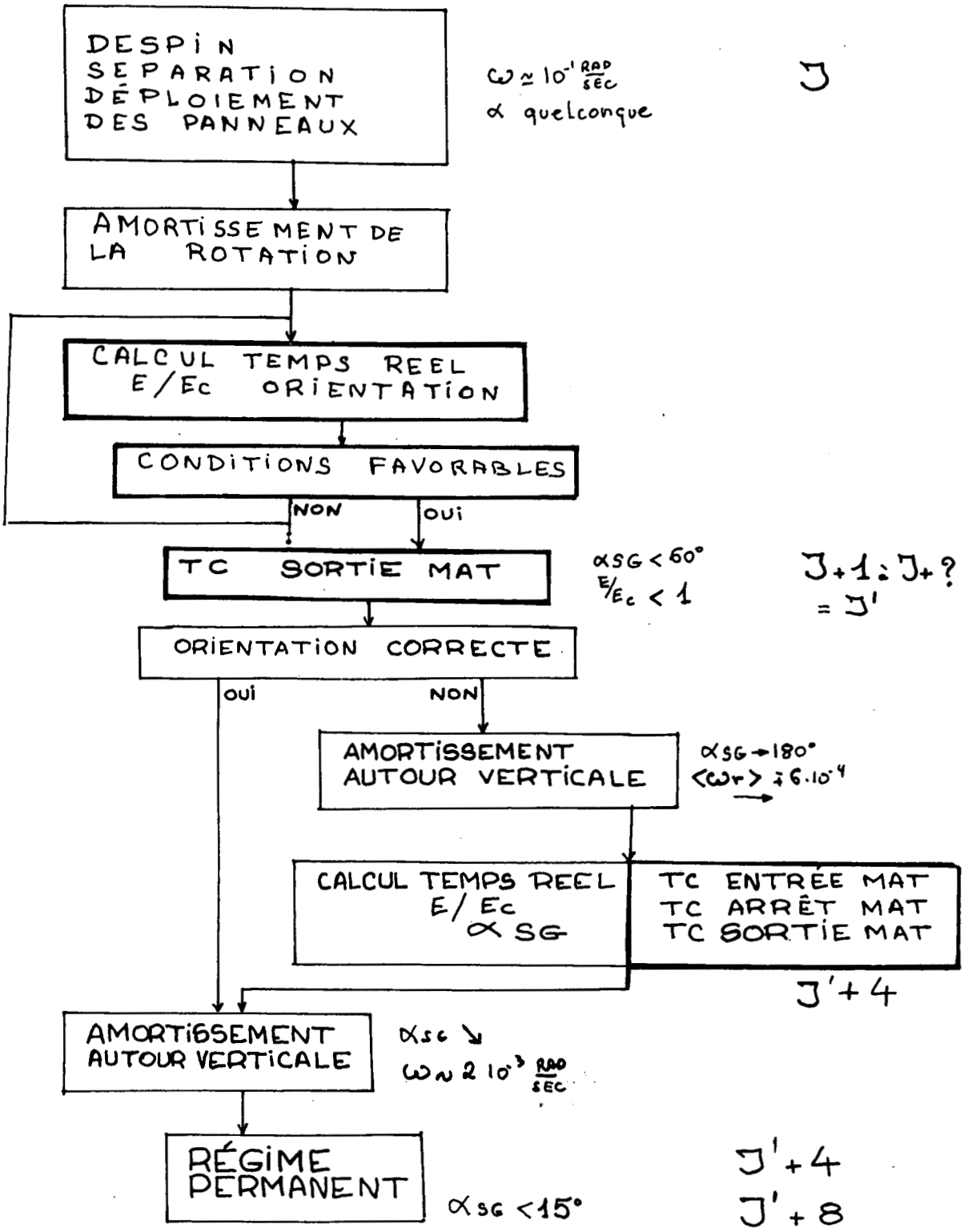

Fig.20 PEOLE capture prévue

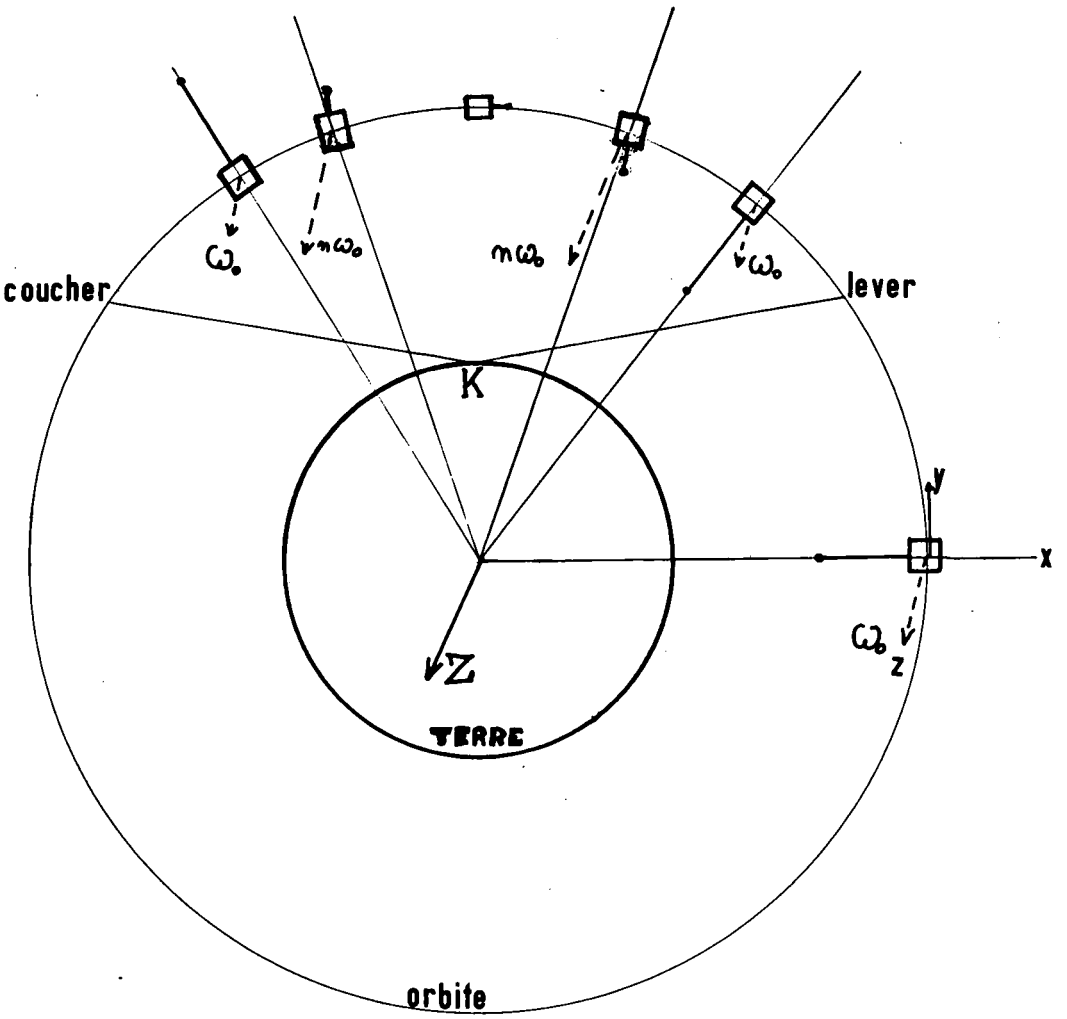

retournement

$$T = \frac{T_0}{2(n-1)} \qquad l_1 < \frac{l}{\sqrt{1+\sqrt{3}}}$$

Figure 21

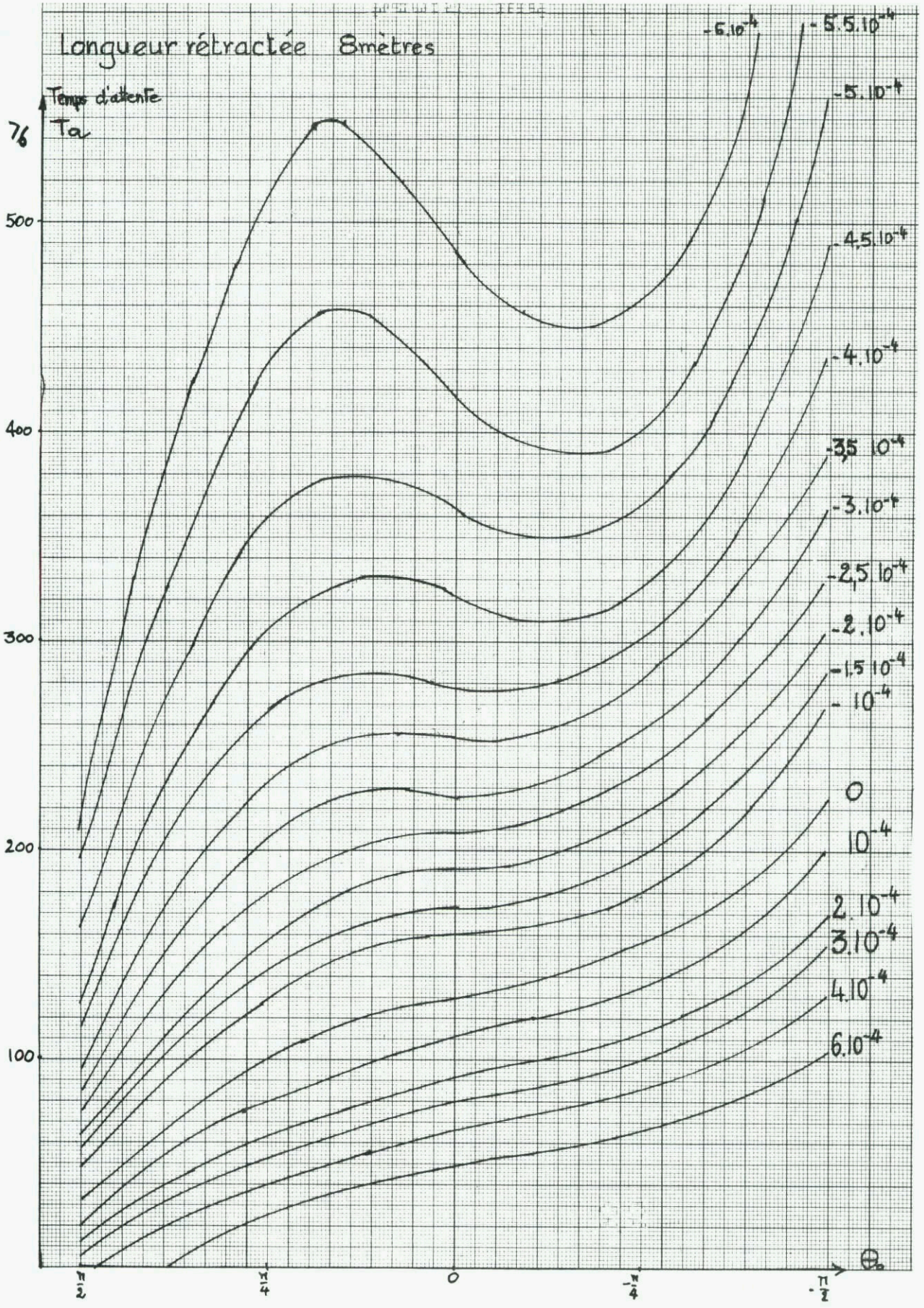

Fig.22 PEOLE mq

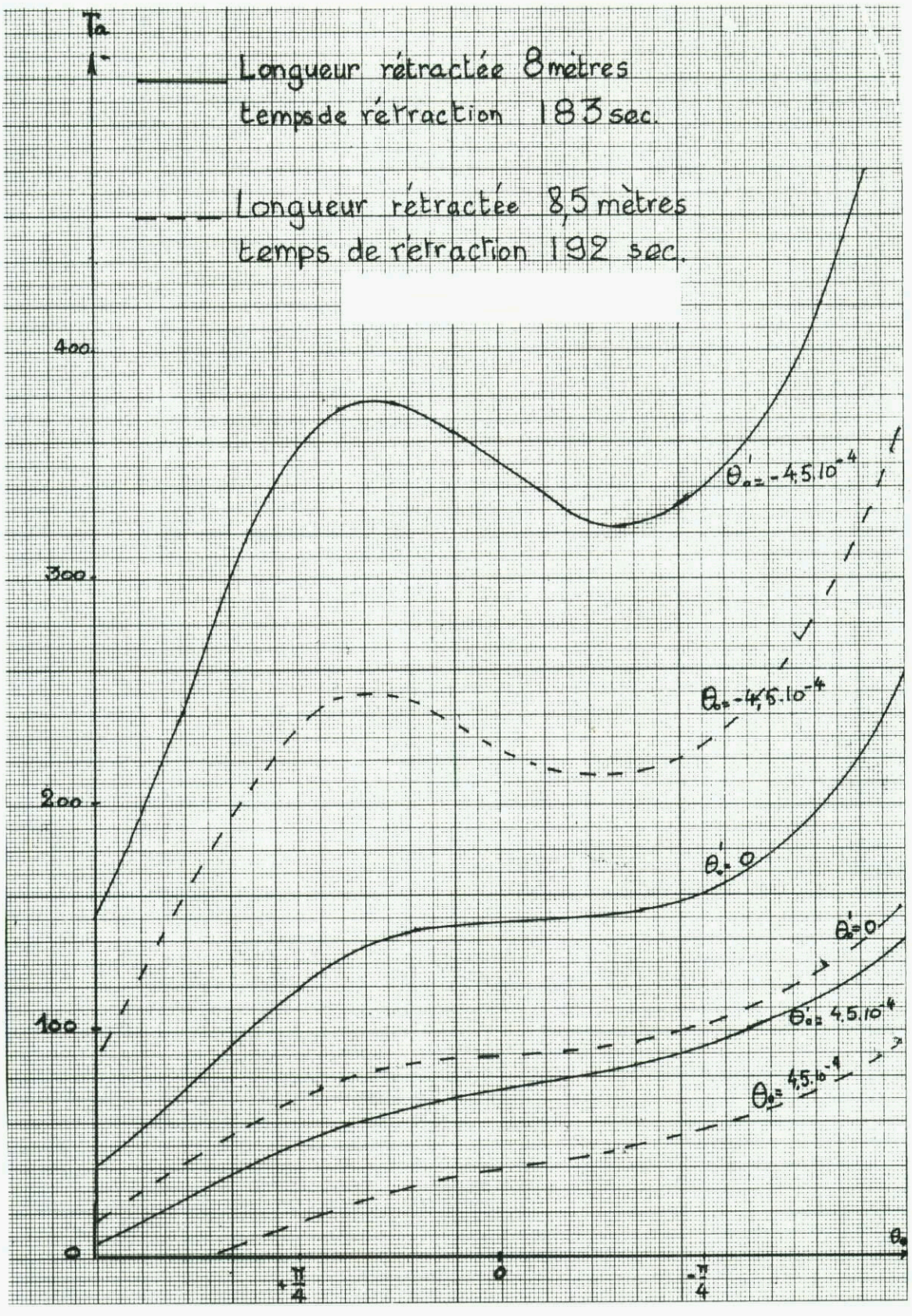

Fig.23 PEOLE mv

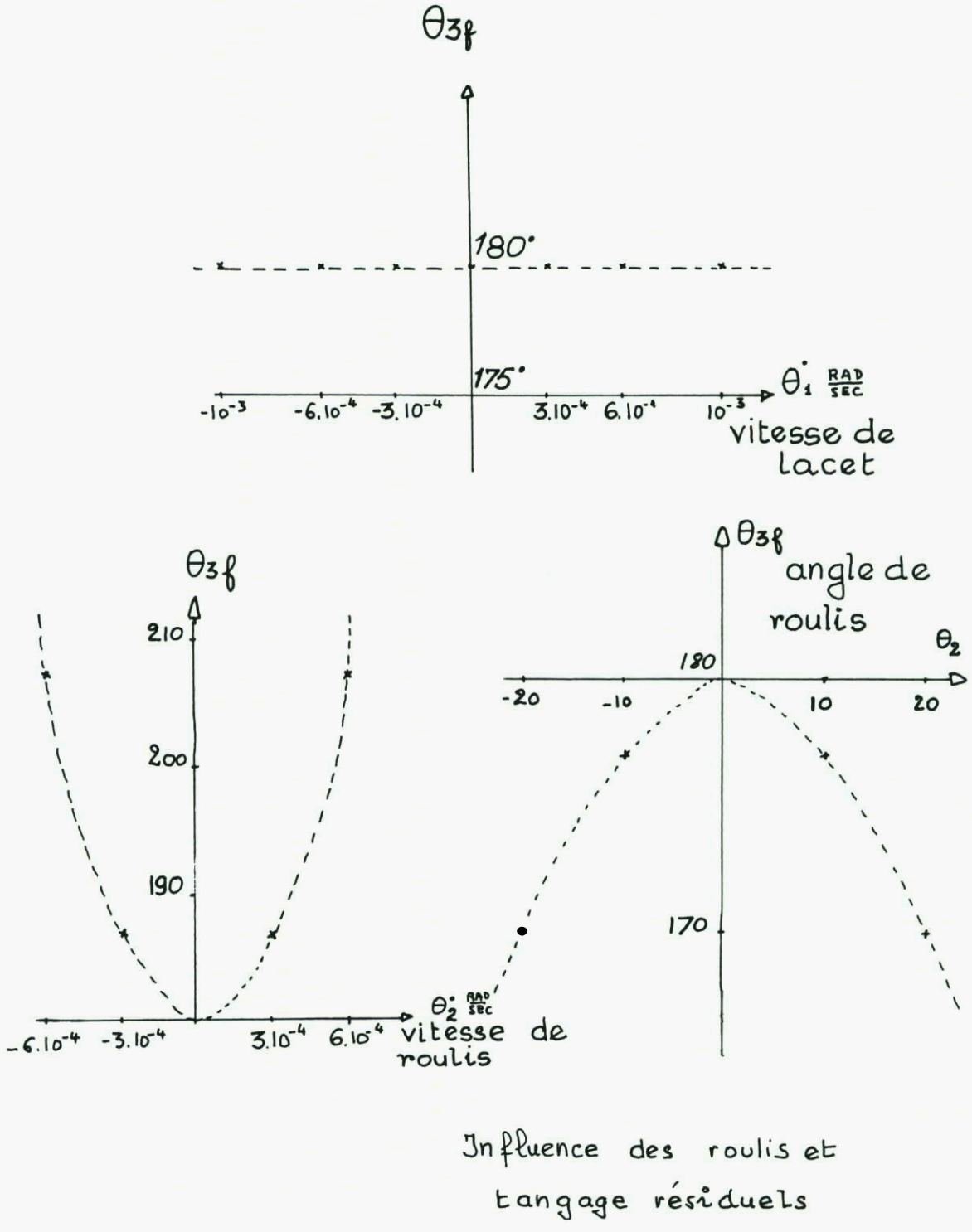

Influence des roulis et tangage résiduels

Fig.24 Retournement

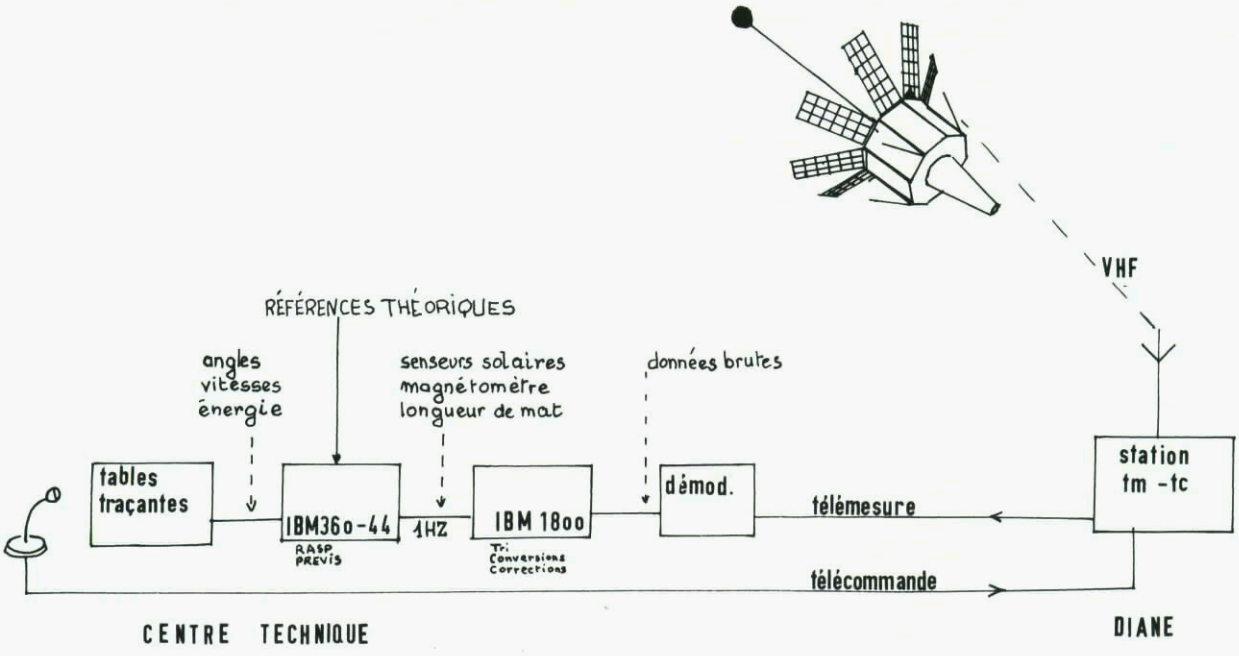

Fig.25 PEOLE: acquisition de la capture à Kourou

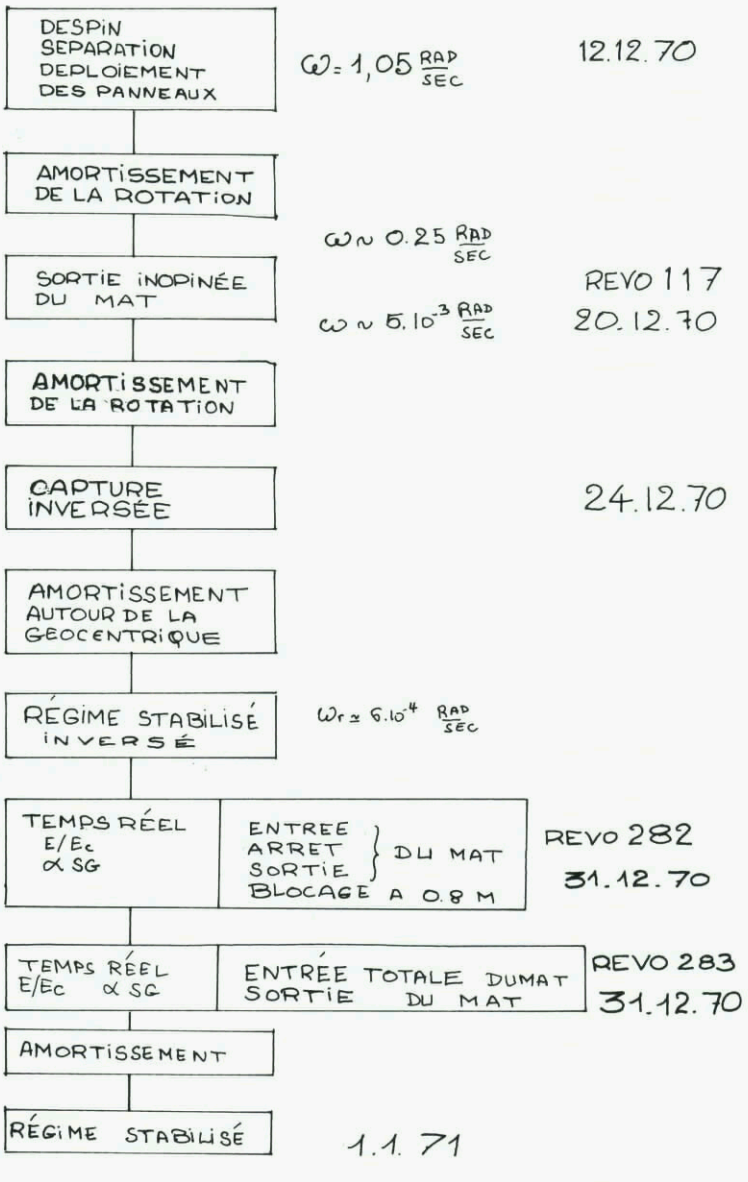

Fig.26 PEOLE: comportement en vol

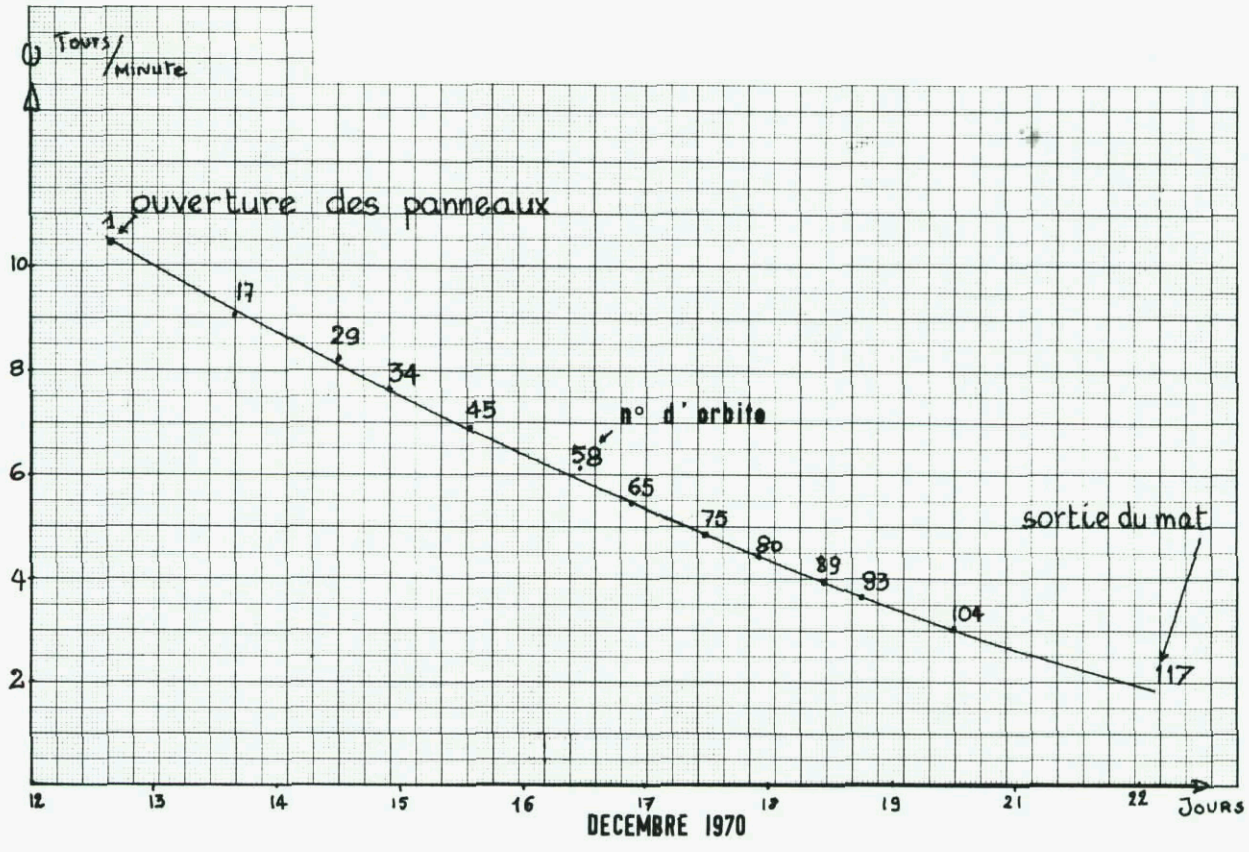

Fig.27 PEOLE: amortissement initial

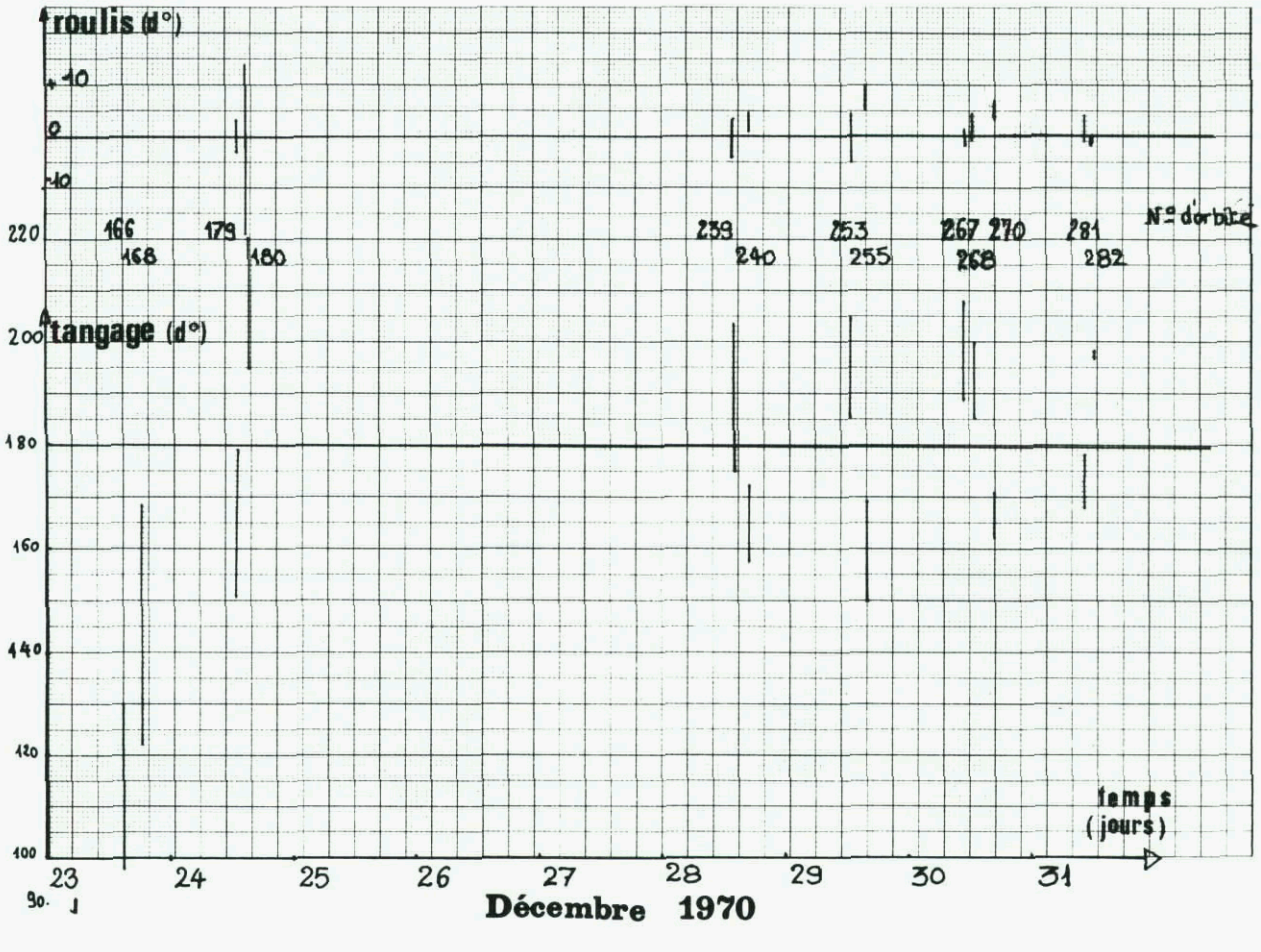

Fig.28 PEOLE: stabilisation sens inverse

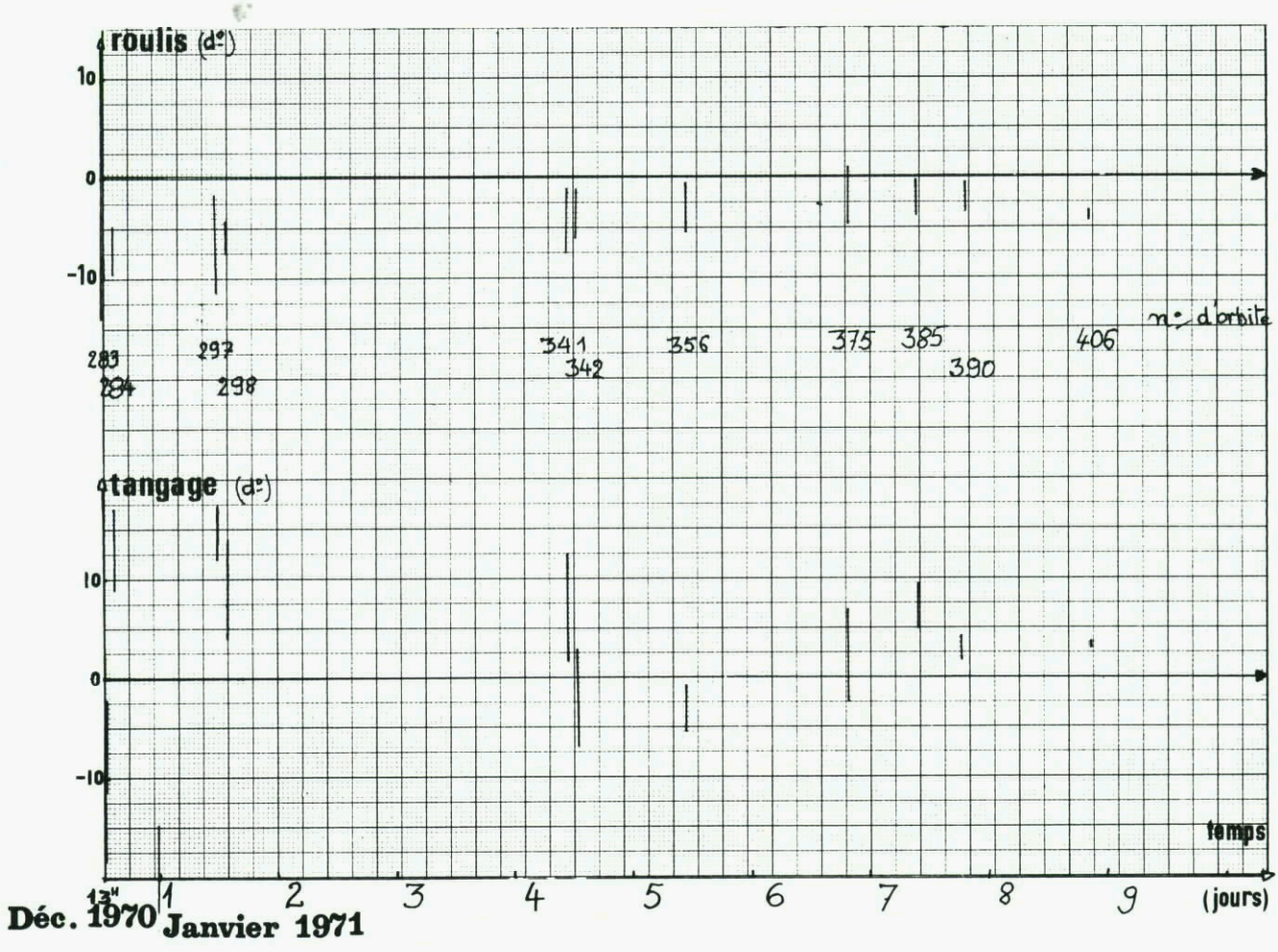

Fig.29 PEOLE: stabilisation sens correct

Development Results of the ESRO TD Satellite Pneumatic System

by
Werner Inden
Dipl.-Ing., Subsystem Leader TD Pneumatic System
and Manager Propulsion Systems

ERNO Raumfahrttechnik GmbH
28 Bremen, Hünefeldstraße 1-5
W.-Germany

Summary

After having payed some attention to the attitude control requirements and principles of the ESRO TD satellite the based upon requirements for the propulsion system are explained. The TD propulsion system is an Argon cold gas system with no redundant parts which is based on the life time of 1/2 to 1 year in orbit.

The design and development philosophy is discussed with some depth to understand the presentation of the test results of development, qualification and flight acceptance. The primary results of these tests are illustrated in form of the influence of the dynamic response on thrust, the problem of leakage and contamination, the regulation as a function of mission time. The successful subsystem qualifications - especially vibration tests - are shown.

In the last paragraph special development techniques for nozzles, system filling and leakage check-out are described. The performance of the smallest nozzles ($2 \cdot 10^{-2}$ N) for a satellite in Europe used on TD is shown to a certain extent. A film will point out the way of subsystem manufacturing under maximum cleanliness conditions and the testing of subsystems.

1. Introduction

This lecture is a survey of the recent design and development history of the pneumatic system used as the active momentum generating device which provides the required impulses to the TD satellite attitude control system for several tasks:

a) to make the initial orientation of the satellite
b) to off-load the on board reaction wheels
c) to conduct the attitude control manoeuvers in case of wheel failures.

TD satellite tasks
The TD satellite is 3 axis stabilized with a pure scientific mission and weights 466 kg. It has seven experiments with 113 kg (24 %) on board. The main characteristics are summarized in table 1.

The main characteristical feature of the TD satellite is the separated compartment design, one for the experiments, the other for the equipment and services. This is shown in figure 1. The great advantage of this concept is that it offers the possibility to provide a family of satellites by changing only the experimental packages. Unfortunately no further TD's are planned by the European organisations. The attention is limited to the equipment case package and there more specifically to the attitude control in general and to the propulsion system in details.

2. The TD attitude control requirements

The following table 2 summarizes the requirements for the attitude control system. As to be seen from this table a very high sun pointing is required, i.e. 1 min. of arc. This high accuracy can only be achieved by a very precise attitude control and leads to the coice of reaction wheels and for redundancy reasons the propulsion system must be capable to fulfill that accuracy too. So a cold gas system with small impulse performance was chosen. The complete attitude control performance depends on the accuracies of the main elements of its control loop:

- the sensors, which discover the deviation
- the electronics, which has to compare it with the allowed tolerances
- the active momentum exchange device (wheels, propulsion system).

3. The TD propulsion system requirements and performances

The translation of the requirements to the attitude control system into those for the propulsion system is the first step. Furtheron satellite requirements must be taken into account. A summary is shown in table 3.

4. TD propulsion system description

In response to the performance characteristics mentioned above the subsystem can be defined. Fig.2 shows the flow scheme of the system which has no redundant components. The simplicity supersedes the risks of failure in the relatively short mission time of 1/2 year.

The argon gas stored at 150 bars (max.) in the tank is reduced to 1,5 bars by a high reliable pressure regulator - used on some American programs -. The six solenoid valve thrusters are provided with this low pressure and deliver the small thrust on electrical command from the attitude control electronics. The low pressure pipes are made of titanium, the high pressure out of steel. Figure 3 shows the real arrangement within the structure. An interesting feature is the use of flexible pipes which allowed the mounting of the thruster manifold at the outer end of the deployable solar paddle. The mass break down of the whole system is noted in table 4. In the following the main components are shown and described.

4.1. Tank

The above figure 3 shows the titanium tank with 448 mm internal diameter and 3,6 medium wall thickness. The manufacturing process is characterized by the following sequence:
- pressing of half shells - machining - heat treatment - final machining of the half shells - electron beam welding. The tank is an ERNO/VFW/Krupp product.

4.2. Regulator assembly

Figure 4 is a photo of the regulator assembly being an integral unit to be screwed into the tank. It provides

- o HP/LP regulation device (HP/LP = high/low pressure)
- o HP-inlet
- o LP-outlet
- o vent port (relief valve)
- o HP-transducer-port
- o LP-transducer-port

4.3. Thruster assembly

Figure 5 shows the 4-thruster manifold with protection caps on the nozzles. Each of these valves is fitted with a 5 µm filter at its inlet to retain any harzardous particles from the piping system. One of the greatest problems is the particle cleanliness. Two kinds are generally distinguished, the parts cleanliness and the area cleanliness. For both tremendous facilities are necessary. Once built up the biggest care must be devoted never to interrupt the clean chaine.

As an example the parts cleanliness level required for TD is:

o metallic:	6 particles max.	3 - 5	µm
	22 particles max.	2 - 3	µm
	437 particles max.	1 - 2	µm
o non metallic:	25 particles max.	10 - 25	µm
	437 particles max.	5 - 10	µm
	unlimited particles	1 - 5	µm

Compared with a normal laboratory air contamination there is a factor of about 100.000 time less number of particles. In fact, even with greatest cleaning efforts human error cannot be excluded so that the use of filters upstream of each critical component is actually the best guarantee against orbit failures due to contamination.

5. Design and development philosophy

Each functional component is covered by a specification defining

- o the performances
- o the environments
- o qualification and acceptance test requirements.

Normally the choice of a component is made with respect to the specification requirements and if available to the qualification status in other programs. The whole development is presented in Figure 6 by a flow scheme.

During the development phase development units of components are tested to verify or adjust them to the specifications. After this period the qualification test program is conducted on a certain number of units. They have to be within all performance limits all over the environmental exposures. In special cases a complete or partial "qualification by similarity" can be made if the component was qualified for another program. The experience shows that such a procedure is complicated since it requires

- o a very good quality control documentaion on the component manufacturers side to demonstrate the differences from type to type;
- o very good test documentation of the test laboratories having conducted the qualification tests;
- o availability of all these documentation for use in other programs than for its origine destination (proprietary etc.);
- o good coincidence of the performance and environmental specification with those of the new program.

Normally a complete requalification is not much more expensive than partial retesting and the troubles with the rest of the above documentaion. Once a component hase been qualified the further units of this component will only be tested for acceptance. This meanse that the environmental exposure conditions are reduced. The aim is to discover production failures or deviations which could effect the mission. The acceptance tests are normally separated in two steps:

- o those at the manufacturer at ambient conditions
- o those at the customer at environmental conditions (temperature, vibration).

The same basic philosophy applies to the subsystem development, qualification and acceptance test.

6. Main test results of the development, qualification and flight hardware

6.1. Component testing

6.1.1. Tank

Two tanks of the batch of five were submitted to the following qualification program: one tank through leakage and burst and one tank through leakage, vibration and burst.

a) Leakage

The leakage of tanks is defined as the leakage of the seam. Leakage through the port is a system leakage. The leakage was measured by means of an evacuated ring (10^{-5} Torr) around the external seam and a He-detector. The tank was pressurized to 150 bars. The test arrangement allowed a leak detection of $5 \cdot 10^{-9}$ Torr ltr/sec. In no case a He-indication could be found, so that the requirement of $1{,}23 \cdot 10^{-5}$ Torr ltr/sec (about 0,05 scc/h) was met.

b) Vibration

One tank has been submitted to a vibration test under nominal high gas pressure of 150 bars in a special test laboratory in the South of France.

The test set up is shown in figure 7 and the test specimen in figure 8 on the slip table. Figure 9 summarizes the results. Due to shaker failures and the lack of an automatic output limitation the outputs on the tank, regulator and fill valve exceeded the acceleration limits considerably (factor 3 max.), i.e. 100 g for the tank at 750 Hz. No explosion or damage occurred.

c) Burst

Both tanks were burst. They withstood 330 bars min. before burst while 306 bars min. are required. The following table compares the burst pressures from tank to tank.

act. burst pressure	tank ser. no. 3	4
p_B (bars)	330	345

Figure 10 shows the stress distribution observed in the seam area, once for the original support with straps on the tank and once in the wood support. The procedure was to pressurize the tank up to the proof pressure within the original structural support to simulate original conditions, then to put the tank into a wood support for the pressurization up to burst. So the destruction of the original support and straps could be avoided.

Figure 11 shows the stress distribution in the pole area with its thicker wall. Figure 12 demonstrates the performance of the tank during pressuration. In Figure 13 the ruptered tank is presented once in the pole area and the other in the seam area.

6.1.2. Regulator

Figure 14 shows the static regulation characteristic over the mission time. The LP regulation within 1,6 bars ± 10 % (required; 1,55 ± 6 % actual) is maintained over the whole HP range of 150 bars down to 10 bars. The regulator has two seats in series for leakage redundancy. The primary seat is of metal/metal, the secondary of soft/metal type. The primary seat closes a little bit earlier (0,2bars) than the secondary. At about 2,1 bars the relief valve - integrated into the regulator assembly - opens and reaches at 2,5 bars the full flow pressure. The relief pressure setting depends on the maximum operating pressure of the thrusters. In case of a leakage failure of the regulator the pressure upstream of the thrusters would increase up to that pressure, so that the system remains operating. A second reason comes from the safety requirements. But with the use of titanium for the low pressure pipes this is not a problem since they withstand pressures up to several hundred bars (1/4 dia; 0,025 in wall thickness).

Figure 15 represents the regulation hysteresis. The following tendencies were observed:

a) the hysteresis is a function of the high pressure inlet, the deviation varies from 0,025 to 0,05 bars between 10 and 150 bars. This corresponds to 1,5 to 3 % of the regulated pressure;

b) the regulation sensitivity is constant up to a mass flow of 0,2 g/sec and independant of the high pressure;

c) above 0,2 g/sec the regulator becomes very sensitive to a mass flow increase. In case of a mass decrease the regulated pressure remains constant.

The dynamic response of the regulator depends on the downstream volume and geometry. During development serious attention must be attached to this problem by testing a simulated system for possible resonancies which could damage the regulator in special cases as for example straight lines in a "T" flow scheme arrangement.

Figure 16 shows the dynamic characteristics for a 20 Hz mode with three thrusters simultaneously. The following observations can be seen:

a) the plenum chamber pressure (about 1,2 bar) does not feel the regulation pressure variations, being in fact small;

b) the pressure oscillations within the plenum chamber (3 mm, 0,3 mm long) due to turbulances;

c) the mass flow readings indicate pressure oscillations in the line of about 50 Hz but they are not in resonance with the regulator, whose resonance frequency lies between 150 and 200 Hz.

6.1.3. The TD nozzles and thrust measurements

The TD nozzles are the smallest nozzles built in Europe for a spacecraft, see figure 17. The tests were conducted in the pressure range of 1,3 to 1,9 bars. Figure 18 shows the results for the thrust and specific impulse which is 10 to 20 % higher than initially estimated. The reason was found to be the extremely good surface roughness. The previous assumption that the surface roughness of the expansion cone is the major determinating parameter and more important than the throat was confirmed. A 0,45 µm repeatable absolute surface roughness (figure 17) was achieved, which exceeds the usual high quality surface roughnesses with a magnitude of 5 to 10. The nozzle is an ERNO-KOHL product. The ERNO developed thrust measuring device (figure 19) for the small thrusts allows an accuracy of better than 2 %. The only problem was that the actual vacuum during mass flow was 5 Torr to high to assure full expansion of the nozzles. Therefore the thrust and I_{sp} of figure 18 is corrected as follows:

The variation of the thrust or thrust coefficient c_F with the ambient chamber pressure for a given fixed nozzle geometry (*) is a linear function:

$$c_F = c_F^{o*} + \frac{A_e^*}{A_t^*}\,\frac{p_e^*}{p_c^*} - \frac{A^*_e}{A^*_t}\cdot\frac{p_a}{p^*_c}$$

$$= c^*_{F_{vac}} - \frac{A^*_e}{A^*_t}\cdot\frac{p_a}{p^*_c}$$

The correction factor is $c^*_{F_{vac}}/c_F$ which is in our case 1,03. The corrected curves are noted in figure 18, too. Some future tests will have to confirm these estimations. Figure 18 contains also the Summerfield and Barrère (1) criterion for the flow separation, being p_e/p_a = 0,4 and 0,286 respectively.
Since in our case p_e/p_a = 0,2 is less than these limits, a separation occurs. An analysis showed that it is to be expected at 80 % of the exit cone length in flow direction.

From the indicated actual regulation band limits the following conclusions can be taken which are of importance for the attitude control:

- The thrust variation over the mission time is 23,3 to 26,9 mN.
  Note: These small thrusters (four) are mounted at the end of the solar paddles. There are two further thrusters of 3 times this thrust on the satellite body, but show similar performance.
- The specific impulse is nearly constant 50 sec. Since initially only 45 sec were estimated and included in the gas mass, a 10 % longer life can be expected than required.

6.2. Subsystem testing

The regulation and dynamic response have been discussed above as well as the vibration performance together with the tank. Therefore only the leakage will be treated here as a function of pressure and temperature. It was found that the leakage depends sensitively on the temperature but not on the supply pressure (figure 20). This can be explained by the very low leakage rate at individual points which is more a Knudson flow than a viscous flow.

7. Special development techniques

In the following some special development test results and special equipments are reported.

7.1. Nozzles and thrust measurements

The very positive test (high spec. impulse over the operating pressure range) results of the TD nozzles leaded to a special test program to investigate the performance of the small nozzles at very low chamber pressures. It was found (figure 21) that the spec. impulse decreases slowly in line with that of the higher pressures of figure 18. It must be noted that the exit pressure was about 3 Torr, consequently again an overexpending nozzle operation occurred. Therefore the correction was made as noted above. The good performance depends on the following criteria:
a) highest manufacturing quality (surface, orifice)
b) accurate measurements of actual dimensions and performance.

In fact our nozzles were measured for the throat diameter being 0,373 mm with an accuracy of 1 /um. An error of 5 /um would mean an error of 2,5 % for the throat area and thus for the thrust, which is quite important. The next step was the manufacturing of an even smaller nozzle. The results of a 0,1 mm throat diameter nozzles are not yet available at the date of the printing of this report. It will be interesting to compare the new results for the spec. impulse in the same thrust range. We await from these tests the answer to the question if - for a given thrust range - the nozzle with the smallest orifice but higher chamber pressure has a better spec. impulse than the nozzle with greater orifice and smaller chamber pressure. The first is preferred because of the regulator performance. We are convinced that the results will open the range of cold gas systems to that of the resistojet by decreasing the actual thrust of about 0,01 N with a magnitude of more than 10.

7.2. Fill and checkout system (FCS)

A special device was developed to fill the pneumatic system and to conduct a functional checkout of the thrusters any time during the satellite ground operations and finally on the launch pad. The FCS is positioned besides the satellite. The operation of filling the tank is a dangerous operation and has therefore to be conducted under various safety roules and requirements. Figure 22 shows the system. Special attention must be payed not to heat the tank too much during pressurization and to keep the gas dry during the passage through the FCS. After having filled the tank a thruster functional control is conducted by an electronic device integrated in the system.

7.3. Leakage checkout system (LCS)

This system serves to control the leakage of the propulsion system every-time during the satellite integration and before the satellite will be mounted on the launcher as a final check. The necessity is immediately understood when the long life steps up to the launch are considered, i.e. the structure with the propulsion system left ERNO in the first days of January 1971. A lot of integration work around the system is done at MATRA. The risk of damages during this period or later during tests is abvious. The device (figure 23) operates at ambient conditions and uses krypton as a tracer gas. The procedure is very simple and as follows:

- Having put the tent around the satellite the increase in krypton concentration in the tent is recorded.
- Afterwards the calibration leak (10 scc/h) is fitted to the wall and again the concentration is recorded over several hours.
  The relation between the two lines defines the leak rate of the system.
- To be sure the recording is continued after having taken away the calibration leak. Normally the same inclination of the line is found as before. A typical diagram is shown in figure 24.

8. Summary and conclusions

The successful development of such a high qualified space system as the propulsion system technology for future European projects depends on sufficient confidence in reliability of the components and last not least of the humans to conduct the work. Very often this item is underestimated against nice paperwork by the customer organisations.

From the technical point of view high gain of experience was obtained in the field of
- tank manufacturing
- thruster development
- integrated subsystem, design and testing

It should be noted that ERNO made the first propulsion system for a European spacecraft. The others as HEOS and HELIOS were completely manufactured in the USA.

Together with the experience of the Intelsat III and recent AEROS satellite propulsion systems on the hydrazine basis ERNO covers the thrust range of 20 N and more, down to 10^{-3} for any satellite orbit and/or attitude control propulsion system based on the simplest propellant solution, i.e. a hot or cold monopropellant.

References

(1) M. Barrère and others, Raketenantriebe, 1961

(2) MESH - TD Specifications

(3) W. Inden, Analyse der Prüfergebnisse von Kaltgas- und Heißgasantriebssystemen für Satelliten, Vortrag auf der DGLR-Fachausschußsitzung "Chemische Antriebe" vom 15. 9. 1970

TABLE 1

Main Characteristics of the TD-1A Satellite

1. Function

to make astronomical measurements in various spectral ranges and to measure space x- and γ-rays.

2. Development

customer	:ESRO/ESTEC
contractor	:MESH-consortium
main-contractor	:S.A.Engins MATRA
devel.period	:1968 to 1972
devel.costs	:47 Mio $ incl. the earlier devel. of the TD 2 satellite in 1967.
launch date	:25.2.72 to 6.4.72
launch site	:Western Test Range/Cal.
launch vehicle	:Thor Delta (2stage
min. life time	: 6 months
orbit	: 550 km circular inclination 97,57°
rotation of orbit	: 0,9855°/day

3. Characteristics

total mass	: 466	kg	
scientific payload	: 113	kg	(24 %)
structure* incl. solar paddles and mechanisms*	: 122	kg	(26 %)
thermal control	: 9,5	kg	(2 %)
attitude control incl. propulsion system*	: 90	kg	(19,3 %)
power supply**	: 36	kg	(7,7 %)
telecommunication***	: 29	kg	(6,2 %)
housekeeping*	: 4	kg	(0,9 %)
electr. wiring	: 52	kg	(11,1 %)

dimensions:

equipment case	: 0,9 x 1 x 0,66 m
experiment case	: 0,9 x 1 x 1,43 m
overall height	2,20 m
paddles, 2 each side	:0,83 x 1,51 m/ea
outfolded length	: 5,5 m
sun pointing accuracy	: 1 min of arc
max electrical power	: 400 watt

* ERNO-Raumfahrttechnik GmbH, Bremen

** HSD-Hawker Siddeley Dynamics, England

*** SAAB-Aktiebolag, Schweden

TABLE 2

Summary of Attitude Control Requirements

MODE OF A.C.S.	PITCH AND YAW ATTITUDE CONTROL 2 SIGMA VALUES		ROLL ATTITUDE CONTROL 2 SIGMA VALUES		ATTITUDE RESTITUTION ACCURACIES VALUES AT 2 SIGMA	
	Sun pointing error	Pointing stability q, r	Pointing error (z, P_3) angle	Roll rate stability p	Pitch, Yaw	Roll
End of initial acquisition	3 degrees of arc	0,2 minute of arc per second of time	10 degrees of arc		2 degrees of arc	2 degrees of arc
Normal	1 minute of arc	0,2 minute of arc per second of time	10 degrees of arc	0,08 minute of arc per second of time	1 minute of arc	0,5 degree of arc
Stand-by	6 degrees of arc	5 minutes of arc per second of time	10 degrees of arc	5 minutes of arc per second of time	10 degrees of arc	10 degrees of arc
M.S.T.L.F.	5 minutes of arc	1 minute of arc per second of time	10 degrees of arc	0,2 minute of arc per second of time	2 minutes of arc	0,5 degree of arc
M.S.R.G	1 minute of arc	0,5 minute of arc per second of time	10 degrees of arc	5 minutes of arc per second of time	1 minute of arc	0,5 degree of arc

REMARK: During the wheel desaturation phase in the normal mode, the drift rate d (x,X)/dt and the roll rate stability shall not exceed 0,5 minute of arc for one second of time.

A.C.S. : Attitude Control System
M.S.T.L.F.: Emergency Fine Pitch and Yaw Mode
M.S.R.G. : Emergency Coarse Roll Mode

TABLE 3

Summary of the Basic Requirements for the TD Propulsion System

	requirements	related performances
• gas:	inert	Argon chosen
• total inert mass :	<17 kg	Real : 13,5 kg
• total momentums :	H_x = 4970 Nms H_y = 1820 Nms H_z = 920 Nms including a safety margin of 1,4.	with the lever arms (2240 mm, 2303 mm, 906 mm) the total impulse is 4630 Ns ≙ 10,8 kg gas incl. residual gas.
• mission time :	0,5 years in normal mode 2 months in back-up mode	full performance, no failures
• cycles/thruster :	10^4 for normal mode 10^6 for back-up mode (incl. safety factor of about 10)	defines the requirements for the solenoid valves.
• minimum/maximum pulses:	50 ms / 300s	defines the requirements for the solenoid valves.
• nozzle torques :	$M = M_{GX} = M_{GY} = M_{GZ}$ 0,03 Nm ≤ M ≤ 0.07 Nm	defines the nozzle thrust range together with the lever arms: 0,02 N on the solar paddles and 0,06 N on the body (both nominal)
• tolerances for c.g.-plane positioning :	± 50 mm along all three axes	defines the attachment points of the thrusters on the structure
• nozzle alignment :	± 0,5°	manufacturing requirement
• reliability :	>0,996 normal mode >0,786 back-up mode } at 90 % confidence level	design goal
• leakage :	< 300 g/year	30 g/year achieved = 4 scc/h
• Western Test Range Safety Requirements	pressure safety factor (burst) 2 x max oper. for tanks 4 x max oper. for all other components	defines the component specifications
• vibration environment induced by the launcher and amplified by the satellite structure	Sinus : 20 - 2000 Hz : 18 $g_2$max. Random: 20 - 2000 Hz : 0,10g^2/Hz qualification 11,8 grms 4 min 20 - 2000 Hz : 0,04g^2/Hz acceptance 7,7 grms 2 min	defines the component specifications

TABLE 4

TD-Propulsion System Mass Breakdown

Equipment case			
tank	10,73	kg	
manifold incl. 2 solenoid thrusters	0,40	kg	
pipes	0,31	kg	
fittings	0,24	kg	
high pressure filter	0,14	kg	
regulator	0,50	kg	
two pressure transducers	0,12	kg	
subtotal equipment case components	12,44	kg	
Solar paddle			
manifold incl. 4 solenoid thrusters	0,79	kg	
pipes	0,23	kg	
fittings	0,04	kg	
subtotal solar paddle components	1,06	kg	
total inert mass	13,50	kg	(17 kg max. allowed)
stored Argon gas	10,80	kg	
total operating subsystem mass	24,30	kg	(5,2 %)

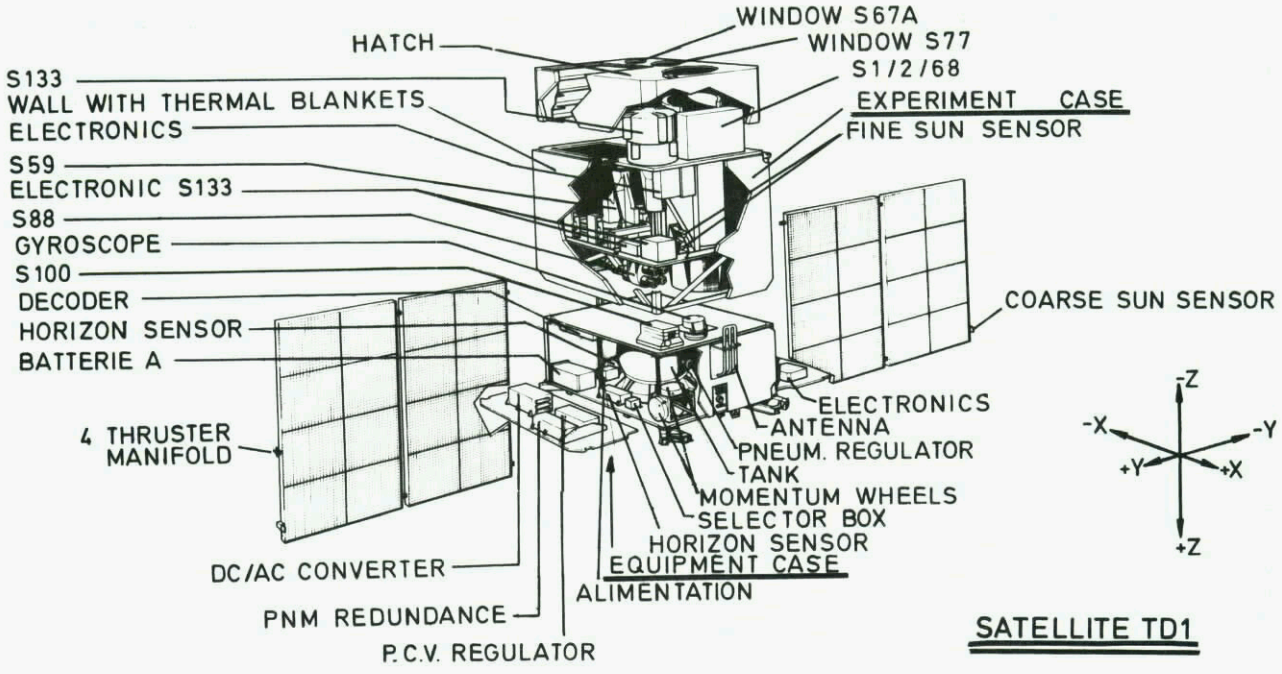

Fig.1 TD-satellite configuration concept

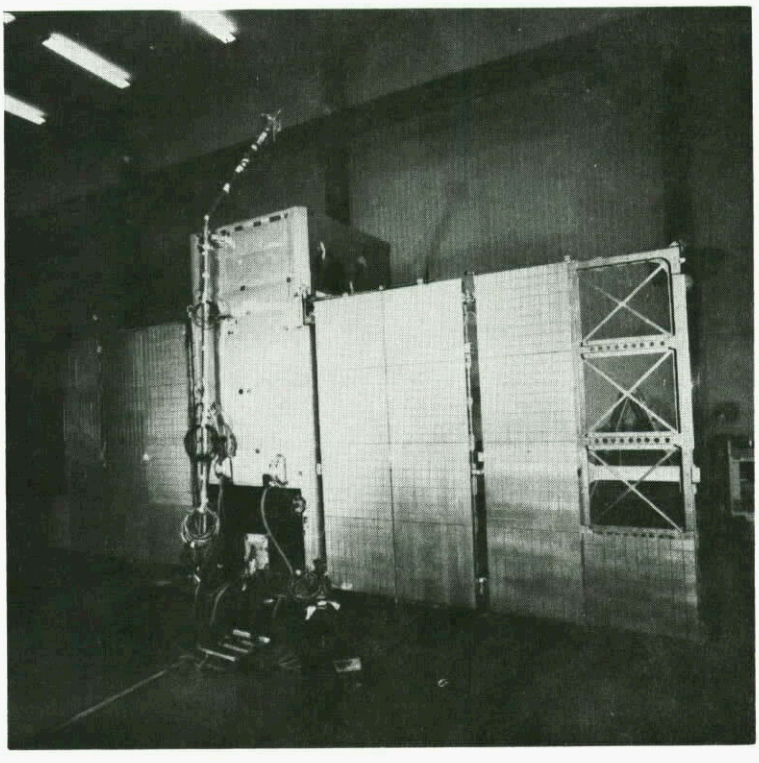

Fig.1(a) TD-satellite before vibration qualification test

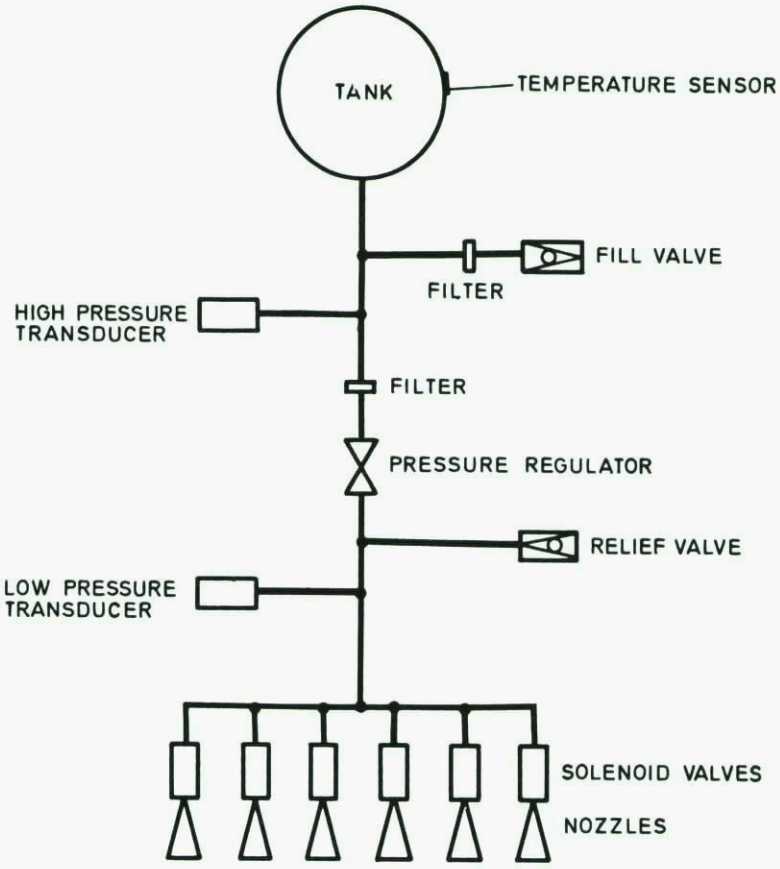

Fig.2 Flow scheme of cold gas propulsion system TD-1A

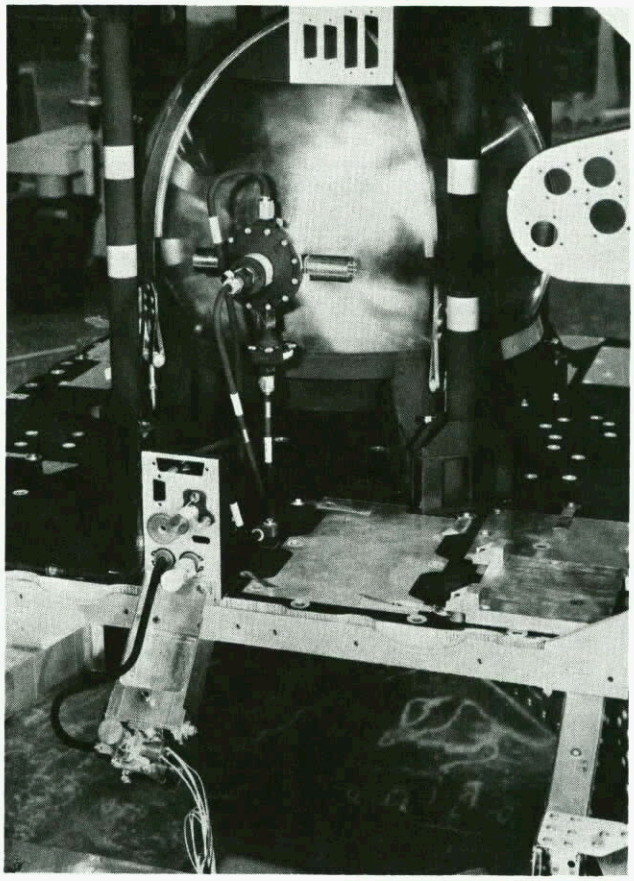

Fig.3 TD-cold gas propulsion system within the original structure

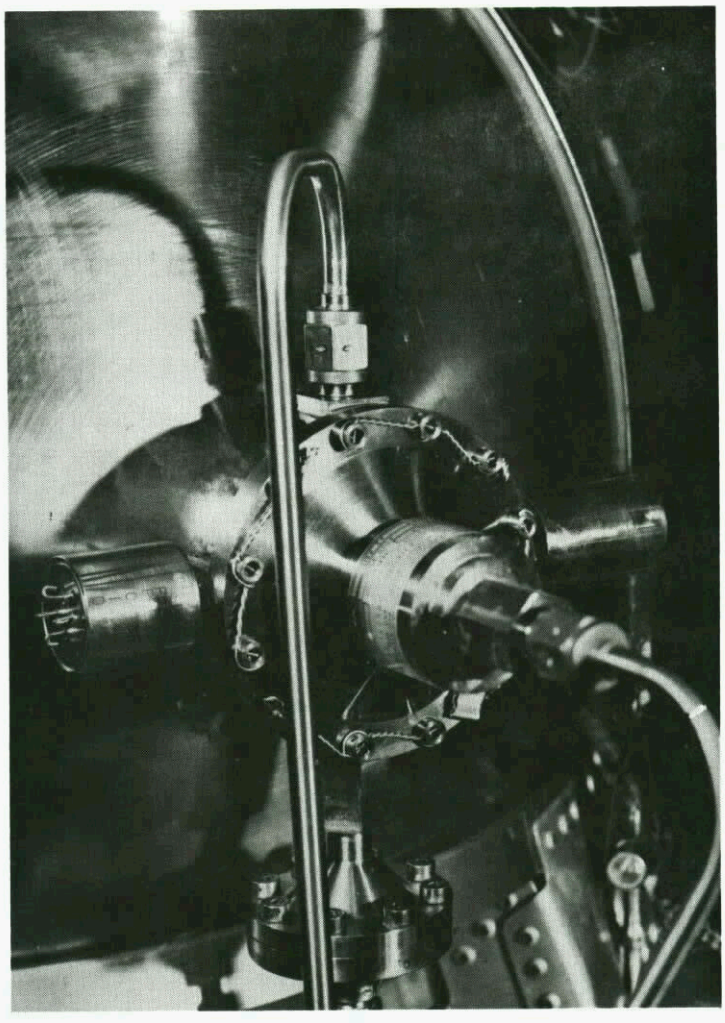

Fig.4 TD-cold gas propulsion system regulator assembly

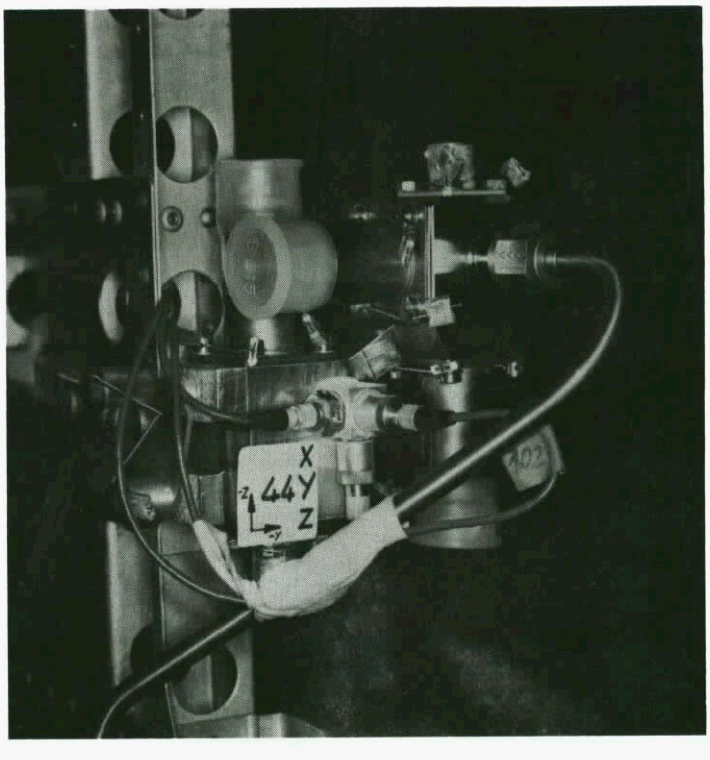

Fig.5 Four thruster manifold mounted on the solar paddle with accelerometers, TD-propulsion system

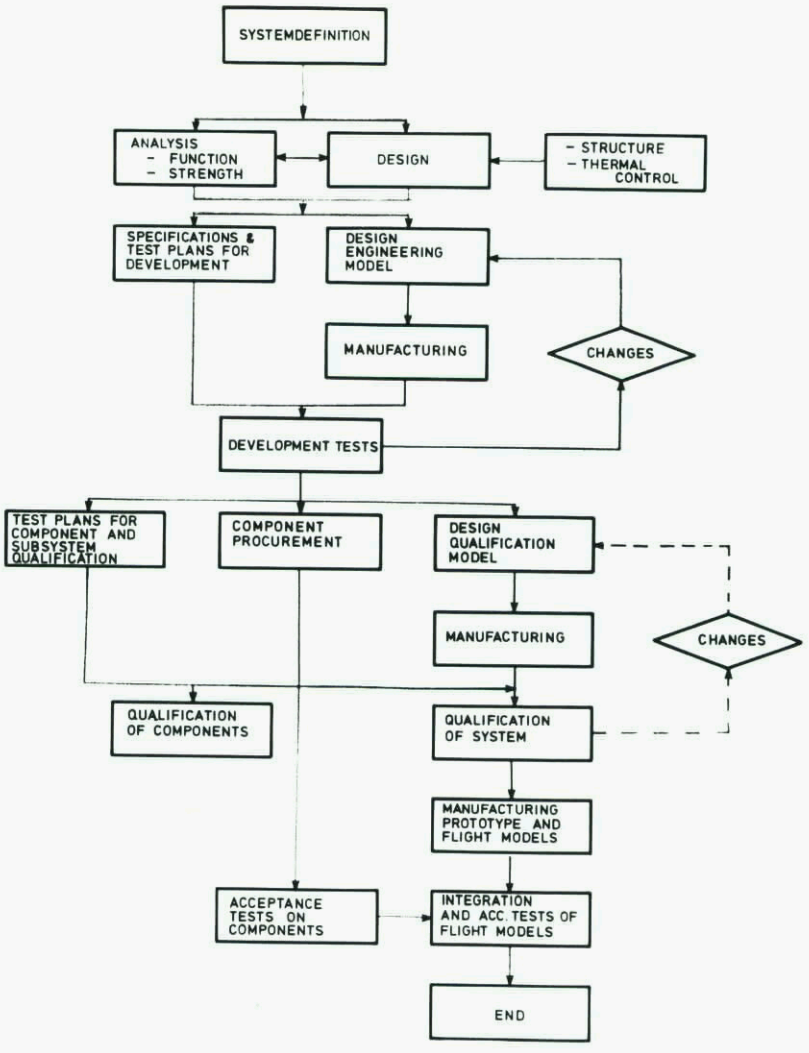

Fig.6 Development flow scheme of the TD-propulsion system

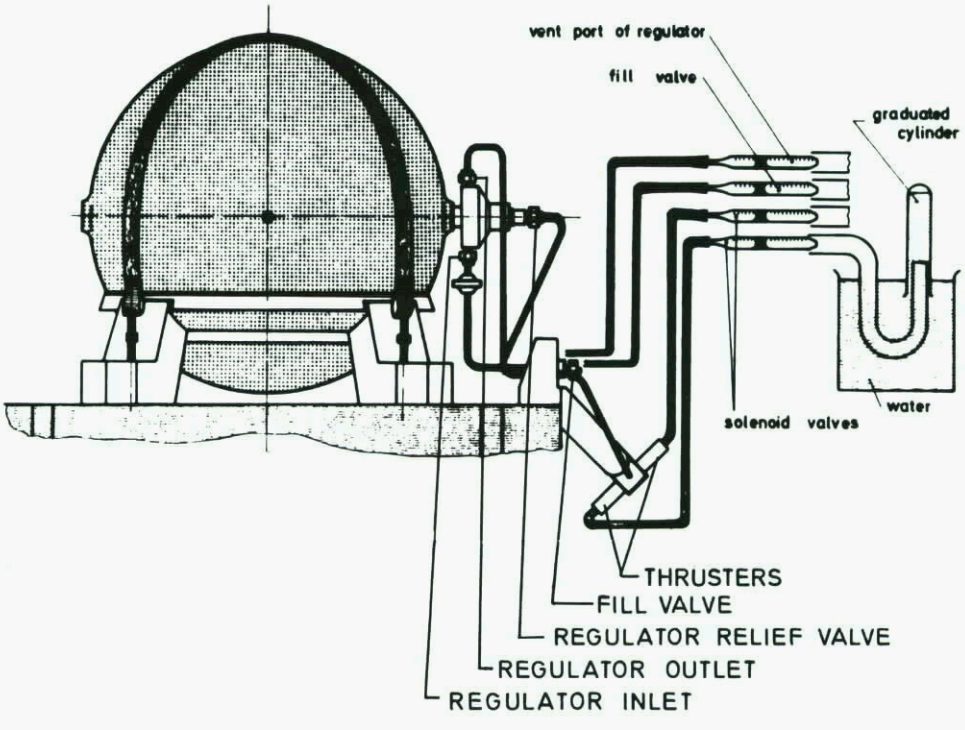

Fig.7 High pressure vibration model test-set-up for leakage monitoring

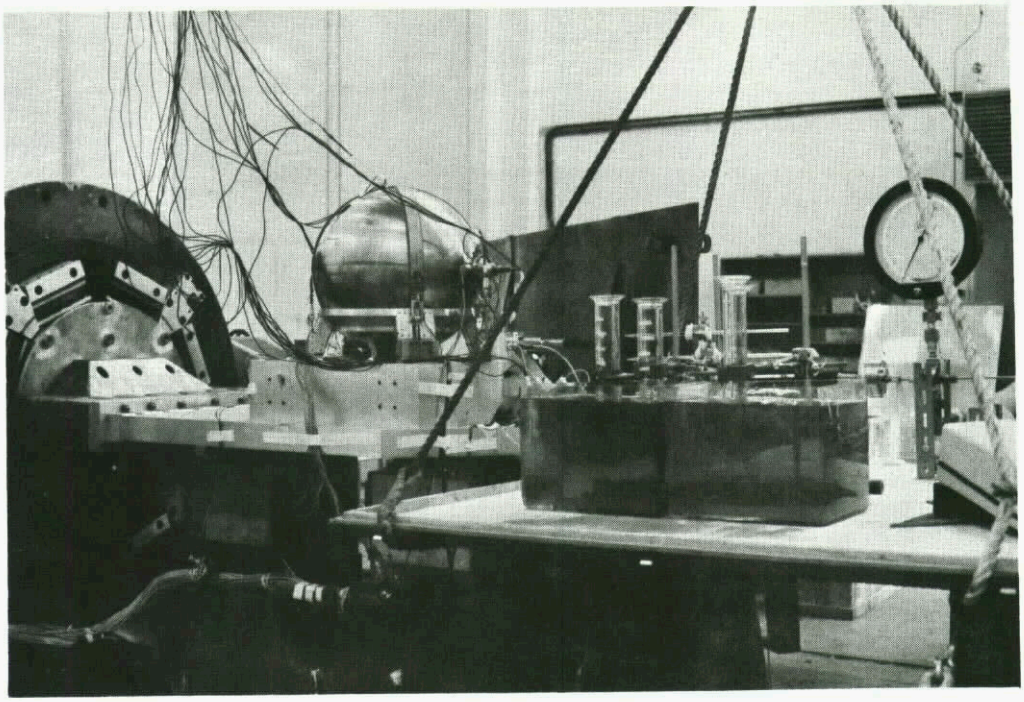

Fig.8 TD-propulsion system under high pressure vibration test (150 bar, gas) on the slip table, axis OX. With continuous leakage monitoring

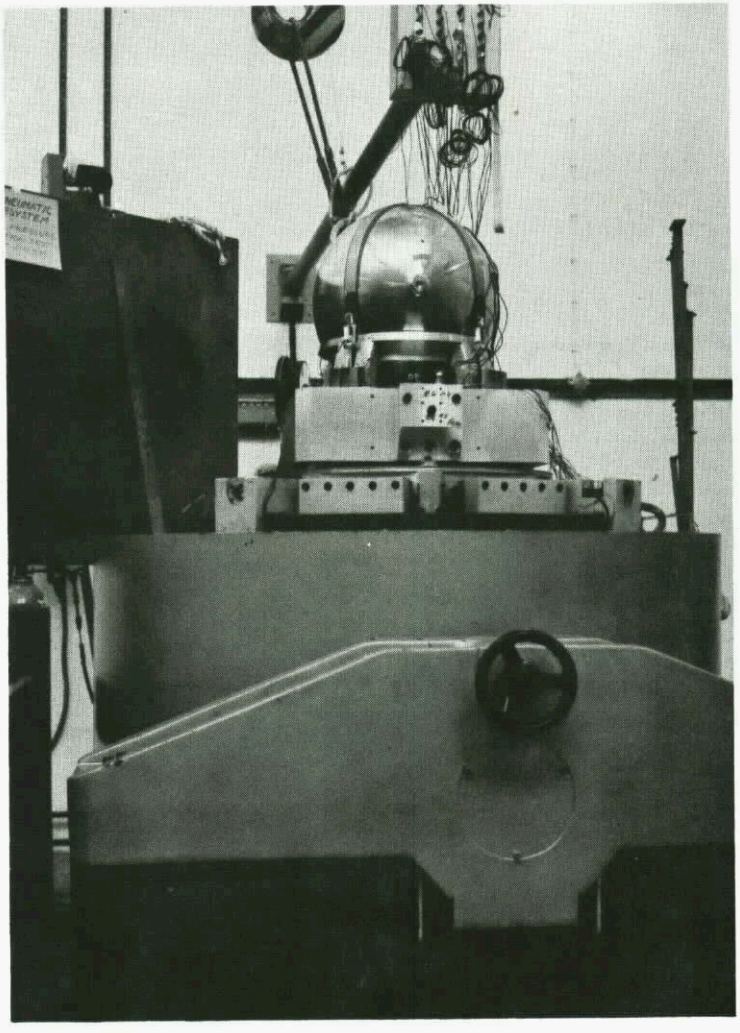

Fig.8(a) TD-propulsion system on the 13to shaker for high pressure vibration test

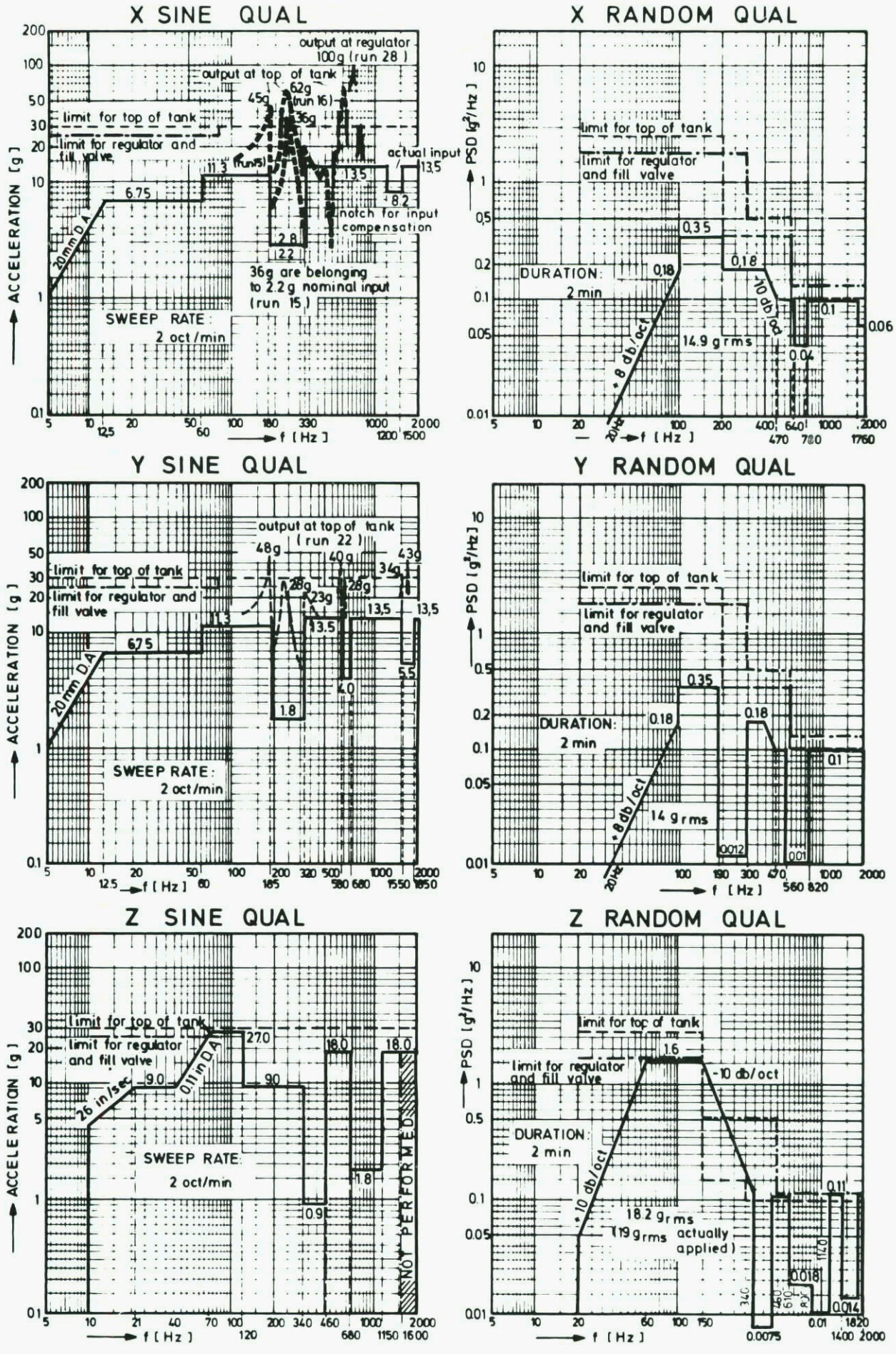

Fig.9 Summary of final qualification inputs

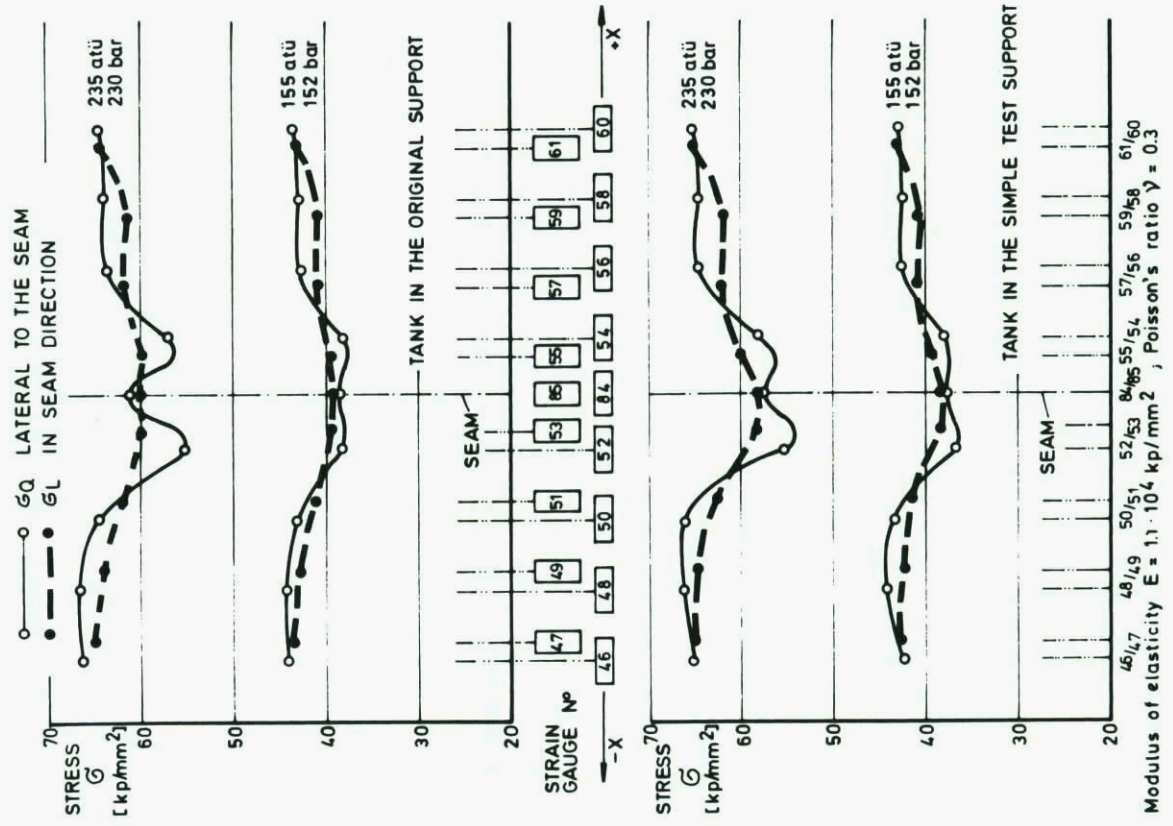

Fig.10 Stresses in a zone the welded seam (+Z – direction)

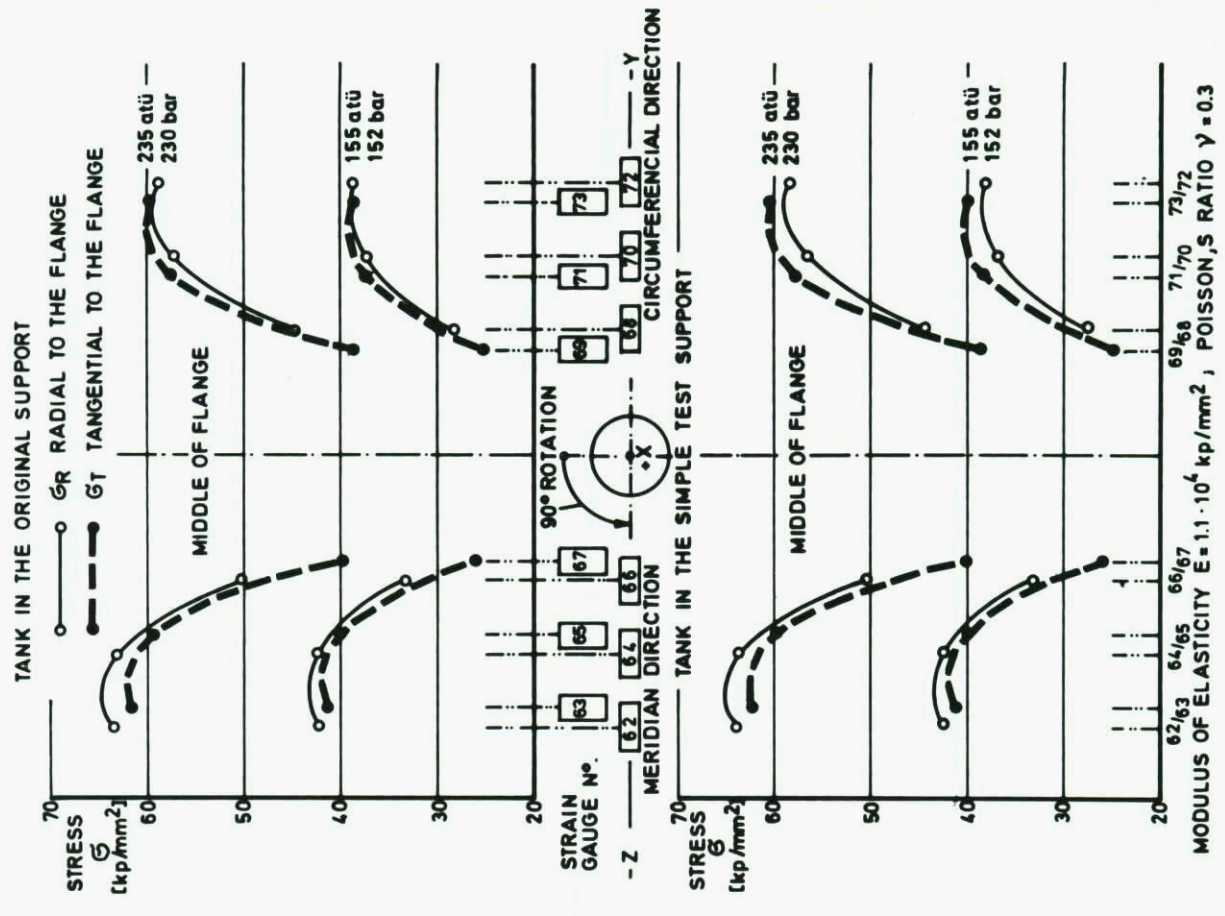

Fig.11 Stresses in the flange zone (tank connection)

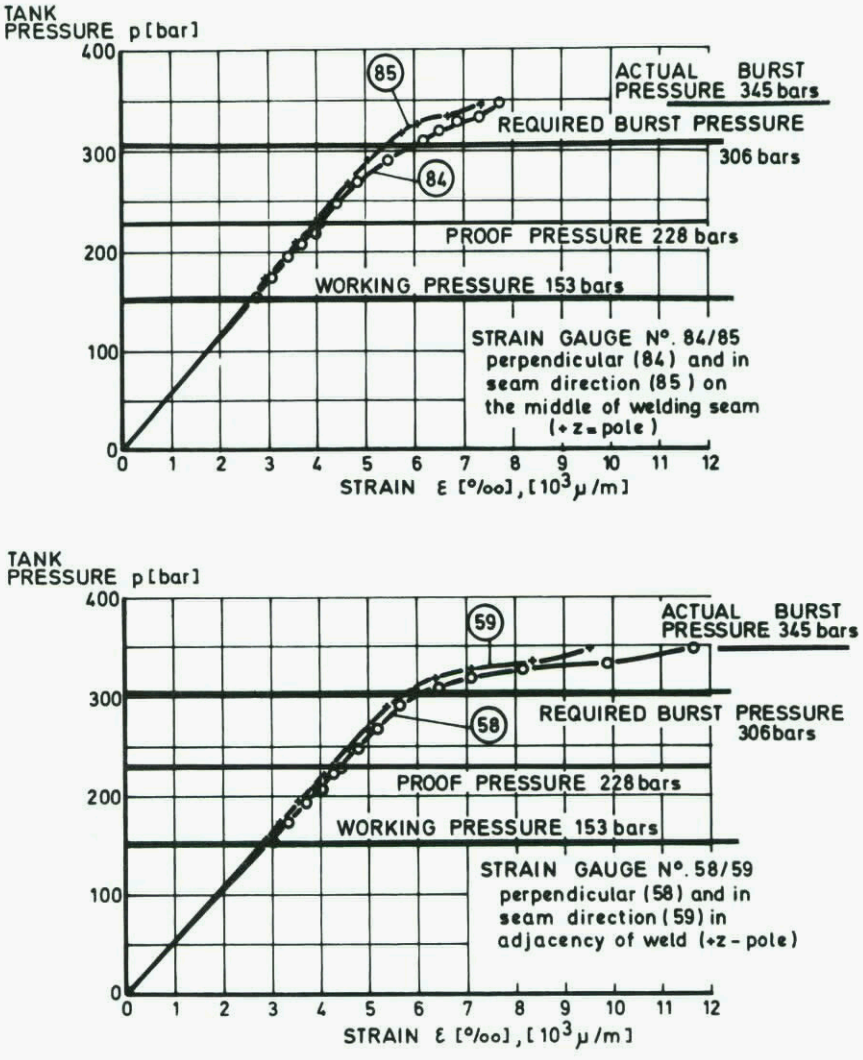

Fig. 12 Pressure/strain-diagrams

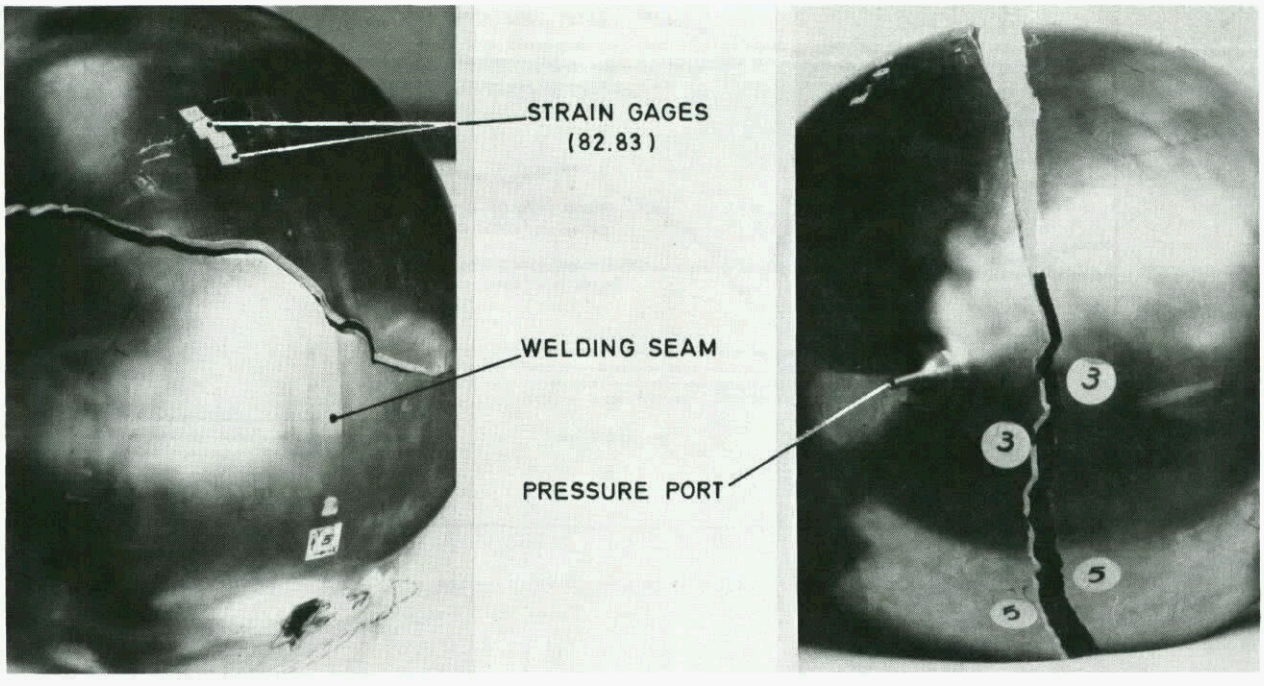

Fig. 13 TD-propulsion system tank No.4 after qualification burst test (345 bar)

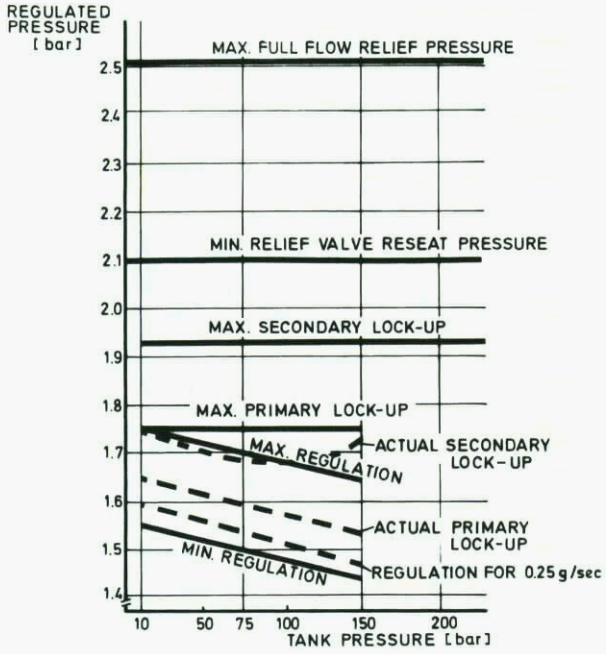

Fig.14 Static regulation characteristic, regulated pressure as a function of the tank pressure

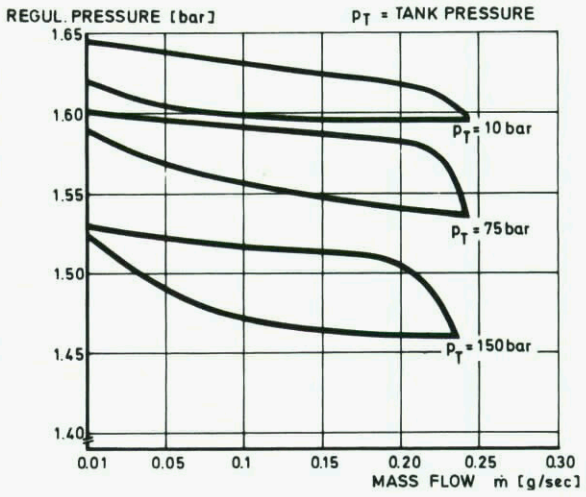

Fig.15 Regulation hysteresis

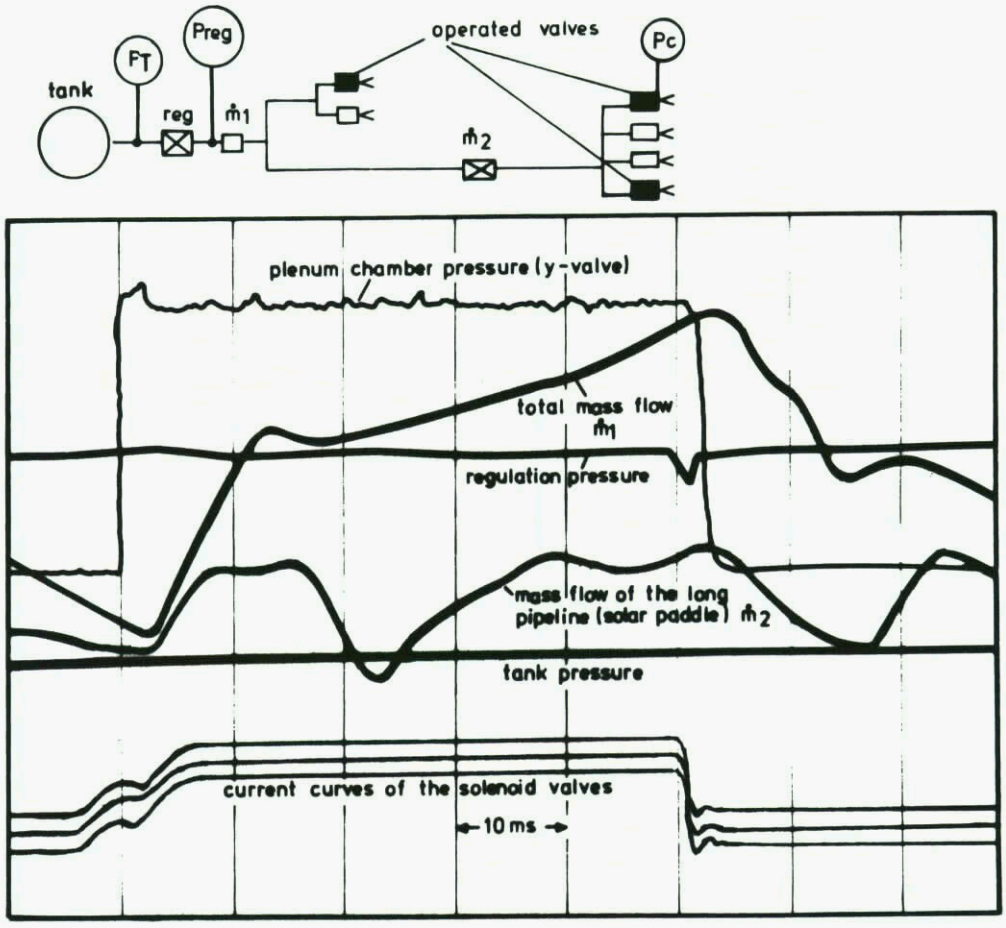

Fig.16 Resonance test and effect of the regulation on the nozzle chamber pressure

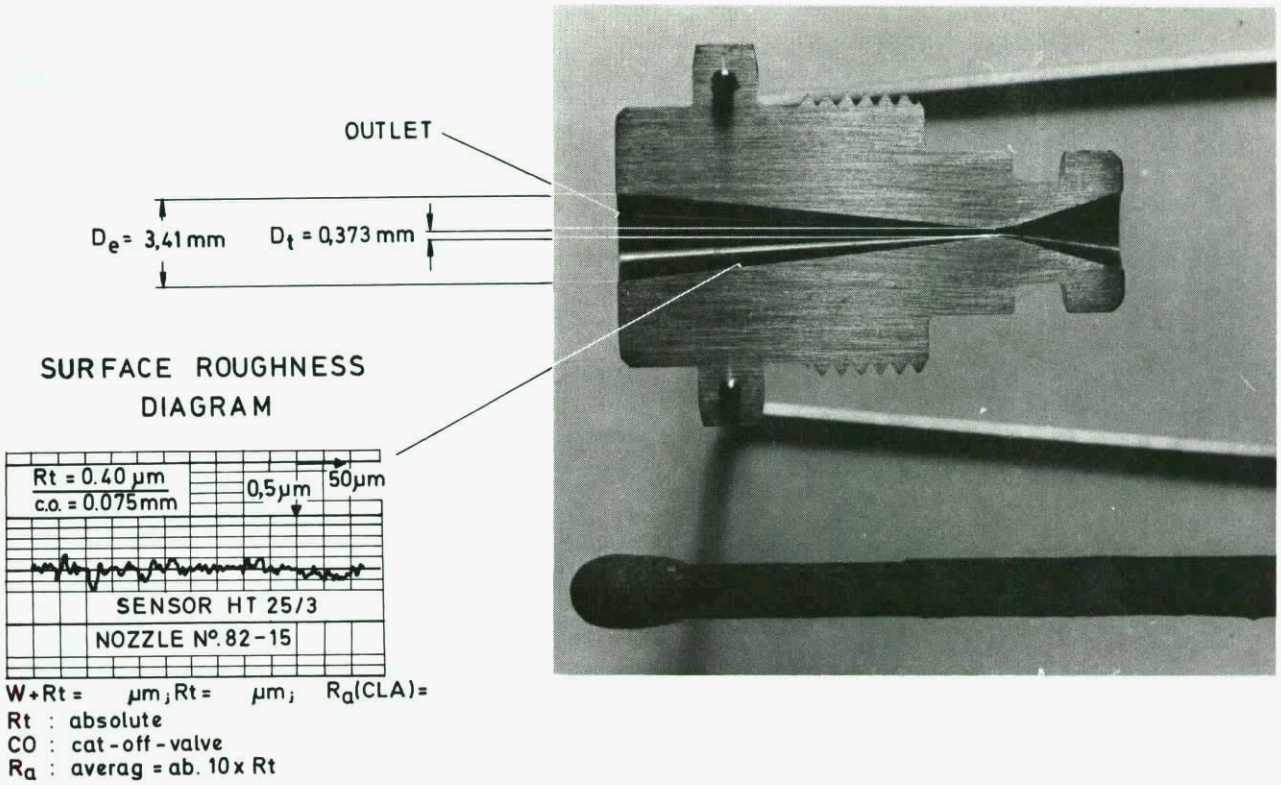

Fig.17 TD-nozzle and surface roughness diagram

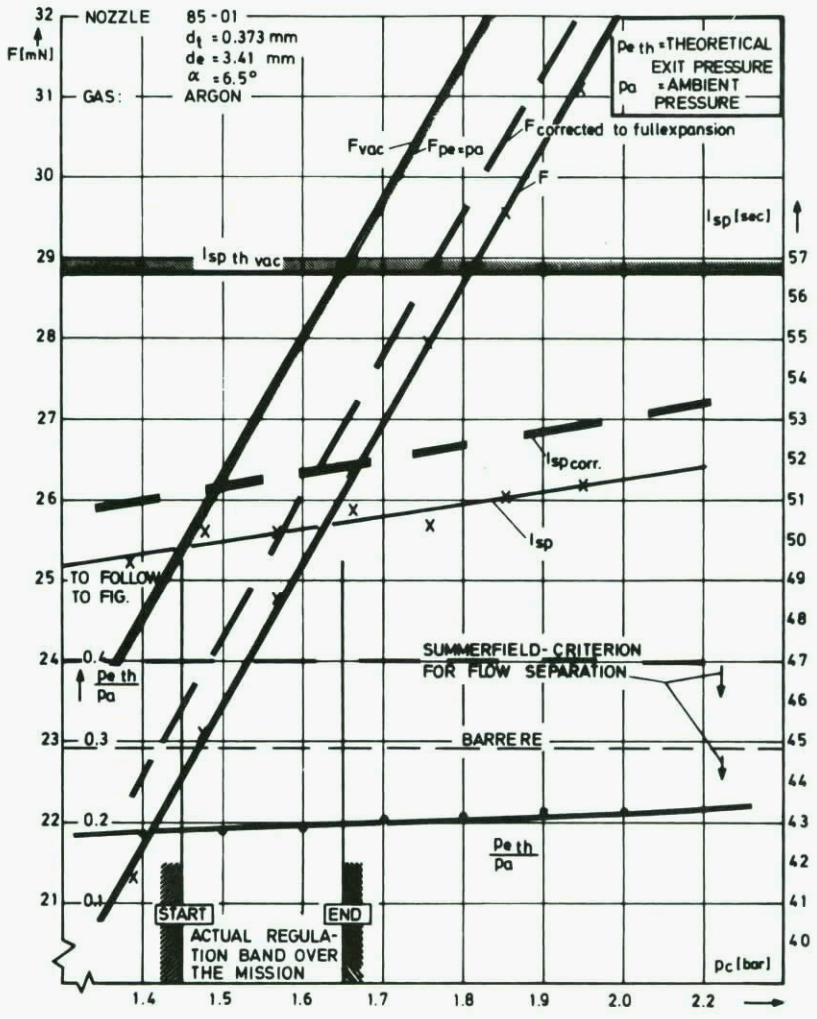

Fig.18 TD-nozzle thrust, spec. impulse and p_e/p_a versus chamber pressure

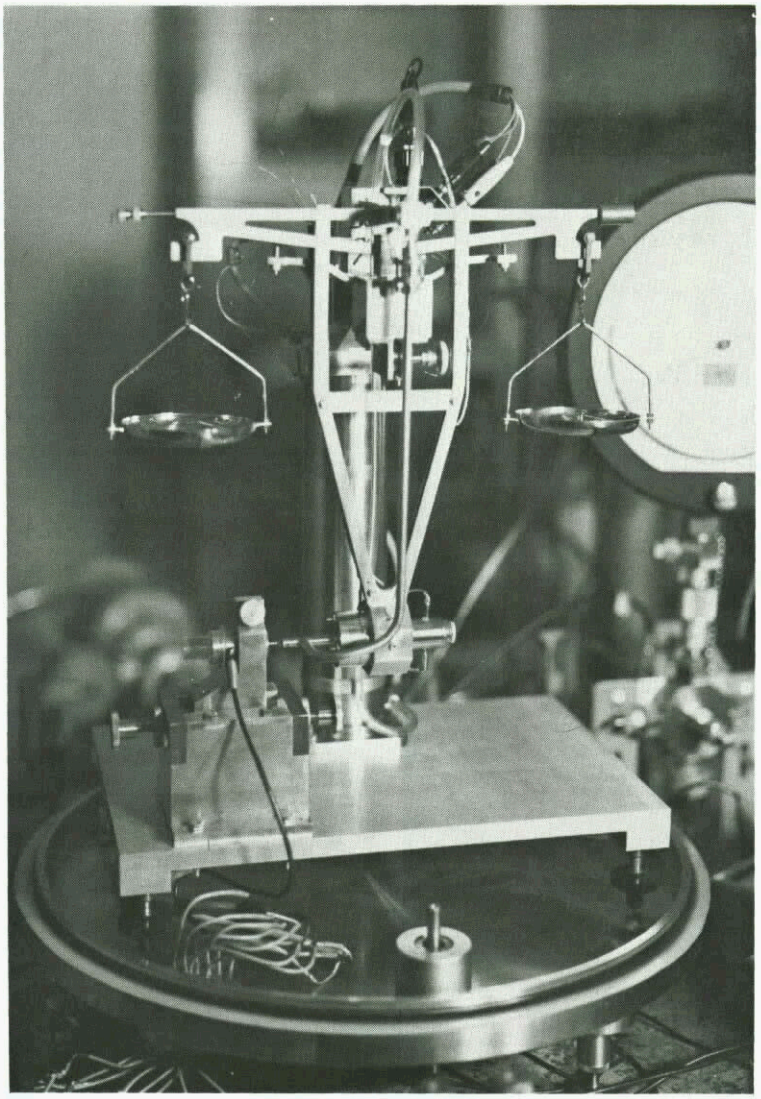

Fig.19 Low thrust measurement balance (10^{-3} N to 1N) without vacuum chamber

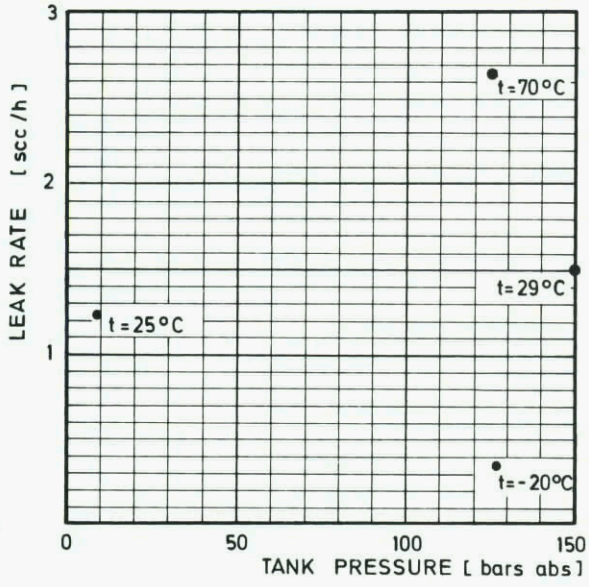

System leakage as a function of the high pressure

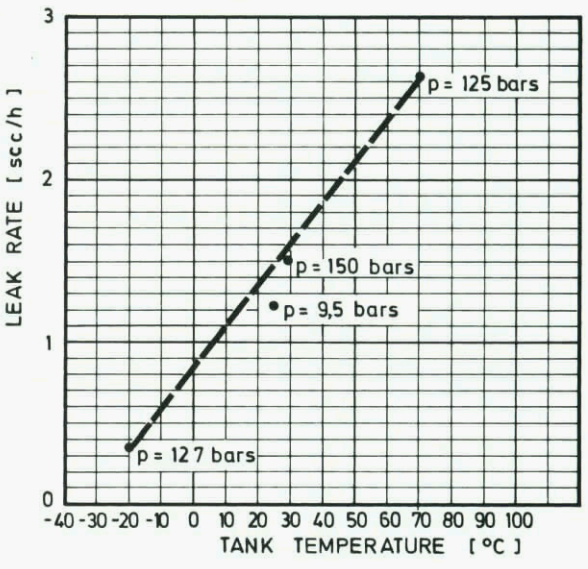

System leakage as a function of temperature

Figure 20

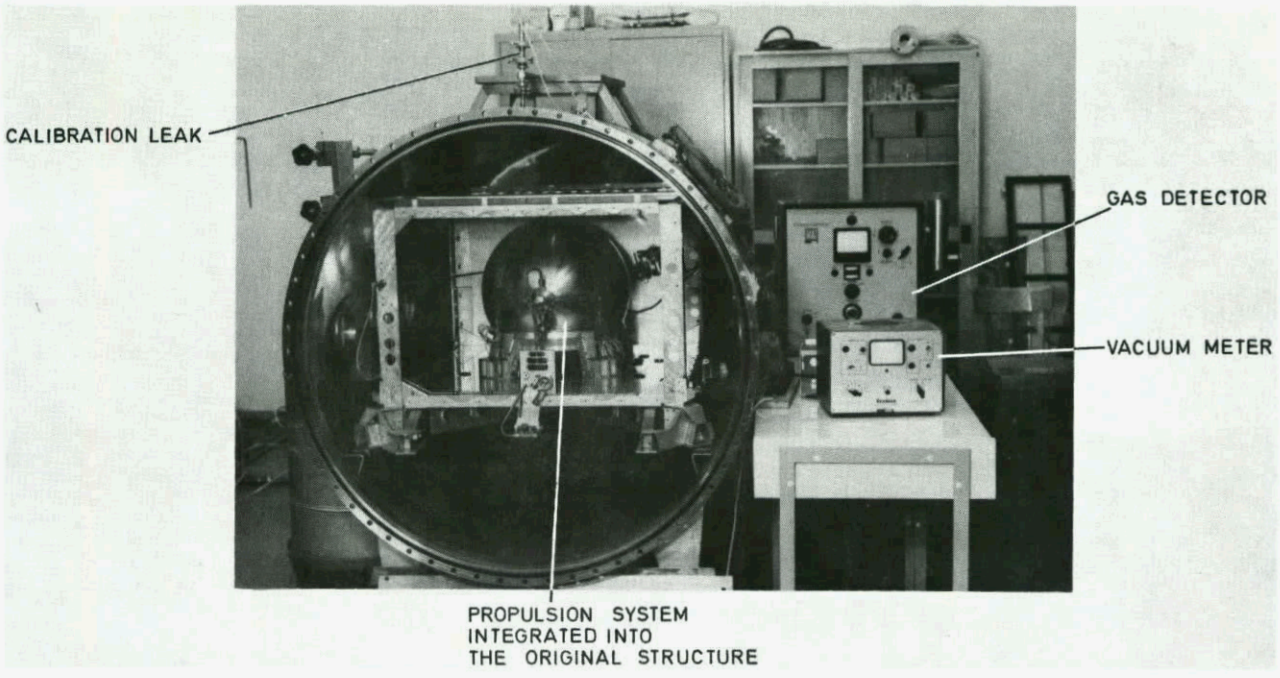

Fig.20(a) TD-propulsion system in a vacuum chamber for leakage measurement

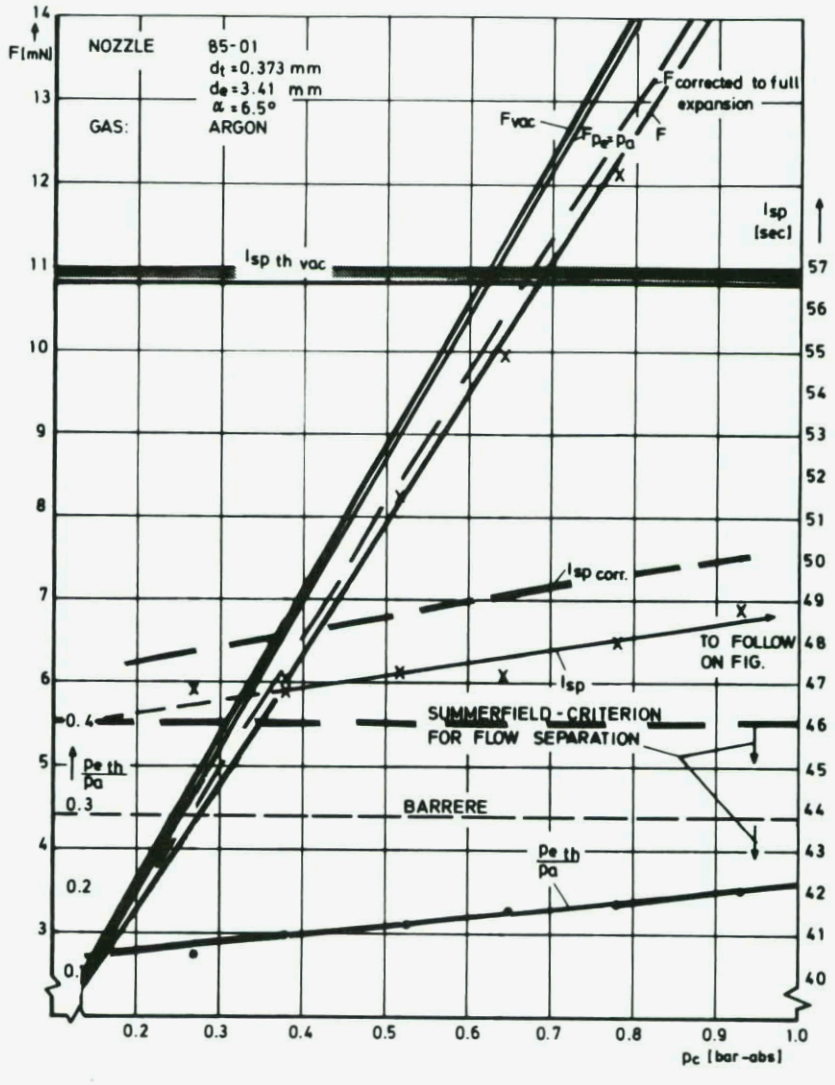

Fig.21 TD-nozzle thrust, spec. impulse and p_e/p_a versus chamber pressure

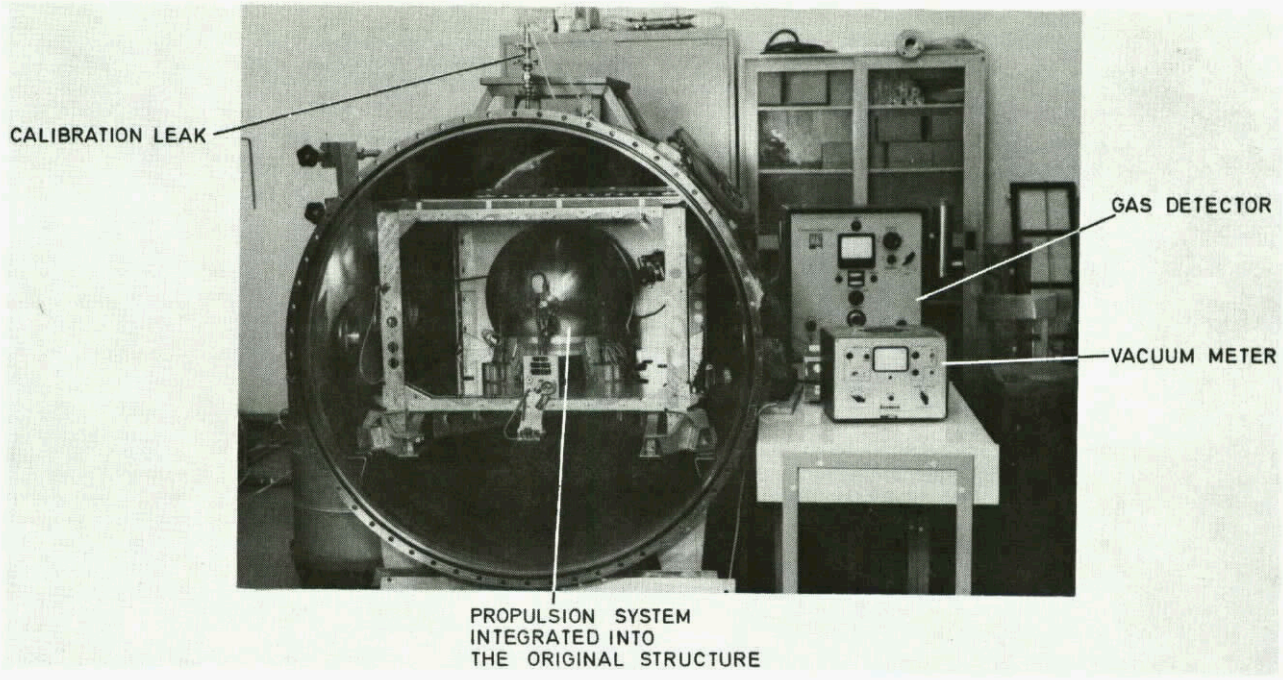

Fig.20(a) TD-propulsion system in a vacuum chamber for leakage measurement

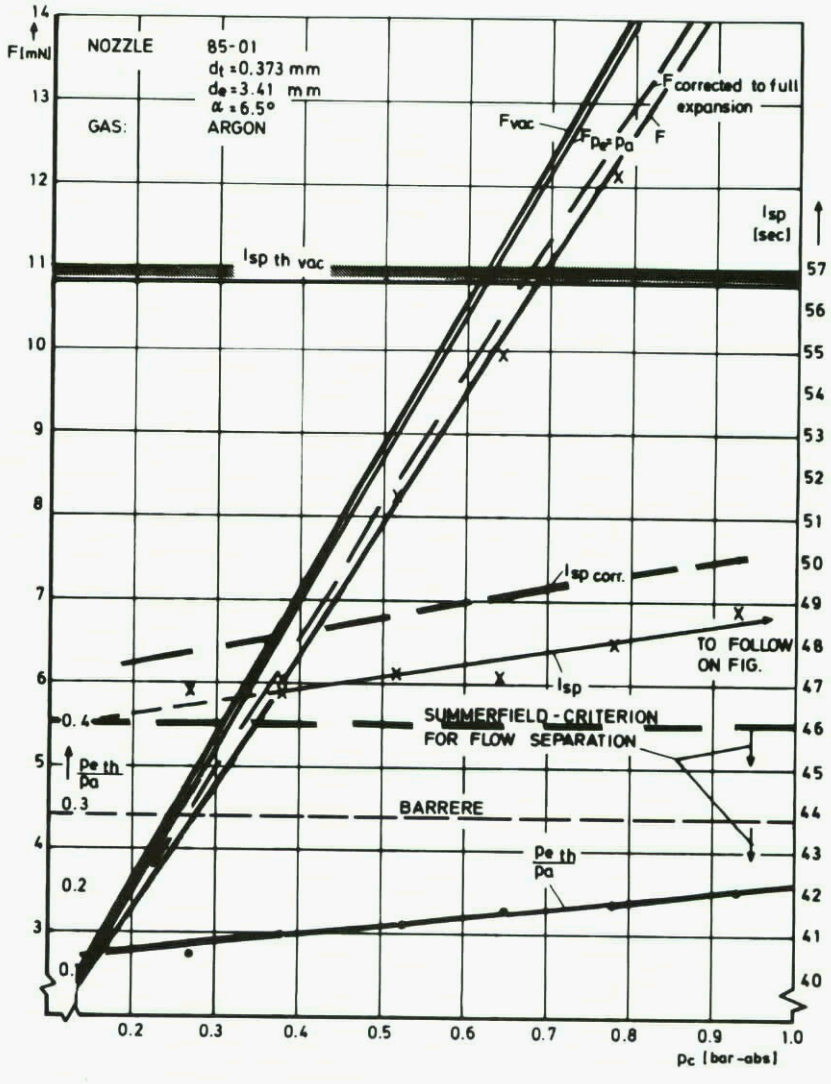

Fig.21 TD-nozzle thrust, spec. impulse and p_e/p_a versus chamber pressure

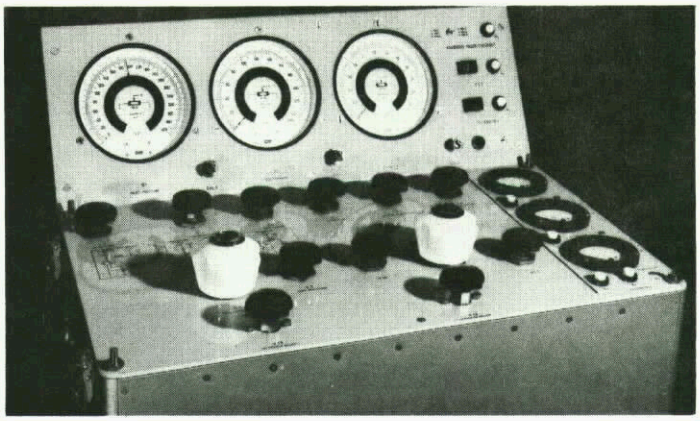

Fig.22 Fill and checkout system for the TD cold gas propulsion system

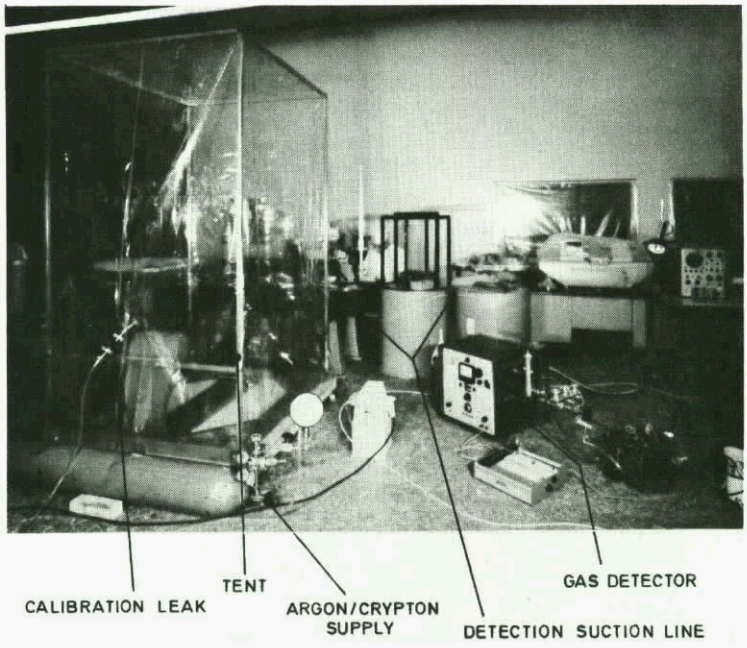

Fig.23 Leakage-checkout-system for the TD-satellite

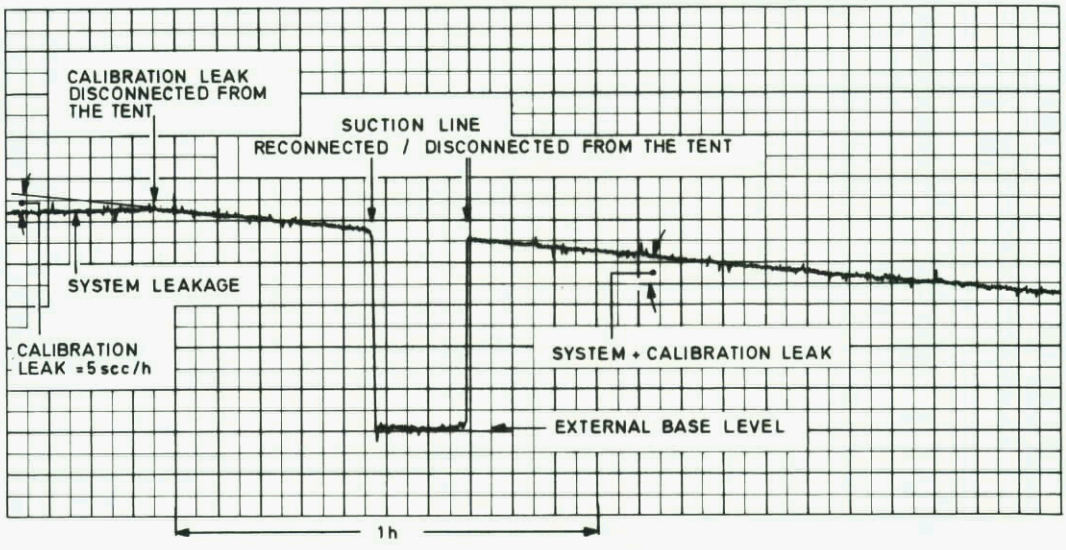

Fig.24 Krypton tracer gas leakage measurement

THE SIRIO ATTITUDE MEASUREMENT AND CONTROL SYSTEM

by

Dr. Ing. Alessandro Buratti
Compagnia Industriale Aerospaziale S.p.A.
Viale di Villa Grazioli, 23
00198 Roma
Italy

SUMMARY

The paper gives a description of the SIRIO attitude measurement and control sub-system components, their characteristics, their interconnection with other units, their mode of operation and how they are employed. Component test problems are discussed where appropriate - as in the case of the sensors and of the nutation damper. Emphasis is given to attitude measurement and an estimate of the accuracy which may be achieved both in the transfer and in the geostationary orbit is given.

1. INTRODUCTION

1.1. SIRIO MISSION

A summary is given in Table 1.

TABLE 1

SIRIO MISSION SUMMARY

Objectives:	Telecommunication Experiment: Atmospheric attenuation at 12÷18 GHz Cosmic Physics Experiment: Magnetic and Particles Fluxes
Final Orbit:	Geostationary, stationed at 15° West
Launch Site:	Cape Kennedy
Launch Vehicle:	Thor-Delta (6 boosters - type 603)
Parking Orbit:	Circular 200 km.high 28.5° Incl.
Transfer Orbit:	Elliptical 6,563 km. perigee 42,134 km. apogee
Year of Launch:	1973
Life:	2 years

1.2. SIRIO MAIN CHARACTERISTICS

These are summarized in Table 2.

TABLE 2

SIRIO MAIN CHARACTERISTICS

Weight (including Apogee Motor):	394 kg
Overall Dimensions:	
Diameter:	1,432 m
Height:	1,919 m
Stabilization:	spin
Spin speed	90 r.p.m.
Spin axis Inertia Moment I_s:	
Before A.M. firing and with A.P. tanks filled	62 kgm^2
After A.M. " " " " " "	57 "
After A.M. " " " " " empty	48 "
Inertia Ratio I_{s/I_t}:	
Before A.M. firing and A.P. tanks filled	1,13
After A.M. " " " " "	1,25
After A.M. " " " " empty	1,17
Propulsion:	
Apogee Motor:	Titanium Case; Solid Propellant
Auxil. Prop.:	Hydrazine Mono-Prop.
Attitude Measurement:	Earth & Sun References
Solar Array Power:	100 W (at end of life at solstice)
Battery Capacity:	2 x 3,5 Ah
Data Links:	
Telemetry:	VHF & SHF
Command:	VHF
Tracking:	VHF (R&RR)

Fig. 1 is a view of the complete satellite.

FIG.1 - SIRIO GENERAL VIEW

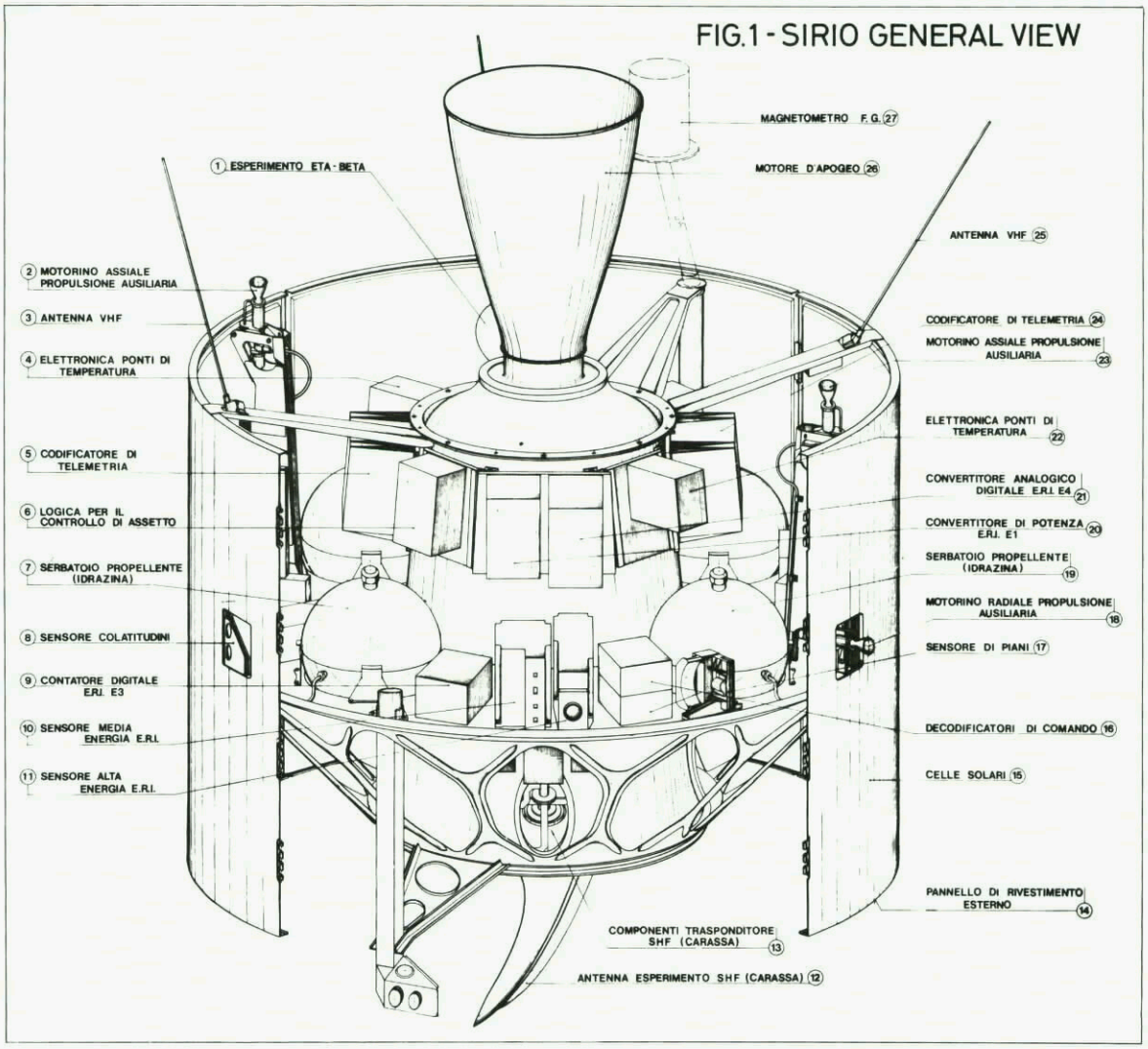

FIG. 2 - ACS LAY-OUT

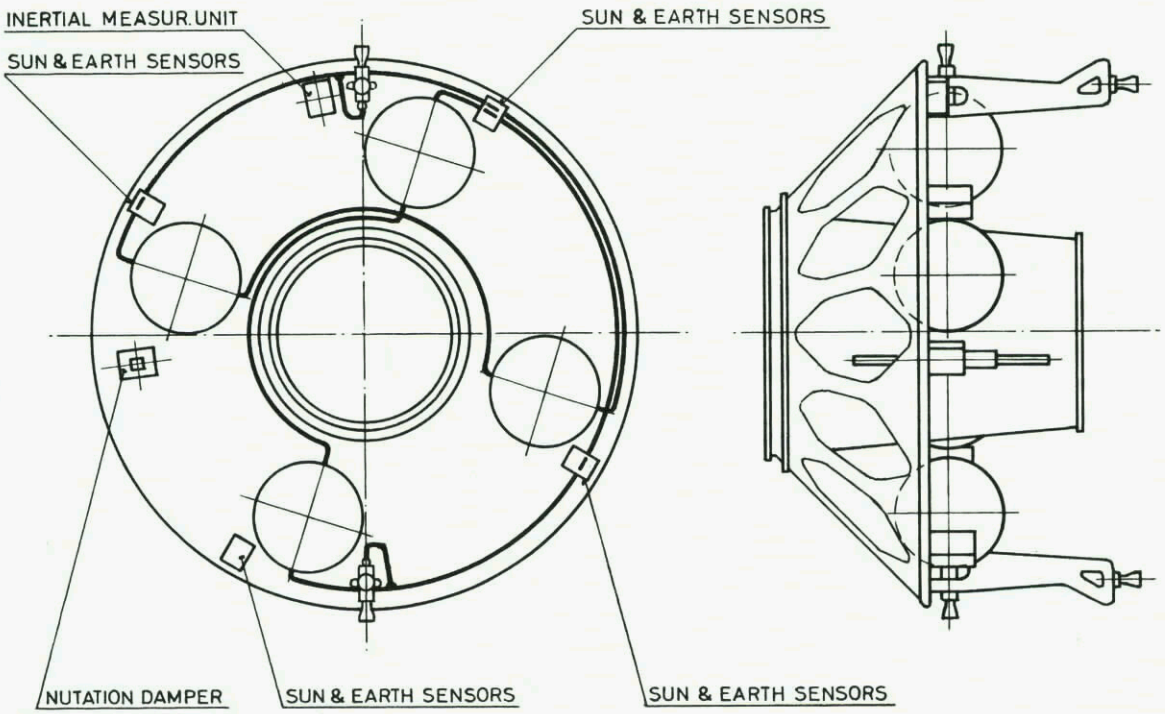

1.3. SIRIO ATTITUDE MEASUREMENT & CONTROL SYSTEM COMPONENTS

These are listed in Table 3.

TABLE 3

SIRIO ATTITUDE MEASUREMENT AND CONTROL SYSTEM COMPONENTS

Sensors:

No. 2 Colatitude Sensors, each consisting of:
- No. 1 NF IR sensor
- No. 1 "V" Sun sensor

No. 2 Plane Sensors, each consisting of:
- No. 1 WF IR sensor
- No. 1 Plane field Sun sensor

Auxiliary Propulsion:

No. 2 fully independent sub-systems, each consisting of:
- No. 2 propellant tanks connected together
- No. 1 radial jet motor, complete with electromagnetic valve
- No. 1 axial jet motor, complete with electromagnetic valve
- 15 kg Hydrazine
- Piping

Attitude Control Logic:

No. 1 unit, fully redundant

Nutation Damper with Caging Device:

No. 1 unit

Inertial Measurement Unit:

No. 1 unit

Fig. 2 shows the geometrical lay-out of the various units on the satellite.

2. ATTITUDE MEASUREMENT

2.1. GENERAL

The sensors output data, properly handled, provide the knowledge of the following "primary" angles:

β = spin axis/satellite position-centre of earth

ϑ_s = spin axis/satellite position - centre of sun

α = angle swept by a satellite meridian plane rotating with the satellite when passing from the earth centre to the sun centre.

The satellite position, with respect to a reference frame, is known through the tracking data.
In principle, with the exception of certain singular conditions and apart from ambiguities which can generally be solved, attitude may be reconstructed from the

knowledge of:

a) any two of the above listed angles at any one satellite position

b) any one of the above listed angles at any two satellite positions, provided the satellite attitude has not changed by an unknown amount, when going from one position to the other.

The error on attitude determination is a complicated function of the following parameters:

a. Sensors errors, which in turn depend generally also on the primary angles values and earth distance as follows:

   1. The IR sensors are affected by errors which vary with the value of β and, to a smaller extend, with earth distance.

   2. The Sun sensors are affected by errors which vary with the value of ϑ .

   3. The determination of α , which depends on both sun and earth sensors is affected by the values of β , ϑ and by earth distance.

b. Sensitivities of primary angle errors with respect to sensor errors, which are strongly dependent on the primary angles values.

c. Tracking errors, greater during the transfer orbit.

d. Sensitivities of errors of attitude angle components to primary angles errors, which are strongly dependent on the positions of the satellite, sun and earth, and satellite attitude.

e. Primary angles selection, which may be dictated by unavailability of other angles due to limitations in sensors field of view, earth sensor blanking by the sun radiation, sun sensor being affected by spurious signals due to earth albedo.

2.2. SENSORS DESCRIPTION

In order to measure the above mentioned primary angles two fully redundant sets of sensors are employed. Each set consists of the following units:

a) one colatitude sensor (fig. 3) which contains a Narrow Field Infrared Earth Sensor (NFIR) and a V-beam Sun Sensor (VSS)

b) one plane sensor (fig. 4) which contains a Wide Field Infrared Earth Sensor (WFIR) and a Plane Field Sun Sensor (PSS).

The NFIR consists of two telescopes in a meridian satellite plane, tilted by 6° in either direction with respect to the satellite equatorial plane. Each telescope contains a germanium lens which focuses the incoming radiation on a bolometer. Between the lens and the bolometer, an optical filter passes only the 14-16 μ radiation, corresponding to the CO_2 absorption band. The bolometer signal is treated in order to obtain pulses whenever the optical axis of the telescope crosses the earth horizon. These pulses determine an output rectangular wave lasting from a space-earth horizon crossing to an earth-space horizon crossing. The β angle is a function of the ratio between the time length of the output rectangular wave and spin period. Fig. 5 is a simplified block diagram of this sensor and fig. 6 shows the signal shapes at various circuit points.

The WFIR consists of a mirror and a bolometer. The arrangement is such that radiation falling within a 1°.5 azimuth angle and within a $\pm$60° elevation angle, with respect to the satellite, is conveyed onto the bolometer. Also in this case a 14-16 μ filter is provided. The bolometer signal is treated in order to provide output pulses whenever the earth crosses the field of view given above. Processing of time delays between two pulses enables the determination of β and processing of the time intervals between these pulses and pulses generated by the PSS allows determinating the α angle. The block diagram of this sensor is similar to half the one of the NFIR sensor.

The PSS consists of a set of photocells placed in such a manner as to be illuminated by the sun whenever the sun is contained in a given half-plane. The plane con-

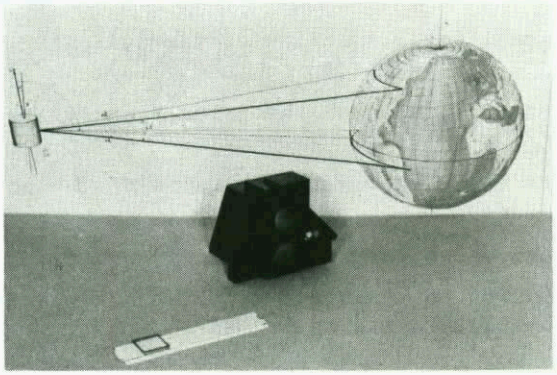

FIG. 3 - COLATITUDE SENSOR

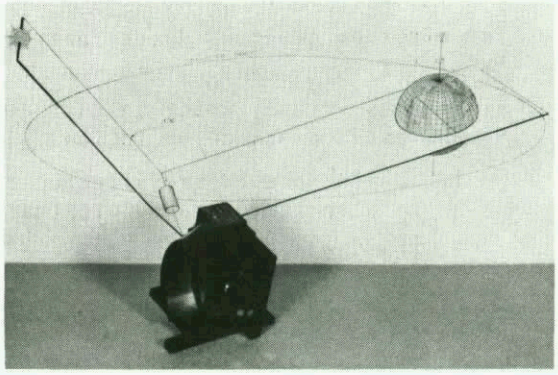

FIG. 4 - PLANE SENSOR

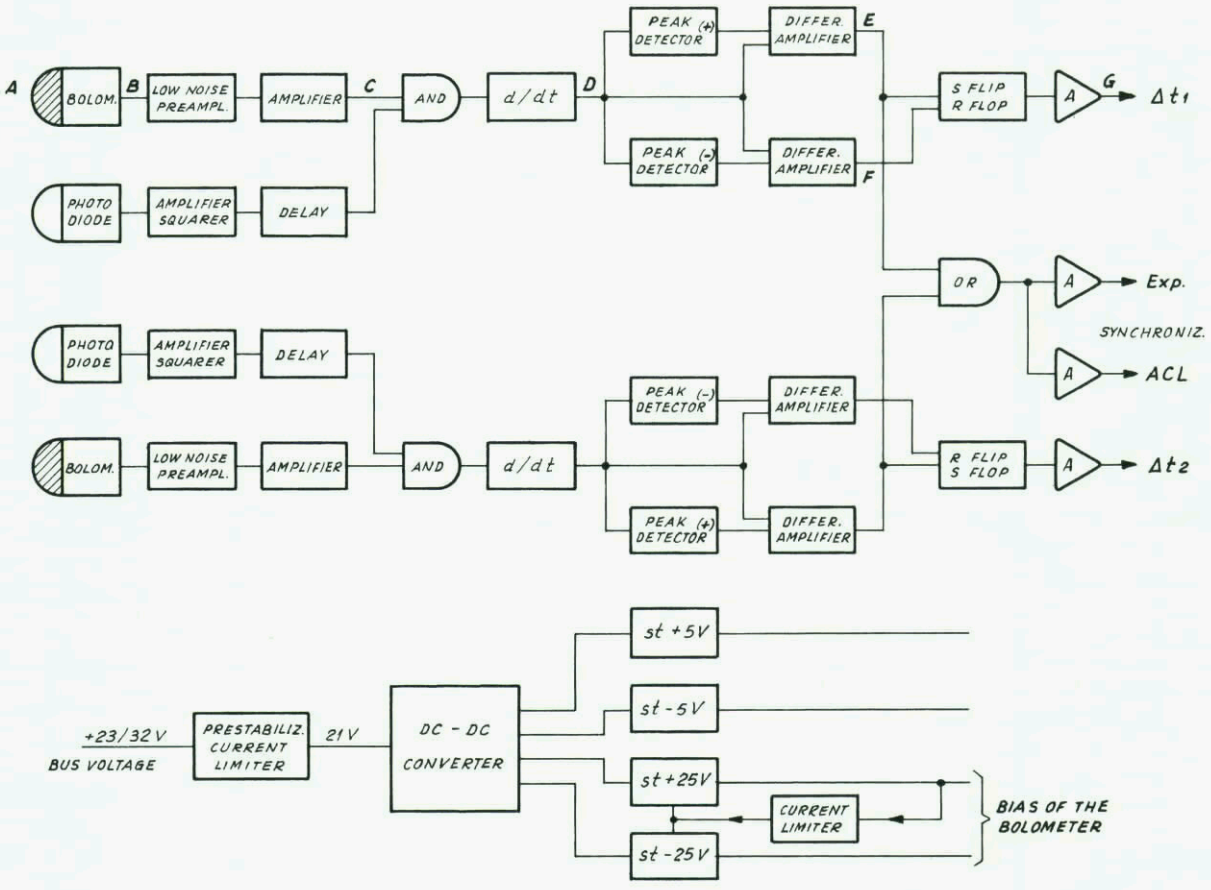

FIG. 5 - NFIR SENSOR BLOCK DIAGRAM

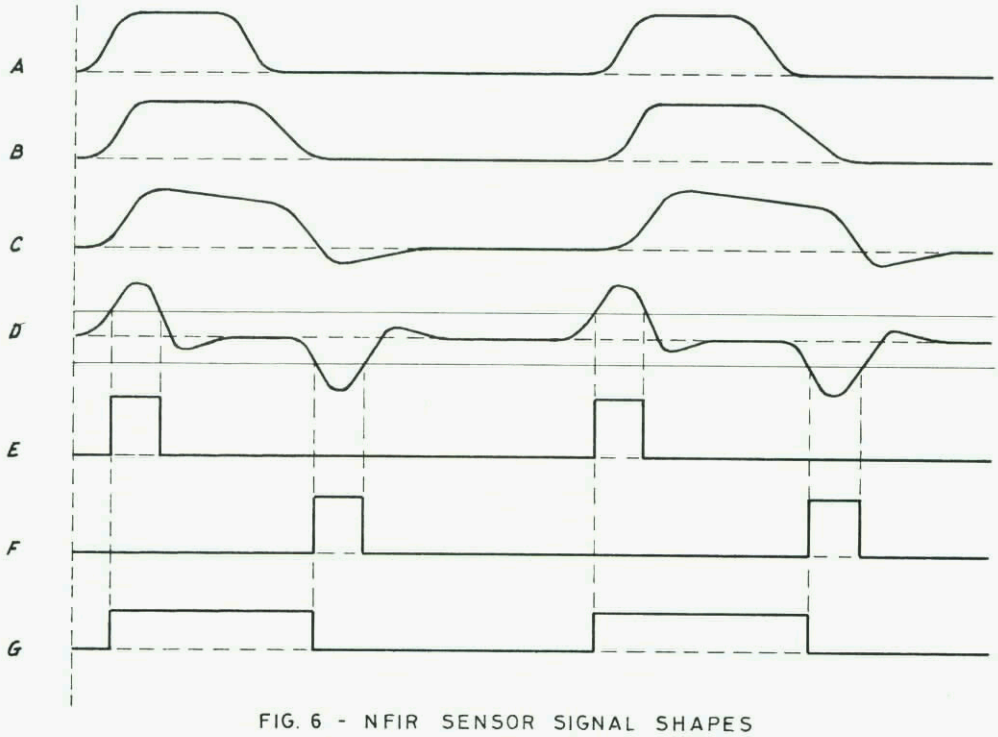

FIG. 6 - NFIR SENSOR SIGNAL SHAPES

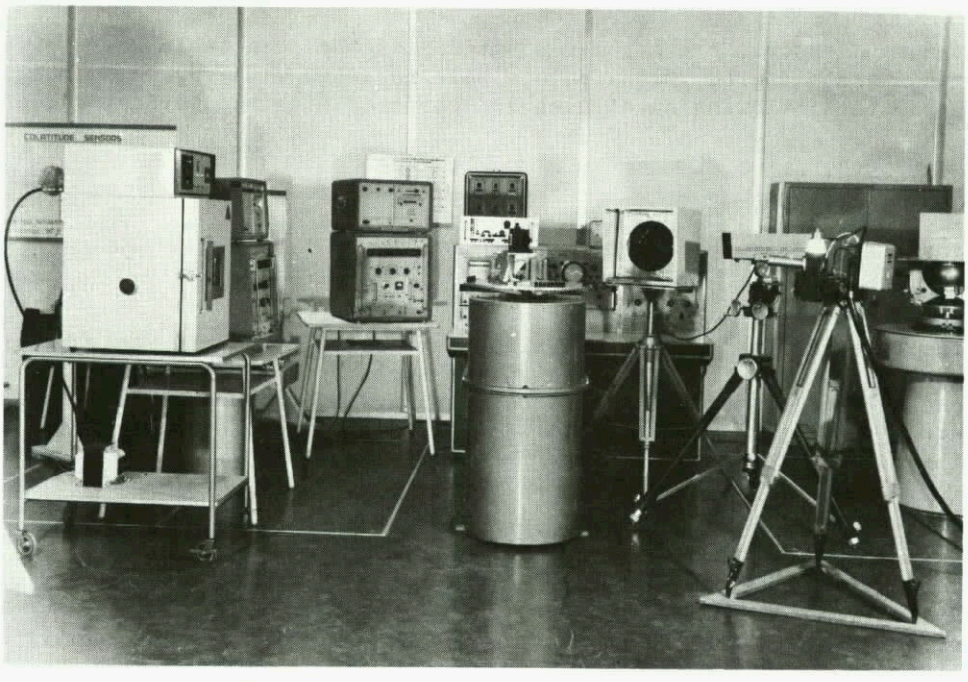

FIG. 7 - SENSOR TEST EQUIPMENT

tains the spin axis. The field of view of this sensor is $\pm 80°$ with respect to the equatorial plane. For each sun crossing a pulse is generated by the cells and associated electronics.

The VSS consists of two sets of photocells each set determining a half-plane as explained above. One plane contains the spin axis, as for the PSS, and the second plane forms an angle of 45° with the previous plane and the intersection of the two planes is perpendicular to the spin axis. Pulses are generated each time either plane crosses the sun. The associated electronics produces an output rectangular wave lasting from when the sun crosses the first plane to when the sun crosses the second one. The ϑ angle is a function of the ratio between the time length of the said rectangular wave and spin period.

Spin period is the time elapsed between two successive pulses of the PSS.

2.3. SENSOR TESTS

Extensive tests have been performed on a prototype set of sensors.
Apart from tests intended to verify optical, electrical and mechanical characteristics and sturdiness, tests were carried out to investigate overall performances, i.e. phase and - where appropriate - duration of output signals.
The basic equipment employed for these tests, was:

- a spin rate controlled rotating table, on which the sensor under test was placed,
- an earth simulator, consisting of a temperature controlled black pan, 30 cm diameter, displaceable along a vertical bar,
- a sun simulator, consisting of a Xenon arc lamp,
- a laser light source,
- 2 photo transistors,
- 2 recording time counters.

Fig. 7 shows the set up.

For the sun sensors, the angular positions of the spin table where pulses were delivered, were measured. Measurements were repeated with various combinations of values of the following quantities and compared with theoretical values:

a) Spin speed,

b) Sun colatitude,

c) Supply line disturbances,

d) Temperature.

For the IR earth sensors, the angular positions of the spin table, where pulses were delivered, together with the angles swept between two successive pulses (corresponding to two successive horizon crossings of the sensor optical axis) were measured. Measurements were repeated with various combinations of the following quantities, and compared with theoretical values:

a) Spin speed,

b) Earth colatitude,

c) Earth radiation constant level,

d) Earth radiation level varying from one extreme of the earth simulator to the other (only for the WFIR),

e) Earth distance,

f) Supply line disturbances,

g) Temperature.

Further tests were carried out in order to check the blanking out of the earth sensor outputs due to the sun falling in the field of view of the earth sensor. Complete simulation of in-orbit conditions is impossible even with the best equipment, and therefore the test results have to be reviewed critically and cor-

rected, where necessary, by computing the effects of the differences between test and in-orbit conditions. This fact requires considerable thought in planning the tests. Moreover, it leaves some doubt on the ultimate calibration accuracy. Here are some examples of the difficulties in simulating in-orbit conditions:

a) When in orbit, the IR sensors see alternatively deep space, having an equivalent temperature of a few degrees Kelvin and earth, which has a temperature of about 300°K and a certain spectrum. On the ground is practically impossible to simulate a back-ground of a few degrees K and to have a source with the same spectrum as the earth.
What we did was to take a black background at ambient temperature and maintain a black body at such a temperature that the difference in radiated power density between the two in the 14-16 μ band was equal to that of the earth, in the same band.
We placed the black body at such a distance from the sensor that it was seen by the same angle the earth is seen in orbit.
Under the above described conditions, the earth simulator (black body) edges are not focussed onto the bolometer, since the optical system is designed to focus points at infinite distance. This fact was theoretically accounted for, when handling the results.
The back-ground and the earth simulator were not and could not be perfect black bodies and their emissivity in the 14-16 μ band had to be measured. This measurement was obviously affected by an error. Moreover, it was impossible to achieve a true step in temperature at the simulator edge.
In order to gain confidence that these and other discrepancies were negligible or were correctly accounted for, tests were repeated by varying the conditions and comparing the results.

b) The visible spectrum of the sun may be only approximated by means of Xenon arc lamps and the level of infrared radiation - which affects the IR sensors - is impossible to achieve. These limitations require extrapolations and indirect measuring methods.

2.4. SENSORS TEST RESULTS

The results shown in table 4 are to be regarded as very preliminary, since:

a) The tests were conducted on prototypes which may be further improved.

b) These were the first overall tests to be carried out by us together with the manufacturers and the test procedures were determined as the tests were going on.

c) The test equipment was somewhat unsophisticated and for some items it was modified during the tests. More than often we found that poor results depended on inaccuracies or faults in the instrumentation rather than in the sensors.

The errors shown in table 4 may be regarded as the sum of the errors of the sensors and of the instrumentation used. It is thus possible to state that the sensor errors are not more than those shown in the table. The values shown are those arising from the worst combination of error causes. A considerable part of the errors is systematically dependent on known parameters, e.g. on spin speed.

Since the satellite spin speed may be measured very accurately and it varies very slowly in orbit, it appears that a large part of the error may be corrected by calibration. Noise errors may be made negligible by filtering on the ground.

TABLE 4

SENSOR ERRORS (degrees)

	Swept angle	Crossing phase
NFIR		
Noise (3 σ)	$\pm$.1	$\pm$.06
Other	$\pm$.2	$\pm$.6
WFIR		
Noise (3 σ)	$\pm$.9	$\pm$.6
Other	$\pm$.7	$\pm$1.0
PSS	-	$\pm$.1
VSS	$\pm$.2	$\pm$.1

2.5. ATTITUDE MEASUREMENT IN THE TRANSFER ORBIT

Table 4 shows that the NFIR and the sun sensors are the most accurate. Remembering what was stated in para. 2.1., it would appear that using either the measure of β, derived from the NFIR sensor or ϑ, derived from the VSS, in two different satellite positions or both these angles in one satellite position, attitude could be well determined. Unfortunately none of these methods can be used, since:

a) Owing to the limited field of view of the NFIR, the satellite positions where the measurements can be done are not very far apart.

b) Owing to the fact that the attitude measurement must be done in a matter of hours at most, the satellite positions are not sufficiently far apart with respect to the sun distance in order to use only the knowledge of ϑ.

c) The geometry of the system leads to an extremely high sensitivity of the attitude declination component to primary angles β and ϑ in the satellite position where the NFIR is within the earth view, i.e. near apogee.
It was thus tought necessary to introduce also the α angle, which is measured by the WFIR in conjunction with the PSS.
A computer program utilizing the information of all sensors in any one satellite position was set up. In order to investigate the reconstructed attitude accuracy which could be obtained once certain sensor errors were given, a second program was written, incorporating the first one. The result was that within the thermal launch window, and after assuming errors of the order of those listed in table 4, the attitude error would be within $\pm 1°$.
As soon as more definite information on sensor errors is acquired, the second program will be run again and - if necessary - a new program for attitude reconstruction will be studied. This would combine measurements taken in several satellite positions.

2.6. ATTITUDE MEASUREMENT IN THE OPERATIONAL PHASE

When the satellite is operational, its spin axis is perpendicular to its orbit plane and the NFIR sensors are continuously viewing the earth.
By measuring the earth colatitude in two orbital positions sufficiently far apart, attitude may be reconstructed with an accuracy of the order of $\pm .2°$, with practically no computation. The above mentioned accuracy is much better than that required by the SIRIO mission.
However, in view of other possible missions, a method for compensating sensor calibration and sensor misalignment errors is under study.

3. ATTITUDE CONTROL

3.1. GENERAL

During the mission, attitude manoeuvres are required:

1) before apogee motor firing, in order to reach the correct apogee velocity increase direction, generally different from the perigee velocity increase direction;
2) during acquisition of the final orbit, station and attitude;
3) during operation, when sun pressure and cross-coupling with station keeping operations impose disturbing torques on the satellite.

The required attitude changes are obtained by imposing torque impulses onto the satellite. The torque impulses are the consequence of firing the auxiliary propulsion (AP) axial jets for a quarter of the spin period. The large attitude variations are achieved by firing a train of impulses. The ratio between the torque impulses and the satellite angular momentum determines the control granularity. Under nominal conditions, this is of the order of .2°. The SIRIO attitude control may be described as a single loop, manual control system. The controlled variable (i.e. attitude) is measured by the on-board sensors, the outputs of which are telemetered to the ground and handled by a computer, together with the desired value. The computer informs the operator on the actual error and on the control action to be followed. The operator will then close the loop, by sending appropriate commands through the telecommand link to the satellite attitude control logic (ACL). The on-board sensors send signals also to the ACL; these are only for the purpose of synchronizing the correcting action pulses, in order that the torque impulse will act on the spacecraft in a known direction with respect to an inertial reference system. The ACL actuates the electro-magnetic valves controlling the propellant flow to the auxiliary propulsion jets.

3.2. AUXILIARY PROPULSION (AP)

This is used both for orbital and for attitude manoeuvres. For the latter only the axial jets are required, fired in a pulsed mode.
The nominal thrust of the jets is 20 N.
Thrust value however is a function of the pressure in the tanks, which is about 25 kg/sq.cm at the beginning of life and about 8 kg/sq.cm when the tanks are exhausted. The specific impulse of the system is 220 sec when the jets are firing continuously. In the pulsed mode, specific impulse is about 180 sec. The motors catalitic packs require warming up. The first jet fired after a period of inactivity has a thrust which is about 65% of the value of the thrust at steady state, which is reached after about ten pulses.

3.3. ATTITUDE CONTROL LOGIC (ACL)

Also this component is used both for orbital and for attitude manoeuvres. On the input side it is connected to the command decoders and the attitude sensors. On the output side to the electro-magnetic valve coils and the telemetry encoder.
The command signals may be grouped into two cathegories: pre-setting and firing.
By means of the pre-setting commands it is possible to select which of the two redundant halves of the ACL will operate, the jet or jets which are to fire, the synchronizing body (sun or earth), the quadrant(s) during which the jet(s) should

be on; by means of the firing commands it is possible to fire either a single pulse, a pulse train or continuously (only the axial jets).
The four earth and the four sun sensors send a pulse to the ACL each time they see the earth or sun respectively, i.e. each sensor sends a pulse per satellite revolution.
Since the sensors are placed on the satellite with their optical axes (or planes) at 90°, one from the other, an earth (and a sun) pulse is received by the ACL every satellite quarter turn.
By means of telemetry, it is possible to verify that the state of the ACL is the one required, before and during jet firing.
The ACL test jig is shown in fig. 8.

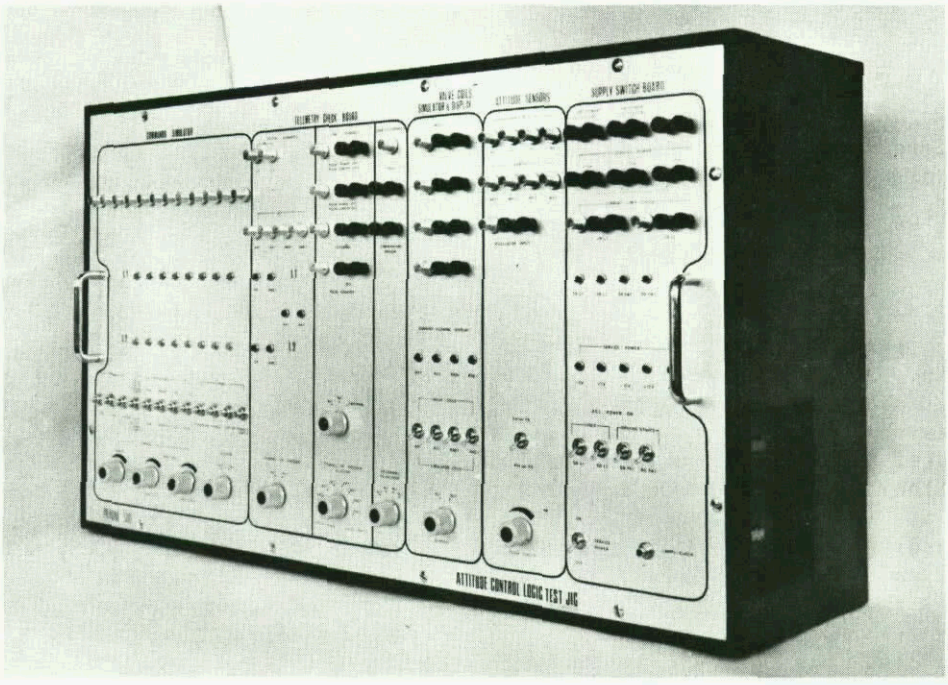

FIG. 8 - ACL TEST JIG

3.4. NUTATION DAMPER (NUD)

The nutation damper consists of a straight tube, partially filled with mercury, mounted parallel to the satellite spin axis. Various types of caging devices have been developed, mono-stable, bistable and passive. The choice between them has yet to be made, on the basis of reliability.
The NUD, a very simple device, poses considerable test problems, due to the presence of gravity on the ground.
Two types of tests have been carried out. Scaled model testing, by means of a pendulum, and real dimension prototype testing on a machine capable of impressing the true in-orbit motion to the NUD and of measuring its reaction forces.
The behaviour of the NUD is non linear. Pendulum tests showed that the oscillation amplitude, once the pendulum is moved from its equilibrium position and set free, decays first linearly with time, then almost exponentially and finally remains constant, when the nutation angle is of the order of .1°.
The non-linearity was confirmed by the tests on the real dimensions prototype, except for very small amplitudes, where the test machine was not sensitive enough anyway.
Tests were performed for various conditions corresponding to a range of satellite inertia ratios and spin speeds.
Testing becomes more and more difficult as inertia ratios approach one.
The time constant of the NUD-satellite combination, under nominal conditions and for nutation angles between .2° and a few degrees is less than five minutes.
Even by assuming as being negligible the NUD contribution, it is reasonable to forecast that nutation angles smaller than .1° will be damped out by the sloshing of the AP propellant in the tanks and by the mechanical hystheresis of the satellite structure.

3.5. INERTIAL MEASUREMENT UNIT (IMU)

It consists essentially of a force-balance accelerometer, to be mounted with its input axis parallel to the spin axis on the satellite main platform, and associated electronics.
The unit will give the following information:

a) Measure amplitude, frequency and shape of nutation angles.

b) Measure acceleration during perigee motor, apogee motor and AP axial jet firing.

c) Indicate the AP propellant contained in the tanks. Since the nutation period is a function of the satellite inertia ratio, and since this varies with the AP propellant quantity in the tanks, it appears that this may be derived from the nutation period. The fact that the fluid is free to slosh in the tanks must of course be accounted for and thus tests must be performed first on the ground in order to calibrate the AP propellant mass against nutation period and, possibly, shape. These tests have not yet been performed, but the presence of gravity will make them somewhat elaborate.

3.6. INTEGRATED TESTS

In order to check the attitude measurement and control system (ACS) design at an early stage of the program, an inertial model of the spacecraft was built. It consists of a structure, very similar to the final one, a number of operating units, amongst which those belonging to the ACS, and a number of mock-up units.

This model is presently being tested.
The most typical test equipment being used is a three axes machine, on which the satellite may be placed and spun up.
The satellite is then free to spin and nutate around a spherical oil bearing, the friction on the bearing being such that the system will spin for hours without being externally driven. Fig. 9 shows a satellite model on the machine.
The test equipment is completed with a mirror-type sun simulator, reflecting the sun on the sensors, a 1.6 m diameter temperature controlled pan simulating the earth and more conventional equipment such as TV cameras, tape recorders, displays, etc.
The test bay allows any attitude control manoeuvre to be performed and the study of the dynamics of the system.

4. ACKNOWLEDGEMENTS

The tests of the sub-systems were carried out in the manufacturers' labs, i.e. OFFICINE GALILEO for the sensors, OTO MELARA for the Auxiliary Propulsion, PIGNONE SUD for the Attitude Control Logic and for the Inertial Measurement Unit, and ELSAG for the Nutation Damper. The integrated tests are being carried out at CIA's Integration Centre.

The author whishes tothank Dr. Ing. G. Bressanin for reading the manuscript.

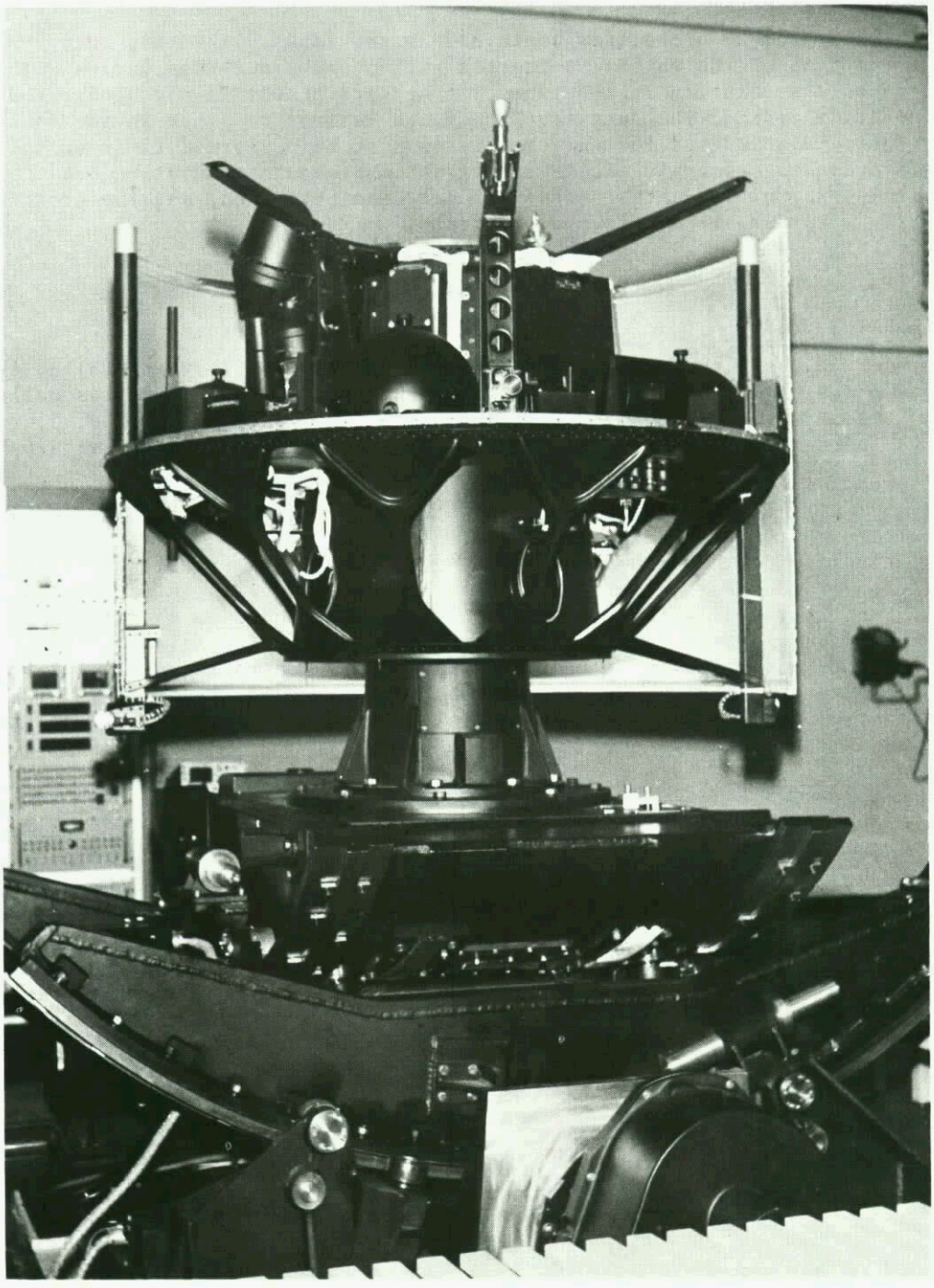

FIG. 9 - SATELLITE MODEL ON THREE AXIS TEST MACHINE

ATTITUDE CONTROL OF THE APOLLO SPACECRAFT

by

Richard H. Battin
Associate Director
Charles Stark Draper Laboratory
Massachusetts Institute of Technology
75 Cambridge Parkway
Cambridge, Massachusetts 02142 USA

SUMMARY

The digital computer is the central control element in the Apollo control, guidance and navigation system. The primary autopilots of the various spacecraft configurations of Apollo are implemented digitally in this general purpose processor. Successful control system design was made possible by capitalizing on the nature of digital processing and exploiting the attendant flexibility and nonlinear computability. After a brief description of the control system hardware, a detailed treatment of one of these autopilots - namely, coasting flight attitude control - is given.

INTRODUCTION

The history making manned landing on the moon was made possible by many significant advances in technology. Among these was the design and implementation of spaceborne digital closed-loop control systems. These autopilot functions are performed by the onboard control, guidance and navigation systems in each of the Apollo vehicles - the Command Service Module (CSM) and the Lunar Module (LM). In this paper, to illustrate the flexibility and optimization that is possible using modern techniques and instrumentation, the operation of the coasting flight attitude control system in the CSM will be described in some detail.

A simplified diagram of the equipment and features of the Apollo flight control system is shown in Fig. 1. The central control element is the digital computer which performs all of the spacecraft navigation, guidance and control functions. Inertially stabilized instruments measure attitude and thrust acceleration and optical sensors determine the spacial orientation of this physical coordinate system. The keyboard and displays, as well as manual hand controllers, allow crew interaction through the computer whenever appropriate. The computer performs the numerical functions of data processing and exercising control over the vehicle orientation and rocket engines. Our primary concern here is with the use of the computer in attitude control so that we shall give only a brief description of the over-all system hardware.

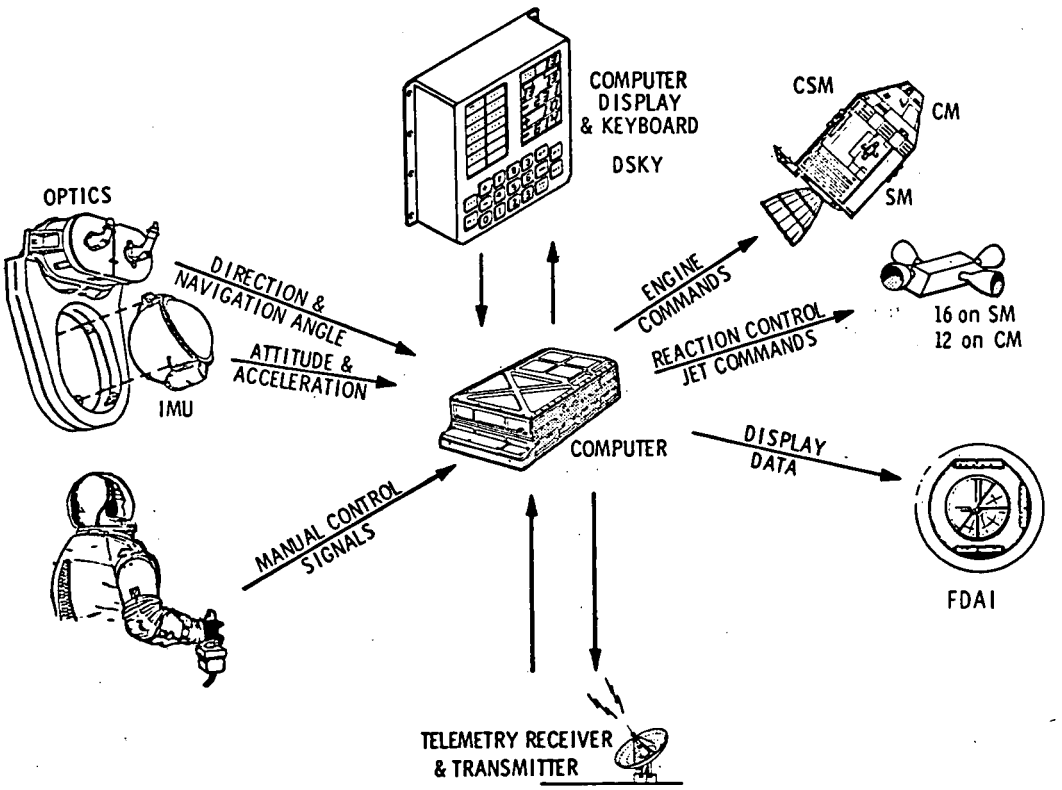

Fig. 1 Apollo Spacecraft Control Schematic Diagram.

1. INERTIAL MEASUREMENT UNIT

The Apollo Inertial Measurement Unit (IMU), as shown schematically in Fig. 2, is a three-degree-of-freedom gimbal system utilizing integrating gyroscopes to detect angular deviations of the stable member with respect to inertial space, and to provide, along with their servo electronics, the establishment of a nonrotating member. On this stable member, in an orthogonal triad, are three accelerometers that are single-degree-of-freedom pendulums with a digital pulse restraining system. Angle information as to the orientation of the computing coordinate frame with respect to the navigation base is derived from a two-speed resolver system mounted on each axis of the IMU. This information is visually displayed to the crew through a ball indicating system with resolvers servo-controlled to follow the IMU resolvers. The same resolver system by means of a Coupling Data Unit (CDU) provides to the computer quantized angle increments corresponding to changes in gimbal angles. The CDU couples angle information to and from the guidance computer, performing both analog to digital and digital to analog conversion.

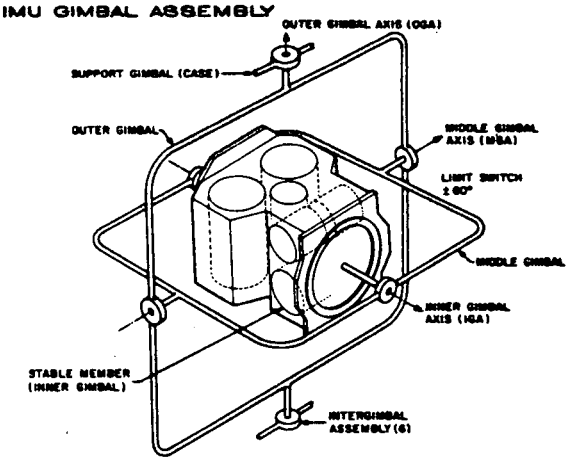

Fig. 2 IMU Schematic Diagram.

IMU Alignment - Since the Apollo IMU is normally not functioning during the long coasting periods, in-flight inertial system alignment against star references has been provided. Since the trajectory and the thrust or drag lie fairly close to a fixed plane, the inner gimbal axis is aligned approximately perpendicular to this plane. All required large maneuvers result mostly in inner gimbal motion, so that the difficulty of approaching gimbal lock associated with large middle gimbal angles is avoided. Finally, because large roll maneuvers are frequently required, the outer gimbal axis is mounted along or near the roll axis.

A rigid structure mounted to the spacecraft, called the navigation base, provides a common mounting structure for a star alignment telescope and the base of the IMU gimbal system. Precision angle transducers on each of the axes of the telescope and on each of the axes of the IMU gimbals permit the indicated angles to be processed to generate the star direction components in inertial system stable-member coordinates.

IMU alignment is normally performed in two stages - coarse and fine. The first step in coarse alignment is to provide the computer with a reasonably accurate knowledge of spacecraft attitude. For this purpose, the navigator sights sequentially two stars using the Scanning Telescope (SCT) which is a single-power, wide-field-of-view instrument. The star image is sensed by the navigator, who uses an optics hand controller to command the SCT prism so as to center the star on the reticle. By depressing a mark button when satisfactory tracking is achieved, the navigator signals the computer to read the SCT angles as transmitted by the optics CDU's. A second star direction at a reasonably large angle from the first is similarly measured. The navigator identifies the stars to the computer through the computer keyboard and the spacecraft attitude in three dimensions is thus determined. This orientation is maintained by the attitude hold autopilot to be described later.

In the second step of coarse alignment, the computer determines the desired IMU gimbal angles based upon its knowledge of spacecraft attitude and the guidance maneuver that will be next performed. These desired angles are sent to the IMU through the CDU to be matched by the IMU gimbal servos in response to error signals developed on the angle transducers on each gimbal axis. The IMU gimbal servos are then driven by the gyro stabilization error signals to hold the achieved orientation.

For fine alignment, two star directions are again measured by the navigator. However, this time he uses the Sextant (SXT), which is a 28-power, narrow-field-of-view instrument, in order to achieve necessary accuracy. When appropriately signalled, the computer simultaneously reads the SXT and IMU angles being transmitted via the CDU's. With these data the computer determines star directions in IMU stable member coordinates from which the spatial orientation of the IMU being held by gyro control can be calculated. From a knowledge of the desired attitude, the computer then determines the existing IMU attitude error and meters out the necessary number of gyro torquing pulses to precess the gyros and the IMU to correct the IMU alignment error.

2. APOLLO GUIDANCE COMPUTER (AGC)

The AGC is designed to handle a relatively large and diverse set of onboard data processing and control functions. Some of the special requirements for this computer include 1) real-time solution of several problems simultaneously on a priority basis, 2) efficient two-way communication with the navigator, 3) capability of ground control through radio links, and 4) multiple signal interfaces of both a discrete and continuously variable type. The memory section has a cycle time of 12 μsec and consists of a fixed (read only) portion of 36,864 words together with an erasable portion of 2048 words. Each word in memory is 16 bits long (15 data bits and an odd parity bit). Data words are stored as signed, 14-bit words using a one's complement convention. Instruction words consist of 3 order-code and 12 address-code bits. Because of the short word length, the address portion does not always determine uniquely the address of a memory word. The ambiguity is removed by auxiliary addresses contained in so-called bank registers which are under program control.

The three bits reserved for instruction codes can provide only eight possible operations. This number is extended through the use of so-called partial codes and an extend instruction. Partial codes exploit the fact that a wider variety of instructions are applicable to erasable than to fixed memory. Since erasable memory addresses are short, the instruction field of a word may be correspondingly lengthened. The extend instruction allows the instruction set of the AGC to be doubled by signalling that the following instruction code is to have an alternate interpretation.

The data words used in the AGC may be divided roughly into two classes: those used for mathematical computations and those used in the control of various subsystems. The latter class can almost always be represented with 15 bits, whereas the former requires double precision arithmetic.

The sequence-generator portion of the AGC provides the basic memory timing and the sequences of control pulses (microprograms) which constitute instructions. It also contains the priority-interrupt circuitry and a scaling network which provides various pulse frequencies used by the computer and the rest of the guidance system. A number of "involuntary" sequences, not under normal program control, may break into the normal sequence of instructions; these are triggered either by external events or by certain overflows within the AGC and are used for counter incrementing and program interruption.

Counter incrementing may take place between any two instructions. External requests for incrementing a counter are stored in a counter priority circuit. At the end of every instruction a test is made to see if any incrementing requests exist. If not, the next instruction is executed directly. If a request is present, an incrementing memory cycle is executed to read the word stored in the counter register, increment or shift it, and store the results back in the same location. This type of interrupt provides for asynchronous incremental or serial entry of information into the working erasable memory at the expense of increasing the time required for normal program steps in direct proportion to the amount of counter activity present at any given time.

Program interruption also occurs between program steps and consists of storing the contents of the program counter together with transfer of control to a location fixed for each interrupt option. Interrupting programs may not be interrupted, but interrupt requests are not lost and are processed as soon as the earlier interrupted program is resumed.

Display and Keyboard - The display and keyboard (DSKY) serves as the communication medium between the computer and the navigator. The principal part of the display is the set of three registers, each containing five decimal digits so that an AGC word of 15 bits can be displayed in one register by five octal digits. Three registers are used because of the frequent need to display the three components of a vector. Digits are entered into the computer from a keyboard of 19 push buttons including the 10 decimal digits, plus and minus, and a number of auxiliary items. Each key depression causes a computer interrupt that initiates a request to the computer's executive program to process the character at the earliest opportunity.

Utility Programs - Most of the AGC programs relevant to guidance and navigation are written in a pseudo-code notation for economy of storage. This notation is encoded and stored in the AGC as a list of data words. An "interpreter" program translates this list into a sequence of subroutine linkages. A pseudo-code program consists of a string of operators and addresses with two 7-bit operators stored in one AGC word. Thus, the instruction set is expanded into a comprehensive mathematical language, which includes matrix and vector operations, using numbers of 28 bits and sign.

All AGC programs operate under control of the "executive" routine except those which are executed in the interrupt mode. The executive routine controls priority of jobs and permits time-sharing of erasable storage. On the other hand, the waitlist routine provides timing control for other program sections. Waitlist tasks are run in the interrupt mode and are restricted to a few milliseconds duration. If an interrupt program were to be longer, it could cause an excessive delay in other interrupts waiting to be serviced since one interrupt program inhibits all others until it calls for resumption of the main program. The waitlist program derives its timing from one of the counter registers in the AGC.

Computer Program Mechanization - Any of the mission programs may be viewed as a chain of computational routines linked together by logical coding, which sets and resets appropriate bits for flags, controls timing and sequencing, and produces DSKY displays. The numbered mission programs are initiated as jobs of specified priority. The job allows all types of interrupts to occur and reestablishes itself after the interrupt period. In fact, during its execution, the job itself must periodically check to determine if a higher-priority job is waiting.

The combination of several jobs with varying priorities, controlled in time by waitlist tasks and DSKY inputs, gives the effect of many computer activities being carried on almost simultaneously. In addition to this structure, other interrupt activities can proceed in the background. The Time 4 counter interrupt routine (T4RUPT) is initiated whenever the Time 4 counter overflows. Normally this counter is set to overflow every 120 msec. Every time this occurs, the T4RUPT routine is initiated and one or more of the following functions is performed: 1) sampling and verification of the IMU mode of operation including turn-on, 2) monitoring the telemetry rates, 3) sampling of malfunction indications from the IMU, and 4) control of the relays of the DSKY for display of information, for commanding IMU and other spacecraft modes, and for control of indicator panel illumination. The Time 4 counter monitors the entire system in search of malfunctions. The Time 5 and Time 6 interrupts usually control digital autopilot timing and jet firing.

During a thrust maneuver, for example, the computer may spend 20 to 25% of its time in the interrupt mode. In particular, the thrust vector control autopilot is cycled every 40 msec and remains in interrupt for 8 msec in each cycle. Additional interrupts which consume time are KEYRUPTS from the depression of DSKY buttons, MARKRUPTS from optics usage, UPRUPTS and DOWNRUPTS signifying up and down telemetry activity, and interrupts generated by the hand controllers.

3. DIGITAL ATTITUDE CONTROL

During periods of coasting flight when there are no significant forces acting on the spacecraft, control of the vehicle is maintained by the Reaction Control System Digital Autopilot (RCS DAP) which provides both attitude rotation and vernier translation control along all three axes. The DAP receives and processes data from various sources such as AGC keyboard input, panel switches and hand controllers, CDU angles and computer generated steering commands for controlling automatic maneuvers. Output from the DAP consists of on and off commands to the reaction jets as well as attitude error signals for display on the flight-director-attitude-indicator (FDAI). Sixteen of these reaction jet engines are mounted on the sides of the service module in quadruple sets at four locations. They are normally fired in pairs to produce control couples and can have pulse durations as short as 14 msec.

The RCS DAP may operate in any of three modes which are selected by the crew using a panel switch. In the so-called FREE mode, direct actuation of the reaction jets by the pilot can be made through a three-axis Rotational Hand Controller (RHC). Each time the RHC is moved out of detent, a single 14 msec. firing of the control jets results. Otherwise, with no crew activity, the spacecraft will drift freely. During the HOLD mode, the attitude of the spacecraft is maintained within a deadband by computer controlled firing of the reaction jets, provided no commands are present from the RHC. Crew commands will override attitude hold and result in rotations at a pre-determined rate on each of the appropriate control axes so long as the RHC is out of detent. When crew activity ceases, attitude hold is again established for the new attitude. Finally, in the AUTO mode, rate and attitude commands are provided by the AGC automatic steering programs to bring the spacecraft to a desired attitude at a specified rate. At any time during an automatic maneuver, the crew may intervene with the RHC and the RCS DAP will again function as it does in the HOLD mode.

Vernier translation commands are provided by the crew, primarily for performing ullage, using the Translation Hand Controller (THC) and may be applied during any mode. The jet selection strategy is designed so that these motions will be combined with vehicle rotations if possible. However, in the event of a quad failure, translation commands will be ignored if they would interfere with desired spacecraft attitude control.

4. ATTITUDE HOLD MODE

In the attitude hold mode, the AGC operates the jet solenoid valve drivers directly based on attitude error and attitude rate information. As illustrated in Fig. 3, the input to the logic is a set of reference angles $\underline{\theta}_d = (\theta_{do}, \theta_{di}, \theta_{dm})^T$ corresponding to the desired outer, inner and middle gimbal angles. These angles are differenced with the current CDU angles and the resulting attitude error signals, resolved along the control axes, are $\underline{\theta}_e$.

The next step is to obtain a set of estimated spacecraft angular rates $\hat{\underline{\omega}}$ also resolved along control axes. Derivation of these body rates from the gimbal angles is complicated by the effects of CDU angle quantization and the effects of body bending modes of the vehicle. They are computed from IMU gimbal angle differences and are smoothed by a second-order filter. To enhance accuracy, the commanded angular acceleration $\underline{\alpha}$ of the jets is included in the computation.

As a function of attitude error and attitude rate, nonlinear switching functions, using a phase plane logic, are employed to generate the necessary firing time intervals. A jet-selection logic is then used to select the individual jets to be fired based both on the rotation commands and the translation commands from the THC. The actual control and timing of the firings is accomplished by the interrupt structure of the computer.

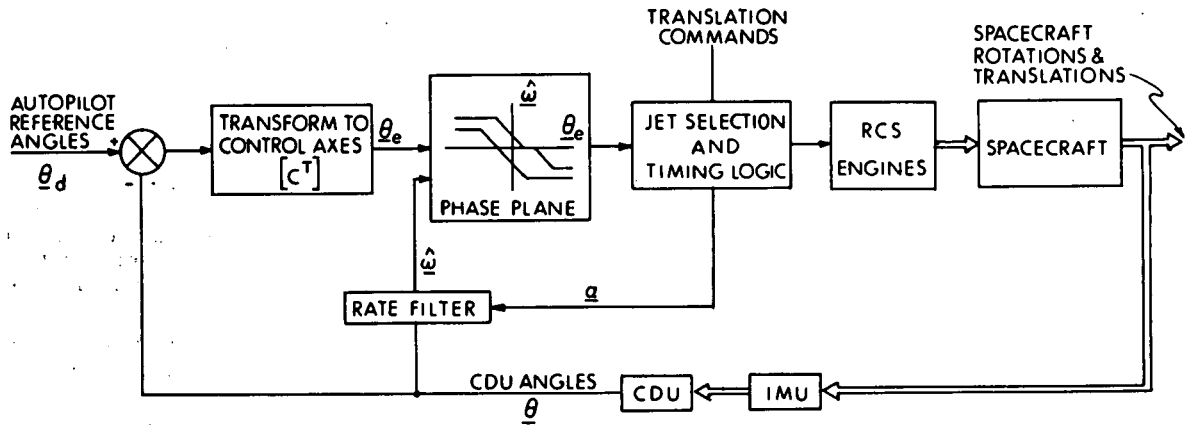

Fig. 3 RCS Attitude Hold Logic.

Attitude Error Computation - Since the RCS jets apply forces along the control axes of the spacecraft, it is necessary to resolve the gimbal angle errors along these directions. For this purpose, we define the direction cosine matrix C that relates the spacecraft navigation base orientation to the stable member frame

$$C = \begin{pmatrix} \cos\theta_i & 0 & \sin\theta_i \\ 0 & 1 & 0 \\ -\sin\theta_i & 0 & \cos\theta_i \end{pmatrix} \begin{pmatrix} \cos\theta_m & -\sin\theta_m & 0 \\ \sin\theta_m & \cos\theta_m & 0 \\ 0 & 0 & 1 \end{pmatrix} \begin{pmatrix} 1 & 0 & 0 \\ 0 & \cos\theta_o & -\sin\theta_o \\ 0 & \sin\theta_o & \cos\theta_o \end{pmatrix} \quad (1)$$

For example, if $\underline{v}_{NB}$ is a vector whose components are expressed in navigation base components and $\underline{v}_{SM}$ is the same vector but with components expressed in stable-member components, then

$$\underline{v}_{SM} = C\,\underline{v}_{NB} \quad (2)$$

(It should be remarked that, in fact, the navigation base axes are tilted at 7.25^o with respect to the control axes. Hence, θ_m should be replaced by $\theta_m - 7.25^o$. However, in the sequel we will ignore this detail.)

The components of the attitude error vector $\underline{\theta}_e$ represent roll, pitch and yaw errors, respectively, and may be obtained from

$$\underline{\theta}_e = C^T(\underline{\theta} - \underline{\theta}_d) \tag{3}$$

where $\underline{\theta}$ is a vector whose components are the current CDU angles. Actually a small angle approximation is used to simplify the computation of C^T which turns out to be sufficiently accurate even though this matrix is updated only once per second. The transformation, as mechanized in the AGC, is simply

$$C^T = \begin{pmatrix} 1 & \sin\theta_m & 0 \\ 0 & \cos\theta_m \cos\theta_o & \sin\theta_o \\ 0 & -\cos\theta_m \sin\theta_o & \cos\theta_o \end{pmatrix} \tag{4}$$

Rate Filter - An estimate of the angular velocity $\hat{\underline{\omega}}$ of the spacecraft must be inferred from the CDU angles since no direct measurement of this rate is available. The rate filter design is motivated by modern statistical estimation theory and leads to a set of recursive difference equations which are readily implemented in a digital computer. The specific argument proceeds as follows.

Let $\hat{\underline{\theta}}_{n-1}$ and $\hat{\underline{\omega}}_{n-1}$ be estimates of the spacecraft attitude and attitude rate at time t_{n-1}. Then at a later time t_n we may write

$$\hat{\underline{\theta}}'_n = \hat{\underline{\theta}}_{n-1} + \hat{\underline{\omega}}_{n-1}\,\Delta t + \int_{t_{n-1}}^{t_n}\int_0^t \underline{\alpha}(\tau)\,d\tau\,dt \tag{5}$$

$$\hat{\underline{\omega}}'_n = \hat{\underline{\omega}}_{n-1} + \int_{t_{n-1}}^{t_n} \underline{\alpha}(t)\,dt \tag{6}$$

where $\underline{\alpha}(t)$ is the control acceleration attributed to the jet firings and $\Delta t = t_n - t_{n-1}$ which happens to be 0.1 sec in the DAP. The prime notation indicates that $\hat{\underline{\theta}}'_n$ and $\hat{\underline{\omega}}'_n$ are extrapolated estimates and do not include the attitude measurement data $\tilde{\underline{\theta}}_n$ at time t_n.

The thrust of an RCS jet is assumed to be constant so that

$$\int_{t_{n-1}}^{t_n} \underline{\alpha}(t)\,dt = \underline{c}\,\Delta t_f \tag{7}$$

where $\underline{c}$ is a constant vector and Δt_f is the single-jet operation jet-on time as required during the interval Δt. It turns out that sufficient accuracy is obtained by neglecting the specific angular increment caused by $\underline{\alpha}$ when extrapolating $\hat{\underline{\theta}}$.

A linear estimate of attitude and attitude rate at time t_n, which utilizes the extrapolated estimates and the measured CDU angles $\tilde{\underline{\theta}}_n$, is simply

$$\begin{aligned} \hat{\underline{\theta}}_n &= \hat{\underline{\theta}}'_n + W_n^{(1)}(\tilde{\underline{\theta}}_n - \hat{\underline{\theta}}'_n) \\ \hat{\underline{\omega}}_n &= \hat{\underline{\omega}}'_n + W_n^{(2)}(\tilde{\underline{\theta}}_n - \hat{\underline{\theta}}'_n) \end{aligned} \tag{8}$$

where $W_n^{(1)}$ and $W_n^{(2)}$ are matrix weighting factors. The proper determination of these matrices to produce a statistically optimum estimate can, of course, be accomplished if the statistical nature of the measurement errors is known. Even so, a recursive calculation of these matrix gains would be far too time consuming for the AGC. Fortunately, sufficient accuracy is possible if the matrices are regarded as diagonal and if these diagonal elements are selected in advance, i.e. preprogrammed.

The filter equations can be put in a more convenient form. For this purpose, we define the vector

$$\underline{\rho}_n = \tilde{\underline{\theta}}_n - \hat{\underline{\theta}}'_n = \tilde{\underline{\theta}}_n - \hat{\underline{\theta}}_{n-1} - \hat{\underline{\omega}}_n\,\Delta t$$

so that $$\hat{\underline{\theta}}_n = \hat{\underline{\theta}}'_n + W_n^{(1)}\underline{\rho}_n$$

or, alternately, $$\tilde{\underline{\theta}}_n - \hat{\underline{\theta}}_n = (I - W_n^{(1)})\,\underline{\rho}_n$$

and $$\tilde{\underline{\theta}}_{n-1} - \hat{\underline{\theta}}_{n-1} = (I - W_{n-1}^{(1)})\,\underline{\rho}_{n-1}$$

Hence $$\underline{\rho}_n = (\tilde{\underline{\theta}}_n - \tilde{\underline{\theta}}_{n-1}) + (\tilde{\underline{\theta}}_{n-1} - \hat{\underline{\theta}}_{n-1}) - \hat{\underline{\omega}}_n\,\Delta t$$

or $$\underline{\rho}_n = (\tilde{\underline{\theta}}_n - \tilde{\underline{\theta}}_{n-1}) + (I - W_{n-1}^{(1)})\,\underline{\rho}_{n-1} \tag{9}$$

This last equation, which gives a recursion formula for the parameter $\underline{\rho}_n$ in terms of the difference between two consecutive sets of measured CDU angles, together with the equation

$$\underline{\hat{\omega}}_n = \underline{\hat{\omega}}_{n-1} + W_n^{(2)} \underline{\rho}_n + \underline{c}\,\Delta t_f \qquad (10)$$

provide the complete description of the RCS DAP rate filter.

The determination of the filter gains $W_n^{(1)}$ and $W_n^{(2)}$ was accomplished in a semi-empirical manner and will not be discussed here. The gain settings depend on the spacecraft configuration, the desired response time of the control system, and the specified size of the limit cycles.

Phase Plane Switching Logic - The dynamics of the switching logic for a single axis can best be understood by interpretation in the phase plane diagram of Fig. 4. Here the horizontal and vertical axes represent attitude error and angular rate, respectively. Paths of zero acceleration are horizontal lines while paths of constant acceleration are parabolas.

In the attitude hold mode, consider the consequences of the vehicle in the state represented by the point A. Since the angular velocity is positive, the point moves to the right until it reaches the decision line at B. The DAP then fires RCS jets to drive the rate to zero. To allow for vehicle torque-to-inertia ratios that are greater than those assumed by the autopilot and to prevent overshoot in this case, the desired impulse is intentionally reduced by 20 per cent. In the normal case, then, the rate change falls short of the desired rate line, producing an over-damped response. The state drops only to point C and moves more slowly toward the decision line. Due to delays in the rate filter, line CD will not be perfectly straight, but will gradually approach the correct rate value. When the decision line is encountered again at point D, the cycle repeats. Because the firing time can never be less than 14 msec., the point will eventually cross the decision line close enough to zero to overshoot on the next jet firing. Since the angular velocity is now negative, the point will now move to the left across the deadband to point F. Jets will fire to drive the rate in the opposite direction, overshooting again to point G. The final result is the minimum-impulse limit cycle EFGH.

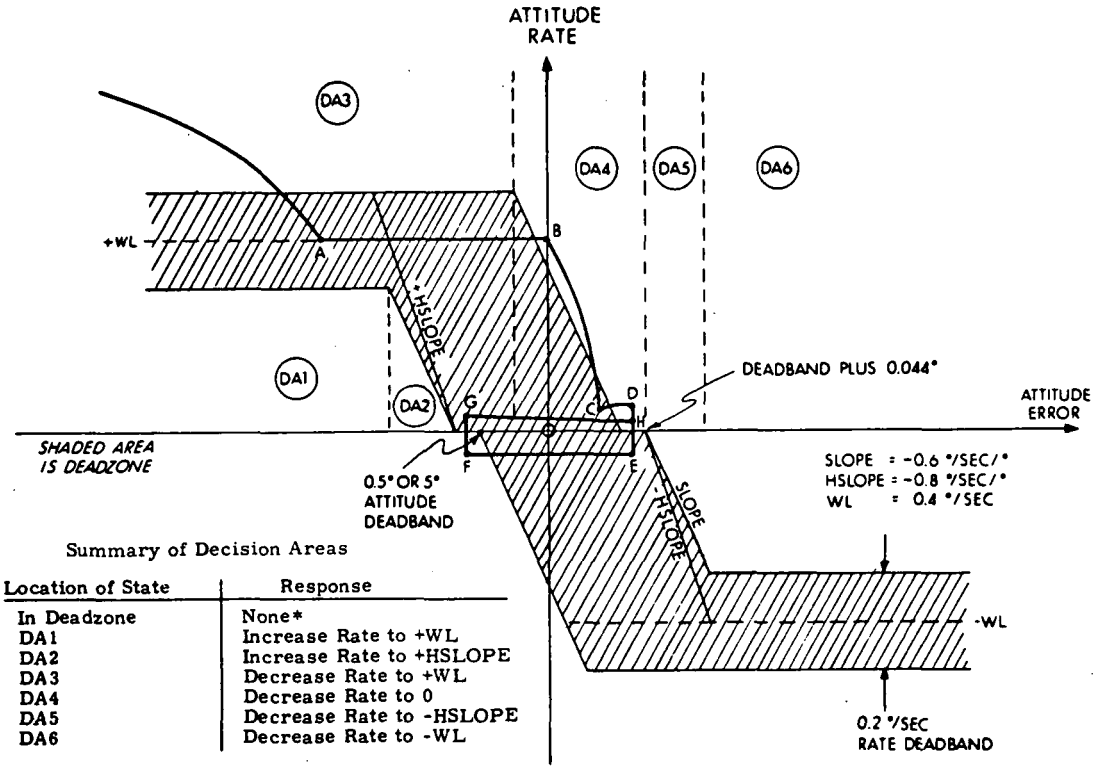

Summary of Decision Areas

Location of State	Response
In Deadzone	None*
DA1	Increase Rate to +WL
DA2	Increase Rate to +HSLOPE
DA3	Decrease Rate to +WL
DA4	Decrease Rate to 0
DA5	Decrease Rate to -HSLOPE
DA6	Decrease Rate to -WL

Fig. 4 Phase Plane.

A summary of decision areas and responses accompanies the figure for the top half of the phase plane. The bottom half is symmetrical with respect to the origin. (Note that from decision areas 2 and 5 the rate is driven to the hysteresis lines +HSLOPE or -HSLOPE to guarantee entry to the deadband zone even for short impulses.) The width of the rate-limit deadband is fixed at 0.2 deg per second. The crew can select either the maximum (5.0 deg) or minimum (0.5 deg) angular deadband through DSKY.

Jet Selection Logic - The RCS DAP causes rotations and translations of the spacecraft by means of the 16 RCS jets located on the forward end of the service module as shown in Fig. 5. They are clustered in four quads of four jets each and lettered A through D. Quads A and C are aligned with the yaw control or Z axis and quads B and D with the pitch control or Y axis.

Rotations about or translations along a given axis are normally executed with a single pair of jets - one each on opposing quads AC or BD. Since a single jet firing will result in both a rotation and a translation, fuel is conserved by combining rotations and translations whenever possible. It is clear from the figure that X translations can be combined with pitch axis rotations using quads AC or with yaw axis rotations using quads BD. Also roll axis rotations can be combined with Y translations using quads AC or with Z translations using quads BD.

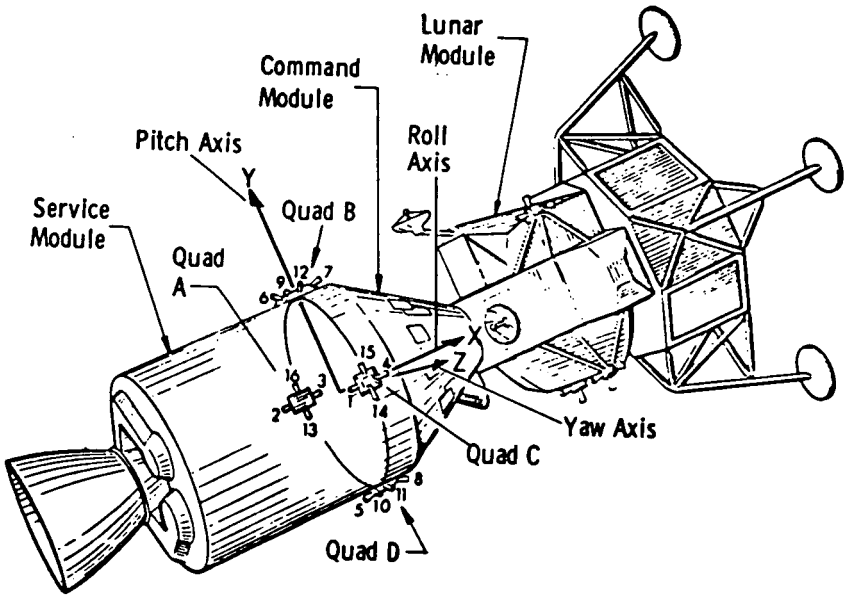

Fig. 5 Service Module Jet Quad Locations.

If one or more jets in a particular quad have failed, the autopilot will continue to function but at a reduced efficiency. However, provision is made for informing the AGC of quad failures. In this event, the computer will not attempt to fire the jets in the designated quad but will, instead, compensate for the reduction of control torque when performing attitude maneuvers. It is interesting to note that a useful by-product of this quad-fail logic feature of the AGC is the possibility of minimizing propellant consumption in attitude hold through the use of a single jet.

Implementation of jet selection in the AGC is by means of a table look-up procedure. Two sets of tables are used - one providing information on combined rotations and translations and the other, translations only. Entries are included for quad failures and a torque parameter is included to indicate the direction and magnitude of the resultant torque. This parameter is used both in calculating jet-on time, accounting for the actual number of jets fired, and in evaluating the effects of quad failures on the resultant torque.

5. AUTOMATIC ATTITUDE MANEUVER MODE

Automatic attitude maneuvers are implemented by exactly the same logic as that used in attitude hold. However, they are based on a specific desired rate ω_d and a reference attitude $\underline{\theta}_d$ which is a function of time. The RCS automatic control logic flow is diagrammed in Fig. 6.

The attitude maneuver routine is designed to provide the necessary data to permit reorientation of the spacecraft from some initial attitude specified by the set of gimbal angles $\underline{\theta}$ to a desired attitude $\underline{\theta}_d$. Optimum solutions of this control problem are quite complex and turn out in practice to be not significantly better than the technique of rotating the spacecraft about a single inertially fixed axis.

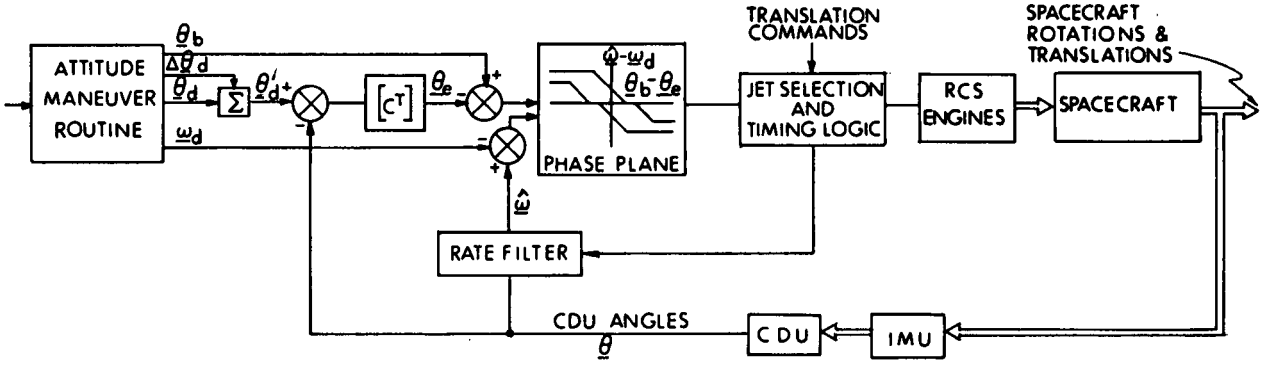

Fig. 6 RCS Automatic Maneuver Logic.

The attitude maneuver program computes according to Eq. (1) two direction cosine matrices: C, using the initial set of gimbal angles $\underline{\theta}$, and C_d, using the final desired set of gimbal angles $\underline{\theta}_d$. Then, following the arguments developed in the Appendix, the rotation matrix R is defined by

$$R = C^T C_d \tag{11}$$

with r_{ij} denoting the element in the i^{th} row and j^{th} column. Finally, the direction in space $\underline{u}$ about which to rotate the vehicle together with the angle of rotation β are determined from

$$\underline{u}^T = \text{Unit}\,(r_{32} - r_{23},\ r_{13} - r_{31},\ r_{21} - r_{12}) \tag{12}$$

$$\beta = \cos^{-1}\left(\frac{\text{tr } R - 1}{2}\right) \tag{13}$$

Instead of specifying the terminal desired gimbal angles $\underline{\theta}_d$, the desired attitude to which the spacecraft is to be aligned can also be specified by two unit vectors: a body-fixed axis vector $\underline{u}_a$ and a desired-direction vector $\underline{u}_d$. This has the advantage of leaving the orientation of the spacecraft about $\underline{u}_d$ unconstrained. Therefore, the crew may utilize this additional degree of freedom to satisfy other requirements such as communication, visibility or thermal effects.

The gimbal angles $\underline{\theta}_d$ may be obtained from the vectors $\underline{u}_a$ and $\underline{u}_d$. The outer and inner products of these vectors will yield $\underline{u}$ and β from which the rotation matrix R is determined. Then from the matrix product

$$C_d = C\,R \tag{14}$$

the terminal desired gimbal angles $\underline{\theta}_d$ may be extracted. Specifically, if we write

$$C_d = \begin{pmatrix} c_1 & c_2 & c_3 \\ c_4 & c_5 & c_6 \\ c_7 & c_8 & c_9 \end{pmatrix} \tag{15}$$

it follows from Eq (1) that

$$\theta_{dm} = \sin^{-1} c_4 \qquad \theta_{di} = \sin^{-1}(-c_7/\cos\theta_{dm}) \qquad \theta_{do} = \sin^{-1}(-c_6/\cos\theta_{dm}) \tag{16}$$

(Note that if $c_1 < 0$, then θ_{di} is replaced by $\pi\,\text{sgn}(\theta_{di}) - \theta_{di}$ and if $c_5 < 0$, then θ_{do} is replaced by $\pi\,\text{sgn}(\theta_{do}) - \theta_{do}$.)

As a result of these calculations it may happen that the magnitude of the desired terminal middle gimbal angle θ_{dm} is so large ($> 59^o$) that a maneuver to this attitude would result in gimbal lock. In most cases, this condition may be avoided by an additional rotation about $\underline{u}_d$ through a sufficently large angle β_m. Under these circumstances, a rotation matrix R_m is computed from $\underline{u}_d$ and β_m. Equation (14) is then replaced by

$$C_d = C\,R\,R_m \tag{17}$$

from which more satisfactory values of $\underline{\theta}_d$ are obtained. For those few instances when this simple procedure will not cure the terminal gimbal lock problem, a platform realignment by the crew is required before reorienting the spacecraft.

Steering during an attitude maneuver is accomplished in the following manner. First, a transformation matrix ΔR is computed representing the rotation about u of the spacecraft through an incremental angle equal to the desired maneuver rate ω_d multiplied by the iteration cycle period of one second. Then, from the matrix product $C_d = C\,\Delta R$ the autopilot reference angles $\underline{\theta}_d$ are extracted and used to compute attitude error signals during the first second of the maneuver. For the next second, and iteratively thereafter for each computation cycle, the C matrix is updated as indicated by

$$C(t_{n+1}) = C(t_n)\,\Delta R \tag{18}$$

Thus, a reference trajectory of desired CDU angles is generated to be tracked by the rotating spacecraft.

The attitude maneuver routine generates the desired gimbal angles $\underline{\theta}_d$ only once per second which is quite infrequent as compared with the autopilot sample rate of 0.1 sec. Therefore, a set of incremental angles $\Delta\underline{\theta}_d$ are also computed so that $\underline{\theta}_d$ can be interpolated at the sample times in order to minimize discontinuity. The attitude maneuver routine also generates a set of desired rates $\underline{\omega}_d = \omega_d\,\underline{u}$ which are subtracted from the estimated spacecraft rate $\hat{\underline{\omega}}$. Then the attitude errors $\underline{\theta}_e = \theta - \theta_d$ and the rate errors $\underline{\omega}_e = \hat{\underline{\omega}} - \underline{\omega}_d$ are applied as inputs to exactly the same phase plane switching logic as used in attitude hold.

In order to improve performance, the maneuver routine may generate a set of attitude error biases $\underline{\theta}_b$ which are added to the attitude errors $\underline{\theta}_e$ to provide additional lead and prevent fuel-consuming overshoot when starting and stopping an automatic maneuver. Also it may be mentioned that various attitude maneuver rates may be selected by the crew. If the largest rate is chosen, the autopilot will increase the frequency response of the rate filter and more effectively counteract the crosscoupling torques that may occur during the maneuver.

The crew has the option of either manually reorienting the spacecraft or having the maneuver performed automatically. Total attitude error displays are available on the FDAI as visual cues for the crew. During the maneuver, the crew must monitor the FDAI ball to detect the approaching of gimbal lock. If the spacecraft attitude is approaching the gimbal lock zone, the crew may stop the maneuver by switching to the attitude hold mode or simply, by using the RHC, steer the spacecraft manually around gimbal lock. Under any circumstances, when the maneuver is complete, the autopilot reverts to the attitude hold mode.

6. APPENDIX

Consider the problem of rotating a vector $\underline{r}_0$ about an axis, defined by the unit vector $\underline{u}$, through an angle β as shown in Fig. 7. If $\underline{r}_1$ is the resulting vector, we desire a relationship between $\underline{r}_0$ and $\underline{r}_1$ as a function of $\underline{u}$ and β.

Let α be the cone angle, i.e. the angle between $\underline{u}$ and $\underline{r}_0$ or $\underline{u}$ and $\underline{r}_1$, and let $\underline{r}(\varphi)$ be the intermediate vector after a rotation through an angle φ. Then, clearly, the vector $d\underline{r}$ has a magnitude of

$$dr = r \sin\alpha \, d\varphi$$

and a direction perpendicular to both $\underline{r}$ and $\underline{u}$. Hence

$$d\underline{r} = (\underline{u} \times \underline{r})\, d\varphi = A\underline{r}\, d\varphi \qquad \text{(A-1)}$$

where the skew-symmetric matrix A is defined in terms of the components of the vector $\underline{u} = (u_x, u_y, u_z)^T$ as

$$A = \begin{pmatrix} 0 & -u_z & u_y \\ u_z & 0 & -u_x \\ -u_y & u_x & 0 \end{pmatrix} \qquad \text{(A-2)}$$

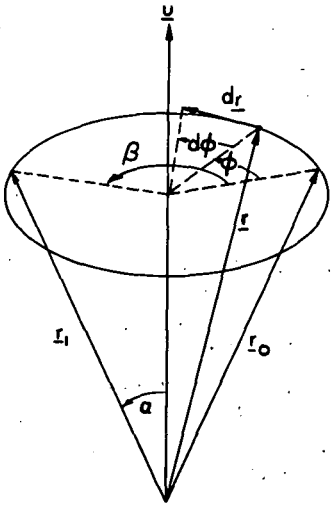

Fig. 7 Vector Rotation Geometry.

Equation (A-1) is a linear vector differential equation with constant coefficient A whose solution, satisfying the boundary conditions $\underline{r}(0) = \underline{r}_0$ and $\underline{r}(\beta) = \underline{r}_1$, is simply

$$\underline{r}_1 = e^{\beta A}\underline{r}_0 = R\underline{r}_0 \qquad \text{(A-3)}$$

where the matrix R is defined by the infinite matrix series

$$R = e^{\beta A} = I + \beta A + \frac{1}{2!}\beta^2 A^2 + \frac{1}{3!}\beta^3 A^3 + \ldots. \qquad \text{(A-4)}$$

Now since

$$\underline{u} \times \underline{r} = A\underline{r} \qquad \text{(A-5)}$$

then

$$\underline{u} \times (\underline{u} \times \underline{r}) = A^2\underline{r} = (\underline{u}\cdot\underline{r})\underline{u} - \underline{r} = (\underline{u}\,\underline{u}^T - I)\underline{r} \qquad \text{(A-6)}$$

and

$$\underline{u} \times [\underline{u} \times (\underline{u} \times \underline{r})] = A^3\underline{r} = -\underline{u} \times \underline{r} = -A\underline{r} \qquad \text{(A-7)}$$

so that

$$A^3 = -A \qquad \text{(A-8)}$$

Hence

$$R = I + (\beta - \frac{\beta^3}{3!} + \ldots)A + (\frac{\beta^2}{2!} - \frac{\beta^4}{4!} + \ldots)A^2$$

$$= I + \sin\beta\, A + (1 - \cos\beta)A^2$$

$$= \underline{u}\,\underline{u}^T + \cos\beta(I - \underline{u}\,\underline{u}^T) + \sin\beta\, A \qquad \text{(A-9)}$$

Consider now the inverse problem. Suppose a linear relationship between $\underline{r}_0$ and $\underline{r}_1$ is specified as

$$\underline{r}_1 = R\underline{r}_0 \tag{A-10}$$

and we require the direction $\underline{u}$ and the angle β for which a simple rotation brings $\underline{r}_0$ into coincidence with $\underline{r}_1$. Clearly, what is required is the solution of Eq. (A-9) for $\underline{u}$ and β in terms of the matrix R.

The solution is simplified by noting that

$$R^T = \underline{u}\,\underline{u}^T + \cos\beta\,(I - \underline{u}\,\underline{u}^T) - \sin\beta\,A \tag{A-11}$$

so that

$$A = \frac{1}{2\sin\beta}\,(R - R^T) \tag{A-12}$$

Hence

$$\underline{u} = \frac{1}{2\sin\beta}\begin{pmatrix} r_{32} - r_{23} \\ r_{13} - r_{31} \\ r_{21} - r_{12} \end{pmatrix} \tag{A-13}$$

where r_{ij} denotes the element in the i^{th} row and the j^{th} column of the matrix R and

$$2\sin\beta = \pm\sqrt{(r_{32} - r_{23})^2 + (r_{13} - r_{31})^2 + (r_{21} - r_{12})^2} \tag{A-14}$$

The ambiguity in quadrant for the angle β is resolved by noting that

$$\begin{aligned} \text{tr } R &= \text{tr}\,(\underline{u}\,\underline{u}^T)(1 - \cos\beta) + 3\cos\beta \\ &= 1 + 2\cos\beta \end{aligned}$$

so that

$$2\cos\beta = \text{tr } R - 1 \tag{A-15}$$

Finally we note that the matrix R has the following interpretation. Let $\underline{r}_1$ be a vector resolved along some orthogonal triad. If this triad is rotated to coincide with a new set of axes as described by the rotation matrix R, then the components of the vector $\underline{r}_1$ in the rotated frame will be numerically equal to the components of $\underline{r}_0$.

7. REFERENCES

(1) Miller, J. E., "Space Navigation Guidance and Control," Technivision Ltd., Maidenhead, England, 1966.

(2) Keene, D. W. and Turnbull, J. F., "Reaction Control System Digital Autopilot," Report R-577, Charles Stark Draper Laboratory, M. I. T., February 1971.

(3) Keene, D. W., "Coasting - Flight Attitude Maneuver Routine," Report R-577, Charles Stark Draper Laboratory, M. I. T., February 1971.

(4) Dixon, M., "Fuel - Time Optimal Spacecraft Reorientation," Ph. D. Thesis T-502, Instrumentation Laboratory, M. I. T., May 1968.

(5) Crisp, R. and Keene, D., "Attitude Maneuver Optimization to Conserve Reaction Control Propellants," Report E-1832, Instrumentation Laboratory, M. I. T., August 1965.

(6) Crisp, R. and Keene, D., "Apollo Command and Service Module Reaction Control by the Digital Autopilot," Report E-1964, Instrumentation Laboratory, M. I. T., May 1966.

NATIONAL DISTRIBUTION CENTRES FOR UNCLASSIFIED AGARD PUBLICATIONS

Unclassified AGARD publications are distributed to NATO Member Nations through the unclassified National Distribution Centres listed below

BELGIUM
Colonel R.DELLEUR
Coordinateur AGARD – V.S.L.
Etat-Major Forces Aériennes
Caserne Prince Baudouin
Place Dailly, Bruxelles 3

CANADA
Director of Scientific Information Services
Defence Research Board
Department of National Defence – 'A' Building
Ottawa, Ontario

DENMARK
Danish Defence Research Board
Østerbrogades Kaserne
Copenhagen Ø

FRANCE
O.N.E.R.A. (Direction)
29, Avenue de la Division Leclerc
92, Châtillon-sous-Bagneux

GERMANY
Zentralstelle für Luftfahrtdokumentation
und Information
Maria-Theresia Str. 21
8 München 27
Attn: Dr Ing. H.J.RAUTENBERG

GREECE
Hellenic Armed Forces Command
D Branch, Athens

ICELAND
Director of Aviation
c/o Flugrad
Reykjavik

ITALY
Aeronautica Militare
Ufficio del Delegato Nazionale all'AGARD
3, Piazzale Adenauer
Roma/EUR

LUXEMBOURG
Obtainable through BELGIUM

NETHERLANDS
Netherlands Delegation to AGARD
National Aerospace Laboratory, NLR
Attn: Mr A.H.GEUDEKER
P.O. Box 126
Delft

NORWAY
Norwegian Defense Research Establishment
Main Library, c/o Mr P.L.EKERN
P.O. Box 25
N-2007 Kjeller

PORTUGAL
Direccao do Servico de Material
da Forca Aerea
Rua de Escola Politecnica 42
Lisboa
Attn: Brig. General Jose de Sousa OLIVEIRA

TURKEY
Turkish General Staff (ARGE)
Ankara

UNITED KINGDOM
Ministry of Technology Reports Centre
Station Square House
St. Mary Cray
Orpington, Kent BR5 3RE

UNITED STATES
National Aeronautics and Space Administration (NASA)
Langley Field, Virginia 23365
Attn: Report Distribution and Storage Unit

* * *

If copies of the original publication are not available at these centres, the following may be purchased from:

Microfiche or Photocopy

National Technical
Information Service (NTIS)
5285 Port Royal Road
Springfield
Virginia 22151, USA

Microfiche

ESRO/ELDO Space
Documentation Service
European Space
Research Organization
114, Avenue de Neuilly
92, Neuilly-sur-Seine, France

Microfiche

Ministry of Technology
Reports Centre
Station Square House
St. Mary Cray
Orpington, Kent BR5 3RE
England

The request for microfiche or photocopy of an AGARD document should include the AGARD serial number, title, author or editor, and publication date. Requests to NTIS should include the NASA accession report number.

Full bibliographical references and abstracts of the newly issued AGARD publications are given in the following bi-monthly abstract journals with indexes:

Scientific and Technical Aerospace Reports (STAR)
published by NASA,
Scientific and Technical Information Facility,
P.O. Box 33, College Park,
Maryland 20740, USA

United States Government Research and Development Report Index (USGDRI), published by the Clearinghouse for Federal Scientific and Technical Information, Springfield, Virginia 22151, USA

Printed by Technical Editing and Reproduction Ltd
Harford House, 7-9 Charlotte St, London. W1P 1HD